CHANGEMENTS CLIMATIQUES PASSES ET VARIABILITE INTERANNUELLE SOUS LES TROPIQUES

Matthieu Carré

UFR Terre, Environnement, Biodiversité

Mémoire Présenté en vue de l'obtention du diplôme
d'Habilitation à Diriger la Recherche

CHANGEMENTS CLIMATIQUES PASSÉS ET VARIABILITÉ INTERANNUELLE SOUS LES TROPIQUES

Matthieu Carré

CR CNRS, Laboratoire d'Océanographie et de Climatologie : Approches numériques et expérimentales (LOCEAN, UMR7159)

Travail présenté le 24 septembre 2018 devant le jury composé de :
Loïc Segalen, Prof Sorbonne Université, Président du jury
Luc Beaufort, DR CNRS, Rapporteur
Frank Bassinot, CEA, Rapporteur
Laurent Chauvaud, DR CNRS, Rapporteur
Mary Elliot, Prof Université de Nantes, Examinatrice
Rachid Cheddadi, DR CNRS, Examinateur

TABLE DES MATIERES

Summary

Past Climate Change and Interannual variability in the tropics

This thesis is a condensed presentation of my main research work since my PhD and of my research prospective for the next few years. My research activities are mainly focused on the reconstruction and the analysis of past climate variability in the tropics. The goals are (1) to assess current climate change in the context of long-term natural climate variability, (2) identify the mechanisms that drive this variability, (3) to test the ability of climate models to reproduce past climate change, and (4) to enlighten the long-term relationship between human societies and environmental changes.

In this large framework, I focused on two regions: first the South-East Pacific including the Peru-Chile coast and the Humboldt current system where the interannual climate variability is almost entirely determined by the El Niño Southern Oscillation (ENSO). Secondly Senegal as a representative area of the Sahel, where climate is essentially governed by the West African monsoon. These two climate features have extreme variations with catastrophic human and economic consequences. In both cases, very large uncertainties in model predictions prevent from designing appropriate adaptation strategies. In both cases, the short observational record prevents statistically robust analyses of the variability and prevents any comparison with pre-industrial conditions. I developed an innovative approach to reconstruct past variations of ENSO and the Sahel rainfall using high resolution isotopic records ($\delta^{18}O$ and $\delta^{13}C$) and sclerochronology of fossil bivalve shells.

Seasonal scale temperature variability of the ocean was reconstructed in Peru for the Holocene period from fossil bivalves collected in archaeological shell middens. We showed that the coastal temperature was significantly cooler in Peru during the early and middle Holocene, as a result of a more intense coastal upwelling confirming a La Niña-like mean state for this period. The statistics of ENSO anomalies in Peruvian shells combined with records from other areas in the tropical Pacific suggest that ENSO variance was slightly lower than today during most of the Holocene, and significantly reduced during a ~3000 years period, 6-3 ka (thousand years ago). A change in ENSO asymmetry *ca*. 7 ka suggests a phase dominated by cold events maybe related to a shift of Niño events towards the central Pacific. These results challenged the hypothesis that ENSO was inactive before 5ka in response to changes in the Earth's orbit. Other forcings such as the presence of remnant polar ice sheets must have affected ENSO during the early Holocene. The objective of my future research is to evaluate ENSO sensitivity by observing its behavior during other key periods: (1) the last 2000 years to test the hypothesis that modern ENSO is beyond the range of preindustrial variability, (2) the Eemian warm period (125ka) to test further the influence of insolation changes, and (3) the Pliocene, a globally warm period, characterized by reduced Walker circulation and atmospheric CO2 concentration similar to the current one.

Past changes of the Sahel hydroclimate can be reconstructed from monumental archaeological shell mounds in the Saloum estuary. The site is located at the maximum latitudinal rainfall gradient and belongs to a small watershed. A long in situ calibration work showed that 85% of shell $\delta^{18}O$ variability is linked to local rainfall, that are themselves strongly coherent with regional Sahel rainfall. Based on a series of well dated shells from multiple sites, we built a 1600-years record of centennial scale hydroclimate variability that is unique in western Sahel. This record shows that modern drought

conditions in the Sahel are unprecedented in the past 1600 years. The most humid period occurred from AD 1500 to AD 1800, which corresponds to the so-called Little Ice Age. An abrupt aridification in the past 200 years points for the first time to an anthropogenic forcing of the current aridity. A significant *negative* correlation is observed between Sahel humidity and global temperature. This shows that global shifts of the intertropical convergence zone mean position cannot be invoked to explain this centennial variability. The result supports climate models that predict reduced rainfall in the Sahel in greenhouse climate. Our future research will aim at (1) quantifying past precipitation changes, (2) determine how the monsoon was affected at the seasonal scale, (3) reconstruct changes in the monsoon seasonality during the termination of the African humid period (4-6ka), (4) understanding the mechanisms that drive monsoon changes using paleoclimate data-model comparisons.

1. Curriculum vitae

Matthieu Carré, Paléoclimatologiste, Chargé de Recherche CNRS

Date de naissance: 12-12-1976

CNRS, INSU, Section 19
Adresse professionnelle :
LOCEAN (Laboratoire d'Océanographie et de Climatologie, expérimentations et approche numérique), UMR 7159 UPMC/CNRS/IRD/MNHN
4 Place Jussieu, 75252 PARIS cedex 5

Tel : (+33) 144 27 75 32
E-mail: matthieu.carre@locean-ipsl.upmc.fr
Page Google scholar
Page ResearchGate

FORMATION

2001-2005 Doctorat de l' Université Montpellier 2
Directeurs: Ilhem Bentaleb (MC, UM2), Michel Fontugne (CEA, LSCE)
Titre: Etude géochimique et sclérochronologique de coquilles de bivalves marins : Paléocéanographie de la côte sud du Pérou à l'Holocène inférieur et implications archéologiques.

2000-2001 DEA Paleontologie, Paleobiologie, Phylogénie, mention B
Université Montpellier 2

1997-2000 Ecole Centrale de Lyon
Spécialité de 3ème année: Technologies pour la santé et l'environnement

Langues Anglais: courant (TOEFL iBT 2006 score: 107/120)
Espagnol: courant
Allemand, Portugais

EXPERIENCE PROFESSIONNELLE

2017 – actuel Professeur honoraire de la Universidad Peruana Cayetano Heredia, Lima, Pérou

2017 – actuel Chercheur CNRS au LOCEAN (UMR 7159), Paris

2008 – 2017 Chercheur CNRS à l'Institut des Sciences de l'Evolution de Montpellier (ISEM, UMR5554).
Responsable de l'équipe paléoclimat de 2003 à 2017.

2006 – 2008 Postdoctoral Research Associate, University of Washington School of Oceanography

2001 – 2005 Doctorant boursier MNRT, Université Montpellier 2.

2000 Stage de fin d'année de Ecole Centrale de Lyon: Conception d'un système de bioremédiation des sols, entreprise pétrolière REPSOL-YPF Oil, Ecuador.

ENSEIGNEMENTS

Universidad Peruana Cayetano Heredia, Lima

2017-2018 Maestria Ciencias del Mar: Cours "Cambio climático pasado y futuro"

Universidade do Estado de Rio de Janeiro

2014 Chaire française at UERJ, July-October 2014
Cours de Master: "Climate change and the El Niño phenomenon"

Université Montpellier 2

2008-2010 Master de Paléontologie: Climate and paleoclimate of the tropics
2005 Module pour doctorants: The El Niño Southern Oscillation and the Pacific Decadal Oscillation

Ecole Centrale de Lyon

2001-2002 Biotechnologie et bioremédiation des sols

THEMES DE RECHERCHE

Histoire du climat dans la zone tropicale
El Niño Southern Oscillation: sa naissance, son histoire et son avenir
Processus saisonniers dans les changements à long terme de l'état moyen de l'environnement
Variabilité de la ceinture de pluie intertropicale aux échelles saisonnière à millénnaire
Variations d'amplitude et de fréquence de la variabilité inter-annuelle
Les carbonates biogéniques comme archives paléoclimatiques
Reconstructions quantitatives
Comparaisons données-modèles
Impacts des changements climatiques passés sur les civilisations humaines.

METRIQUES DE PRODUCTION SCIENTIFIQUE

Peer-reviewed articles: 38
12 comme premier auteur
3 comme encadrant
23 comme co-auteur
Chapitres de livres: 3
Communications de colloques ou congrès internationaux: 25

12 comme présentant
2 comme encadrant
11 comme co-auteur

h-index: 16 (Google scholar)

PROJETS DE RECHERCHE

Comme chercheur principal

National Geographic Foundation (2006-2007), Human adaptations and climate changes on the Chilean coast. 25,000 US$

Université Montpellier 2, programme EAU (2009-2010), Variations physico-chimiques des milieux lagunaires et côtiers du Languedoc : Calibration de nouveaux indicateurs géochimiques malacologiques. 10,000 €

Projet SALOUM, West African Monsoon variability in Senegal for the last 2000 years.
Université Montpellier 2, programme EAU (2011), 10,000 €
CNRS-INSU, programme LEFE, (2011-2013), 40,000 €
CNRS-INSU, programme LEFE, (2014-2016), 60,000 €

CNRS-INSU, programme LEFE : El Niño, Seasonality and teleconnections during the Eemian warming (2017-2019). 48,000 €.

Magnet program, Peru: Clima, Paleoambientes y biodiversidad en el Peru. Development of a research area at the Universidad Peruana Cayetano Heredia. (2017-20120). 905,000 US$.

Comme Participant

CONCHAS (2002-2004), PNEDC project , P.I. Luc Ortlieb, Calibration of the coastal molluscan proxy for reconstructing sea water temperature variations and El Niño conditions in the eastern tropical Pacific since deglaciation.

PEROU-SUD (participant de 2001 à 2012) (MAE, CNRS, IFEA), P.I. Danièle Lavallée, Study of the early human adaptations in the southern coast of Peru

US National Science Foundation (2008-2010), P.I. Julian P. Sachs: Holocene SST & ENSO Reconstructions from Peruvian Mollusks (Project designed by Matthieu Carré)

US NOAA (2009-2011), P.I. Julian P. Sachs: Tropical Pacific Climate Variability During the Last Millennium from Sediments, Corals & Mollusks

Agence Nationale pour le Recherche, France, P.I. Pascale Braconnot, (2011-2014): El Niño: Lessons from the Past using simulations and observations.

CNRS – Institut National d'Ecologie et Environnement (2014-2015), P.I. Rachid Cheddadi.

Belmont Forum grant (2016-2018), Mountains, sentinels of climate change, P.I. Rachid Cheddadi. Vulnerability of montane ecosystems: lessons from the past.

FONDECYT, Chile (2016-2018), P.I. Maria E. de Porras. Past climatic and environmental dynamics of the southern Atacama Desert (24-27°S) since the Late Glacial

Belmont Forum/JPI-climate grant (2017-2019), Climate services collaborative research actions, P.I. Pascale Braconnot. Palaeo-constraints on Monsoon Evolution and Dynamics (PACMEDY).

US National Science Foundation (2017-2018), P.I. Kurt Rademaker. Chronology, seasonality, and inter-zonal connections in a Terminal Pleistocene-Early Holocene settlement system, southern Peru.

ENCADREMENT

Postdocs

2017 – 2020	Juan Valqui, biologiste : Influence d'El Niño sur la structure de la biodiversité marine du Pérou. Projet Magnet, Universidad Peruana Cayetano Heredia.
2017-2020	Diana Ochoa, Géologue : Stratigraphie de la formation Pisco, Pérou, et reconstruction des conditions environnementales de la transition Miocène-Pliocène dans le système de Humboldt. Projet Magnet, Universidad Peruana Cayetano Heredia.
2017-2020	Rodolfo Salas, Paléontologue : Influence de la surrection Andine sur l'évolution des communautés de vertébrés sur la côte et en Amazonie Péruvienne. Projet Magnet, Universidad Peruana Cayetano Heredia.
2017-2020	Jorge Cardich, Paléocéanographe : Variabilité de la zone de minimum d'oxygène au Pérou reconstruite par l'étude des foraminifères benthiques. Projet Magnet, Universidad Peruana Cayetano Heredia.

Doctorants

2014	Rita Abou Nader, Université Montpellier 2 (Co-encadrement avec Rachid Cheddadi). Echec de l'étudiante, thèse interrompue par le comité de thèse.
2009-2012	Moufok Azzoug. Université Montpellier 2 (Co-encadrement avec Marie-Pierre Ledru) "Reconstruction of seasonal to multidecadal variations of the West African monsoon during the last 2000 years from the sclerochronological study of fossil shell middens in the Saloum Delta, Senegal."

Projets de Master

2017-2018	Stephanie Gruver, co-encadrement avec Kurt Rademaker. University of northern Illinois.
2016	Océane Perrot (M2), Université de Montpellier "West African monsoon seasonality during the little ice age"
2016	Marion Lacand (M1), Université de Montpellier "Stable Isotopes in Baobab tree rings along a rainfall gradient"
2016	Julia Morarin (M1), Université de Montpellier "Seasonality of mollusk shell gathering in a preceramic shell middens of the lower Ica valley, Peru"
2016	Aurélien Fruy (M1), Université de Montpellier "potential of fossil mollusks in the Pisco formation for Pliocene paleoclimatic reconstructions"

2015	Alexandre Mariller (M2), co-encadrement avec Myriam Khodri, Université de Versailles St- Quentin "Processes driving the decadal variability of the West African monsoon in simulations and observations"
2014	Anastasia Lebedeva (M1), co-encadrement avec Rachid Cheddadi, université Montpellier 2 "Late Holocene paleoenvironmental changes in Moroccan Sahara"
2013	Alexandre Supply (M1), co-encadrement avec Myriam Khodri, Université Paris 6 "Natural and forced variability of the West African Monsoon in the last 100 years"
2009-2010	James Sadler, co-encadrement avec Eelco Rohling, University of Southampton "Insights into the Peruvian Upwelling System during the Holocene from Stable Isotopes in Mollusc Shells"
2009	Guillaume d'Herbes (M1), Université Montpellier 2 "Etude géochimique et reconstruction climatique d'EL Niño à l'Holocene moyen par l'analyse de coquilles de *Mesodesma donacium*"

Publications d'étudiants :

Sadler, J., M. Carré, M. Azzoug, A. J. Schauer, J. Ledesma, F. Cardenas, B. M. Chase, I. Bentaleb, S. Müller, E. J. Rohling, and J. P. Sachs , (2012). Reconstructing past upwelling intensity and the seasonal dynamics of primary productivity along the Peruvian coastline from mollusk shell stable isotopes, ***Geochem. Geophys. Geosyst.*** , 13, Q01015. doi:10.1029/2011GC003595.

Azzoug, M., Carré, M., Schauer, A.J. (2012). Reconstructing the duration of the West African Monsoon season from growth patterns and isotopic signals of shells of Senilia senilis (Saloum Delta, Senegal). ***Palaeogeography, Palaeoclimatology, Palaeoecology*** 346-347, 145-152.

Azzoug, M., Carré, M., Chase, B.M., Deme, A., Lazar, A., Lazareth, C.E., Schauer, A.J., Mandeng-Yogo, M., Simier, M., Thierno-Gaye, A., de Morais, L.T., 2012. Positive Precipitation-Evaporation budget from AD 460 to 1090 in the Saloum Delta (Senegal) indicated by mollusk oxygen isotopes. ***Global and Planetary Change***, 98-99, 54-62.

EXPEDITIONS DE TERRAIN

En tant qu'organisateur

2002	Ecuador-Peru, 4 weeks, survey of coastal archaeological shell middens, and Pleistocene marine terraces
2004	Peru, 2 weeks, Environmental monitoring and sampling in Tumbes Mangrove estuary for sclerochronological calibration
2007	Chile, 3 weeks, Excavation and sampling of archaeological shell middens in Los Vilos, sediment cores for pollen-derived paeo-environmental reconstructions
2007	Peru, 4 weeks, survey and sampling of shell middens in the central and southern coast.
2010	Peru, 2 weeks, survey and sampling of shell middens in the central coast
2012	Peru, 2 weeks, survey and sampling of pleistocene marine terraces, southern coast
2011-2016	Senegal, 4x2 weeks, Environmental monitoring, survey and sampling of archaeological shell middens and Holocene natural deposits, collection of tree cores along a rainfall transect.
2014	Brazil, 4 weeks, survey and sampling of coastal archaeological shell middens
2017	Peru, 3 weeks, survey of Eemian marine terrasses, fossil mollusk sampling. Sampling of water and mollusk shells in mangroves of Northern Peru.

Comme participant

2002	Oceanographic cruise on the Marion Dufresne ship, Vancouver-Panama-Cancoon, 4 weeks. Ocean sediment piston cores in high primary production upwelling zones
2007	Peru, 4 weeks, archaeological excavation at Quebrada de los Burros.
2013	Morocco, 2 weeks, collection of lake sediment cores, Middle Atlas

MEDIAS

The Holocene history of El Niño

2014	Science Mag News, University of Washington UW Today, Earth Magazine, La Gran Epoca, Global Climat, Sciencedaily, Labnews
15/07/2015	Live TV/Radio interview in Ampliacion de noticias, RPP
15/07/2015	Live TV interview in 7.13 news program, TV PERU

LISTE COMPLETE DE PUBLICATIONS

ARTICLES DE REVUES A COMITE DE LECTURE

38. **Carré M.**, M. Azzoug, P. Zaharias, A. Camara , R. Cheddadi , M. Chevalier, D. Fiorillo, A. Gaye, S. Janicot, M. Khodri, A. Lazar, C. E. Lazareth, J. Mignot, N. Mitma Garcia, N. Patris, O. Perrot, M. Wade, Modern drought conditions in western Sahel unprecedented in the past 1600 years. ***Climate Dynamics***, in press.

37. Shi C., V. Daux, Z. Li, X. Wu, T. Fan, Q. Ma, X. Wu, H. Tian, **M. Carré**, D. Ji, W. Wang, A. Rinke, W. Gong, Y. Liu, Y. Chen, V. Masson-Delmotte. Tree-ring evidence of constant relative humidity with centennial warming over southeastern Tibetan Plateau. ***Climate Dynamics***, doi: 10.1007/s00382-018-4107-5.

36. Cheddadi R., A. Henrot, L. Francois, F. boyer, M. Bush, **M. Carré**, E. Coissac, P. Deoliveira, F. Ficetola, A. Hambuckers, K. Huang, A.-M. Lézine, M. Nourelbait, A. Rhoujjati, P. Taberlet, F. Sarmiento, D. Abel-Schaad, F. Alba-Sánchez, Z. Zheng (2017). Microrefugia, climate change, and conservation of Cedrus atlantica in the Rif Mountains, Morocco. ***Frontiers in Ecology And Evolution***, 5, 114. doi: 10.3389/fevo.2017.00114

35. **Carré M.**, Cheddadi R. (2017). Seasonality in long-term climate change. ***Quaternaire***, **28** (2), 173-177.

34. Camara A., K. Hardy, E. Dioh, M. Gueye, R. Pique, **M. Carré**, M. Sall, M.W. Diouf (2017). Amas et sites coquilliers du Delta du Saloum (Sénégal) : Passé et présent. ***L'anthropologie***, **121**, 204-214.

33. Christol A., P. Wuscher, N. Goepfert, S. Mogollon, P. Béarez, B. Gutiérrez, **M. Carré** (2017). The Las Salinas palaeo-lagoon in the Sechura Desert (Peru): evolution during the last two millennia. ***The Holocene* 27**, 26-38. DOI: 10.1177/0959683616646182

32. Cheddadi, R., Araújo, M. B., Maiorano, L., Edwards, M., Guisan, A., **Carré, M.**, Chevalier, M., and Pearman, P. B. (2016). Temperature Range Shifts for Three European Tree Species over the Last 10,000 Years. ***Frontiers in Plant Science* 7**. Doi : 10.3389/fpls.2016.01581

31. Nourelbait, M., Rhoujjati, A., Benkaddour, A., **Carré, M.**, Eynaud, F., Martinez, P., and Cheddadi, R. (2016). Climate change and ecosystems dynamics over the last 6000 years in the Middle Atlas, Morocco. ***Climate of the Past* 12,** 1029-1042.

30. **Carré, M**., D. Jackson, A. Maldonado, B.M. Chase, J.P. Sachs (2016). Variability of the ^{14}C activity and ocean-atmosphere flux of CO_2 in the Peru-Chile upwelling region during the past 12,000 years. ***Quaternary research***, **85**, 87-93

29. Tabel, J., C. Khater, A.Rhoujjati, L. Dezileau, I. Bouimetarhan, **M. Carré**, L. Vidal, A. Benkaddour, M. Nour El Bait, R. Cheddadi. Environmental changes over the past 5,000 years in the southern Middle Atlas, Morocco. ***Journal of Quaternary Science***. doi: 10.1002/jqs.2841.

28. Emile-Geay, J., Cobb, K., Carre, M., Braconnot, P., Leloup, J., Zhou, Y., Harrison, S. P., Correge, T., McGregor, H. V., Collins, M., Driscoll, R., Elliot, M., Schneider, B., and Tudhope, A. (2015). Links between tropical Pacific seasonal, interannual and orbital variability during the Holocene. ***Nature Geoscience,*** doi:10.1038/ngeo2608.

27. Hardy, K., Camara, A., Piqué, R., Dioh, E., Guèye, M., Diadhiou, H. D., Faye, M., and **Carré, M.** (2016). Shellfishing and shell midden construction in the Saloum Delta, Senegal. ***Journal of Anthropological Archaeology* 41,** 19-32.

26. Chase, B. M., Boom, A., Carr, A. S., **Carré, M.**, Chevalier, M., Meadows, M. E., Pedro, J. B., Stager, J. C., and Reimer, P. J. (2015). Evolving southwest African response to abrupt deglacial North Atlantic climate change events. ***Quaternary Science Reviews*** 121, 132-136.

25. Wade, M., Mignot, J., Lazar, A., Gaye, A., and **Carré, M**. (2015). On the spatial coherence of rainfall over the Saloum delta (Senegal) from seasonal to decadal time scales. ***Frontiers in Earth Science*** 3, 30. doi: 10.3389/feart.2015.00030

24. **Carré, M.**, J. P. Sachs, S. Purca, A. J. Schauer, P. Braconnot, R. Angeles Falcón, M. Julien, and D. Lavallée (2014), Holocene history of ENSO variance and asymmetry in the eastern tropical Pacific, ***Science***, *345*, 1045-1048.

23. Shi, C., V. Masson-Delmotte, V. Daux, Z. Li, **M. Carré**, and J. Moore (2014), Unprecedented recent warming rate and temperature variability over the east Tibetan Plateau inferred from Alpine treeline dendrochronology, ***Climate Dynamics***, 1-14.

22. Xu, J.X., Zheng, Z., Huang, K.Y., Yue, Y., Li, J., Chase, B.M., Ledru, M.P., **Carré, M.**, Cheddadi, R. (2013). Impacts of human activities on ecosystems during the past 1300 years in Pingnan area of Fujian Province, China. ***Quaternary International***, 286, 29-35.

21. **Carré, M.**, Sachs, J.P., Schauer, A.J., Rodríguez, W.E., Ramos, F.C., (2013). Reconstructing El Niño-Southern Oscillation activity and ocean temperature seasonality from short-lived marine mollusk shells from Peru. ***Palaeogeography, Palaeoclimatology, Palaeoecology*** 371, 45-53.

20. Amami, B., S. D. Muller, L. Rhazi, M. Chaibi, S. Fauquette, A. Charif, M. Ayt Ougougdal, M. Ridaoui, S. Bouahim, **M. Carré**, A. Daoud-Bouattour, and P. Grillas (2013), Late Quaternary history of a Mediterranean temporary pool of western Morocco, based on sedimentological and palynological evidence, ***Palaeogeogr. Palaeoclimatol. Palaeoecol.***, 392, 281-292.

19. Li, J., Z. Zheng, K. Huang, S. Yang, B. Chase, V. Valsecchi, **M. Carré**, and R. Cheddadi (2013), Vegetation changes during the past 40,000 years in Central China from a long fossil record, ***Quaternary International***, *310*, 221-226.

18. **Carré, M.**, Azzoug, M., Bentaleb, I., Chase, B. M., Fontugne, M., Jackson, D., Ledru, M.-P., Maldonado, A., Sachs, J. P., and Schauer, A. J.: Mid-Holocene mean climate in the south-eastern Pacific and its influence on South America, ***Quaternary International***, 253, 55-66, doi:10.1016/j.quaint.2011.02.004, 2012.

17. Ballester, B., D. Jackson, **M. Carré**, A. Maldonado, C. Méndez, and R. Seguel (2012). An Early Holocene task camp (~ 8.5 ka cal. BP) on the coast of the semi-arid north of Chile., ***Antiquity***, 86, 88-98.

16. Sadler, J., M. **Carré, M.** Azzoug, A. J. Schauer, J. Ledesma, F. Cardenas, B. M. Chase, I. Bentaleb, S. Müller, E. J. Rohling, and J. P. Sachs , (2012). Reconstructing past upwelling intensity and the seasonal dynamics of primary productivity along the Peruvian coastline from mollusk shell stable isotopes, ***Geochem. Geophys. Geosyst.*** , 13, Q01015. doi:10.1029/2011GC003595.

15. Muller, S.D., Miramont, C., Bruneton, H., **Carré, M**., Sottocornola, M., Court-Picon, M., de Beaulieu, J.-L., Nakagawa, T., Schevin, P., 2012. A palaeoecological perspective for the conservation and restoration of wetland plant communities in the central French alps, with particular emphasis on alder carr vegetation. ***Review of Paleaobotany and Palynology*** 171, 124-139.

14. **Carré, M.**, J. P. Sachs, J. M. Wallace, and C. Favier (2012), Exploring errors in paleoclimate proxy reconstructions using Monte Carlo simulations: paleotemperature from mollusk and coral geochemistry, ***Climate of the Past***, 8, 433-450, doi:10.5194/cp-8-433-2012.

13. Lerosey-Aubril, R., Hegna, T. A., Kier, C., Bonino, E., Habersetzer, J., and **Carré, M.** (2012). Controls on Gut Phosphatisation: The Trilobites from the Weeks Formation Lagerstätte (Cambrian; Utah), ***PLoS ONE***, 7, e32934, doi:10.1371/journal.pone.0032934

12. Azzoug, M., **Carré, M**., Schauer, A.J. (2012). Reconstructing the duration of the West African Monsoon season from growth patterns and isotopic signals of shells of Senilia senilis (Saloum Delta, Senegal). ***Palaeogeography, Palaeoclimatology, Palaeoecology*** 346-347, 145-152.

11. Azzoug, M., **Carré, M**., Chase, B.M., Deme, A., Lazar, A., Lazareth, C.E., Schauer, A.J., Mandeng-Yogo, M., Simier, M., Thierno-Gaye, A., de Morais, L.T., 2012. Positive Precipitation-Evaporation budget from AD 460 to 1090 in the Saloum Delta (Senegal) indicated by mollusk oxygen isotopes. ***Global and Planetary Change***, 98-99, 54-62.

10. Yue, Y., Zheng, Z., Huang, K.Y., Chevalier, M., Chase, B.M., **Carré, M.**, Ledru, M.P., Cheddadi, R., 2012. A record of vegetation and climate change over the past 50,000 years in the Fujian Province of eastern subtropical China. ***Palaeogeogr. Palaeoclimatol. Palaeoecol.***, 365-366, 115-123.

9. Lavallée, D., M. Julien, P. Béarez, A. Bolaños, **M. Carré**, A. Chevalier, T. Delabarde, M. Fontugne, C. Rodríguez-Loredo, L. Klaric, P. Usselmann, and M. Vanhaeren (2011), Quebrada de los burros.

Los primeros pescadores del litoral Pacífico en el extremo sur peruano, ***Chungara***, 43, Numero Especial 1, 333-351.

8. **Carré M.**, Lavallée, D., Julián, M., Klaric, L., Bentaleb, I., Fontugne, M., Kawka, O.E., 2009. Insights into Early Holocene hunter-gatherer mobility on the Peruvian Southern Coast from mollusk gathering seasonality. ***Journal of Archaeological Science***, 36, 1173-1178.

7. Jackson, D., Maldonado, A., **Carré, M.**, 2009. Early Archaic occupation (9265 Cal.Yr.BP.) on the semi-arid coast of Chile. ***Current Research in the Pleistocene***, 26, 3-5.

6. **Carré M.**, 2007, El mes de recolección de la macha (*Mesodesma donacium*) determinado por sus lineas de crecimiento: aplicaciones arqueológicas, ***Bull. Inst. Fr. Etudes Andines***, 36(2), 299-304.

5. Bentaleb, I., Langlois, C., Martin, C., Iacumin, P., **Carré, M**., Antoine, P.-O., Duranthon, F., Moussa, I., Jaeger, J.-J., Barrett, N., Kandoorp, R., 2006. Rhinocerotid tooth enamel $^{18}O/^{16}O$ variability between 23 and 12 Ma in southwestern France. ***C. R. Geosciences***, 338, 172-179.

4. **Carré M**., Bentaleb I., Bruguier O., Ordinola E., Fontugne M., 2006. Calcification rate influence on trace elements incorporation in marine bivalve aragonite: evidences and mechanisms. ***Geochimica et Cosmochimica Acta***, 70(19), 4906-4920.

3. **Carré M**., Bentaleb I., Fontugne M. & Lavallée D. 2005, Strong El Niño events during the early Holocene: stable isotope evidence from Peruvian sea-shells. ***The Holocene***, 15 (1), 42-47.

2. **Carré, M**., Bentaleb, I., Blamart, D., Ogle, N., Cardenas, F., Zevallos, S., Kalin, R.M., Ortlieb, L., Fontugne, M., 2005, Stable isotopes and sclerochronology of the bivalve *Mesodesma donacium*: Potential application to Peruvian paleoceanographic reconstructions. ***Palaeogeography, Palaeoclimatology, Palaeoecology***, 228, 4-25.

1. Fontugne M., **Carré M**., Bentaleb I., Julien M., Lavallée D., 2004 Radiocarbon reservoir age variations in the south Peruvian upwelling during the Holocene. ***Radiocarbon***, 46(2), 531-537.

CHAPITRES DE LIVRES

3. **Carré, M.**, Dufour, E., 2012. Estrategias estacionales de explotación del medio marino - el aporte de la esclerocronologia y del estudio isotópico -. In: Lavallée, D., Julien, M. (Eds.), Prehistoria de la costa extremo-Sur del Perú. Los Pescadores arcaicos de la quebrada de los Burros (10000 - 7000 a.P.). Travaux de l'Institut Français d'Etudes Andines, Lima, 195-203.

2. Fontugne, M. ; Usselmann, P., Carré, M., Dufour, E., 2012. La QLB en el Holoceno temprano y medio : el impacto del fenómeno ENSO. In: Lavallée, D., Julien, M. (Eds.), Prehistoria de la costa extremo-Sur del Perú. Los Pescadores arcaicos de la quebrada de los Burros (10000 - 7000 a.P.). Travaux de l'Institut Français d'Etudes Andines, Lima, 77-89.

1. Jackson, D., Maldonado, A., **Carré, M**., Seguel, R., 2011. Huentelauquén Cultural Complex: The earliest peopling of the Pacific Coast in the South-American southern Cone. In: Peuplements et préhistoire en Amériques, Vialou, D. (Ed.), CTHS, Documents préhistoriques n°28, p 221-232.

PRESENTATIONS DE CONGRES ET COLLOQUES

31. **Carré M**., Azzoug M., Camara A., Cheddadi R., Gaye A., Janicot S., Khodri M., Lazar A., Lazareth C.E., Mignot J., Wade M., Anthropogenic forcing brings Sahel drought to unprecedented level in the past 1600 years. Climate Change in Africa, Marrakech, 7-9 Nov. 2017.

30. **Carré M**., M. Elliot, T. Corrège, A. Tudhope, R. Cheddadi, C. Brierley, S. Harrison, P. Braconnot. Seasonality and interannual variability in the tropics: A synthesis of Holocene coral and mollusk records. PMIP4 meeting, Stockholm, 25-29 Sept 2017.

29. **Carré M**., M. Elliot, T. Corrège, A. Tudhope, R. Cheddadi, C. Brierley, S. Harrison, P. Braconnot. Seasonality and interannual variability in the tropics: A synthesis of Holocene coral and mollusk records. PMIP4 meeting, Stockholm, 25-29 Sept 2017.

28. **Carré M**., M. Azzoug, A. Camara, R. Cheddadi , A.T. Gaye, S. Janicot, M. Khodri, A. Lazar, C.E. Lazareth, J. Mignot, M. Wade. Sahel rainfall negatively linked to global temperature during the past 1600 years. OSM PAGES meeting, Zaragoza, 9-13 May 2017.

27. Cheddadi R., M. Araujo, L. Maiorano, M. Edwards, A. Guisan, **M. Carré**, M. Chevalier, P. Pearman. Temperature range shifts of three European tree species over the last 10,000 years. OSM PAGES meeting, Zaragoza, 9-13 May 2017.

26. **Carré, M.**, J. P. Sachs, S. Purca, A. J. Schauer, P. Braconnot, R. Angeles Falcón, M. Julien, and D. Lavallée, Holocene history of ENSO variance and asymmetry in the eastern tropical Pacific. Q10 conference, Bordeaux, 16-18 Feb. 2016

25. Cheddadi R. , **M. Carré**. Ecosystèmes et changement climatique : du passé au futur, reculer pour mieux voir. Colloque CeMEB : Environnement, société et changements climatiques, Montpellier, 28-29 sept. 2015

24. **Carré M.**, M. Azzoug, P. Zaharias, A. Camara, R. Cheddadi, A. Gaye, S. Janicot, M. Khodri, A. Lazar, J. Mignot, N. Mitma Garcia, N. Patris, M. Wade. Rainfall in the Sahel and global temperature: lessons from a 1500-year long paleoclimate record. Symposium in memory of Françoise Gasse, Tropical deserts and lakes through time. CEREGE, 1-2 July 2015, France.

23. Emile-Geay, J., K. Cobb, **M. Carré**, P. Braconnot, J. Leloup, Y. Zhou, S.P. Harrison, T. Corrège, H.V. McGregor, M. Collins, R. Driscoll, M. Elliot, B. Schneider, A.W. Tudhope. Holocene constraints on simulated tropical Pacific climate. AGU Fall meeting, 14-18 Dec. 2015, San Francisco, USA

22. **Carré, M.**, M. Azzoug, P. Zaharias, M. Wade, A. T. Gaye, N. Patris, R. Cheddadi, A. Lazar, J. Mignot, Precipitation variability in the Sahel during the last 2000 years revealed by archaeological shell middens in Senegal. AFQUA conference, 30 Jan. – 04 Feb. 2015, Cape Town, South Africa.

21. **Carré, M.**, J. P. Sachs, S. Purca, A. J. Schauer, P. Braconnot, R. Angeles Falcón, M. Julien, and D. Lavallée, Holocene history of ENSO variance and asymmetry in the eastern tropical Pacific. EGU General Assembly, 27 April- 2 May 2014,Vienna, Austria.

20. **Carré, M.**, Azzoug, M., Quantified paleo-seasonality of the West African Monsoon in Senegal, PAGES Open Science Meeting, 13-16 Feb. 2013, Goa, India.

19. **Carré, M.**, Purca, S., Angeles Falcon, R., Sachs, J., The Holocene history of ENSO in the Eastern Tropical Pacific reconstructed from Peruvian mollusk shells, PAGES Open Science Meeting, 13-16 Feb. 2013, Goa, India.

18. Azzoug, M., **Carré, M**., Schauer, A.J., The West African Monsoon duration and intensity fom A.D. 450 to 950 inferred from high resolution isotope sclerochronology of modern and fossil shells in the Saloum estuary, Senegal. 4th AMMA international conference, 2-6 July 2012, Toulouse, France.

17**. Carré, M.**, Sachs, J., Schauer, A.J., Elliott Rodriguez, W., Cardenas Ramos, F., El Niño Southern Oscillation variability and ocean temperature seasonality recorded by short-lived marine mollusk shells from Peru. AGU Ocean Science Meeting, Salt Lake City, Feb. 20-24, 2012.

16. Maldonado, A., C. Gonzalez, C. Mendez, D. Jackson, **M. Carré**, Climatic changes and human occupation in subtropical semiarid region of Chile (32ºS) during the Late Pleistocene and Holocene. **Segundo Congreso de Oceanografía Física, Meteorología y Clima del Pacifico Sudoriental, 5-7 Oct. 2011, La Serena, Chile.**

15. Sachs, J.P., **Carré, M.,** Tudhope, A., Mügler, I., Lough, J., Richey, J., Little Ice Age Climate in the Tropical Pacific from Sediment, Mollusks and Corals, *AGU Fall meeting 2011, San Francisco.*

14. Azzoug M., **Carré M.**, Strengthening of the West African Monsoon in Senegal during the Medieval Warm Period inferred from fossil mollusk shells in the Salum Estuary. *INQUA meeting 2011, Bern.*

13. MaldonadoA., Mendez C., Jackson D., **Carré M.**, Late Pleistocene-Holocene climatic changes and human occupation in subtropical semiarid region of Chile (32ºS), *INQUA meeting 2011, Bern.*

12. Sachs, J.P., **Carré M.**, Tudhope A., Mügler I., Lough J., Richey J., Little Ice Age Climate in the Tropical Pacific from Sediment, Mollusks and Corals, *American Geophysical Union, Fall Meeting 2011*.

11. Fontugne M., **Carré M.**, Bentaleb I., Julien M., Lavallée D., Impact of ENSO phenomenon on the prehistoric occupation and environment of Quebrada de los Burros in coastal southern Peru. *10th International Conference "METHODS OF ABSOLUTE CHRONOLOGY", 22-25th April 2010 Gliwice, Poland.*

10. Sachs J. P., Sachse D., Zhang Z., Smittenberg R., **Carré M.**, Mügler I., Nelson D. B., Atwood A., Ladd N., ITCZ Shifts During the Last Millennium from Lipids on Tropical Pacific Islands, *American Geophysical Union, Fall Meeting 2009*, abstract #PP53A-02.

9. Carré M., J. Sachs, J.M. Wallace, I. Bentaleb, M. Fontugne, ENSO activity during the Holocene: quantitative reconstruction from mollusk isotopic records. *PMIP2 Workshop, Estes Park, CO, 11-15 September 2008.*

8. Carré M., J. Sachs, J.M. Wallace, I. Bentaleb, M. Fontugne, Early to mid-Holocene changes of ENSO-related interseasonal variability in the Eastern Pacific: evidences from mollusk shell isotopic records. *INQUA 2007 abstracts, Quaternary International*, 167-168 Supp., p60.

7. Carré M., D. Lavallee, M. Julien, I. Bentaleb, M. Fontugne, Favorable environmental conditions allowed early permanent hunter-gatherer settlements on the southern Peruvian coast. *INQUA 2007 abstracts, Quaternary International*, 167-168 Supp., p60.

6. Bentaleb I., Martin C., Pisapia, C., **Carré M**., France-Lanord C., Kaandorp R., Jaeger J.J., Bruguier O., Iacumin P., Chatri K., Monsoon seasonality inferred from thai rhino-teeth stable isotope records: evidence of the 1986-87 El-Niño event. *EGU-CIIFEN AVH1 Conference*, *Guayaquil, 16-20 may 2005, Abstract p. 111*.

5. Carré M., Bentaleb I., Lavallée D., Julien M., Vonhof H., Kaandorp R., Fontugne M., Insights into the ENSO system at early to mid-Holocene using high resolution stable isotope records of bivalve shells from southern Peru. *EGU-CIIFEN AVH1 Conference*, *Guayaquil, 16-20 may 2005, Abstract p. 37*.

4. Carré M., Bentaleb I., Blamart D., Fontugne M., Ogle N. and Ortlieb L., The usefulness of *Mesodesma donacium* for paleoceanographic reconstructions: Stable Isotopes and growth pattern, *Eos Trans. AGU, 84(52), Ocean Sci. Meet. Suppl., Abstract OS42B-10, Portland 2004*

3. Ortlieb L., Guzmán N., El Jouhari L., **Carré M**. & PNEDC CONCHAS Project members (2003) Calibration studies on mollusc shells in the Peru-Chile coastal region submitted to ENSO impacts. EGS - AGU - EUG Joint Assembly, Nice, France, April 2003, Geophysical Research Abstracts, 5, 13681.

2. Fontugne M., Usselman P., Lavallée D., Julien M., Hatté C., **M. Carré**, Bentaleb I., Plagnes V., El Niño intensity and frequency during the Holocene and its relationship with prehistoric settlements in the coastal southern Peru. In *Colloque International Quaternaire 3*, «Evénements rapides, instabilités, changements culturels au Quaternaire», *2002, volume pré-actes, résumé p. 32.*

1. Carré M., Bentaleb I., Fontugne M., Lavallée D., Existence of strong El Niño events at the early Holocene: Evidence from carbonate stable isotopes in *Mesodesma donacium* shells from Southern Peru. *Colloque international Quaternary 3, Aix-en-Provence, 2002*.

AUTRES DOCUMENTS

Carré, M., Purca, S., Sachs, J.P., 2013. Reconstructing ENSO in the Eastern Tropical Pacific from short-lived marine mollusks, PAGES News, 21(2), 56-57.

Carré M., Géochimie isotopique des coquilles de *Mesodesma donacium,* Mission archéologique au Pérou : Projet « Pérou-Sud » (MAE-CNRS), Rapport 2003 dirigé par D. Lavallée et M. Julien, pp. 61-64.

Carré M., Stries de croissance et géochimie des coquilles de *M. donacium,* apports à la problématique de saisonnalité d'occupation. Mission archéologique au Pérou : Projet « Pérou-Sud » (MAE-CNRS), Rapport 2004 dirigé par D. Lavallée et M. Julien, pp. 86-90.

Carré M., Etude géochimique et sclérochronologique de coquilles de bivalves marins : Paléocéanographie de la côte sud du Pérou à l'Holocène inférieur et implications archéologiques. Thèse de doctorat, 2005, Université Montpellier 2, pp 348.

2- Synthèse des travaux de thèse de doctorat

Titre : ETUDE GEOCHIMIQUE ET SCLEROCHRONOLOGIQUE DE COQUILLES DE BIVALVES MARINS : PALEOCEANOGRAPHIE DE LA COTE SUD DU PEROU A L'HOLOCENE INFERIEUR ET IMPLICATIONS ARCHEOLOGIQUES.

Les objectifs de mon travail de doctorat ont été (1) l'exploration des potentialités des coquilles de bivalves marins comme qu'archives paléoclimatiques au Pérou, (2) la mise au point des bases méthodologiques pour une reconstruction de l'activité passée d'El Niño dans cette région, (3) une proposition préliminaire sur les conditions océanographiques de cette région d'upwelling côtier à l'Holocène inférieur. Les coquilles fossiles utilisées provenant de sites archéologiques, celles-ci ont également apporté des informations concernant la saisonnalité d'occupation des sites et le contexte environnemental des premières occupations humaines sur la côte Pacifique Sud-Américaine.

Afin de reconstituer à une échelle saisonnière l'histoire Holocène du climat de la côte péruvienne et en particulier de l'ENSO (El Niño Southern Oscillation), j'ai étudié la géochimie isotopique ($\delta^{18}O$, $\delta^{13}C$), les teneurs en éléments traces (Sr, Mg, Ba, Mn) et les structures périodiques de croissance (sclérochronologie) de deux espèces de bivalves. J'ai démontré que la croissance des coquilles de *Mesodesma donacium* et de *Chione subrugosa,* était rythmée par les marées et formait des structures cycliques d'un demi-mois lunaire, fournissant un cadre temporel interne précis. L'incorporation des éléments traces, en particulier le Sr et le Mg, est, pour ces deux espèces, principalement dépendante de la vitesse de calcification. Leur concentration ne peut donc pas être utilisée comme indicateur de température comme chez d'autres organismes carbonatés comme les coraux. En revanche, le rapport isotopique de l'oxygène ($\delta^{18}O$) de l'oxygène des coquilles de *M. donacium* s'est révélé un indicateur fidèle des températures de surface de la mer (SST) notamment grâce à l'absence d'influence significative d'eau douce le long des côtes désertiques du Pérou. Une relation entre le fractionnement isotopique de l'oxygène et les SST a été calibrée spécifiquement pour l'aragonite de *M. donacium*. Des courbes de SST, de résolution infra-mensuelle, ont ainsi pu être obtenues à partir de 12 coquilles du site archéologique « La Quebrada de los Burros », datées entre 9900 et 6700 cal. BP. Durant cette période, la température moyenne de l'océan à l'extrême sud du Pérou (18,1°S) était inférieure de 3°C par rapport à aujourd'hui indiquant un renforcement de l'upwelling côtier à cette époque et une situation générale de type La Niña. Des âges réservoirs importants à la même époque suggèrent une circulation océanique modifiée. La variabilité climatique interanuelle, qui dans cette région est liée à l'ENSO, était peu importante à l'Holocène moyen mais plus forte à l'Holocène inférieur avec une prédominance probable des évènements froids La Niña. Grâce à l'upwelling qui assurait une forte productivité marine et un apport d'humidité sur la côte par des brouillards, les conditions environnementales étaient très favorables à l'occupation humaine. L'examen sclérochronologique de coquilles archéologiques montra que la collecte des mollusques était une activité principalement estivale qui devait être remplacée en hiver par l'exploitation des ressources végétales.

Ces premiers travaux de recherche ouvrent l'accès à la saisonnalité et la variabilité interannuelle des températures dans le Pacifique tropical Est, offrant alors la possibilité d'étudier la variabilité de l'upwelling du Pacifique Sud-Est à de nouvelles échelles de temps et surtout l'activité de l'ENSO, incluant à la fois évènements froids et chauds, dans une région clé du Pacifique où les indicateurs directement liés aux anomalies de SST étaient encore inexistants.

Publications associées :

7- Lavallée, D., M. Julien, P. Béarez, A. Bolaños, M. Carré, A. Chevalier, T. Delabarde, M. Fontugne, C. Rodríguez-Loredo, L. Klaric, P. Usselmann, and M. Vanhaeren (2011), Quebrada de los burros. Los primeros pescadores del litoral Pacífico en el extremo sur peruano, *Chungara*, 43, Numero Especial 1, 333-351.

6- Carré M., Lavallée, D., Julián, M., Klaric, L., Bentaleb, I., Fontugne, M., Kawka, O.E., 2009. Insights into Early Holocene hunter-gatherer mobility on the Peruvian Southern Coast from mollusk gathering seasonality. *Journal of Archaeological Science*, 36, 1173-1178.

5- Carré M., 2007, El mes de recolección de la macha (Mesodesma donacium) determinado por sus lineas de crecimiento: aplicaciones arqueológicas, *Bull. Inst. Fr. Etudes Andines*, 36(2), 299-304.

4- Carré M., Bentaleb I., Bruguier O., Ordinola E., Fontugne M., 2006. Calcification rate influence on trace elements incorporation in marine bivalve aragonite: evidences and mechanisms. *Geochimica et Cosmochimica Acta*, 70(19), 4906-4920.

3- Carré M., Bentaleb I., Fontugne M. & Lavallée D. 2005, Strong El Niño events during the early Holocene: stable isotope evidence from Peruvian sea-shells. *The Holocene*, 15 (1), 42-47.

2- Carré, M., Bentaleb, I., Blamart, D., Ogle, N., Cardenas, F., Zevallos, S., Kalin, R.M., Ortlieb, L., Fontugne, M., 2005, Stable isotopes and sclerochronology of the bivalve Mesodesma donacium: Potential application to Peruvian paleoceanographic reconstructions. *Palaeogeography, Palaeoclimatology, Palaeoecology*, 228, 4-25.

1- Fontugne M., Carré M., Bentaleb I., Julien M., Lavallée D., 2004 Radiocarbon reservoir age variations in the south Peruvian upwelling during the Holocene. *Radiocarbon*, 46(2), 531-537.

3- Activités de recherche : Evaluation des changements de saisonnalité et de la variabilité climatique interannuelle au cours de l'Holocène dans le Pacifique tropical et dans le Sahel.

3.1. Contexte et problématique

Mes activités de recherche sont dédiées à la reconstruction et à l'analyse de l'histoire passée de la variabilité climatique dans la zone tropicale, les enjeux étant (1) de mettre en perspective les changements climatiques observés actuellement par rapport à la variabilité climatique naturelle à long terme, (2) d'identifier les forçages et les mécanismes qui déterminent cette variabilité, (3) de tester à partir des simulations du climat passé les modèles climatiques utilisés dans les prédictions du GIEC, (4) d'éclairer les relations entre sociétés humaines et changements environnementaux.

Dans ce cadre très large, ma recherche s'est concentrée essentiellement sur deux zones géographiques : d'une part le Pacifique Sud-Est comprenant les côtes Péruvienne et Chilienne et le système de Humboldt, et d'autre part le Sénégal comme zone représentative de l'ouest du Sahel. Ces deux régions sont soumises à des phénomènes climatiques cruciaux dans la variabilité globale interannuelle à multi-décennale : El Niño et l'Oscillation australe (ENSO) dans le Pacifique et la mousson Ouest Africaine au Sénégal. La variabilité de l'ENSO et de la mousson Ouest Africaine ont des répercussions écologiques et socio-économiques très fortes mais l'incertitude sur leur réponse au forçage anthropique actuel et futur est si grande qu'aucune stratégie d'adaptation claire ne peut être envisagée. Les observations à long-terme (multiséculaires à millénaires) sont donc essentielles pour appréhender la gamme de variabilité naturelle de ces systèmes, étudier leur réponse aux changements climatiques passés, contraindre les simulations.

La difficulté essentielle pour la reconstruction de l'activité passée de ces phénomènes tient à l'échelle de temps qui leur est propre : inter-annuelle pour l'ENSO, saisonnière pour la mousson. Rares sont les archives paléoclimatiques permettant l'accès à des échelles de temps aussi fines. Mon travail s'est donc concentré sur l'étude des amas coquilliers (accumulations anthropiques de coquilles de mollusques liées à une ancienne activité de pêche) qui représentent à ce jour l'unique archive permettant une reconstitution « directe » de l'ENSO dans la Pacifique Est, et de la mousson ouest Africaine pour la période Holocène.

Mes travaux peuvent se diviser en trois grands volets présentés plus en détail ci-après. Le premier volet, fondamental, est lié au développement de méthodes de reconstruction paléoclimatique quantifiées à partir des enregistrements géochimiques des amas coquilliers. Les volets suivants concernent l'histoire Holocène du système de Humboldt et de l'ENSO, et l'histoire des précipitations Sahéliennes au cours des 2000 dernières années.

Encadré : El Niño Southern Oscillation

L'ENSO se manifeste par une alternance d'anomalies chaudes (phase El Niño) et froides (phase La Niña) des eaux de surface du Pacifique tropical centre et Est qui durent environ une année. L'état de l'ENSO est évalué par des indices dont le plus commun est l'indice Niño3.4 calculé comme l'anomalie de température dans la boîte [170°W - 120°W, 5°S - 5°N] du Pacifique central. L'indice le plus significatif pour le Pérou est l'indice Niño1+2 défini par les anomalies de TSM dans la boîte [90°W - 80°W, 10°S - 0°N]. Les évènements El Niño se déclenchent suite à une relaxation des vents alizés qui maintiennent l'upwelling équatorial. Cette relaxation génère un train d'ondes de Kelvin qui traversent l'océan Pacifique tropical d'Ouest en Est en abaissant la thermocline, ce qui élève la température superficielle dans l'océan oriental. Le fort gradient Est-Ouest de température maintenu en condition normale par une rétroaction positive avec le gradient de pression et les vents alizés est alors rompu. Lors d'un évènement El Niño, le réchauffement des eaux de surface déplace et étend la zone de convexion atmosphérique vers l'Est du Pacifique tropical, perturbant profondément la circulation atmosphérique et l'hydrologie de la zone intertropicale. Les évènements les plus forts comme ceux de 1983 et 1998 provoquèrent des précipitations catastrophiques en Equateur et au Pérou, et une sécheresse accompagnée d'incendies en Indonésie et Australie. Ces oscillations ne sont pas véritablement périodiques mais se caractérisent par un pic de fréquence entre 3 et 5 ans. L'ENSO est la principale source de variabilité climatique interannuelle à l'échelle globale. Son évolution future dans un climat d'effet de serre est très incertaine (Collins et al., 2010). Les modèles climatiques, malgré leurs difficultés à représenter l'ENSO de façon réaliste (Guilyardi et al., 2006, 2009), s'accordent à prédire un impact hydrologique accru des anomalies océaniques de l'ENSO (Cai et al., 2014). On ne sait pas, cependant, si la fréquence des anomalies de TSM (température superficielle de la mer) de l'ENSO, leur amplitude, la distribution des évènements froids et chauds, leur structure spatiale, seront affectés ni comment. L'hypothèse que ces caractéristiques de l'ENSO puissent être sensibles aux forçages externes reste elle-même débattue (Cobb et al., 2013). Pouvoir estimer de façon robuste la statistique de l'ENSO dans des conditions climatiques passées différentes de l'actuel est donc plus que jamais nécessaire. Pour plus de détails sur l'ENSO, voir Wyrtki (1975) ; Cane and Zebiak (1985) ; Trenberth (1997).

3.2. Les isotopes stables des coquilles de bivalves : vers une quantification des paléoclimats

Les coquilles de mollusques aquatiques et en particulier de bivalves croissent par l'accrétion de couches de carbonate de calcium précipité à partir du calcium et des ions carbonates dissous dans l'eau. Il s'agit d'une réaction biologiquement contrôlée dans le temps et l'espace par l'intermédiaire d'une matrice organique protéique et d'enzymes permettant de bloquer ou de catalyser la biominéralisation. Ce bio-carbonate de calcium, calcite ou aragonite, se forme en intégrant des isotopes de l'oxygène, ^{16}O et ^{18}O, dans des proportions (notées $\delta^{18}O$ exprimées en pourmille (‰) de déviation par rapport à un standard) qui dépendent de la température de l'eau d'une part et du $\delta^{18}O$ de l'eau d'autre part (McCrea, 1950 ; Epstein et al., 1953 ; Grossman and Ku, 1986). Ainsi, les bivalves, comme d'autre organismes carbonatés, contiennent préservée dans leur coquille la trace des variations environnementales qu'elles ont vécues. Bien que le potentiel paléoclimatique des enregistrements isotopiques des coquilles de mollusques soit connu depuis longtemps (Shackleton, 1973 ; Killingley and Berger, 1979), les applications ont été peu nombreuses et l'utilisation des amas coquilliers pour reconstituer la variabilité climatique passée est encore peu connue par la

communauté scientifique. Une difficulté majeure tient à la multiplicité des échelles de temps abordées : premièrement les coquilles à fort taux de croissance fournissent des enregistrements *mensuels* des variations environnementales de leur milieu mais généralement sur une durée courte de quelques années ; deuxièmement, elles sont accumulées à des rythmes très variables pour former des amas anthropiques qui représentent des périodes d'activité de pêche allant d'une saison à plusieurs millénaires. La discontinuité des échelles de temps de cette archive (mensuelle d'une part, séculaire à millénaire d'autre part) rend difficile la reconstruction sous forme de série temporelle continue classique. L'approche que j'ai développée est statistique : un échantillon de coquille d'un amas (ou d'une strate) permet de reconstituer la *climatologie* (moyenne, saisonnalité, variance) de la période d'accumulation. Une série temporelle paléoclimatique peut être produite par la succession de tels échantillons fournissant une estimation de la variabilité à plus basse fréquence de cette climatologie (multidécennale à millénaire selon la résolution de la série composite).

Pour mettre au point cette méthode, plusieurs étapes sont nécessaires, qui doivent être renouvelées pour chaque nouvelle espèce et chaque nouvelle région d'étude. Le développement de la méthode est détaillé ci-dessous par étape plutôt que par zone géographique. Le perfectionnement des calibrations est un processus qui se poursuit continuellement.

3.2.1. Sclérochronologie

Les exosquelettes calcaires comme les coquilles de bivalves se forment par accumulation de microcouches, visibles en section radiale par les lignes de croissance qui les séparent (Figure 1). La sclérochronologie est l'étude des rythmes de formation, de la structure et de la géochimie de ces incréments, et de leurs liens avec la biologie, le milieu et ses conditions physico-chimiques (Rhoads and Lutz, 1980).

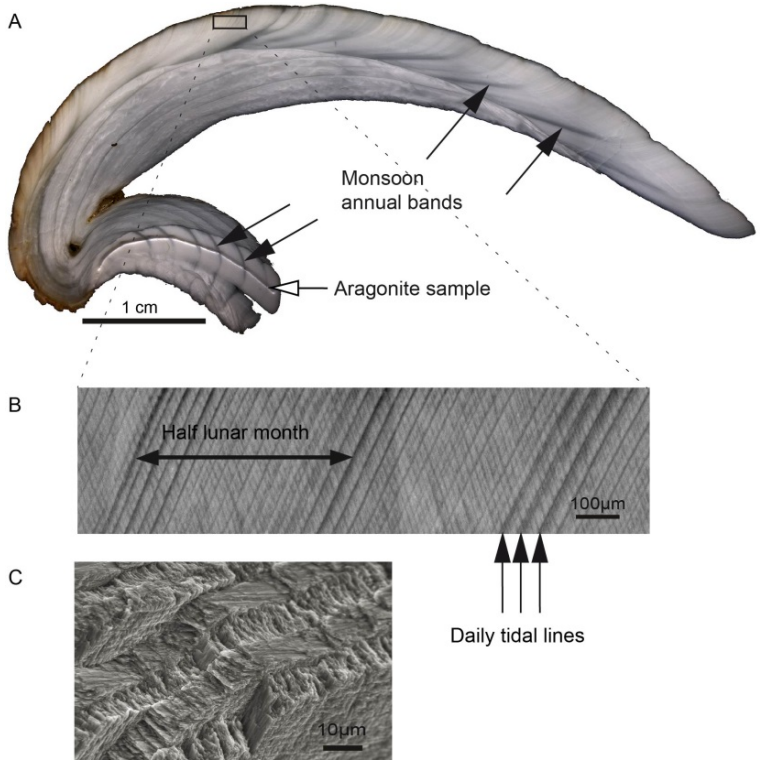

Figure 1. (A) Coupe radiale d'une coquille *de Senilia senilis* et position de bandes sombres annuelles formées durant la saison de mousson. (B) Grossissement des lignes de croissance où apparaissent les lignes de marée journalières et les « paquets » de lignes marquant les phases de marées de vives eaux. (C) Photo prise au microscope électronique à balayage de la microstructure lamellaire croisée de l'aragonite de la couche externe de *S. senilis*.

Une étude des patrons de croissance a été menée dans le cadre du doctorat de M. Azzoug sur l'espèce *Senilia senilis* présente sur toute la côte Ouest Africaine et en particulier dans les mangroves du Saloum au Sénégal. Nous avons montré que les lignes de croissance de cette espèce se forment quotidiennement à chaque marée basse et constituent des structures périodiques (un demi mois lunaire) liée à l'amplitude des marées. Ces structures fournissent un calendrier interne très précis pour les enregistrements isotopiques. Les rapports isotopiques ($\delta^{18}O$) des coquilles mesurés à haute résolution présentent une saisonnalité très marquée en réponse aux précipitations de la mousson (Figure 2). La combinaison des signaux isotopiques des coquilles qui permettent de marquer le début et la fin de la mousson, et des lignes de croissance qui permettent d'estimer le temps écoulé, offre la possibilité d'estimer la durée des saisons sèches et humides avec une précision d'environ 21 jours (Azzoug et al., 2012a). on peut améliorer cette précision statistiquement avec la taille de l'échantillon de coquilles étudié. Ce résultat obtenu sur *Senilia senilis* ouvre une voie importante vers l'étude de la saisonnalité de la mousson, sa variabilité à long terme et ses forçages. Il s'agit à notre connaissance de la seule technique paléoclimatique existant aujourd'hui pour reconstituer quantitativement la durée des saisons en Afrique de l'Ouest au-delà du registre instrumental. Plus que le montant total des précipitations, la durée des saisons sèches et humides est le paramètre principal qui gouverne l'agriculture et la répartition des biomes en Afrique.

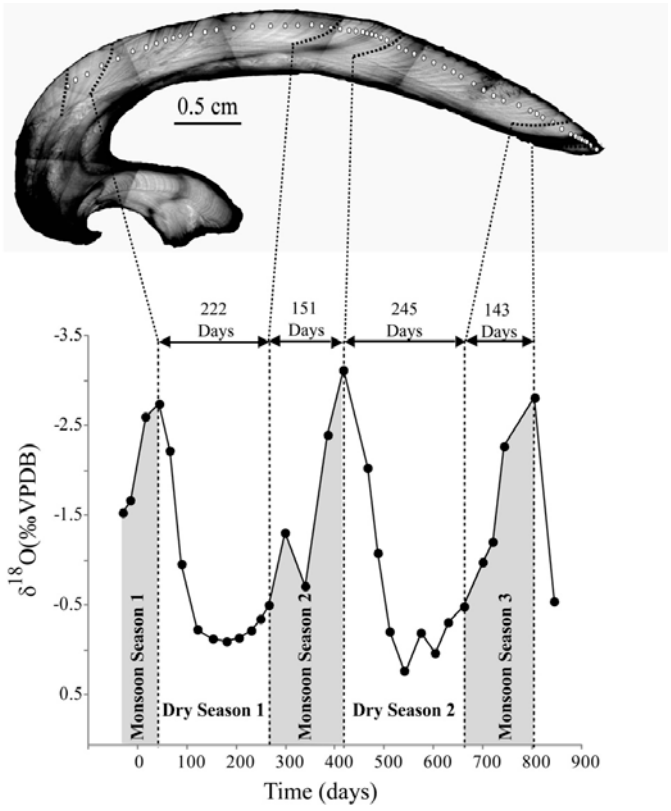

Figure 2. Profil isotopique d'une coquille fossile de *S. senilis* du Delta du Saloum. L'axe de temps a été reconstitué grâce aux structures d'un demi-mois lunaire de la coquille, indiquées par des cercles blancs. Le début de la mousson est marqué par le début du pic isotopique négatif (échelle inversée) et la fin de la mousson par le sommet du pic. (d'après Azzoug et al., 2012a)

3.2.2. Calibration des indicateurs

Quantifier l'activité de l'ENSO

Une première relation empirique entre la température de l'eau et le fractionnement isotopique de l'oxygène avait été calculé à partir de données *in situ* et d'individus pêchés vivants de *Mesodesma*

donacium (Carré et al., 2005), l'espèce de bivalve qui est encore pour l'instant le principal support de mes travaux au Pérou et au Chili.

Reconstituer les paléotempératures n'est pas suffisant pour reconstituer l'activité de l'ENSO. L'enregistrement d'une coquille de *M. donacium* ne représentant que rarement plus de 3 ans, l'ENSO ne peut être identifiée par un filtrage ou une analyse de fréquence. Celle-ci devra donc être estimée par la variance des anomalies mesurées dans un échantillon de coquilles. Ici, les anomalies sont définies à partir des amplitudes saisonnières de température ($\Delta T = Max_{été} - Min_{Hiver}$). Les évènements El Niño génèrent des amplitudes supérieures à la normale tandis que les années La Niña se caractérisent par des amplitudes saisonnières faibles. Ceci est dû au fait que les anomalies ENSO sont maximales pendant l'été austral. L'utilisation des anomalies d'amplitude au lieu des anomalies de température absolue a plusieurs avantages : (1) on évite l'effet de l'hétérogénéité spatiale des températures côtières qui rend incertaine l'estimation d'une température moyenne de référence à partir d'enregistrements courts de 1 à 3 ans, (2) les valeurs de ΔT ne sont pas affectées par l'incertitude sur la valeur moyenne du $\delta^{18}O$ de l'eau et l'effet du volume des glaces.

D'autre part, les conditions côtières étant particulières, surtout dans cette zone d'upwelling, il convient de déterminer l'extension géographique de la représentativité des conditions enregistrées sur la côte. Ce point est particulièrement important dans la perspective d'une comparaison avec les modèles climatiques globaux qui, en raison de leur résolution spatiale limitée, ne peuvent pas reproduire les conditions côtières. L'analyse des séries temporelles de température instrumentales côtières et de l'indice Niño1+2 depuis 1950 montre des coefficients de corrélation entre l'indice Niño1+2 et les amplitudes saisonnières de TSM supérieurs à 0.7 sur toute la côte du Pérou. Ceci confirme (1) l'influence majeure de l'ENSO sur les conditions côtières, (2) que l'amplitude saisonnière de TSM est un indicateur fiable de l'ENSO, (3) que les conditions côtières reflètent fidèlement un signal climatique régional. Sachant que les variations isotopiques des coquilles de *M. donacium* reproduisent correctement les variations de température de l'eau (Carré et al., 2005), ce résultat signifie que l'activité moyenne de l'ENSO dans le Pacifique Est pour une période donnée peut être quantitativement estimée par la variance des amplitudes annuelles des signaux isotopiques fournis par un échantillon de coquilles pêché au cours de cette période (Carré et al., 2013).

Cependant, il faut noter que les évènements chauds extrêmes de type 1997-1998 ne peuvent pas être enregistrés pour cause de mortalité des bivalves. Pour cette raison, la distribution de fréquence des anomalies liées à l'ENSO reproduite par la distribution des amplitudes des signaux isotopiques est tronquée des valeurs positives extrêmes (Figure 3). Toutefois, ces évènements extrêmes, bien qu'important du point de vue de leurs impacts, le sont moins sur le plan statistique en raison de leur très faible fréquence. Le registre sédimentaire côtier qui permet de comptabiliser ces évènements de crue extrême reporte environ 13 évènements de ce type pour les trois derniers millénaires (Wells, 1990). La distribution des anomalies ENSO obtenue par un échantillon de coquilles actuelles est donc peu affectée par cette limitation et reproduit bien l'asymétrie positive (des anomalies chaudes plus intenses que les anomalies froides) caractéristique de l'ENSO, ce qui représente une validation supplémentaire de notre méthodologie (Figure 3). Un échantillon de coquille permet donc de capturer la grande majorité de la gamme de variance, hors évènement extrême de l'ENSO, alors que la plupart des indicateurs sédimentaires utilisés jusqu'ici n'était sensible qu'aux impacts hydrologiques liés à ce type d'évènement extraordinaire. Nous avons ici une représentation plus

étendue de l'ENSO, incluant amplitude et fréquence des anomalies froides et chaudes, que l'on pourra compléter par les enregistrements sédimentaires des évènements extraordinaires.

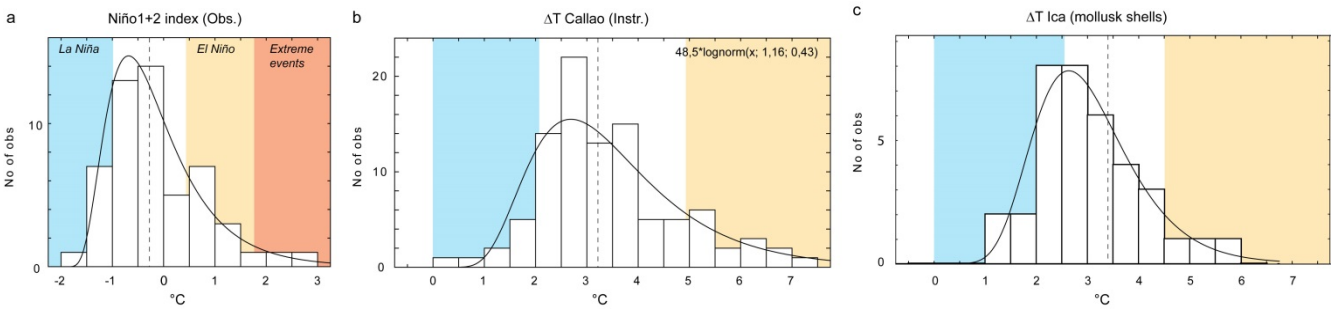

Figure 3. Distributions (a) des valeurs annuelles de l'indice Niño1+2, (b) des amplitudes saisonnières de températures mesurées à Callao depuis 1950, et (c) des amplitudes saisonnières de température enregistrées par un échantillon de 13 coquilles modernes de la zone de Ica (~15°S), pêchées durant les dernières décennies du 20ème siècle.

Au 20ème siècle, la distribution des anomalies de SST dans le Pacifique Est n'est pas symétrique. Ceci est dû à l'asymétrie entre évènements El Niño et La Niña dans leur type canonique : les évènements El Niño produisent des anomalies chaudes fortes centrées sur le Pacifique Est alors que les anomalies froides de La Niña sont de moindre amplitude et centrées d'avantage sur le Pacifique central. Depuis quelques années, un autre mode de variabilité spatiale de l'ENSO a été décrit, caractérisé par des évènements El Niño de faible amplitude et localisés dans le Pacifique central, parfais appelés Niño Modoki ou Central Pacific Niños (CP) (Ashok et al., 2007 ; Ashok and Yamagata, 2009 ; Kao and Yu, 2009 ; Takahashi et al., 2011). Dans le Pacifique Est et sur la côte du Pérou, les modes Pacifique Est (EP) et Pacifique central (CP) se distinguent par leur distribution d'anomalies de SST, déviée vers droite (coefficient d'asymétrie positif) pour le mode EP et vers la gauche (coefficient d'asymétrie négatif) pour le mode CP (Dewitte et al., 2012). Ces changements de contribution des modes EP et CP pourraient donc être détectés par l'asymétrie des distributions de ΔT des coquilles fossiles.

Ces résultats apportent un saut qualitatif substantiel dans le degré de précision des investigations de la variabilité passée de l'ENSO dans le Pacifique Est. L'enregistrement direct de la variabilité saisonnière et inter-annuelle n'était alors possible que grâce à l'étude des coraux fossiles du Pacifique Ouest et Central. Nous espérons désormais entamer une reconstitution de la variabilité temporelle et *spatiale* de l'activité de l'ENSO, une question particulièrement importante étant donné les incertitudes sur un possible changement de régime de l'ENSO en réponse au changement climatique (Lee and McPhaden, 2010 ; Collins et al., 2010).

A travers les rapports isotopiques de carbone ($\delta^{13}C$), les coquilles de mollusques enregistrent également les variations de $\delta^{13}C$ du carbone inorganique dissous (CID), qui à leur tour reflètent différents aspects du cycle du carbone côtier en intégrant l'intensité de l'upwelling, la productivité primaire et la dégradation locale de la matière organique. Au cours du stage de James Sadler (Etudiant de Master de l'Université de Southampton), nous avons utilisé un large jeu de données isotopiques de coquilles de *M. donacium* du Pérou pour construire un modèle interprétatif permettant d'identifier ces différentes influences. Nous avons ainsi montré qu'en combinant les données isotopiques de l'oxygène et celles du carbone il était possible d'estimer (1) les variations

moyennes de l'intensité de l'upwelling côtier et (2) la saison du pic de productivité primaire (Sadler et al., 2012). Ce dernier paramètre est une clé pour l'interprétation des proxies paléocéanographiques basés sur les microfossiles dont la productivité est souvent saisonnière.

Modélisation de proxy et quantification des incertitudes

Pour être comparables aux sorties de modèles climatiques, les reconstitutions paléoclimatiques doivent être quantitatives et associées à des estimations d'incertitude. Un gros effort de la part de l'ensemble de la communauté est nécessaire pour quantifier les barres d'erreur des reconstitutions, trop souvent absentes ou calculées de manière sommaire et sous-estimées. L'intégration du signal climatique dans le proxy puis son extraction représentent de nombreuses étapes amenant chacune son lot d'incertitudes et de biais. Hughes et Ammann (2009) écrivaient : *" the study of the processes by which climate proxy records are formed [...] should be accorded high priority".* Vis à vis des reconstitutions de l'activité de l'ENSO à partir d'échantillons de coquilles, se posaient en plus des difficultés liées aux limites du proxy associées au problème de la représentativité statistique de l'échantillon. Pour répondre à ces questions, j'ai utilisé une approche numérique de type Monte Carlo. Le processus de reconstitution paléoclimatique est simulé numériquement en intégrant les sources d'incertitudes connues (erreur analytique, variabilité isotopique de l'eau de mer, incertitudes de la calibration isotopique, limites physiologiques de température, arrêts de croissance aléatoires…) et appliquées à une série temporelle connue. En répétant des milliers de fois l'expérience de reconstitution avec un tirage aléatoire des incertitudes, la population d'erreurs obtenue permet d'estimer les biais systématiques et l'erreur standard de la méthode sur plusieurs variables comme la température moyenne, l'amplitude saisonnière moyenne, et la variance des températures (Figure 4). Le code Matlab utilisé, baptisé MoCo, est en accès libre et permet d'estimer quantitativement les incertitudes des reconstitutions paléoclimatiques obtenues à partir des enregistrements géochimiques d'échantillons de coraux ou de mollusques (Carré et al., 2012a). L'apport principal de cette approche est qu'elle permet, en jouant sur le paramétrage des différentes sources d'incertitude, d'évaluer par des tests de sensibilité leur influence respective sur les reconstructions paléoclimatiques.

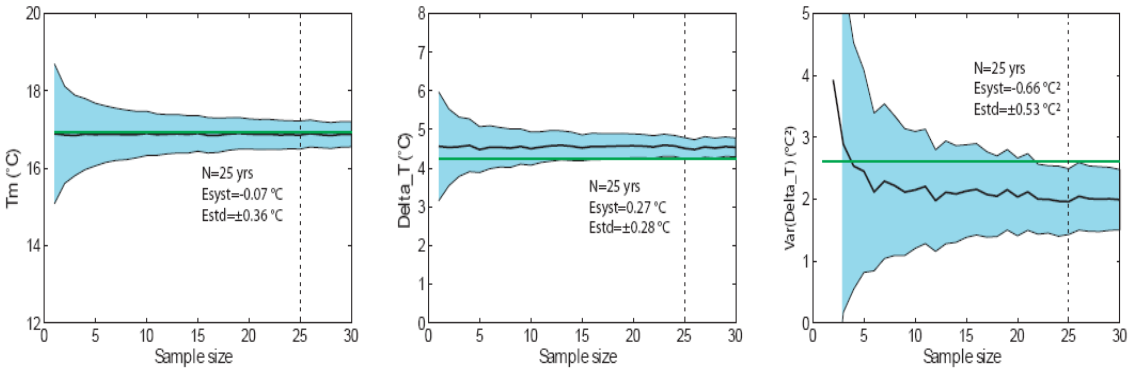

Figure 4. Résultats de simulations Monte Carlo reproduisant le processus de reconstruction paléoclimatique à partir des courbes isotopiques d'échantillons de coquilles de mollusques, pour la température moyenne (gauche), l'amplitude saisonnière des températures (centre) et la variance de l'amplitude saisonnière (droite). Sont représentées la valeur moyenne (courbe noire épaisse) comparée à la valeur attendue (vert) et l'erreur standard (1σ) (bleu) en fonction de la taille de l'échantillon. Carré et al. (2012a).

Pour être fiables, ces estimations d'incertitude doivent se baser sur des paramétrages réalistes des sources d'erreur, ce qui nécessite des mesures de terrain, en particulier un suivi de la composition isotopique de l'eau (effectuées au Pérou en collaboration avec l'Institut de la Mer du Pérou, et au Chili central avec des collaborateurs de l'université de Santiago). Cette approche est transposable à d'autres sites ou d'autres organismes.

Reconstruire la mousson au Sahel (Projet SALOUM)

Un travail de calibration est mené depuis 2010 dans le cadre du projet SALOUM (INSU-LEFE) sur la relation entre les précipitations au Sénégal, la variabilité isotopique des eaux de l'estuaire du Saloum et celle des coquilles de *Senilia senilis*. L'objectif de cette calibration est de pouvoir utiliser les coquilles fossiles de cette espèce accumulées dans de très nombreux amas coquilliers comme enregistreurs des précipitations passées. Des missions de terrain régulières ont été menées pour installer des capteurs automatisés de température et de précipitation, prélever des échantillons d'eau et de coquilles sur plusieurs transects, et mettre en place un échantillonnage hebdomadaire avec des partenaires locaux. Les premiers résultats ont montré (1) un fort gradient spatial du $\delta^{13}C$ du CID reflété dans les coquilles et permettant de contraindre la localisation d'origine des coquilles fossiles, (2) un couplage fort entre les variations du $\delta^{18}O$ de l'eau et les précipitations locales (Figure 5), (3) que les coquilles précipitent leurs carbonates en équilibre isotopique avec leur milieu et que les variations de $\delta^{18}O$ des coquilles sont principalement déterminées par les précipitations et secondairement par la température.

Suivant l'hypothèse que l'amplitude du pic isotopique dans les coquilles est liée au montant des précipitations de mousson, il devrait être possible d'utiliser cette amplitude pour quantifier les précipitations passées. Nous travaillons à établir une relation empirique entre les précipitations de mousson et les variations isotopiques saisonnières de l'eau. La principale difficulté tient au fait que cette calibration ne produit qu'un point par an ($P_{annuelle}$, $\Delta(\delta^{18}O_w)$). Nous disposons pour l'instant d'un suivi continu de 2011 à 2015 (les échantillons de 2016 et 2017 sont en cours d'analyse), c'est-à-dire uniquement 5 points, ce qui reste trop peu pour une calibration statistiquement robuste. Cependant, les précipitations annuelles enregistrées à Toubakouta ayant varié de 593 à 1042 mm sur cette période, une gamme de valeur assez étalée nous permet d'observer déjà une relation significative, encourageante pour de futures reconstructions quantifiées de paléo-précipitation, jusqu'à présent quasi inexistantes en Afrique (Figure 6).

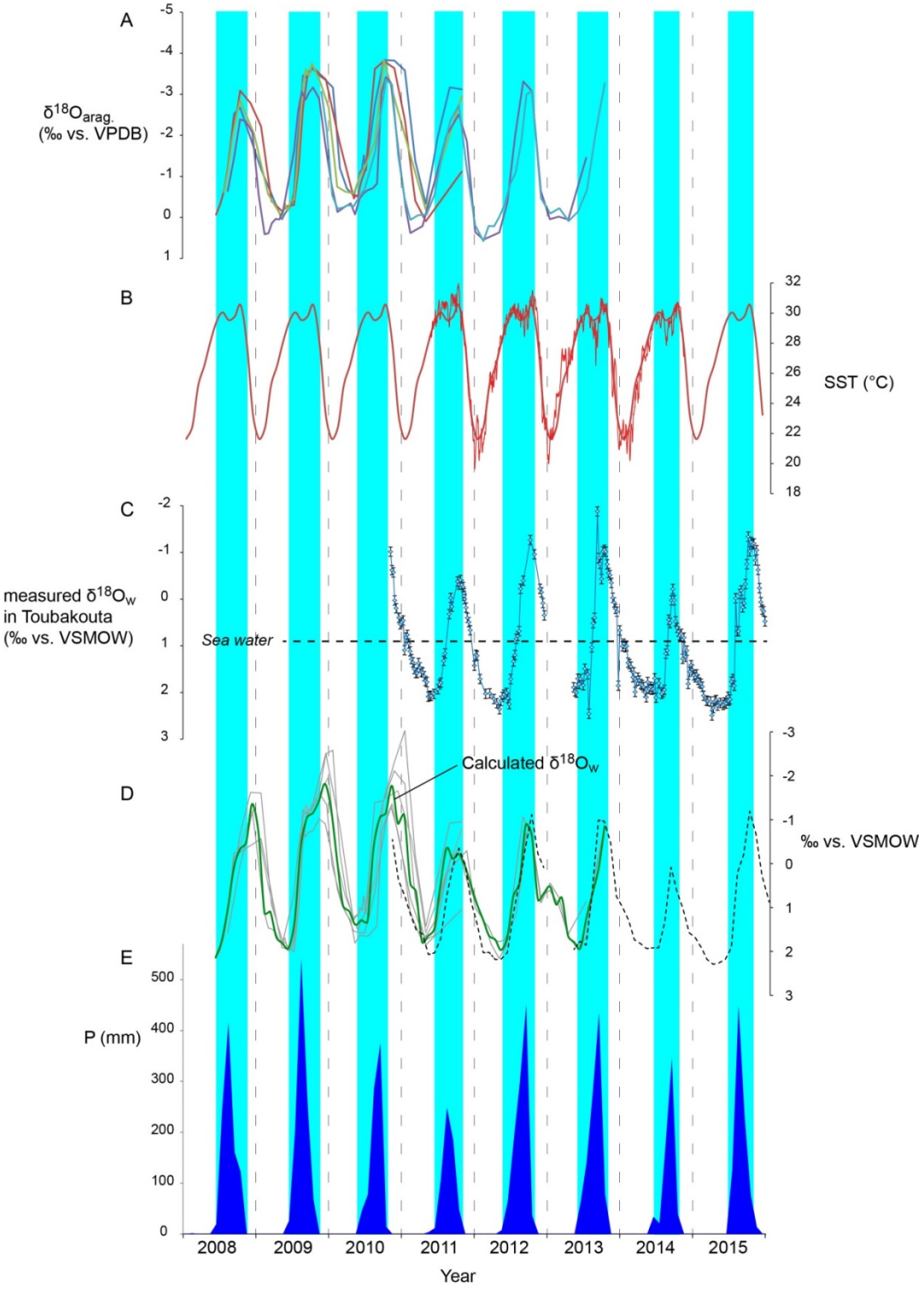

Figure 5. Monitoring *in situ* à Toubakouta. (A) Enregistrements isotopiques de coquilles modernes. (B) Variations journalières de SST de 2011 à 2014, et cycle annuel moyen des SST représenté sur toute la période. (C) Variations hebdomadaires du $\delta^{18}O$ de l'eau de l'estuaire à Toubakouta. (D) Comparaison du $\delta^{18}O$ de l'eau calculé à partir des valeurs isotopiques des coquilles et du cycle moyen des températures d'après la 3ème équation de Grossman et Ku (1986) (coquilles individuelles en gris, valeur moyenne en vert), et des variations mensuelles du $\delta^{18}O$ de l'eau mesuré (pointillés). (E) Précipitations mensuelles mesurées à Toubakouta. La saison des pluies est indiquée par les bandes verticales bleu clair.

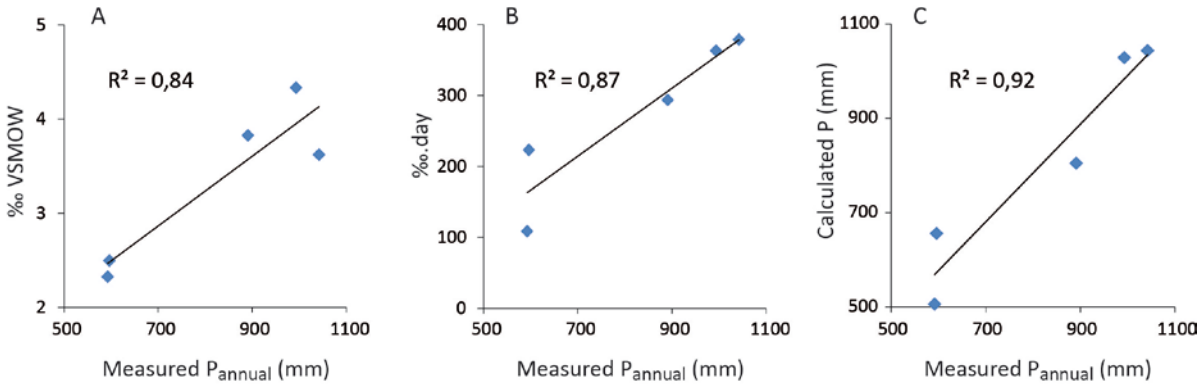

Figure 6. Regressions linéaires entre les précipitations annuelles totales mesurées de 2011 à 2015 à toubakouta et (A) l'amplitude de la variation saisonnière de $\delta^{18}O_w$, (B) l'aire de la variation saisonnière de $\delta^{18}O_w$ corrigée des pertes d'eau douce par le courant, le mélange tidal et l'évaporation (ces pertes sont estimées par le taux de variation de $\delta^{18}O_w$ observé pendant la saison sèche multiplié par la durée de la saison humide), (C) les précipitations calculées par une relation linéaire entre les précipitations annuelles, l'aire de la variation saisonnière $\delta^{18}O_w$ et la durée de la saison humide, dont les paramètres sont estimés par une méthode Monte Carlo de manière à optimiser la regression.

3.3. El Niño est-il sensible aux changements du climat global ?

L'ENSO est un mode de variabilité interannuelle interne à l'océan Pacifique qui résulte de la dynamique couplée de l'océan et de l'atmosphère. Bien que les modèles climatiques soient capables de simuler des évènements El Niño, les caractéristiques spatio-temporelles de l'ENSO sont très variables d'un modèle à l'autre (Guilyardi et al., 2009). Les mécanismes qui conditionnent le déclenchement des évènements, leur amplitude, leur fréquence et leur structure spatiale sont multiples et subtils, si bien que la sensibilité de l'ENSO aux forçages externes et aux conditions globales moyennes reste mal comprise et la réponse de l'ENSO au réchauffement globale inconnue. Aujourd'hui, nous ne savons toujours pas si les variations de régime de l'ENSO observées dans le registre instrumental vers 1976 (Wallace et al., 1998) puis vers les années 2000 (Lee and McPhaden, 2010) sont une réponse à des facteurs externes ou simplement l'expression d'une variabilité interne stochastique. Une expérience de simulation climatique à l'équilibre (sans variation des forçages) sur 2000 ans a produit des variations significatives décennales et séculaires de l'ENSO, parfois similaires à celles observées (Wittenberg, 2009), soulignant ainsi clairement l'insuffisance de la durée du registre instrumental pour évaluer la sensibilité de l'ENSO. En revanche, sur des échelles de temps plus longues, les modèles suggèrent une sensibilité de l'ENSO aux variations d'insolation dues aux changement de géométrie de l'orbite terrestre (Clement et al., 1999). Les simulations du climat de l'Holocène moyen (6ka) en particulier montrent pour la plupart une réduction de variance de l'ENSO en réponse au contraste saisonnier d'insolation renforcé dans l'hémisphère nord (Clement et al., 2000 ; Brown et al., 2008 ; Braconnot et al., 2012 ; Emile-Geay et al., 2016). Les changements climatiques passés constituent donc le meilleur laboratoire expérimental pour l'étude de la sensibilité de l'ENSO, en raison de l'amplitude des forçages et des variations globales, et des échelles de temps longues qui peuvent dépasser celles de la variabilité interne du phénomène. J'ai donc étudié au cours des dernières années et dans la continuité de mon travail de doctorat le comportement de l'ENSO au Pérou au cours de l'Holocène, une période caractérisée d'abord par la

fin de la déglaciation et par des changements importants de l'insolation ayant affecté considérablement les climats tropicaux. Malgré, ou peut-être en raison de la relative abondance des archives paléoclimatiques à l'Holocène, l'histoire de l'ENSO pour cette période est très débattue.

3.3.1. Les conditions moyennes de l'Océan Pacifique à l'Holocène inférieur et moyen

L'Holocène moyen est une période particulière sous les tropiques. Les calottes polaires étaient alors à leur niveau actuel mais l'insolation d'été était plus importante dans l'hémisphère nord ce qui généra un optimum climatique et des systèmes de mousson renforcés (Jousseaume et al., 1999 ; Fleitmann et al., 2003 ; Wang et al., 2005). Des précipitations renforcées dans le bassin de Cariaco (Vénézuela) sont interprétées comme le signe d'une position plus septentrionale de la zone de convergence intertropicale (Haug et al., 2001). Dans l'océan Pacifique, des comparaisons de reconstructions de températures de surface entre l'Est et l'Ouest suggèrent un gradient zonal renforcé qui correspondrait à une situation moyenne de type La Niña (Koutavas et al., 2002). Cependant les indications paléocéanographiques comportent d'importantes incertitudes notamment liées à la différente nature des indicateurs de température (Mg/Ca et $U^{k'}_{37}$) utilisés de part et d'autre du Pacifique.

Pour déterminer l'état moyen de l'upwelling côtier au Pérou et au Chili à cette période, j'ai comparé à des valeurs actuelles les données isotopiques obtenues sur des coquilles fossiles de l'Holocène moyen de sites archéologiques étalés du nord du Pérou au Chili central (Figure 7). Les résultats montrent systématiquement des conditions plus froides et sèches sur l'ensemble de la côte Pacifique, traduisant clairement un renforcement de l'upwelling côtier à cette époque (Carré et al., 2012b). Cette situation peut s'expliquer par un renforcement des vents côtiers et du pompage d'Ekmann.

Je me suis alors intéressé à l'influence de ce changement océanique sur le climat d'Amérique du Sud. Sur le continent Sud-américain, les traces d'un changement climatique sont très nettes à l'Holocène moyen. En réponse à une insolation d'été plus faible dans l'hémisphère sud, le système de mousson Sud-américaine était affaibli, provoquant une forte aridité sur la partie sud du bassin amazonien. Mais les signes de changement climatiques dépassaient largement cette zone. Pour isoler la part de changement climatique due à l'océan Pacifique, j'ai sélectionné 4 régions sujettes à de fortes téléconnections atmosphériques avec le Pacifique, mais situées hors de l'influence directe du système de mousson ou de la ceinture de vents d'ouest (southern westerlies), et fait la synthèse des évidences paléoclimatiques disponibles dans la littérature pour l'Holocène moyen (~5-8 ka). Le résultat est très homogène, indiquant des conditions clairement arides dans les zones qui reçoivent aujourd'hui des excès de précipitation dans les situations El Niño, et des conditions relativement humide dans les zones qui au contraire reçoivent moins de précipitation en condition El Niño. L'image obtenue est donc très cohérente, associant des conditions océaniques froides caractéristiques d'une situation moyenne de type La Niña à des conditions continentales caractéristiques d'une réponse de type La Niña selon les schémas de téléconnection atmosphériques actuels (Figure 8). L'étude clarifie et confirme la situation paléoclimatique de l'Holocène moyen de la région et met en évidence le rôle de la téléconnection atmosphérique avec le Pacifique tropical à l'échelle millénaire (Carré et al., 2012b).

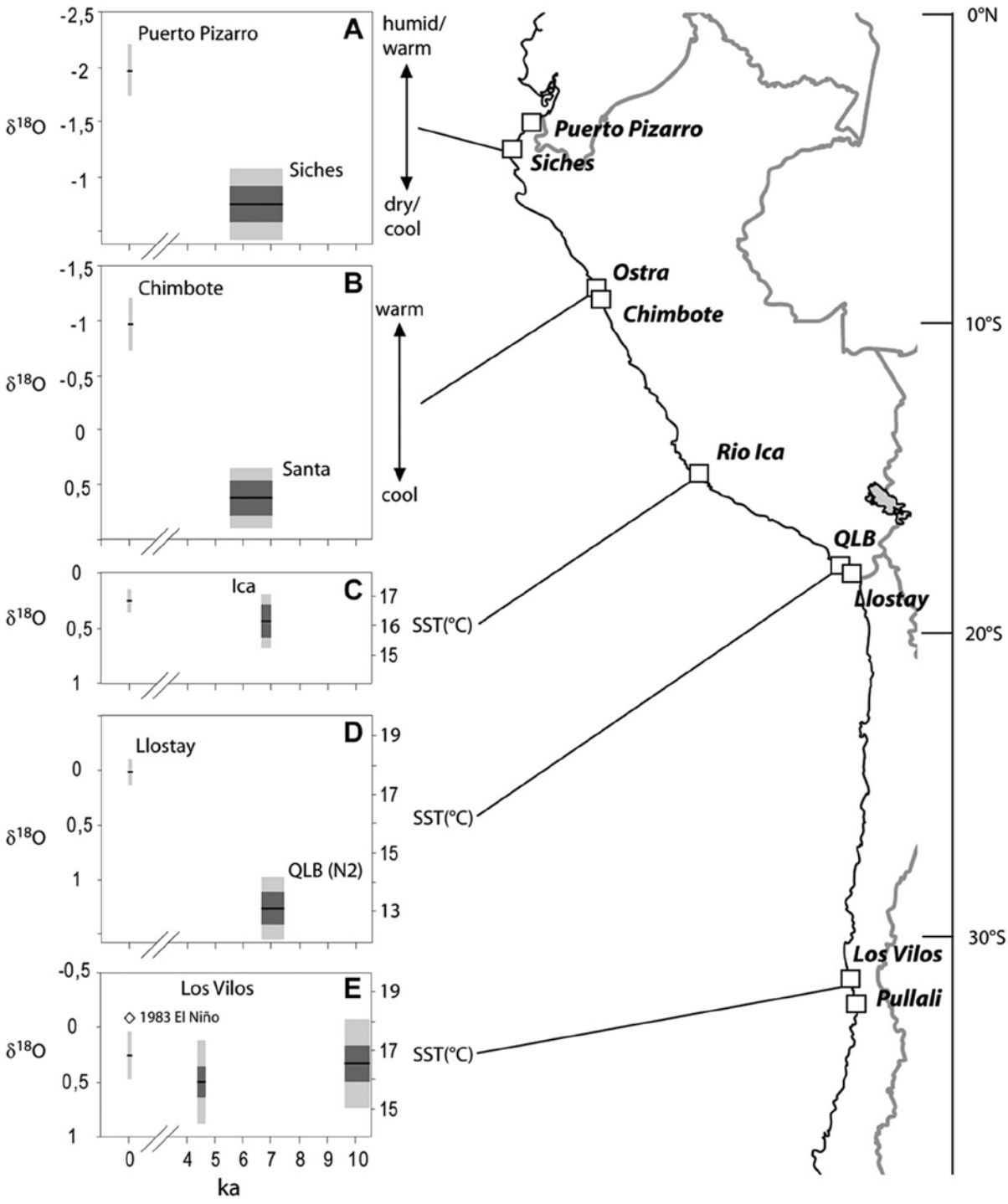

Figure 7. Carte de la côte Pacifique Sud-américaine indiquant les sites archéologiques et modernes où les coquilles de mollusque ont été prélevées (Carré et al., 2012b). Les valeurs isotopiques sont des moyennes issues de plusieurs coquilles analysées. Les valeurs ont été corrigées de l'effet du volume des glaces. Les biais systématiques potentiels (barres gris foncé) incluent l'incertitude sur les valeurs moyennes de la composition isotopique de l'eau de mer. L'erreur standard (gris clair) a été calculée par des simulations Monte carlo (voir section 3.2.2. ; Carré et al., 2012a).

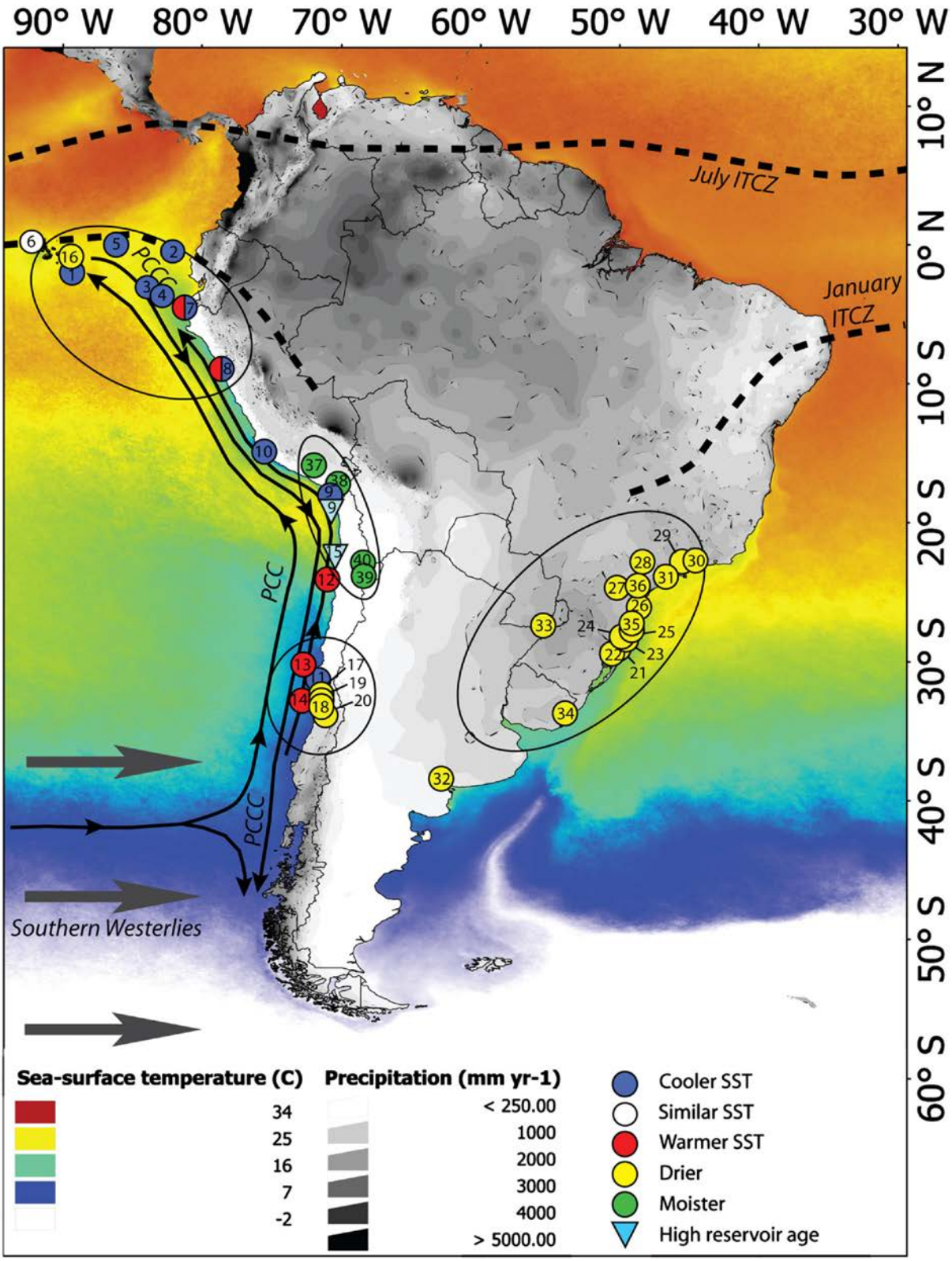

Figure 8. Carte d'Amérique du Sud indiquant les précipitations annuelles (niveau de gris) et les températures océaniques moyennes (échelle de couleur). Les courants océaniques, les positions saisonnières de l'ITCZ et la ceinture de vent d'ouest sont indiquées. 4 régions sélectionnées pour leur forte téléconnection avec l'ENSO sont entourées. Les sites de l'Holocène moyen sont représentés par des symboles indiquant le type de changement observé (voir Carré et al., (2012b) pour les références associées aux sites).

3.3.2. El Niño Southern Oscillation à l'Holocène

Le climat de l'Holocène moyen et inférieur dans la zone Pacifique et sud-américaine est aussi communément associé dans la littérature à une réduction, voire une disparition, de l'activité de l'ENSO. Cette hypothèse, qui, à force d'être utilisée dans de multiples interprétations paléoenvironnementales semble être acceptée comme un fait, est en réalité assise sur des bases très fragiles. En 1999 furent publiés deux articles, l'un montrant dans les sédiments d'un lac Andin une augmentation progressive au cours de l'Holocène de la fréquence de dépôts détritiques interprétés comme le résultats de pluies dues à El Niño (Rodbell et al., 1999). L'autre était une expérience de modélisation climatique montrant une diminution de l'amplitude et de la fréquence d'El Niño lors des phases de plus forte insolation d'été comme à l'Holocène inférieur (Clement et al., 1999). L'association de ces deux articles indépendants donna à cette hypothèse une autorité qui perdure encore alors qu'il a été montré d'une part que ce lac andin est hors de la zone d'influence directe d'El Niño (Sulca et al., 2018) et que ces dépôts sont dûs à l'érosion des glaciers (Rodbell et al., 2008), et qu'on sait d'autre part que le modèle utilisé par Clement et al. (1999) est très simplifié (Cane et al., 1986). L'histoire de l'ENSO à l'Holocène reste donc encore largement à découvrir.

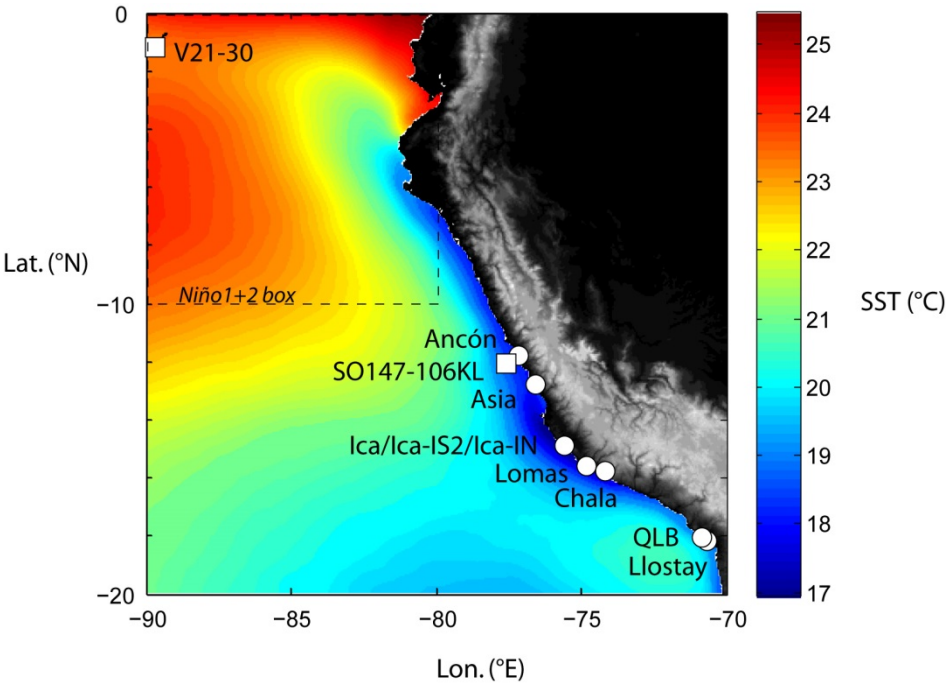

Figure 9. Carte de la topographie du Pérou et des températures océaniques moyennes (échelle de couleur) indiquant la position des sites archéologiques étudiés (cercles), de carottes marines citées dans le texte (carrés), et de la zone Niño1+2.

Dans le Pacifique tropical Est, elle peut être reconstruite grâce aux amas coquilliers archéologiques que l'on trouve dispersés le long de la côte péruvienne (Figure 9). Ces amas coquilliers sont de dimensions très variables et en général très bien conservés en raison des conditions d'aridité extrêmes (Figure 10). Les principales dégradations sont dues à des pillages de sépultures. Les amas les plus anciens remontent à environ 12 ka. Le plus ancien étudié ici date de 9.5 ka et provient de la

Quebrada de los burros (QLB), une petite vallée à l'extrême sud du Pérou (Figure 9, 11) où les brumes côtières alimentent une source d'eau douce permanente. Ce site a été étudié de manière très complète durant plus de 10 ans par le projet archéologique Pérou-Sud (Lavallée et al., 2011 ; Lavallée et Julien, 2012). Les autres sites ont été identifiés et sélectionnés lors de plusieurs prospections de terrain de 2007 à 2011 et échantillonnés stratigraphiquement sur des affleurements plus ou moins grands (Figure 12). Les strates de ces sites ont été datées au ^{14}C à partir de fragments de charbon.

Figure 10. Amas coquillier IS2 de la partie inférieure de la vallée de Ica, Pérou, daté de la période Inca. Il s'agit d'un site de grande dimension, n'ayant fait l'objet d'aucune fouille, et comportant des habitations d'argile et de bois, des restes de céramique et de tissus et d'outils de pêche et de chasse, des tombes contenant des momies. (Photo : M. Carré)

Figure 11. Fouille du site de la QLB, niveau N6, 2007. En arrière-plan se trouvent les postes de tamisage et de tri. (photo : projet archéologique Pérou-Sud)

Figure 12. Coupe du l'amas archéologique de Lomas due au passage d'une route. L'affleurement a été échantillonné sur ses 6m de hauteur, accumulés en un siècle de1340 à 1430 A.D.. (Photo : M. Carré)

Les données isotopiques obtenues sur les coquilles fossiles permettent une reconstruction quantitative des variations de températures côtières. Les changements de température moyenne (Figure 13) indiquent des variations importantes de l'intensité de l'upwelling côtier depuis le Chili central jusqu'au Pérou central. L'upwelling était généralement plus intense de 10 ka à 4,5 ka en réponse à des vents plus forts et un anticyclone Sud Pacifique renforcé. Ceci se traduisait par des eaux côtières plus froides de 1 à 4°C à ces époques, la période la plus froide étant comprise entre 8 et 5ka. Nos résultats montrent cependant que les gradients côtiers de température étaient alors différents probablement en raison d'un changement d'intensité et de taille des cellules d'upwelling (Sadler et al., 2012). La première moitié de l'Holocène mais plus particulièrement l'Holocène moyen se caractérisait donc dans le Pacifique Est par des conditions moyennes de type La Niña associées à une position plus au nord de la zone de convergence intertropicale (ITCZ) (Carré et al., 2012b). Une transition semble avoir eu lieu entre 4.5ka et 3ka dans le régime de circulation océanique vers des conditions proches de l'actuel. Cette transition s'observe également dans un shift de la saisonnalité des températures de surface (SST) (Figure 14B). La saisonnalité des SSTs sur la côte dépend de la saisonnalité de l'ensoleillement avec une rétroaction positive du couvert nuageux, mais aussi fortement de l'upwelling qui tamponne ces variations (Takahashi, 2005).

Concernant la variabilité interannuelle liée à l'ENSO, la première observation est que le niveau de variance actuel est supérieur à celui de toute autre période de l'Holocène (Figure 14). L'enregistrement n'étant pas continu, on ne peut écarter la possibilité que des périodes de forte activité se soient produites, notamment entre 1000 et 3000 BP. Ensuite, le niveau de variance de l'ENSO dans le Pacifique Est à l'Holocène inférieur n'est pas statistiquement différent de celui de

l'Holocène tardif, ce qui contredit le paradigme d'une ENSO inactive à l'Holocène inférieur. La période de plus faible activité est enregistrée par un échantillon daté de 4.7 ka qui montre une baisse d'environ 50% de la variance ENSO par rapport à aujourd'hui, avec un niveau de confiance statistique de 87%. Cette réduction du niveau de variance est également enregistrée par la dispersion des valeurs isotopiques de foraminifères individuels d'une carotte des Galapagos (Koutavas et al., 2012) et par des enregistrements coralliens du Pacifique central (Cobb et al., 2013) (Figure 14). La cohérence de ces trois jeux de données du Pacifique tropical soutient un signal régional et l'existence d'une phase de très faible activité de l'ENSO sur la majeure partie du Pacifique tropical de 4 à 6 ka.

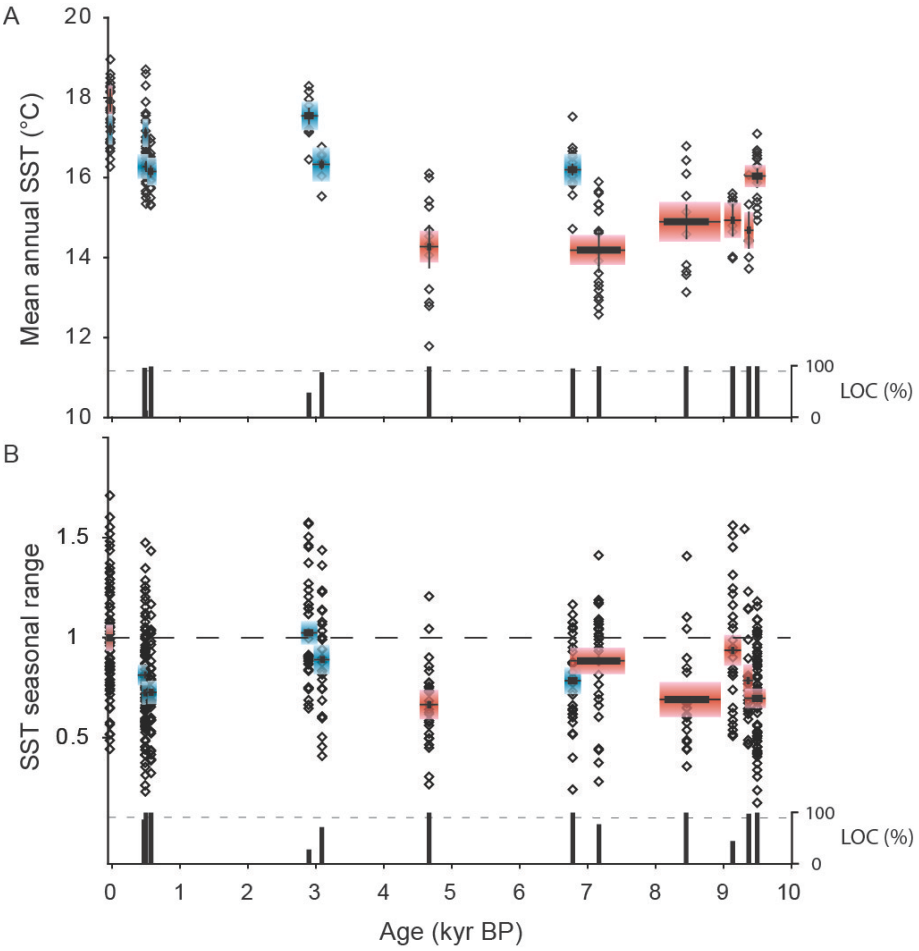

Figure 13. Reconstitutions paléoclimatiques pour la période Holocène au Pérou obtenues d'après les enregistrements isotopiques de coquilles fossiles de *M. donacium*. Haut : températures moyennes annuelles de l'océan obtenues pour chaque coquille (losanges) et moyennes par période (barres épaisses). La couleur bleue correspond aux sites de la zone de Ica et le rouge à la zone de Ilo (site Quebrada de los Burros). Les barres d'erreur sur les moyennes sont estimées par simulation Monte Carlo. La différence avec les conditions actuelles implique un niveau de confiance statistique (LOC) représenté par les barres en contrebas avec le niveau de confiance à 90% indiqué par une ligne pointillé. Bas : même légende pour l'amplitude saisonnière des températures de l'océan. (Carré et al., 2014)

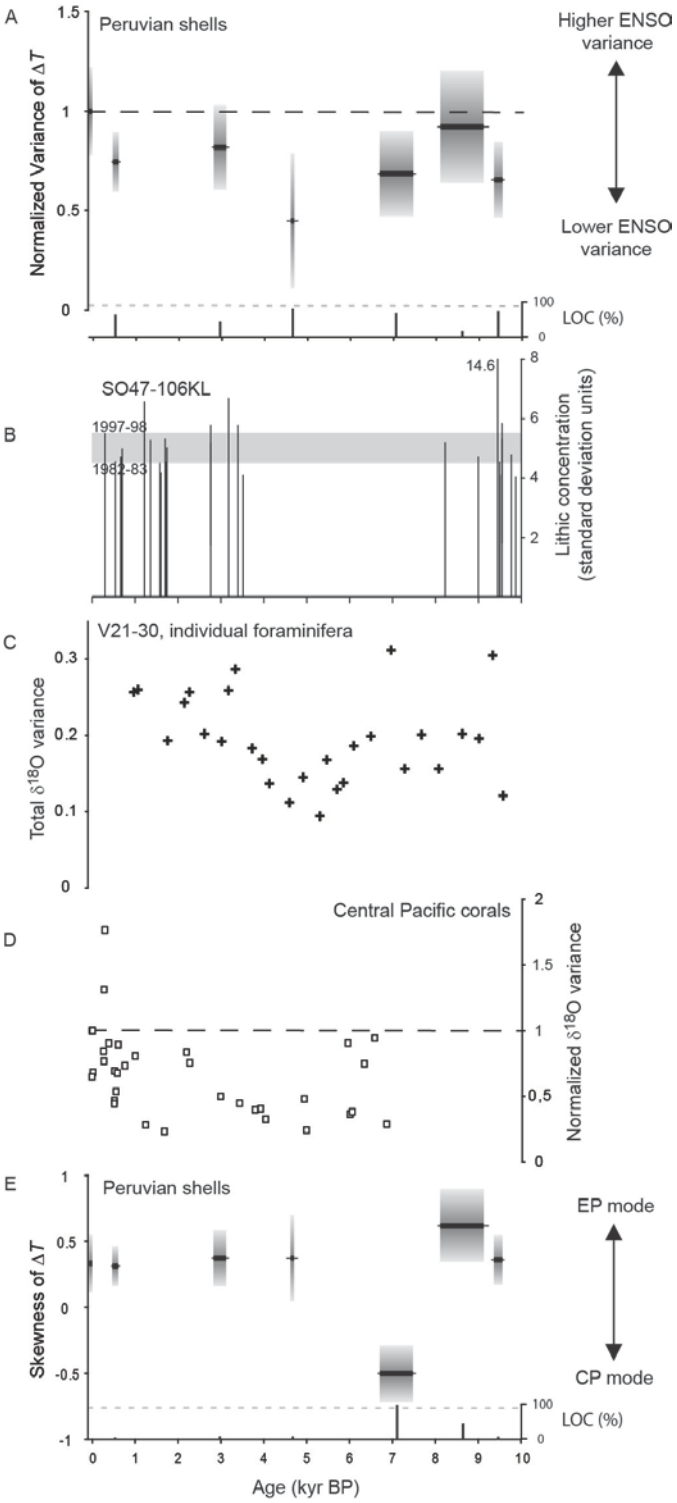

Figure 14. (A) variance normalisée des valeurs de ΔT des échantillons de coquilles fossiles du Pérou indiquant les changements de variance ENSO dans la zone Niño1+2. Les barres d'erreur (+/-σ) (grises) sont estimées par des simulations Monte Carlo (Carré et al., 2012a). La différence avec les conditions actuelles implique un niveau de confiance statistique (LOC) représenté par les barres en contrebas avec le niveau à 90% indiqué par une ligne pointillé. (B) Evènements extrêmes de concentration lithique dans la carotte SO47-106KL (Rein, 2007) indiquant les évènements El Niño extrêmes. (C) variance des valeurs de $\delta^{18}O$ des foraminifères individuels dans la carotte V21-30 (Koutavas et al., 2012). (D) variance interannuelle (filtre passe-bande 2-7 ans) et normalisée des enregistrements de $\delta^{18}O$ de coraux des Line Islands (Cobb et al., 2013). (E) Coefficient d'asymétrie des valeurs de ΔT des coquilles fossiles du Pérou. Légende identique à (A). (Figure tirée de Carré et al., 2014)

Enfin, les variations du coefficient d'asymétrie des anomalies enregistrées par les coquilles apportent pour la première fois des informations sur l'histoire de la dimension spatiale de l'ENSO. La plupart de l'Holocène apparaît plutôt dominé par le mode EP produisant des distributions d'asymétrie positive. Une période cependant se démarque de façon très significative avec une valeur d'asymétrie très négative de 7.5 à 6.8 ka. Ceci indique une variabilité climatique dominée par des anomalies chaudes de faible amplitude et de fortes anomalies froides, similaire à ce qui est observé aujourd'hui au Pérou avec le mode CP (Dewitte et al., 2012). Notre résultat est cohérent avec les données d'une carotte sédimentaire marine proche de Lima qui enregistre des décharges détritiques liées à des crues (Rein et al., 2005). Si nous sélectionnons uniquement les évènements extrêmes (>4 σ) qui reflètent les évènements El Niño extraordinaires de type 1982-83 et 1997-98 (de type EP), nous obtenons un enregistrement paléoclimatique complémentaire de celui des coquilles. Cette carotte indique clairement l'existence d'évènements extrêmes au début et à la fin de l'Holocène lorsque l'asymétrie des anomalies indique une domination du mode EP, et aucun lorsque l'ENSO apparaît faible ou bien dominé par le mode CP.

Ces résultats modifient profondément et complexifient l'histoire Holocène de l'ENSO qui était interprétée jusqu'à présent sur la base d'indicateurs indirects et liés aux précipitations continentales dont la relation avec les anomalies de température de l'océan Pacifique est complexe et non stationnaire. Cela signifie par conséquent d'une part qu'un grand nombre d'interprétations paléoenvironnementales continentales sont à réviser et d'autre part que les critères d'évaluation des simulations de l'ENSO à l'Holocène sont à revoir.

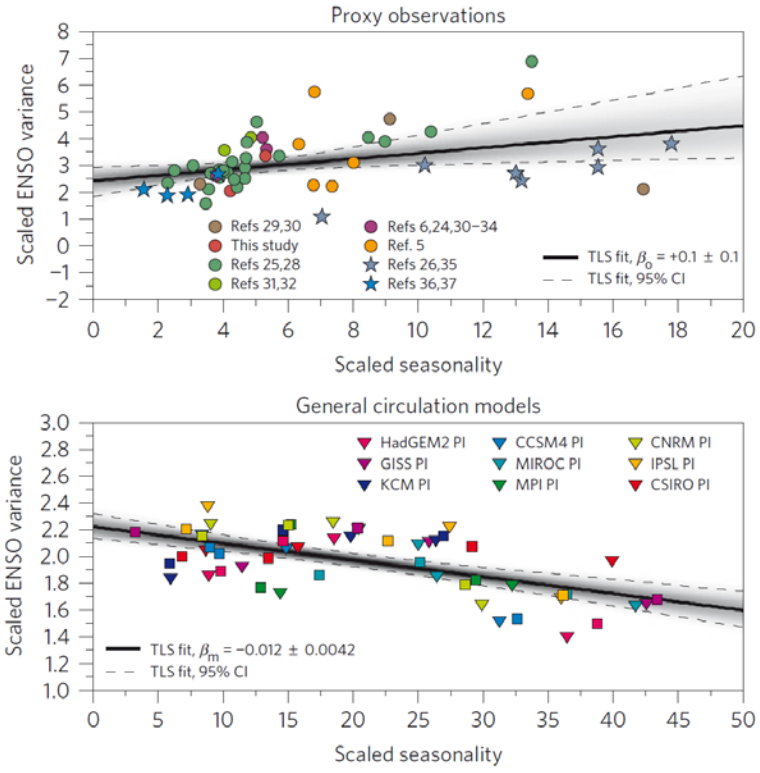

Figure 15. Relation entre la variabilité interannuelle et saisonnière dans les observations (haut) et les modèles de PMIP3 (bas). (Voir Emile-Geay et al., 2016 pour les références et les détails méthodologiques).

Ces résultats ont été intégrés dans un travail collaboratif de synthèse d'une équipe internationale en lien avec le projet ANR EL PASO (dir. P. Braconnot) visant à regrouper l'intégralité des enregistrements « directs » d'El Niño basés sur les données géochimiques de haute résolution obtenus sur des coraux et mollusques fossiles Holocène du Pacifique. Cette synthèse publiée récemment (Emile-Geay et al., 2016) représente une reconstruction discrète de la variabilité saisonnière et interannuelle des conditions de surface de l'ensemble du Pacific tropical au cours de l'Holocène. Confirmant les conclusions de 2014, une période de 64% de réduction d'activité de l'ENSO est détectée entre 3 et 5ka, cette fois sur l'ensemble du bassin. Cette période de faible activité de l'ENSO n'est pas en phase avec les variations d'insolation liées à la précession des équinoxes. La comparaison du cycle saisonnier et de la variance de l'ENSO observés dans les coraux et bivalves du Pacifique avec ceux simulés par neuf modèles climatiques forcés par les paramètres orbitaux montre que ceux-ci ne capturent ni le timing ni l'amplitude des changements d'activité de l'ENSO. D'autre part, la corrélation négative qui apparaît entre le cycle saisonnier et l'ENSO dans les modèles est au contraire positive dans les observations (Figure 15). Cette étude démontre que l'ENSO n'est pas simplement forcée par l'insolation et que la génération actuelle de modèles climatiques ne simule pas correctement les processus qui lient l'état moyen, le cycle annuel et l'ENSO. La période de réduction de l'ENSO entre 3 et 5ka constitue une nouvelle cible de simulation qu'il reste à expliquer.

Ce travail est actuellement poursuivi dans le projet PACMEDY (ANR-Belmont Forum, P.I. P. Braconnot) qui regroupe un consortium international et dont l'objectif est d'étudier la variabilité climatique haute et basse fréquence en zone tropicale et en particulier des systèmes de mousson, à partir d'une approche intégrant données et simulations paléoclimatiques sur des périodes clés de l'Holocène. J'ai assemblé dans le cadre de ce projet une base de données relationnelle MySQL compilant l'ensemble des données géochimiques de résolution mensuelle de coraux et de mollusques fossiles disponibles pour la période Holocène (0-12700 BP) dans la zone tropicale. La base de données, qui contient 139 jeux de données paléoclimatiques (représentant 75,000 données) (Figure 16), est complète pour l'Holocène mais n'est pas exhaustive pour les coraux « modernes » qui ont été inclus essentiellement dans la mesure où ils peuvent constituer une référence moderne pour les données passées.

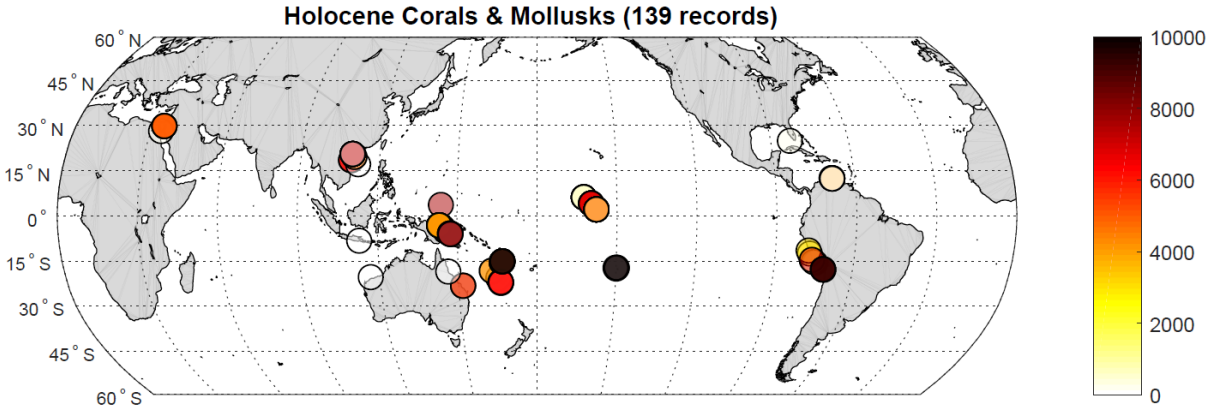

Figure 16. Carte des jeux de données mensuels de coraux et de bivalves disponibles pour l'Holocène. L'échelle de couleur indique l'âge (BP) des archives. On remarque une disparité spatiale très importante avec des lacunes majeures sur les Océans Indien et Atlantique.

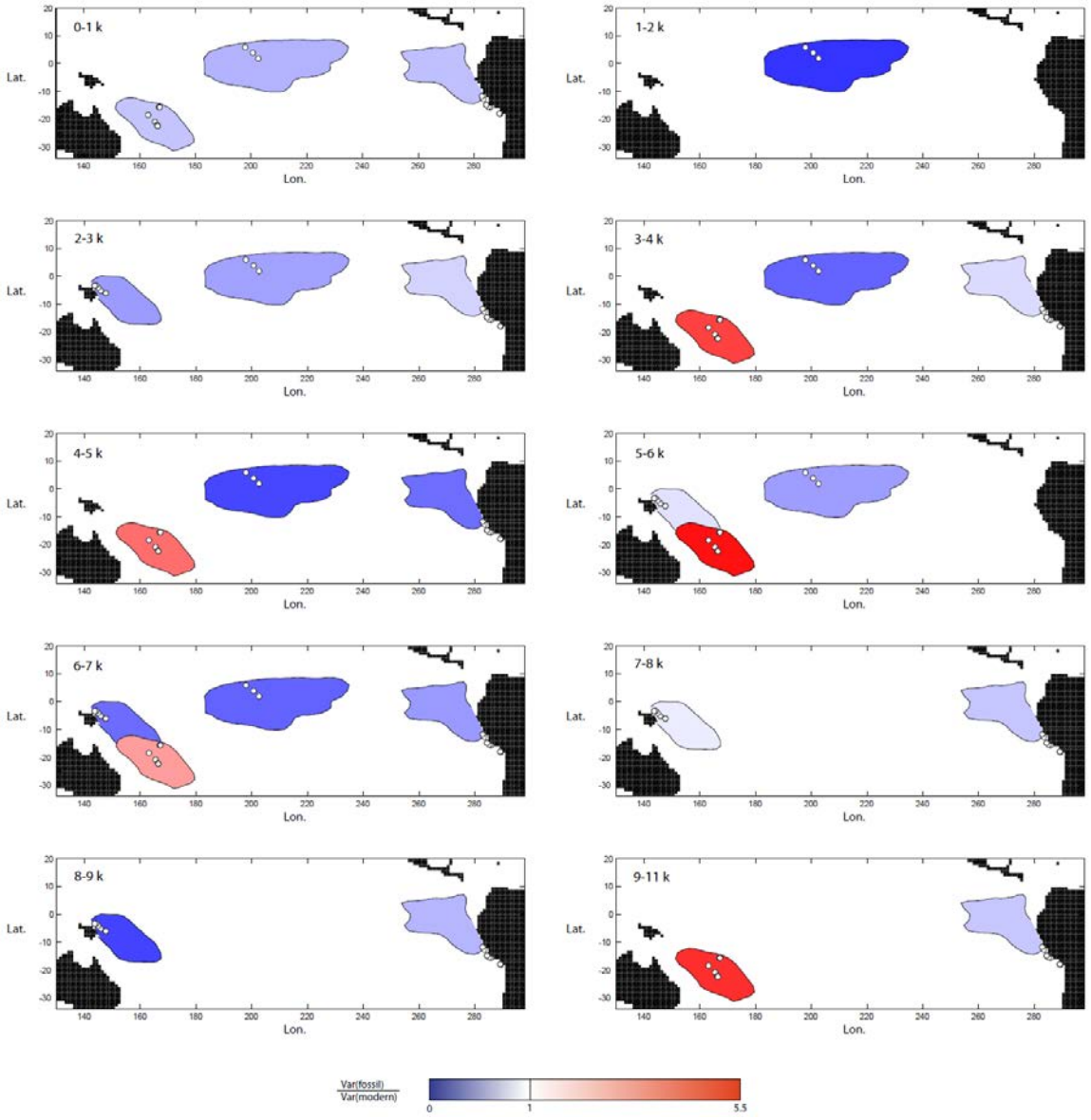

Figure 17. Variance interannuelle normalisée (couleur) reconstruite par des enregistrements de coraux et de coquilles sur 10 tranches de temps de 1000 ans. La répartition géographique des données permet de les diviser en 4 régions dont les contours sont ici définis par la zone où les anomalies de SST présentent un coefficient de détermination R^2>0.7 avec les anomalies de SST des sites d'étude.

Cette synthèse permet d'observer les disparités spatiales des changements de variabilité interannuelle du Pacifique tropical à l'Holocène. En regroupant les données paléoclimatiques en quatre zones (Pacifique Ouest, Sud-Ouest, Central, et Est) et par tranche de 1000 ans, il apparaît d'une part que la variance liée à l'ENSO était inférieure à l'actuelle dans tout le Pacifique équatorial, et d'autre part que la zone Sud-Ouest se comporte très différemment. La variabilité interannuelle dans cette région proche de la SPCZ (South Pacific Convergence Zone) était jusqu'à 5 fois supérieure à la variabilité actuelle avant 3 ka (Figure 17). Ceci suggère que la variabilité interannuelle de la SPCZ, en grande partie liée à l'ENSO aujourd'hui, était liée à d'autres mécanismes au cours de l'Holocène inférieur et moyen.

3.4. La variabilité multiséculaire de l'Hydroclimat du Sahel (projet SALOUM)

La mousson ouest Africaine (MOA) détermine l'écologie et l'économie d'un immense territoire, y compris le Sahel, particulièrement sensible à ses moindres fluctuations. Les précipitations liées à la MOA ont chuté de 30% dans le Sahel au cours des années 60, initiant une longue phase de sécheresse qui dura plus de 30 ans et provoqua des famines catastrophiques. Cette sécheresse représente à l'échelle globale le signal climatique multi-décennal le plus fort du 20ème siècle (IPCC, 2007). Le registre instrumental ne permet cependant pas de mesurer le caractère exceptionnel de cet évènement au regard de la variabilité naturelle. Le projet de recherche SALOUM au Sénégal a pour objectif de produire un enregistrement de 2000 ans des variations de la MOA, de sa saisonnalité et de sa variabilité interannuelle. La durée des saisons sèches et humides est un paramètre clé pour les écosystèmes et l'agriculture. Il n'existait jusqu'à présent aucune méthode paléoclimatique pour le reconstituer quantitativement en Afrique.

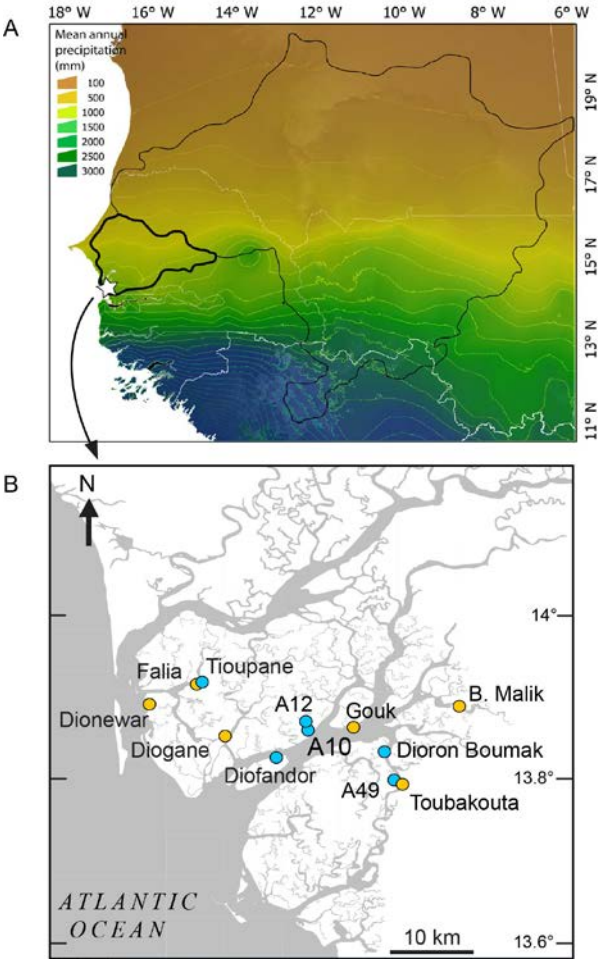

Figure 18. (A) Carte des précipitations annuelles moyennes dans la région du Sénégal (couleur), indiquant le bassin versant du Sénégal (ligne noire fine), celui du Sine-Saloum (ligne noire épaisse) et le site d'étude (étoile). (B) Carte du delta du Saloum montrant la position des sites de calibration (cercles jaunes) et les sites archéologiques échantillonnés et datés (cercles bleus).

Le potentiel unique du site du delta du Saloum pour réaliser ces objectifs tient à sa situation géographique au maximum du gradient latitudinal de précipitation et à son bassin versant réduit

(Figure 18A), qui en font un estuaire très sensible aux variations locales de la mousson. Cette sensibilité s'observe à l'échelle décennale par l'augmentation continue de la salinité de l'estuaire en réponse à la sécheresse des années 60 à 80 (Pagès et Citeau, 1990). Ces variations de salinité, peuvent être enregistrées par les rapports isotopiques de l'oxygène des coquilles fossiles de *Senilia senilis*, un bivalve très abondant sur les fonds sablo-vaseux de l'espace intermaréal du delta. Ces coquilles ont été collectées pendant des millénaires par les habitants de l'estuaire, formant de très nombreux amas coquilliers mesurant jusqu'à 15 m de hauteur et dispersés dans les iles à mangrove, parfois difficiles d'accès (Figure 18).

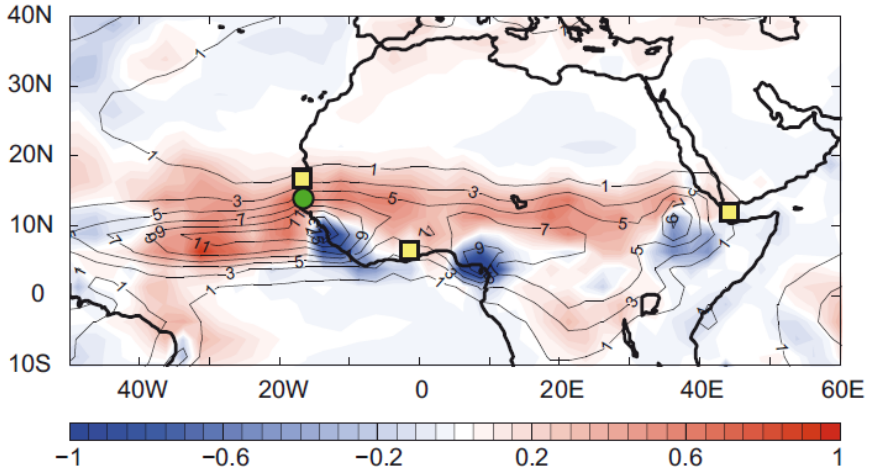

Figure 19. Régression linéaire entre la variabilité décennale des précipitations d'été (JAS) (1972-2012) sur le bassin du Saloum (cercle vert) et celles sur le reste du domaine (échelle de couleur). Les lignes noires indiquent les précipitations moyennes annuelles (mm/d). L'analyse montre une cohérence spatiale très forte avec l'ensemble de la bande Sahélienne (Wade et al., 2015). Les carré jaunes montrent la position de sites de comparaison des données paléoclimatiques, avec d'Ouest en Est : Carotte GeoB9501 (Mulitza et al., 2010), lac Bosumtwi (Shanahan et al., 2009), carotte P178-15 (Tierney et al., 2015a).

La cohérence spatiale des précipitations à diverses échelles de temps et leur lien avec les conditions océaniques a été étudiée par Malik Wade, postdoctorant au LPAO (Dakar), dans le but d'estimer l'extension géographique de la représentativité des variations de précipitations enregistrées dans le Delta du Saloum. Son analyse de régression montre une forte relation entre les précipitations sur le Saloum et celles de toute la bande Sahélienne aussi bien à l'échelle interannuelle qu'à l'échelle décennale (Figure 19). Si on émet l'hypothèse que cette relation est stationnaire aux échelles séculaires et millénaires, la remarquable cohérence spatiale des précipitations de cette région suggère que les variations hydrologiques passées reconstruites par l'analyse de ces amas coquilliers sont représentatives de l'ensemble du Sahel. Bien que certaines projections futures montrent des réponses différentes entre le Sahel central et l'ouest du Sahel (Biasutti, 2013), la très grande majorité des simulations actuelles et passées conserve la cohérence spatiale et la structure latitudinale caractéristique des précipitations du Sahel.

Nous avons produit un nouvel enregistrement des variations de condition d'aridité au cours des 1600 dernières années au Sénégal, à partir des valeurs isotopiques moyennes de 47 coquilles modernes et 114 coquilles fossiles provenant de 6 sites archéologiques du Sine-Saloum (figure 18B). En calculant un ensemble de moyennes mobiles construit à partir d'un ré-échantillonnage aléatoire des

incertitudes chronologiques et des incertitudes isotopiques, nous avons, à partir d'un jeu de données discontinu, calculé les variations continues multidécennales à séculaire de la distribution de probabilité du signal isotopique moyen (figure 20). Cette reconstruction montre une aridification abrupte du Sahel au cours des 200 dernières années. **Au regard de cette nouvelle perspective historique, les conditions actuelles apparaissent comme des conditions de sécheresse sans précédent au cours des 1600 dernières années**. La période la plus humide du dernier millénaire se situe de 1500 à 1800 A.D., soit lors de la période la plus froide du petit âge de glace.

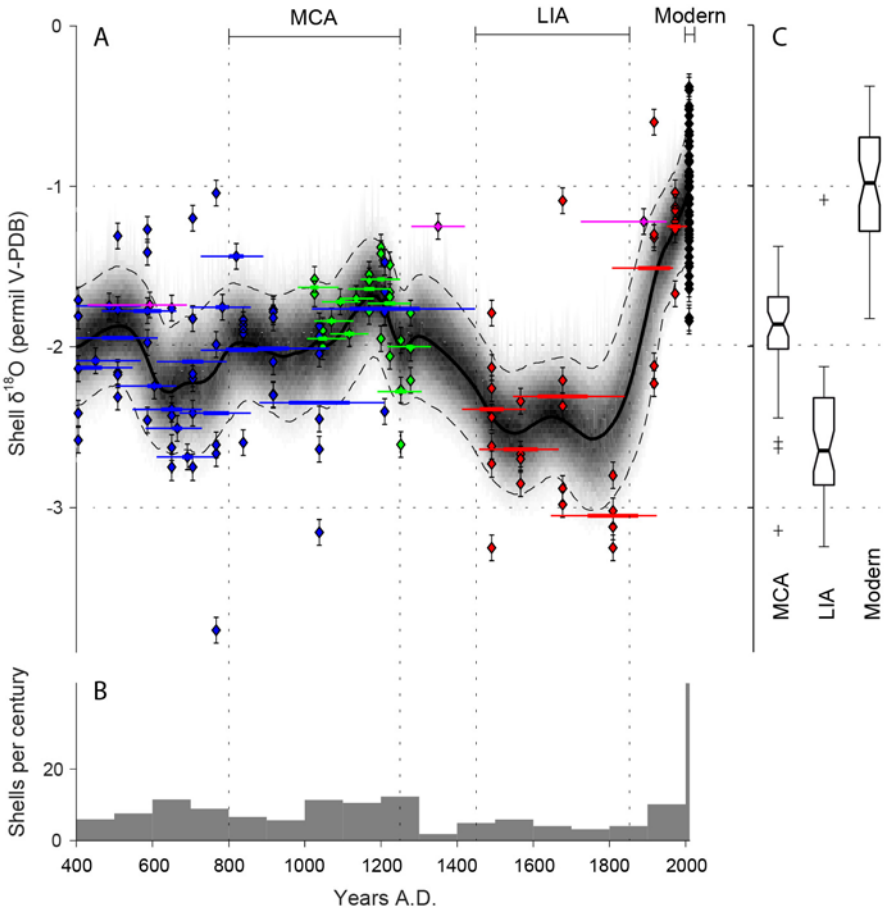

Figure 20. Variations des valeurs isotopiques de S. senilis au cours des 1600 dernières années dans le delta du Saloum. Les valeurs mesurées sur les coquilles individuelles (losanges, barres d'erreur ±2σ) modernes (noir), et des sites Diofandor (rouge), Tioupane (vert), Dioron Boumak (bleu), et A10, A12, A49 (rose), sont moyennées par niveau stratigraphique (barres horizontales). Les variations continues de la valeur moyenne de $\delta^{18}O$ sont indiquées par la distribution de probabilité (niveau de gris), la valeur médiane (ligne noire) et l'intervalle de confiance à 95% (pointillés). La représentativité statistique de l'échantillon au cours du temps est estimée par le nombre moyen de coquille par siècle (en bas), sachant que chaque coquille intègre les conditions environnementales sur une durée de 5 ans en moyenne.

Une corrélation forte et statistiquement significative avec les reconstructions de température de l'hémisphère nord (R^2=0.54 avec Moberg et al.(2005)) révèle un lien, direct ou indirect, entre le climat global et les précipitations au Sahel (figure 21). Un enregistrement très similaire obtenu à

partir d'une carotte marine du golfe d'Aden (Tierney et al., 2015a) suggère une cohérence spatiale sur toute la bande Sahélienne des variations de précipitation au cours des 1600 dernières années. Cette relation entre températures de l'hémisphère nord et l'hydroclimat du Sahel est opposée à celle observée à l'échelle multidécennale dans les interactions entre les précipitations au Sahel et l'AMO (Atlantic multidecadal oscillation) puisque les phases positives de l'AMO sont associées à des températures élevées de l'hémisphère nord et une augmentation des précipitations sur le Sahel (Folland et al. 1986; Giannini et al. 2003; Zhang and Delworth 2006; Mohino et al. 2011). Cette relation est également contradictoire par rapport aux observations faites dans d'autres régions tropicales qui suggèrent un déplacement vers le sud de la zone de convergence intertropicale (ITCZ) durant la période froide du petit âge de glace, réduisant ainsi les précipitations sur la partie nord de la zone intertropicale (Haug et al., 2001 ; Sachs et al., 2009 ; Bird et al., 2011 ; Yan et al., 2015). Les changements de latitude de la position moyenne de l'ITCZ, qui sont fréquemment invoqués pour expliquer les variations de précipitation dans les tropiques, ne peuvent donc pas expliquer la variabilité séculaire des précipitations au Sahel.

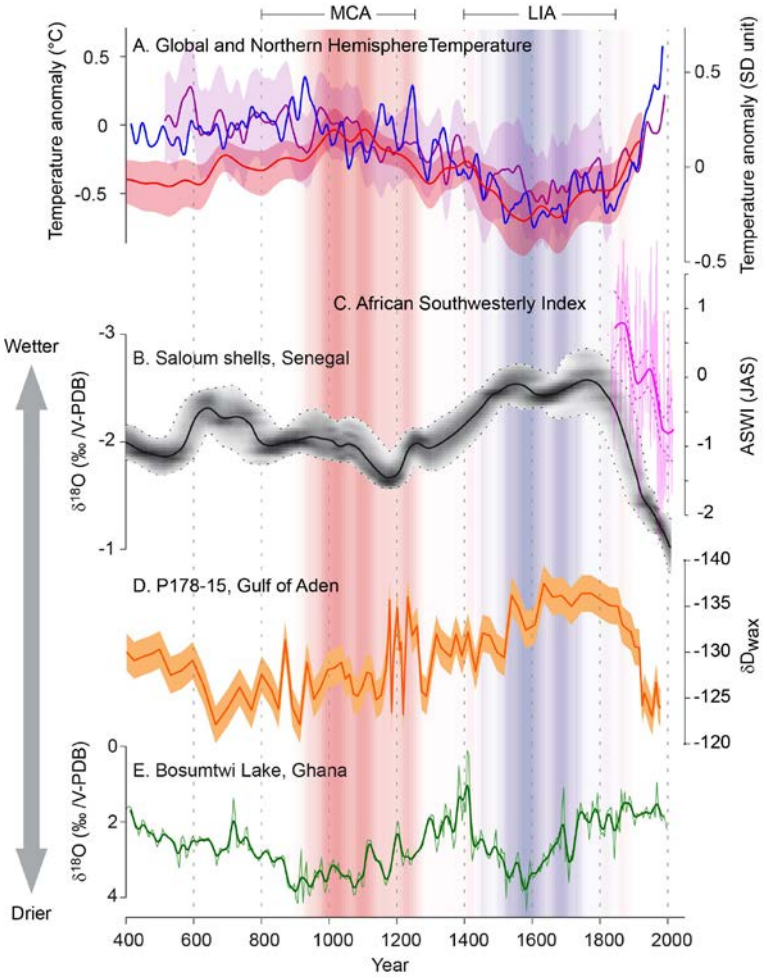

Figure 21. (A) Reconstructions des températures de l'hémisphère nord : Mann et al. (2009) (violet), Moberg et al., (2005) (rouge) et globales (Pages2K, 2013) (bleu). (B) Courbe isotopique du Saloum (notre étude), (C) African Southwesterly index, indicateur des précipitations de mousson sur le Sahel (Gallego et al., 2015), (D) Enregistrement du δD des alkanes dans les sédiments de la carotte P178-15 du Golfe d'Aden (Tierney et al., 2015). (E) $\delta^{18}O$ de la calcite des sédiments du lac Bosumtwi au Ghana (Shanahan et al., 2009). Les périodes

MCA et LIA sont indiquées dans la partie supérieure et les anomalies de température correspondantes respectivement chaudes et froides sont indiquées par des bandes verticales rouges et bleues.

L'aridification brutale des 200 dernières années et le fait que l'hydroclimat du Sahel soit sorti de la gamme de variabilité naturelle indiquent un impact anthropique sur les conditions hydroclimatiques du Sahel. En plus d'un effet anthropique lié au réchauffement global, il est probable qu'un impact anthropique ait eu lieu à l'échelle locale en raison d'un changement de l'usage des sols. En effet, Mulitza et al. (2010) ont montré que les flux de poussières atmosphériques au large du Sénégal avait augmenté de façon abrupte depuis 200 ans, indiquant une érosion éolienne accrue en raison du développement de l'agriculture industrielle. Ce changement de couvert végétal pourrait avoir contribué à la diminution des précipitations en perturbant la rétroaction positive végétation-précipitation.

Cette nouvelle perspective historique du climat du Sahel soutient les modèles qui prédisent un futur déclin des précipitations au Sahel avec le réchauffement global. Elle doit cependant encore être confirmée par de nouvelles reconstructions. Il reste également à déterminer comment les précipitations ont été affectées à l'échelle saisonnière à partir des enregistrements isotopiques de haute résolution des coquilles fossiles. Ces enregistrements nous permettront d'estimer la durée des saisons sèches et humides (figure 22).

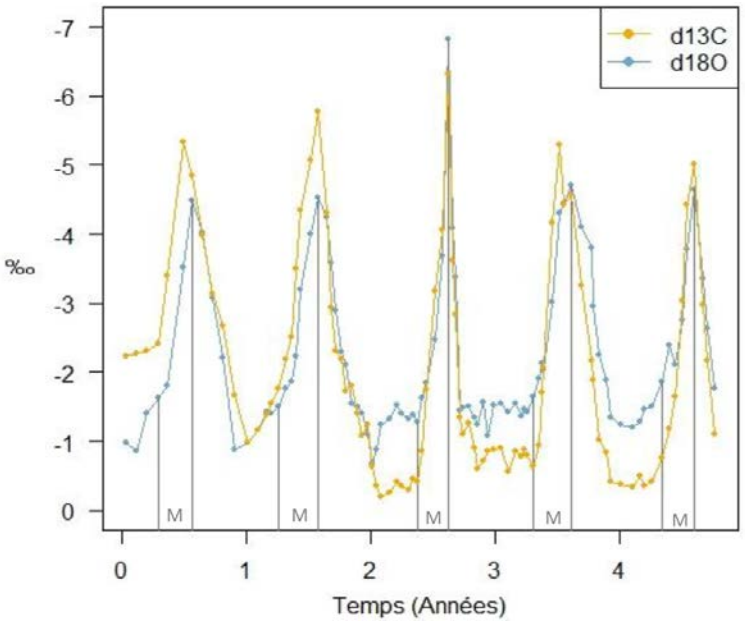

Figure 22. Profils isotopiques (carbone et oxygène) de la coquille DF-N4-1 sur un axe temporel reconstitué par l'analyse des lignes de croissance (sclérochronologie). Les périodes de mousson sont ici identifiées par les lignes verticales et les lettres « M ».

4- Programme de recherche

4.1. ENSO durant les périodes géologiques de réchauffement

Mes recherches sur l'histoire de l'ENSO se sont pour l'instant essentiellement concentrées sur la période Holocène, dont l'un des intérêts est d'estimer la variabilité millénaire de l'ENSO et de tester sa sensibilité aux changements d'insolation liés à la précession des équinoxes. Cela reste cependant insuffisant pour estimer la sensibilité de l'ENSO aux changements globaux et en particulier aux phases de réchauffement. Cette question, loin d'être encore résolue par les expériences de simulation, requiert des observations fiables et quantifiées sur une gamme de conditions globales beaucoup plus vaste. Mon objectif pour les prochaines années est d'utiliser le passé comme laboratoire naturel pour tester la sensibilité de l'ENSO en observant son comportement lors de plusieurs périodes de réchauffement global : (1) le réchauffement anthropique actuel par rapport aux deux derniers millénaires, (2) l'optimum climatique de l'Holocène moyen, (3) le stade isotopique 5e (125 ka), (4) le Pliocène (~5-3 Ma). Ces reconstructions seront principalement basées sur les registres isotopiques de bivalves fossiles de la côte péruvienne, couplés si possible par des indicateurs complémentaires, sédimentaires et faunistiques.

Les deux derniers millénaires

2018-2019 Financements : Concytec-Magnet : Postdoc Alexander Perez

Cette tâche, déjà entamée il y a quelques années à partir des coquilles fossiles du site de Pachacamac au Pérou, a été brièvement présentée dans la section 2.4. L'activité de l'ENSO dans le Pacifique Est sera estimée de façon statistique sur 4 périodes d'environ 200 ans distribuées entre 500 et 1500 A.D. et comparée au niveau d'activité actuel enregistré de manière identique par des coquilles modernes. La période clé du 16ème au 19ème siècle est malheureusement absente du registre fossile (sites archéologiques abandonnés suite à la conquête espagnole) et sera complétée par des reconstructions existantes basées sur des coraux (Tierney el al., 2015b), des archives historiques (Ortlieb, 2000), des sédiments marins (Rein et al., 2004), bien que ces dernières archives n'enregistrent que les anomalies de précipitation liées aux évènements chauds extrêmes.

Malgré ces limites nous espérons pouvoir reconstituer en partie la variabilité séculaire récente de l'ENSO dans le Pacifique Est et vérifier objectivement si la variabilité de l'ENSO observée au cours des dernières décennies est, ou non, statistiquement distincte de la variabilité préindustrielle des deux derniers millénaires. Une synthèse récente basée sur des cernes d'arbres et des coraux indique une augmentation importante de variabilité au 20ème siècle par rapport au 600 dernières années (McGregor et al., 2013) mais on ne sait pas clairement s'il s'agit d'un renforcement de la variabilité des SST ou à un renforcement de la réponse hydrologique d'ENSO.

Ce jeu de données préindustriel récent, en outre, représentera la période de contrôle pour évaluer les changements mesurés dans des périodes plus anciennes.

L'Holocène

2018-2022 Financements : ANR-Pacmedy Concytec-Magnet : posdoc Alexander Perez NSF (Kurt Rademaker) : thèse Master S. Gruver ERC (David Beresford Jones, soumis): thèse doctorat

Bien que les nouvelles observations que nous avons produites pour le Pacifique Est aient modifié profondément notre vision de la variabilité à long-terme de l'ENSO, ce registre reste trop discontinu pour déterminer la nature des transitions qui se sont produites en particulier à l'Holocène moyen. Les causes du minimum d'activité détecté entre 6 et 3 ka restent peu claires, et encore davantage celles qui auraient déterminé la phase dominée par El Niño Modoki vers 7 ka. D'innombrables sites archéologiques contenant des bivalves fossiles existent sur la côte du Pérou et pourraient permettre de combler les lacunes du registre pour s'approcher d'une reconstruction continue. Celle-ci permettrait alors des comparaisons avec des simulations transitoires de l'Holocène.

L'ENSO étant la principale cause des aléas climatiques sur la côte du Pérou, son histoire est également d'un intérêt primordial pour les archéologues pour comprendre les conditions environnementales de l'évolution des sociétés humaines dans cette région. La côté péruvienne est en effet l'un des 5 sites mondiaux qui ont vu l'apparition indépendante d'une transition néolithique. Nous étudierons, en collaboration avec des archéologues, l'ENSO du tardiglaciaire (13-10 ka) qui correspond aux premières occupations humaines (projet NSF, P.I. Kurt Rademaker, D. Sandweiss). Nous étudierons également la période qui précède la transition néolithique (8-5 ka) en collaboration avec David Beresford-Jones (ERC, soumis), et la transition néolithique elle-même en collaboration avec Ruth Shady à partir des restes du site de Caral, la plus ancienne cité d'Amérique (Shady Solis et al., 2001).

Dans le cadre du projet ANR/Blemont Forum Pacmedy (P.I. Pascale Braconnot), nous développerons les analyses de la variabilité spatio-temporelle de l'ENSO à l'Holocène à partir de la base de données présentée dans la section précédente, qui seront comparées aux simulations de la base PMIP3 et à de nouvelles simulations climatiques transitoires (6-0 ka).

L'ENSO au dernier interglaciaire

2018-2021, Financements: INSU-LEFE : collaboration avec Mary Elliot, Kevin Pedoja, Laurent Husson, Ioanna Bouloubassi, Dimitri Gutierrez, Renato Salvatecci Concytec-Magnet : postdoc Jorge Cardich, thèse de master Rolf Rivas, thèse de master de Juan Carlos Guerra

L'Eemien, qui correspond approximativement au stade isotopique marin 5e (MIS5e) (Sanchez-Goñi et al., 1999), représente la phase la plus chaude du dernier interglaciaire et s'étend environ de 130,000 à 116,000 ans BP (Kukla et al., 2002), une durée similaire à celle de l'Holocène. La température du stade 5e était environ 2°C plus élevée qu'aujourd'hui selon l'enregistrement isotopique de Vostok (Jouzel et al., 1987). Les températures de surface reconstituées dans les différents océans sont en général 2 à 4°C plus élevées au stade 5e (Leduc et al., 2010). Le niveau de la mer était de 4 à 6 m au-dessus du niveau actuel (Rohling et al., 2008). Les reconstructions de température à l'Est et à l'Ouest du Pacifique tropical (Lea et al., 2000) suggèrent des températures très élevées dans le Pacifique Est (+3-4°C) et un gradient Est-Ouest des SST fortement réduit, impliquant une circulation atmosphérique réduite et une situation moyenne de type El Niño (Contreras et al., 2010). Les conditions globales de l'Eemien possèdent donc les caractéristiques majeures du réchauffement global prédit dans un avenir proche. Pourtant, le climat chaud de l'Eemien ne fut pas la conséquence d'un effet de serre comme celui observé aujourd'hui, mais des variations orbitales d'insolation, si bien que la réponse de la variabilité climatique au stade 5e pourrait être différente de la réponse future. Bien que nous ne considérions pas le stade 5e comme un analogue direct des conditions futures, notre objectif est de fournir un contexte observationnel permettant de quantifier la gamme potentielle de variabilité du Pacifique tropical dans des conditions aux limites similaires en moyenne à celles attendues dans l'avenir. D'autre part, le stade 5e est caractérisé par un contraste saisonnier d'insolation similaire à celui de l'Holocène mais de plus grande amplitude, offrant ainsi les conditions expérimentales pour tester la sensibilité de l'ENSO aux paramètres orbitaux et ses liens avec le cycle saisonnier.
Les reconstructions au Pérou se baseront sur l'analyse de bivalves fossiles des terrasses marines côtières déposées lors du dernier interglaciaire et aujourd'hui émergées par l'activité tectonique. Nous analyserons également la carotte sédimentaire ODP686 qui présente de fines laminations sur quelques zones de l'Holocène et pour toute la partie du stade 5e (Brodie and Kemp, 1994). La variabilité interannuelle et decennale de la zone de minimum d'oxygène de la côte péruvienne sera estimée grâce aux profils de métaux (U, Mb) obtenus par XRF de très haute résolution. Sont également associés dans ce projet des collègues des universités de Nantes (Mary Elliott), de Caen (Kevin Pedoja) et de Grenoble (Laurent Husson) pour l'étude d'archives contemporaines (coraux et bivalves) situées de l'autre côté du Pacifique, sur les terrasses marines émergées de la péninsule de Huon en Papouasie nouvelle Guinée.
Nous tenterons d'autre part de calibrer les enregistrements isotopiques de bivalves de mangrove du nord du Pérou pour disposer d'une archive de la variabilité des précipitations côtières (thèse de master de Juan Carlos Guerra). Cette nouvelle archive nous permettrait de tester dans quelle mesure l'impact hydrologique des évènements El Niño est modulé par les conditions climatiques globales.

Le Pliocène

2018-2022, Financements : Concytec-Magnet : postdoc Diana Ochoa, Postdoc Rodolfo Salas Projet à soumettre en 2019/2020

Le Pliocène est, à l'échelle globale, une période de transition entre les climats chauds du tertiaire et les glaciations du quaternaire. Avec une concentration de CO_2 atmosphérique d'environ 400 ppm

(Pagani et al., 2010), cette période est aussi considérée comme le meilleur analogue passé du climat d'effet de serre actuel. Les causes profondes de la baisse progressive des températures globales au Pliocène restent mal comprises. L'activité tectonique de la côte Américaine a certainement eu un impact sur l'océan et le climat et aurait contribué à la mise en place du système de courants océaniques de Humboldt actuel. On suppose que la circulation océanique actuelle s'est installée avec le soulèvement de l'Isthme de Panama qui coupa la connexion entre les océans Pacifique et Atlantique, avec des conséquences climatiques à l'échelle globale (Haug et Tiedemann, 1998 ; Zachos et al, 2001). Cet évènement n'est cependant daté que de façon très approximative entre 10 et 3 Ma selon l'approche utilisée. Le climat Sud-Américain a été également profondément transformé par la surrection des Andes (Hartley, 2003). Celles-ci bloquent les précipitations venant du bassin amazonien et contribuent à l'aridité de la côte Ouest. Ce phénomène existait probablement déjà au Miocène moyen et s'est accentué au Miocène supérieur et au Pliocène. L'installation des conditions hyperarides du désert d'Atacama reste cependant sujette à débat. Elle est parfois datée du Pliocène (Hartley, 2003) mais certains auteurs soutiennent une hyperaridité beaucoup plus ancienne, antérieure à la surrection des Andes (Alpers and Brimhall, 1988 ; Dunai et al., 2005) ce qui suggèrerait un rôle secondaire de la tectonique et une influence plus déterminante des conditions marines. L'interaction est toutefois complexe puisque les expériences de modélisation ont montré que la surrection des Andes provoque une intensification de l'upwelling côtier et un refroidissement général du Pacifique Est, provoquant en retour une aridification du climat (Takahashi et al., 2007 ; Feng et al., 2014). Une hypothèse a même été avancée proposant que la surrection andine aurait pu être accentuée par une augmentation des contraintes de cisaillement dans la zone de subduction péruvienne à cause d'un fort déficit de sédimentation, c'est-à-dire forcée par l'aridité du climat (Lamb and Davis, 2003).

Il est clair que nous manquons d'observations paléoclimatiques robustes et bien datées pour contraindre les différents scénarios proposés. Les reconstructions de températures à partir des carottes sédimentaires marines montrent des températures plus élevées d'environ de 3 °C au début du Pliocène au large du Pérou et jusqu'à 9°C dans d'autres systèmes d'upwelling (Dekens et al., 2007) et une baisse progressive de ces températures au cours du Pliocène. De nombreux auteurs se sont penchés sur la dynamique du Pacifique au Pliocène. En comparant les reconstructions de SST entre l'Est et l'Ouest du Pacifique, Wara et al. (2005) reconstruisent un gradient zonal de température fortement réduit et l'hypothèse d'une situation de Niño permanent fut proposée (Fedorov et al., 2006). Les expériences de simulation climatique obtiennent une réduction de la circulation de Walker en moyenne, additionnée d'une variabilité interannuelle de type ENSO (Haywood et al., 2007 ; von der Heydt et al., 2011). Les seules données de variabilité existantes aujourd'hui proviennent de deux enregistrements coralliens des philippines (Watanabe et al., 2011) et de la variance des valeurs isotopiques de foraminifères de sédiments du Pacifique Est (Scroxton et al., 2011) et suggèrent toute l'existence d'une variabilité interannuelle de type ENSO dès le Pliocène.

Mon objectif est de fournir les premières reconstructions paléoclimatiques du Miocène supérieur et Pliocène de la côte Pacifique Sud-Américaine incluant des estimations du régime de précipitation, de l'activité de l'ENSO et ses impacts hydrologiques en conditions globales chaudes, et une caractérisation de l'activité saisonnière de l'upwelling côtier. Ces premières observations pourraient être obtenues au Pérou grâce aux fossiles de la Formation Pisco constituées de roches sédimentaires d'une mer épicontinentales du Miocène supérieur jusqu'au début du

Pléistocène. Les assemblages fauniques montrent au Pliocène une transition d'environnements de type tropical humide (crocodiles, mangroves) vers les conditions modernes froides caractéristiques de l'upwelling péruvien. Cette caractérisation de la transition océanographique et climatique vers le système de Humboldt moderne sera effectuée grâce à une étude multi-indicateurs des sédiments de la formation Pisco au Pérou, et en particulier grâce aux enregistrements isotopiques à haute résolution de bivalves fossiles de différentes écologies (de condition lagunaire pour une reconstruction des régimes de pluie, et de condition marine pour les SST). Des mesures de « clumped isotopes » (Δ47) sur les bivalves fourniront des estimations de paléotempérature indépendantes des hypothèses sur la composition isotopique de l'eau (Eiler, 2007). Les premières expéditions de terrain et d'échantillonnage ont été réalisées en 2017 et se poursuivent en 2018.

4.2. La Biodiversité du système de Humboldt

Une base de données de la biodiversité côtière

2018-2023 Financement s: Concytec-Magnet : Postdoc Juan Valqui

Le système de courants côtiers de Humboldt abrite un écosystème très productif d'une importance économique et sociale fondamentale. Pourtant, son étude est essentiellement limitée à celle de la biologie et de la dynamique de population de quelques espèces d'intérêt commercial. Les travaux et thèses de biologie marine sur les communautés intermaréales et submaréales sont rarement publiés et n'ont jamais fait l'objet d'une synthèse. Les bases de données existantes sont souvent limitées à une simple liste de taxons, dispersées et non accessibles à la communauté scientifique ou au public. Il est donc également impossible de faire des analyses statistiques sur ces données biologiques.

L'un des objectifs du projet Concytec-Magnet est de constituer une base de données relationnelle accessible en ligne regroupant toutes les observations disponibles de taxons côtiers (taxon, date, coordonnées, observateur, et informations connexes). Il s'agit avant tout de regrouper les observations dispersées dans divers instituts et dans la littérature grise et de la compléter avec des observations de nouvelles campagnes de terrain. Les deux principales difficultés sont d'une part d'obtenir l'accord et les conventions nécessaires des organismes partenaires, et d'autre part de vérifier l'homogénéité taxonomique des données compilées. La structure de la base de données est créée et celle-ci est actuellement alimentée par Juan Valqui, biologiste postdoc du projet Concytec-Magnet à l'UPCH, Lima.

L'objectif à long-terme de ce travail est de mettre à la disposition de la communauté scientifique un outil permettant de déterminer de façon objective et robuste la distribution des taxons et de suivre les variations temporelles de ces distributions. Cet outil nous permettra de caractériser les influences océanographiques, climatiques sur la répartition des espèces et la structure des communautés,

d'estimer l'impact du changement climatique et de l'acidification de l'océan, ainsi que l'impact anthropique direct sur la biodiversité côtière. Il s'agit de l'outil indispensable pour la connaissance et la gestion à long-terme de l'écosystème. L'objectif est aussi d'arriver à une standardisation des nouvelles observations et une alimentation systématique de la base de données de la part des instituts scientifiques locaux et internationaux qui étudient la biodiversité de la côté péruvienne. Après cette première étape, il sera également nécessaire d'élargir cette base de données à toute la côte Pacifique Sud-Américaine par des collaborations avec les groupes Chiliens et Equatoriens.

La première question que nous souhaitons résoudre à partir des premières données collectées est de déterminer comment l'ENSO qui représente 85% de la variabilité interannuelle dans cette région, façonne les communautés marines intermaréales, influence leur variabilité, oriente les stratégies adaptatives, et comment ces adaptations biologiques peuvent être mises à profit pour une gestion durable de l'écosystème et une meilleure résilience des communautés de pêcheurs.

Mise en place de l'écosystème moderne de Humboldt.

2018-2021 Financement s: Concytec-Magnet : Postdoc Rodolfo Salas, postdoc Diana Ochoa

Connaître réellement un écosystème signifie aussi connaître son histoire. Dans ce sous-projet de la ligne de recherche financée par Concytec-Magnet, notre objectif est de déterminer quand et comment les caractéristiques modernes du système océanographique de Humboldt et l'écosystème qui l'accompagne se sont mises en place. Ce projet accompagne évidemment l'objectif 4.1.4 qui vise à caractériser la transition climatique miocène-Pliocène. Ici, il s'agit d'étudier la transformation des communautés fossiles de vertébrés et d'invertébrés, de comprendre, par une analyse de l'espace morpho-fonctionnel de ces fossiles, dans quelle mesure ces transformations furent une réponse aux changements environnementaux de cette période. Les associations fossiles constituent également des indications sur le type d'environnement. Les signes d'une transition climatique au cours du Miocène-Pliocène viennent en effet d'abord de l'observation d'une transformation des communautés contenant au Miocène des espèces typiques d'environnements chauds et humides qui disparaissent pour laisser la place à des espèces caractéristiques des conditions froides et désertiques actuelles comme le lion de mer et le manchot.

La formation Pisco est constituée de roches sédimentaires marines peu profondes de la marge continentale de la côte centrale du Pérou (~14-16°S). Il s'agit d'une formation fossilifère d'une richesse exceptionnelle, particulièrement connue pour ses fossiles de cétacés (figure 23) d'une diversité et d'une qualité de préservation inégalée (de Muizon et DeVries, 1985). Sont également présents de nombreux fossiles de poissons, crocodiles, oiseaux, requins, mammifères marins (paresseux aquatiques, lions de mer), mollusques, microfossiles, permettant ainsi une caractérisation des communautés marines, des réseaux trophiques, et de l'histoire évolutive et phylogénétique associée. Les couches de cendre volcaniques sont relativement fréquentes et seront datées par la méthode U-Pb pour consolider la biostratigraphie par une chronologie absolue.

Figure 23. Baleine fossile, désert d'Ocucaje, Pérou .

4.3. Variabilité passée de la Mousson Ouest Africaine

Les deux derniers millénaires

2018-2020 Financements : ANR PACMEDY

Mon objectif à court terme est de finaliser le projet SALOUM en terminant la phase d'analyses de laboratoire pour (1) établir et valider une relation permettant la quantification des précipitations à partir des courbes isotopiques mensuelles de bivalves, (2) produire une histoire quantitative des changements de précipitation annuelle et de saisonnalité des précipitations pour les 2 derniers millénaires, (3) estimer les changements séculaires de variabilité interannuelle de la mousson, de fréquence des évènements extrêmes.

A moyen terme, je souhaite étudier en collaboration avec les climatologues du LOCEAN (Myriam Khodri, Juliette Mignot et Serge Janicot) les simulations climatiques du dernier millénaire de PMIP4 pour déterminer les mécanismes responsables de la variabilité séculaire des précipitations Sahélienne observée et identifier les principaux biais des modèles dans leur représentation de la variabilité séculaire des pluies du Sahel. L'objectif est également d'utiliser les enregistrements paléoclimatiques de la mousson au Sahel pour établir un critère d'évaluation des performances de ces modèles. La sélection des modèles les plus réalistes pourrait permettre de réduire l'incertitude

sur les prédictions futures des précipitations au Sahel, actuellement tellement larges qu'aucun scénario ne peut être privilégié. Ce travail serait l'objet d'un sujet de doctorat à proposer en 2019.

La fin de la période Africaine humide

2020-2023 Financements : projet à soumettre en 2019/2020

Le changement climatique et environnemental le plus marqué de l'Holocène s'est produit en Afrique lorsque la période Africaine humide de l'Holocène inférieur et moyen, caractérisée par une mousson nord-Africaine nettement renforcée et un couvert végétal sur la majeure partie du Sahara, s'est terminée par une aridification entre 6 et 4 ka vers des conditions proches de l'actuel (Lézine et al., 2011). La vitesse de cette transition reste le sujet d'un intense débat (DeMenocal et al., 2000 ; Kröpelin et al., 2008 ; Shanahan et al., 2015). Alors que des mécanismes de rétroaction avec la végétation sont invoqués pour expliquer une transition abrupte (Claussen et al., 1999), les enregistrements polliniques du Lac Yoa montrent au contraire une transition plutôt graduelle (Kröpelin et al., 2008). D'autre part, les reconstructions paléoclimatiques sont jusqu'à présent qualitatives, à l'exception d'une récente reconstruction basée sur les isotopes de l'hydrogène d'alkanes synthétisés par les plantes et préservés dans les sédiments marins (Tierney et al., 2017). Cependant, malgré de très grandes incertitudes, les auteurs proposent des précipitations atteignant 2000 mm au tardiglaciaire en Mauritanie incompatibles avec les évidences polliniques. Nous ne disposons toujours d'aucune estimation fiable du montant des précipitations au cours de la période Africaine humide, ce qui limite fortement les possibilités de validation modèle-données. Enfin, la dernière inconnue est la saisonnalité des précipitations.

Mon hypothèse est que la saisonnalité des précipitations est le paramètre qui permettra de résoudre les contradictions entre les différents types d'indicateurs et permettra également de contraindre l'éventail des mécanismes responsables de la fin de la période Africaine humide. En effet, aucun des indicateurs paléoclimatiques utilisés ne possède la résolution temporelle pour résoudre la saisonnalité des pluies. Les changements environnementaux observés sont donc tous interprétés dans un schéma climatique supposant une saisonnalité similaire à l'actuelle, une hypothèse peu vraisemblable à l'échelle de l'Holocène.

Il existe au Sénégal des terrasses marines datant de la dernière transgression marine du Nouakchottien, datée d'environ 5 à 7 ka, une période qui correspond à la fin de la période humide Africaine (Michel et al., 1967 ; Faure et al., 1980). J'ai collecté en 2014 dans ces niveaux des échantillons de coquilles de *Senilia senilis* dont les dates ^{14}C ont confirmé qu'elles appartenaient à cette période (Figure 24). Des dépôts similaires sont également disponibles en Mauritanie permettant ainsi une vision latitudinale, nécessaire pour contraindre les mouvements de l'ITCZ.

Comme pour les derniers siècles, cette espèce offre la possibilité d'estimer la durée des saisons sèches et humides et la variabilité interannuelle. La quantification des précipitations sera plus incertaine en raison de changements profonds de la géomorphologie côtière qui affectent la relation entre salinité et précipitation. L'objectif principal sera de tester l'hypothèse que la fin de la période

Africaine humide a été liée à une augmentation de la saisonnalité des précipitations, passant d'un régime de pluie d'avantage étalé sur l'année au régime actuel de précipitations intenses, érosives, et concentrées sur 3 à 4 mois. L'apparition d'une saison sèche très longue aurait été responsable du changement de végétation, de l'aridification, et de l'augmentation des flux sédimentaires. Nous testerons cette hypothèse en appliquant la même méthode que celle utilisée pour les coquilles plus récentes. Ce travail pourra faire l'objet d'un projet de doctorat en 2020.

Figure 24. Terrasse marine contenant des coquilles fossiles de *Senilia senilis*, dans la région de St Louis au Sénégal. Le dépôt est daté d'environ 6000 ans BP.

Références bibliographiques

Alpers, C. N., and G. H. Brimhall (1988), Middle Miocene climatic change in the Atacama Desert, northern Chile: Evidence from supergene mineralization at La Escondida, *Geological Society of America Bulletin*, *100*, 1640-1656.

Ashok, K., S. K. Behera, S. A. Rao, H. Weng, and T. Yamagata (2007), El Niño Modoki and its possible teleconnection, *J. Geophys. Res.*, *112*, C11007, doi:10.1029/2006JC003798

Ashok, K., and T. Yamagata (2009), The El Niño with a difference, *Nature*, *461*, 481-484.

Azzoug, M., M. Carré, and A. J. Schauer (2012a), Reconstructing the duration of the West African Monsoon season from growth patterns and isotopic signals of shells of Anadara senilis (Saloum Delta, Senegal), *Palaeogeography, Palaeoclimatology, Palaeoecology*, *346-347*, 145-152.

Azzoug, M., M. Carré, B. M. Chase, A. Deme, A. Lazar, C. E. Lazareth, A. J. Schauer, M. Mandeng-Yogo, M. Simier, A. Thierno-Gaye, and L. T. de Morais (2012b), Positive precipitation-evaporation budget from AD 460 to 1090 in the Saloum Delta (Senegal) indicated by mollusk oxygen isotopes, *Global and Planetary Change*, *98-99*, 54-62.

Biasutti, M. (2013), Forced Sahel rainfall trends in the CMIP5 archive, *Journal of Geophysical Research: Atmospheres*, *118*, 1613-1623, doi:10.1002/jgrd.50206.

Bird, B. W., M. B. Abbott, M. Vuille, D. T. Rodbell, N. D. Stansell, and M. F. Rosenmeier (2011), A 2,300-year-long annually resolved record of the South American summer monsoon from the Peruvian Andes, *Proc. Natl Acad. Sci. USA*, *108*, 8583-8588, doi:10.1073/pnas.1003719108.

Braconnot, P., Y. Luan, S. Brewer, and W. Zheng (2012), Impact of Earth's orbit and freshwater fluxes on Holocene climate mean seasonal cycle and ENSO characteristics, *Climate Dynamics*, *38*, 1081-1092, doi:10.1007/s00382-011-1029-x

Brodie, I., and A. E. S. Kemp (1994), Variation in biogenic and detrital fluxes and formation of laminae in late Quaternary sediments from the Peruvian coastal upwelling zone, *Marine Geology*, *116*, 385-398.

Brown, J., M. Collins, A. Tudhope, and T. Toniazzo (2008), Modelling mid-Holocene tropical climate and ENSO variability: towards constraining predictions of future change with palaeo-data, *Climate Dynamics*, *30*, 19-36.

Cai, W., S. Borlace, M. Lengaigne, P. van Rensch, M. Collins, G. Vecchi, A. Timmermann, A. Santoso, M. J. McPhaden, L. Wu, M. H. England, G. Wang, E. Guilyardi, and F.-F. Jin (2014), Increasing frequency of extreme El Nino events due to greenhouse warming, *Nature Clim. Change*, *4*, 111-116, doi:10.1038/nclimate2100.

Cane, M. A., and S. E. Zebiak (1985), A Theory for El Niño and the Southern Oscillation, *Science*, *228*, 1085-1087, doi:10.1126/science.228.4703.1085.

Cane, M. A., S. E. Zebiak, and S. C. Dolan (1986), Experimental forecasts of El Niño, *Nature*, *321*, 827.

Carré, M., J. P. Sachs, J. M. Wallace, and C. Favier (2012a), Exploring errors in paleoclimate proxy reconstructions using Monte Carlo simulations: paleotemperature from mollusk and coral geochemistry, *Climate of the Past*, *8*, 433-450, doi:10.5194/cp-8-433-2012.

Carré, M., M. Azzoug, I. Bentaleb, B. M. Chase, M. Fontugne, D. Jackson, M.-P. Ledru, A. Maldonado, J. P. Sachs, and A. J. Schauer (2012b), Mid-Holocene mean climate in the south-eastern Pacific and its influence on South America, *Quaternary International*, *253*, 55-66, doi:10.1016/j.quaint.2011.02.004.

Carré, M., I. Bentaleb, D. Blamart, N. Ogle, F. Cardenas, S. Zevallos, R. M. Kalin, L. Ortlieb, and M. Fontugne (2005), Stable isotopes and sclerochronology of the bivalve Mesodesma donacium:

potential application to peruvian paleoceanographic reconstructions, *Palaeogeography, Palaeoclimatology, Palaeoecology*, *228*, 4-25.

Carré, M., J. P. Sachs, S. Purca, A. J. Schauer, P. Braconnot, R. Angeles Falcón, M. Julien, and D. Lavallée (2014), Holocene history of ENSO variance and asymmetry in the eastern tropical Pacific, *Science*, *345*, 1045-1048, doi:10.1126/science.1252220.

Carré, M., J. P. Sachs, A. J. Schauer, W. E. Rodríguez, and F. C. Ramos (2013), Reconstructing El Niño-Southern Oscillation activity and ocean temperature seasonality from short-lived marine mollusk shells from Peru, *Palaeogeography, Palaeoclimatology, Palaeoecology*, *371*, 45-53.

Clement, A. C., R. Seager, and M. A. Cane (1999), Orbital controls on the El Niño/Southern Oscillation and the tropical climate, *Paleoceanography*, *14*, 441-456.

Clement, A. C., R. Seager, and M. A. Cane (2000), Suppression of El Niño during the mid-Holocene by changes in earth's orbit., *Paleoceanography*, *15*, 731-737.

Cobb, K. M., N. Westphal, H. R. Sayani, J. T. Watson, E. Di Lorenzo, H. Cheng, R. L. Edwards, and C. D. Charles (2013), Highly Variable El Niño-Southern Oscillation Throughout the Holocene, *Science*, *339*, 67-70, doi:10.1126/science.1228246.

Collins, M., S.-I. An, W. Cai, A. Ganachaud, E. Guilyardi, F.-F. Jin, M. Jochum, M. Lengaigne, S. Power, A. Timmermann, G. Vecchi, and A. Wittenberg (2010), The impact of global warming on the tropical Pacific Ocean and El Nino, *Nature Geosci*, *3*, 391-397, doi:10.1038/ngeo868

Contreras, S., C. B. Lange, S. Pantoja, G. Lavik, D. Rincón-Martínez, and M. M. M. Kuypers (2010), A rainy northern Atacama Desert during the last interglacial, *Geophysical Research Letters*, *37*, L23612, doi:10.1029/2010GL045728

De Muizon, C., and T. J. De Vries (1985), Geology and paleontology of late Cenozoic marine deposits in the Sacaco area (Peru), *Geologische Rundschau*, *74*, 547-563.

Dekens, P. S., A. C. Ravelo, and M. D. McCarthy (2007), Warm upwelling regions in the Pliocene warm period, *Paleoceanography*, *22*, PA3211, doi:10.1029/2006PA001394.

deMenocal, P., J. Ortiz, T. Guilderson, J. Adkins, M. Sarnthein, L. Baker, and M. Yarusinski (2000), Abrupt onset and termination of the African humid period: rapid climate response to gradual insolation forcing, *Quaternary Science Reviews*, *19*, 347-361.

Dewitte, B., J. Vazquez-Cuervo, K. Goubanova, S. Illig, K. Takahashi, G. Cambon, S. Purca, D. Correa, D. Gutierrez, A. Sifeddine, and L. Ortlieb (2012), Change in El Niño flavours over 1958-2008: Implications for the long-term trend of the upwelling off Peru, *Deep Sea Research Part II: Topical Studies in Oceanography*, *77-80*, 143-156.

Dunai, T. J., G. A. G. Lopez, and J. Juez-Larré (2005), Oligocene-Miocene age of aridity in the Atacama Desert revealed by exposure dating of erosion-sensitive landforms, *Geology*, *33*, 321-324.

Eiler, J. M. (2007), "Clumped-isotope" geochemistry—The study of naturally-occuring, multiply-substituted isotopologues, *Earth and Planetary Science Letters*, *262*, 309-327.

Emile-Geay, J., K. M. Cobb, M. Carre, P. Braconnot, J. Leloup, Y. Zhou, S. P. Harrison, T. Correge, H. V. McGregor, M. Collins, R. Driscoll, M. Elliot, B. Schneider, and A. Tudhope (2016), Links between tropical Pacific seasonal, interannual and orbital variability during the Holocene, *Nature Geosci*, *9*, 168-173, doi:10.1038/ngeo2608.

Epstein, S., R. Buchsbaum, H. A. Lowenstam, and H. C. Urey (1953), Revised carbonate-water isotopic temperature scale, *Bulletin of the Geological Society of America*, *64*, 1315-1326.

Faure, H., J. C. Fontes, L. Hebrard, J. Monteillet, and P. A. Pirazzoli (1980), Geoidal Change and Shore-Level Tilt Along Holocene Estuaries: Senegal River Area, West Africa, *Science*, *210*, 421-423, 10.1126/science.210.4468.421.

Fedorov, A. V., P. S. Dekens, M. McCarthy, A. C. Ravelo, P. B. deMenocal, M. Barreiro, R. C. Pacanowski, and S. G. Philander (2006), The Pliocene Paradox (Mechanisms for a Permanent El Niño), *Science*, *312*, 1485-1489, doi:10.1126/science.1122666.

Feng, R., and C. J. C. P. A. Poulsen (2014), Andean elevation control on tropical Pacific climate and ENSO, *Paleoceanography*, *29*, 795-809, doi:10.1002/2014PA002640

Fleitmann, D., S. J. Burns, M. Mudelsee, U. Neff, J. Kramers, A. Mangini, and A. Matter (2003), Holocene forcing of the Indian monsoon recorded in a stalagmite from southern Oman, *Science*, *300*, 1737-1739.

Folland, C. K., T. N. Palmer, and D. E. Parker (1986), Sahel rainfall and worldwide sea temperatures, 1901-85, *Nature*, *320*, 602-607.

Gallego, D., P. Ordóñez, P. Ribera, C. Peña-Ortiz, and R. García-Herrera (2015), An instrumental index of the West African Monsoon back to the nineteenth century, *Q. J. R. Meteorol. Soc.*, *141*, 3166-3176, doi:10.1002/qj.2601

Giannini, A., R. Saravanan, and P. Chang (2003), Oceanic forcing of Sahel rainfall on interannual to interdecadal time scales, *Science*, *302*, 1027-1030.

Grossman, E. L., Ku, Teh-Lung (1986), Oxygen and carbon fractionation in biogenic aragonite: temperature effect, *Chemical Geology*, *59*, 59-74.

Guilyardi, E. (2006), El Niño-mean state-seasonal cycle interactions in a multi-model ensemble, *Climate Dynamics*, *26*, 329-348.

Guilyardi, E., A. Wittenberg, A. Fedorov, M. Collins, C. Wang, A. Capotondi, G. J. van Oldenborgh, and T. Stockdale (2009), Understanding El Niño in Ocean-Atmosphere General Circulation Models: Progress and Challenges, *Bulletin of the American Meteorological Society*, *90*, 325-340.

Hartley, A. (2003), Andean uplift and climate change, *Journal of the Geological Society*, *160*, 7-10, doi:10.1144/0016-764902-083.

Haug, G. H., K. A. Hughen, D. M. Sigman, L. C. Peterson, and U. Röhl (2001), Southward migration of the intertropical convergence zone through the Holocene, *Science*, *293*, 1304-1308.

Haug, G. H., and R. Tiedemann (1998), Effect of the formation of the isthmus of Panama on Atlantic Ocean thermohaline circulation, *Nature*, *393*, 673-676.

Haywood, A. M., P. J. Valdes, and V. L. Peck (2007), A permanent El Niño–like state during the Pliocene?, *Paleoceanography*, *22*, PA1213, doi:10.1029/2006PA001323

Hughes, M., and C. Ammann (2009), The future of the past—an earth system framework for high resolution paleoclimatology: editorial essay, *Climatic Change*, *94*, 247-259.

IPCC (2007), *Climate change 2007: The Physical Science Basis. Contribution of Working Group I to the Fourth Assessment Report of the Intergovernmental Panel on Climate Change (IPCC)*, 1009 pp., Cambridge University Press.

Joussaume, S., K. E. Taylor, P. Braconnot, J. F. B. Mitchell, J. E. Kutzbach, S. P. Harrison, I. C. Prentice, A. J. Broccoli, A. Abe-Ouchi, P. J. Bartlein, C. Bonfils, B. Dong, J. Guiot, K. Herterich, C. D. Hewitt, D. Jolly, J. W. Kim, A. Kislov, A. Kitoh, M. F. Loutre, V. Masson, B. McAvaney, N. McFarlane, N. de Noblet, W. R. Peltier, J. Y. Peterscmitt, D. Pollard, D. Rind, J. F. Royer, M. E. Schlesinger, J. Syktus, S. Thompson, P. Valdes, G. Vettoretti, R. S. Webb, and U. Wyputta (1999), Monsoon changes for 6000years ago: results of 18 simulations from the Paleoclimate Modeling Intercomparison Project (PMIP), *Geophysical Research Letters*, *26*, 859-862.

Jouzel, J., C. Genthon, C. Lorius, J. R. Petit, and N. I. Barkov (1987), Vostok ice core-A continuous isotope temperature record over the last climatic cycle (160,000 years), *Nature*, *329*, 403-408.

Kao, H.-Y., and J.-Y. Yu (2009), Contrasting Eastern-Pacific and Central-Pacific Types of ENSO, *Journal of Climate*, *22*, 615-632.

Killingley, J. S., and W. H. Berger (1979), Stable isotopes in a mollusk shell: Detection of Upwelling events, *Science*, *205*, 186-188.

Koutavas, A., and S. Joanides (2012), El Niño–Southern Oscillation extrema in the Holocene and Last Glacial Maximum, *Paleoceanography*, *27*, doi: 10.1029/2012PA002378.

Koutavas, A., J. Lynch-Stieglitz, T. M. Marchitto Jr., and J. P. Sachs (2002), El Niño-like pattern in ice age tropical sea surface temperature, *Science*, *297*, 226-230.

Kröpelin, S., D. Verschuren, A.-M. Lézine, H. Eggermont, C. Cocquyt, P. Francus, J.-P. Cazet, M. Fagot, B. Rumes, J. M. Russell, F. Darius, D. J. Conley, M. Schuster, H. von Suchodoletz, and D. R. Engstrom (2008), Climate-driven ecosystem succession in the Sahara: The past 6000 years, *Science*, *320*, 765-768.

Kukla, G. J., M. L. Bender, J.-L. de Beaulieu, G. Bond, W. S. Broecker, P. Cleveringa, J. E. Gavin, T. D. Herbert, J. Imbrie, J. Jouzel, L. D. Keigwin, K.-L. Knudsen, J. F. McManus, J. Merkt, D. R. Muhs, H. Müller, R. Z. Poore, S. C. Porter, G. Seret, N. J. Shackleton, C. Turner, P. C. Tzedakis, and I. J. Winograd (2002), Last Interglacial Climates, *Quaternary Research*, *58*, 2-13.

Lamb, S., and P. Davis (2003), Cenozoic climate change as a possible cause for the rise of the Andes, *Nature*, *425*, 792-797.

Lavallée, D., and M. Julien (2012), *Prehistoria de la costa extremo-Sur del Perú. Los Pescadores arcaicos de la quebrada de los Burros (10000 - 7000 a.P.)*, 478 pp., Travaux de l'Institut Français d'Etudes Andines, Lima.

Lavallée, D., M. Julien, P. Béarez, A. Bolaños, M. Carré, A. Chevalier, T. Delabarde, M. Fontugne, C. Rodríguez-Loredo, L. Klaric, P. Usselmann, and M. Vanhaeren (2011), Quebrada de los burros. Los primeros pescadores del litoral Pacífico en el extremo sur peruano, *Chungara, Revista de Antropología Chilena*, *43*, 333-351.

Lea, D. W., D. K. Pak, and H. J. Spero (2000), Climate impact of late Quaternary equatorial Pacific sea surface temperature variations, *Science*, *289*, 1719-1724.

Leduc, G., R. Schneider, J. H. Kim, and G. Lohmann (2010), Holocene and Eemian sea surface temperature trends as revealed by alkenone and Mg/Ca paleothermometry, *Quaternary Science Reviews*, *29*, 989-1004.

Lee, T., and M. J. McPhaden (2010), Increasing intensity of El Niño in the central-equatorial Pacific, *Geophys. Res. Lett.*, *37*, L14603, doi:10.1029/2010GL044007

Lézine, A.-M., C. Hély, C. Grenier, P. Braconnot, and G. Krinner (2011), Sahara and Sahel vulnerability to climate changes, lessons from Holocene hydrological data, *Quaternary Science Reviews*, *30*, 3001-3012.

Mann, M. E., Z. Zhang, S. Rutherford, R. S. Bradley, M. K. Hughes, D. T. Shindell, C. Ammann, G. Faluvegi, and F. Ni (2009), Global signatures and dynamical origins of the Little Ice Age and Medieval Climate Anomaly, *Science*, *236*, 1256-1260.

McCrea, J. M. (1950), On the isotopic chemistry of carbonates and a paleotemperature scale, *The Journal of Chemical Physics*, *18*, 849-857.

Michel, P., P. Elouard, and H. Faure (1967), Nouvelles recherches sur le quaternaire récent de la région de Saint-Louis (Sénégal), Laboratoire de Géologie de la Faculté des Sciences de l'Université de Dakar, Dakar.

Moberg, A., D. M. Sonechkin, K. Holmgren, N. M. Datsenko, and W. Karlén (2005), Highly variable northern hemisphere temperatures reconstructed from low- and high-resolution proxy data, *Nature*, *433*, 613-617.

Mohino, E., S. Janicot, and J. Bader (2011), Sahel rainfall and decadal to multi-decadal sea surface temperature variability, *Climate Dynamics*, *37*, 419-440, doi:10.1007/s00382-010-0867-2.

Mulitza, S., D. Heslop, D. Pittauerova, H. W. Fischer, I. Meyer, J.-B. Stuut, M. Zabel, G. Mollenhauer, J. A. Collins, H. Kuhnert, and M. Schulz (2010), Increase in African dust flux at the onset of commercial agriculture in the Sahel region, *Nature*, *466*, 226-228, 10.1038/nature09213.

Ortlieb, L. (2000), The documented historical record of El Niño events in Peru: an update of the Quinn record (sixteenth through nineteenth century), in *El Niño and the Southern Oscillation, multiscale variability and global and regional impacts*, edited by H. F. Diaz and V. Makgraf, pp. 207-295, Cambridge University Press, Cambridge.

Pagani, M., Z. Liu, J. LaRiviere, and A. C. Ravelo (2010), High Earth-system climate sensitivity determined from Pliocene carbon dioxide concentrations, *Nature Geosci*, *3*, 27-30, doi:10.1038/ngeo724.

Pagès J, Citeau J (1990), Rainfall and salinity of a Sahelian estuary between 1927 and 1987. *Journal of Hydrology, 113*, 325-341.

PAGES-2k (2013), Continental-scale temperature variability during the past two millennia, *Nature Geosci*, *6*, 339-346, doi:10.1038/ngeo1797.

Rein, B. (2007), How do the 1982/83 and 1997/98 El Niños rank in a geological record from Peru?, *Quaternary International*, *161*, 56-66.

Rein, B., A. Lückge, and F. Sirocko (2004), A major Holocene ENSO anomaly during the Medieval period, *Geophysical Research Letters*, *31*, doi:10.1029/2004GL020161.

Rhoads, D. C., and R. A. Lutz (1980), *Skeletal growth of aquatic organisms*, Plenum Press, New York.

Rodbell, D. T., G. O. Seltzer, D. M. Anderson, M. B. Abbott, D. B. Enfield, and J. H. Newman (1999), An ~15,000-year record of el nino driven alluviation in southwestern Ecuador, *Science*, *283*, 516-520.

Rodbell, D. T., G. O. Seltzer, B. G. Mark, J. A. Smith, and M. B. Abbott (2008), Clastic sediment flux to tropical Andean lakes: records of glaciation and soil erosion, *Quaternary Science Reviews*, *27*, 1612-1626.

Rohling, E. J., K. Grant, C. Hemleben, M. Siddall, B. A. A. Hoogakker, M. Bolshaw, and M. Kucera (2008), High rates of sea-level rise during the last interglacial period, *Nature Geosci*, *1*, 38-42.

Sachs, J. P., D. Sachse, R. H. Smittenberg, Z. Zhang, D. S. Battisti, and S. Golubic (2009), Southward movement of the Pacific intertropical convergence zone A.D. 1400-1850, *Nature Geoscience*, *2*, 519-525.

Sadler, J., M. Carré, M. Azzoug, A. J. Schauer, J. Ledesma, F. Cardenas, B. M. Chase, I. Bentaleb, S. D. Muller, M. Mandeng, E. J. Rohling, and J. P. Sachs (2012), Reconstructing past upwelling intensity and the seasonal dynamics of primary productivity along the Peruvian coastline from mollusk shell stable isotopes, *Geochem. Geophys. Geosyst.*, *13*, Q01015, doi:10.1029/2011GC003595.

Sánchez Goñi, M. F., F. Eynaud, J. L. Turon, and N. J. Shackleton (1999), High resolution palynological record off the Iberian margin: direct land-sea correlation for the Last Interglacial complex, *Earth and Planetary Science Letters*, *171*, 123-137.

Scroxton, N., S. G. Bonham, R. E. M. Rickaby, S. H. F. Lawrence, M. Hermoso, and A. M. C. P. Haywood (2011), Persistent El Niño–Southern Oscillation variation during the Pliocene Epoch, *Paleoceanography*, *26*, doi:10.1029/2010PA002097.

Shackleton, N. J. (1973), Oxygen isotope analysis as a means of determining season of occupation of prehistoric midden sites, *Archaeometry*, *15*, 133-141.

Shady Solis, R. S., J. Haas, and W. Creamer (2001), Dating Caral, a preceramic site in the Supe Valley on the Central Coast of Peru, *Science*, *292*, 723-726.

Shanahan, T. M., N. P. McKay, K. A. Hughen, J. T. Overpeck, B. Otto-Bliesner, C. W. Heil, J. King, C. A. Scholz, and J. Peck (2015), The time-transgressive termination of the African Humid Period, *Nature Geosci*, *8*, 140-144, doi:10.1038/ngeo2329.

Sulca, J., K. Takahashi, J.-C. Espinoza, M. Vuille, and W. Lavado-Casimiro (2018), Impacts of different ENSO flavors and tropical Pacific convection variability (ITCZ, SPCZ) on austral summer rainfall in South America, with a focus on Peru, *International Journal of Climatology*, *38*, 420-435, doi:10.1002/joc.5185

Takahashi, K. (2005), The annual cycle of heat content in the Peru current region, *Journal of Climate*, *18*, 4937-4954.

Takahashi, K., and D. S. Battisti (2007), Processes controlling the mean tropical Pacific precipitation pattern: I. The Andes and the Eastern Pacific ITCZ, *Journal of Climate*, *20*, 3434-3451, doi:10.1175/JCLI4198.1.

Takahashi, K., A. Montecinos, K. Goubanova, and B. Dewitte (2011), ENSO regimes: Reinterpreting the canonical and Modoki El Niño, *Geophys. Res. Lett.*, *38*, doi:10.1029/2011GL047364.

Tierney, J. E., C. C. Ummenhofer, and P. B. deMenocal (2015a), Past and future rainfall in the Horn of Africa, *Science Advances*, *1*, doi:10.1126/sciadv.1500682.

Tierney, J. E., N. J. Abram, K. J. Anchukaitis, M. N. Evans, C. Giry, K. Halimeda Kilbourne, C. P. Saenger, H. C. Wu, and J. Zinke (2015b), Tropical sea-surface temperatures for the past four centuries reconstructed from coral archives, *Paleoceanography*, 2014PA002717, doi:10.1002/2014PA002717

Tierney, J. E., F. S. R. Pausata, and P. B. deMenocal (2017), Rainfall regimes of the Green Sahara, *Science Advances*, *3*, doi:10.1126/sciadv.1601503.

Trenberth, K., E. (1997), The Definition of El Niño, *Bull. Amer. Meteor. Soc.*, *78*, 2771-2777, 10.1175/1520-0477(1997)078<2771:tdoeno>2.0.co;2.

von der Heydt, A. S., A. Nnafie, and H. A. Dijkstra (2011), Cold tongue/Warm pool and ENSO dynamics in the Pliocene, *Clim. Past*, *7*, 903-915.

Wade, M., J. Mignot, A. Lazar, A. T. Gaye, and M. Carré (2015), On the spatial coherence of rainfall over the Saloum delta (Senegal) from seasonal to decadal time scales, *Frontiers in Earth Science, Atmospheric Science*, *3*, 30, doi:10.3389/feart.2015.00030.

Wallace, J. M., E. M. Rasmusson, T. P. Mitchell, V. E. Kousky, E. S. Sarachik, and H. Von Storch (1998), On the structure and evolution of ENSO-related climate variability in the tropical Pacific: Lessons from TOGA, *Journal of Geophysical Research*, *103*, 14,241-214,259.

Wang, P., S. Clemens, L. Beaufort, P. Braconnot, G. Ganssen, Z. Jian, P. Kershaw, and M. Sarntheim (2005), Evolution and variability of the Asian monsoon system: state of the art and outstanding issues, *Quaternary Science Reviews*, *24*, 595-629.

Wara, M. W., A. C. Ravelo, and M. L. Delaney (2005), Permanent El Niño-like conditions during the Pliocene warm period, *Science*, *309*, 758-761.

Watanabe, T., A. Suzuki, S. Minobe, T. Kawashima, K. Kameo, K. Minoshima, Y. M. Aguilar, R. Wani, H. Kawahata, K. Sowa, T. Nagai, and T. Kase (2011), Permanent El Nino during the Pliocene warm period not supported by coral evidence, *Nature*, *471*, 209-211, doi:10.1038/nature09777.

Wells, L. E. (1990), Holocene history of the El Nino phenomenon as recorded in flood sediments of northern coastal Peru, *Geology*, *18*, 1134-1137.

Wyrtki, K. (1975), El Niño—The Dynamic Response of the Equatorial Pacific Ocean to Atmospheric Forcing, *Journal of Physical Oceanography*, *5*, 572-584.

Yan, H., W. Wei, W. Soon, Z. An, W. Zhou, Z. Liu, Y. Wang, and R. M. Carter (2015), Dynamics of the intertropical convergence zone over the western Pacific during the Little Ice Age, *Nature Geosci*, *8*, 315-320, doi:10.1038/ngeo2375.

Zachos, J., M. Pagani, L. Sloan, E. Thomas, and K. Billups (2001), Trends, rythms, and aberrations in global climate 65 Ma to present, *Science*, *292*, 686-693.

Zhang, R., and T. L. C. L. Delworth (2006), Impact of Atlantic multidecadal oscillations on India/Sahel rainfall and Atlantic hurricanes, *Geophysical Research Letters*, *33*, doi:org/10.1029/2006GL026267.

Documents annexes: Publications majeures des 5 dernières années

Carré, M., J. P. Sachs, A. J. Schauer, W. E. Rodríguez, and F. C. Ramos (2013), Reconstructing El Niño-Southern Oscillation activity and ocean temperature seasonality from short-lived marine mollusk shells from Peru, *Palaeogeography, Palaeoclimatology, Palaeoecology*, *371*, 45-53.

Carré, M., J. P. Sachs, S. Purca, A. J. Schauer, P. Braconnot, R. Angeles Falcón, M. Julien, and D. Lavallée (2014), Holocene history of ENSO variance and asymmetry in the eastern tropical Pacific, *Science*, *345*, 1045-1048.

Emile-Geay, J., K. M. Cobb, M. Carre, P. Braconnot, J. Leloup, Y. Zhou, S. P. Harrison, T. Corrège, H. V. McGregor, M. Collins, R. Driscoll, M. Elliot, B. Schneider, and A. Tudhope (2016), Links between tropical Pacific seasonal, interannual and orbital variability during the Holocene, *Nature Geosci*, *9*, 168-173.

Carré, M., D. Jackson, A. Maldonado, B. M. Chase, and J. P. Sachs (2016), Variability of 14C reservoir age and air-sea flux of CO2 in the Peru-Chile upwelling region during the past 12,000 years, *Quaternary Research*, *85*, 87-93.

Carré M., M. Azzoug, P. Zaharias, A. Camara , R. Cheddadi , M. Chevalier, D. Fiorillo, A. Gaye, S. Janicot, M. Khodri, A. Lazar, C. E. Lazareth, J. Mignot, N. Mitma Garcia, N. Patris, O. Perrot, M. Wade, Modern drought conditions in western Sahel unprecedented in the past 1600 years. *Climate Dynamics*, in press.

Palaeogeography, Palaeoclimatology, Palaeoecology 371 (2013) 45–53

Contents lists available at SciVerse ScienceDirect

Palaeogeography, Palaeoclimatology, Palaeoecology

journal homepage: www.elsevier.com/locate/palaeo

Reconstructing El Niño-Southern Oscillation activity and ocean temperature seasonality from short-lived marine mollusk shells from Peru

Matthieu Carré [a,*], Julian P. Sachs [b], Andrew J. Schauer [c], Walter Elliott Rodríguez [d], Fredy Cardenas Ramos [e]

[a] UM2-CNRS-IRD, Institut des Sciences de l'Evolution de Montpellier, Université Montpellier 2, CC065, Pl. Eugène Bataillon, 34095 Montpellier, France
[b] University of Washington School of Oceanography, Box 355351, Seattle, WA 98195, USA
[c] University of Washington Department of Earth and Space Sciences, Box 351310, Seattle, WA 98195, USA
[d] IMARPE, Laboratorio Costero de Huacho, Avenida San Martin 710 Carquín, Huacho, Peru
[e] IMARPE, Laboratorio Costero de Ilo, Ilo, Peru

ARTICLE INFO

Article history:
Received 18 June 2012
Received in revised form 30 November 2012
Accepted 12 December 2012
Available online 28 December 2012

Keywords:
Eastern tropical Pacific
ENSO
Paleoclimate
Sea surface temperature
Mollusk
Stable isotopes

ABSTRACT

A critical need exists for quantitative reconstructions of long-term El Niño Southern Oscillation (ENSO) variability in the eastern tropical Pacific. Presented here is a method to quantitatively estimate past changes 1) in the seasonal amplitude of sea surface temperature (SST) in the Peruvian coastal upwelling system and 2) in the amplitude of ENSO-related interannual variability in the eastern tropical Pacific. The seasonal amplitude of SST (ΔT) along the length of the Peruvian coast is strongly correlated with the Niño1 + 2 index. We show that the frequency distribution of ΔT values provided by a modern sample of 13 *Mesodesma donacium* shells faithfully reflects modern ENSO variability at the regional scale, including the range of anomalies from La Niña to moderate El Niño events, but excludes extreme warm anomalies because of high shell mortality. We propose to use the frequency distribution of ENSO anomalies in paleoclimate studies for comparisons between shell records, coral records, and GCM simulations. Reconstruction uncertainties can be quantified using Monte Carlo simulations. The method presented here opens new perspectives for quantitative paleo-ENSO reconstructions in the Eastern Pacific since it may be applied with any mollusk species from Peru provided at least one annual cycle of SST is faithfully recorded by shell $\delta^{18}O$.

1. Introduction

Reconstructing a long-term record of El Niño Southern Oscillation (ENSO) is critical to identify the forcings that influence its activity and to estimate its sensitivity to global climate change. Past changes in ENSO variability not only involve changes of the event intensity and frequency, but also changes in the distribution of cold and warm events, and changes in the spatial pattern of sea surface temperature (SST) anomalies. This means that records of interannual SST are needed from across the tropical Pacific, from the warm pool to the cold tongue, to properly evaluate past ENSO modes.

So far, proxy records of the tropical Pacific SST with seasonal resolution have been obtained primarily from Sr/Ca and $\delta^{18}O$ analyses of coral (Cole and Fairbanks, 1990; Dunbar et al., 1994; McCulloch et al., 1996; Corrège et al., 2000; Tudhope et al., 2001; Evans et al., 2002; Cobb et al., 2003; Kilbourne et al., 2004; McGregor et al., 2010). Fossil corals faithfully record past interannual climate variability in the Pacific warm pool and in the central Pacific but they are very scarce in the eastern tropical Pacific. The most ancient coral analyzed in the eastern tropical Pacific was collected in the Galapagos Islands and reached 1587 A.D. (Dunbar et al., 1994).

On the eastern side of the Pacific, most paleoclimate studies dedicated to ENSO reconstruction for long intervals are based on rainfall proxies of the American continent (D'Arrigo and Jacoby, 1992; Stahle et al., 1998; Rodbell et al., 1999; Moy et al., 2002; Riedinger et al., 2002; D'Arrigo et al., 2005; Rein et al., 2005; Conroy et al., 2008). However, all these signals are communicated through atmospheric teleconnections that are likely to change over time. Changes in the rainfall regime may also be linked to changes in the intensity or in the seasonal movement of the intertropical convergence zone (ITCZ). In the tropical Andes, the Atlantic Ocean and the South American monsoon system also have a large influence on rainfall variability (Garreaud et al., 2009). Consequently, rainfall-related paleoclimate records provide valuable data for the study of continental rainfall variability but yield only indirect and often mixed information for past ENSO activity.

Marine indications for past changes in ENSO activity in the eastern tropical Pacific have been obtained from the variance of individual foraminifera $\delta^{18}O$ values in marine sediment samples (Koutavas et al., 2006; Leduc et al., 2009). Since marine cores have a centennial resolution and foraminifera live about a month, the variance of a foraminifera sample yields a mixed signal that involves temperature

* Corresponding author. Tel.: +33 4 67 14 38 08; fax: +33 4 67 14 40 44.
E-mail address: matthieu.carre@univ-montp2.fr (M. Carré).

0031-0182/$ – see front matter © 2013 Elsevier B.V. All rights reserved.
http://dx.doi.org/10.1016/j.palaeo.2012.12.014

seasonality, temperature gradient in the mixed layer, ENSO-related interannual variability, and multidecadal variability.

Here we present a technique that responds to the critical need for quantitative estimates of the marine interannual variability in the eastern tropical Pacific. We show how short-lived marine mollusk shells, despite the brevity of their timespan, can be used as a paleoclimate archive for reconstructing the seasonal range of SST and ENSO variability in the tropical Pacific cold tongue, and how these data can be compared to coral records and model outputs. The technique shares similarities with the coral-based approach since it involves short high resolution windows at a monthly time scale, but also with the individual foraminifera technique since paleoclimate is estimated by the statistics of a random sample. The advantage of the mollusk-based technique compared to foraminifera is that it allows independent reconstruction of the seasonal cycle and more comprehensive characterization of ENSO variance.

It has been previously established that marine mollusk shell $\delta^{18}O$ may be a reliable SST proxy as long as water $\delta^{18}O$ can be reasonably constrained (Grossman and Ku, 1986; Hickson et al., 1999; Schöne et al., 2004). On the Peruvian coast, the monthly sea water $\delta^{18}O$ variations are very small (typically <0.1‰) because precipitation is virtually nonexistent and river discharge is minimal, so that mollusk species such as *Mesodesma donacium* faithfully record coastal SST variations at a monthly time scale over 1–3 year long windows (Carré et al., 2005). Although continuous records of at least several decades are generally preferred to study ENSO variability, we will examine here how a discontinuous sample of short-lived shells from Peru can also yield a reliable statistical estimate of ENSO variability.

We will examine the relationship between coastal SSTs in the Peruvian upwelling system and the Niño1+2 index to assess the spatial range of representativeness of coastal records. Uncertainties will also be quantitatively assessed using the MoCo program (Carré et al., 2012). Our approach, presented here with one species, is valid for any coastal mollusk species that faithfully records at least one annual SST cycle. Our study potentially opens new opportunities for direct and quantitative paleo-ENSO reconstructions in the eastern tropical Pacific, using anthropogenic or natural fossil shell accumulations in Peru.

2. Materials

M. donacium is an endemic intertidal bivalve species of Peruvian and Chilean sandy beaches that has been gathered for food since the first human occupation of the Peruvian coast (Sandweiss et al., 1989, 1998; Carré et al., 2009; Lavallée et al., 2011). In 1980, the northern limit of *M. donacium* was 10°S in Sechura Bay (Tarifeño, 1980). Its distribution today is restricted to south of ~15°S because of mass mortality induced by the extreme El Niño events of 1983 and 1998 (Riascos et al., 2009). This means that *M. donacium* shells cannot record extreme warm anomalies (9.5 °C in 1983 and 8.8 °C in 1998 in Puerto Chicama). After the 1983 event, populations recovered within a few years but the 1998 event had a much more prolonged impact since populations have not fully recovered so far, 15 years after the mortality event, perhaps because of competition or changes in the beaches slope and granulometry. Some periods following similar extreme events might therefore not exist in the fossil record but such potential gaps are not expected to produce any bias since there is no evidence that ENSO activity may be systematically stronger or weaker during the decade following an extreme event.

A sample of 13 *M. donacium* shells was collected in 2007 from modern shell mounds behind the long sand beach close to the Ica River mouth (14°52′19″S; 75°33′21″W) (Fig. 1). Based on fishermen testimonies and newspaper fragments found in shell mounds, we know that these shells were gathered by fishermen during the last decades of the 20th century, when these surf clams were a significant economical resource. These shells cannot be cross-dates. To minimize the probability of collecting shells from the same year, every shell was collected in a separate mound. This modern shell sample thus represents a random sample of 13 short-term windows which combined represent the environmental conditions during the last decades of the 20th century. In this, our modern sample would mimic shell samples from archeological middens and could therefore be used as a modern reference.

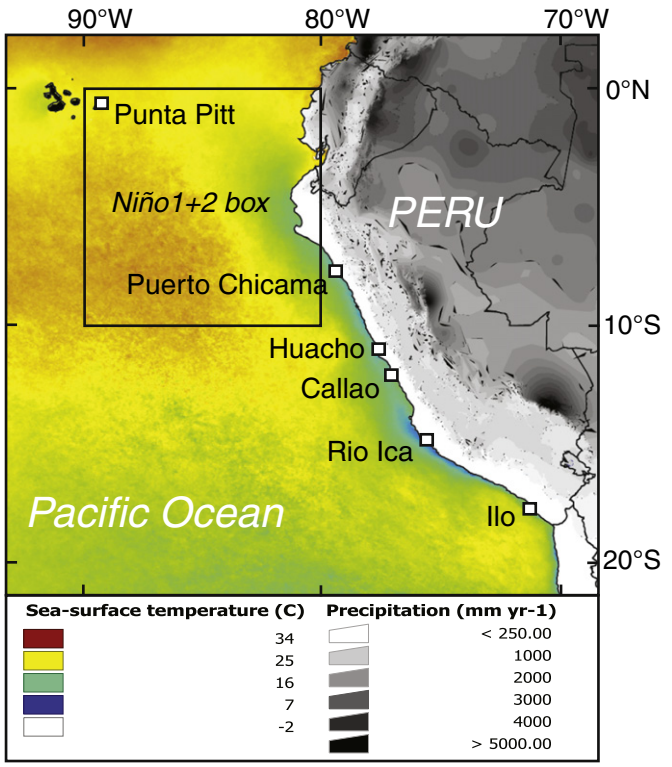

Fig. 1. Map of the study area with mean annual SST and annual precipitation on the continent. The Niño1+2 area and the sites mentioned in the text were indicated.

3. Methods

3.1. Microsampling and isotopic analyses

Radial shell sections were polished and serially microsampled in the outer layer using an automated microdrilling system (Micromill, Merchantek™) with a three-edged pyramidal dentist drill. Microsamples consisted in a ~0.15 mm deep and ~0.2 mm wide groove and were adjacent for a continuous sampling (Fig. 2). Based on shell growth lines, the length of the groove was adapted to the growth rate so the sample would integrate about a month.

The oxygen isotopic composition of powdered aragonite microsamples (~50 μg) was analyzed at the University of Washington Isolab using a Finnigan Delta Plus isotope ratio mass spectrometer coupled to a Kiel III carbonate device. Aragonite samples were digested in 100% phosphoric acid at 70 °C. The standard deviation for repeated measurements of the internal standard was better than 0.08‰. Raw $\delta^{18}O$ values were corrected as per Tobin et al. (2011) for temperature-induced isotopic drift observed in micromilled aragonite (−0.1‰/day at 70 °C). $\delta^{18}O$ values were reported with respect to the Vienna Pee Dee Belemnite (VPDB) scale using NBS19 ($\delta^{18}O = -2.2‰$) and NBS18 ($\delta^{18}O = -23.01‰$) (Coplen, 1996). Data points corresponding to seasonal extrema were re-sampled on the shell and re-analyzed. Values from replicate microsamples were then averaged. Isotopic values were not corrected for the difference of CO_2-acid fractionation factors between calcite and aragonite

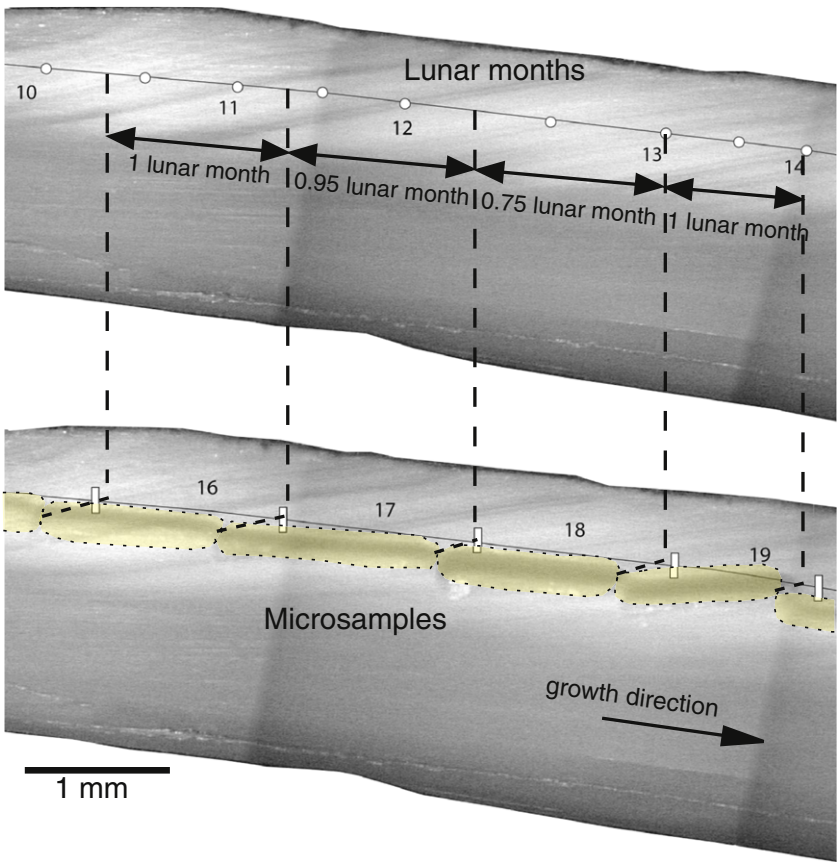

Fig. 2. Detail of Ica-3 shell section illustrating the method used to determine subannual chronology of shell isotopic records. Top: polished section showing fortnightly growth lines (open circles on an arbitrary line following the growth axis) and numbers of lunar months from the microsampling starting point. Bottom: same section after microsampling. Microsample grooves were indicated in yellow and numbered. Their limits were indicated by open rectangles on the same growth axis. Time intervals represented by microsamples were estimated on the growth axis in the top section by the intervals between vertical dotted lines.

(Kim et al., 2007) because paleotemperature equations mentioned further in the text were calculated with uncorrected values (Grossman and Ku, 1986; Carré et al., 2005).

Sea water samples were collected from the surface water close to the shoreline in glass vials avoiding the presence of air bubbles. Vials were sealed with tape and stored at 5 °C. Water $\delta^{18}O$ values were analyzed by mass spectrometry using the classical CO_2–H_2O equilibration method (Cohn and Urey, 1938), with a precision of ±0.1‰. Seawater samples were equilibrated for 8 h at 40 °C. Water oxygen isotope ratios are reported with respect to Vienna Standard Mean Ocean Water (VSMOW).

3.2. Shell inner chronology and seasonal extrema

Polished shell sections were observed and photographed with a binocular microscope under reflected light. In fast growing parts of *M. donacium* shells, thin growth lines can be observed that were shown to be produced during daily low tides (Carré et al., 2005). These lines form darker clusters during spring tide periods with a fortnightly periodicity. These fortnightly growth lines were used in a first phase to keep microsampling resolution close to one month. There is, however, uncertainty in the identification of these fortnightly lines due to the pattern variability (Carré, 2007; Carré et al., 2009). Subannual chronology was thus more precisely determined during a second phase combining isotopic records with growth lines. In a simultaneous process, we defined seasonal extrema, and selected the sclerochronological reading that would allow them to be separated by ~12 ± 1 months. Based on this adjusted interpretation of shell growth lines, the timespan of every microsample was calculated (Fig. 2), and shell isotopic records were plotted on a monthly time axis (Fig. 3). Local extrema related to the strong intra-seasonal variability on the Peruvian coast rather than to the annual cycle could be discriminated in this process (for example in shells Ica-3 and Ica-4, Fig. 3). Temporal resolution of the records ranged from ~0.5 to 3 months. The average resolution of the whole record was 1.2 months ($\sigma = 0.5$ months). There was no systematic bias in time resolution related to growth rate changes since microsampling resolution was adjusted growth rate. The lowest resolution in extrema values was 2.5 months. The seasonal amplitude of shell $\delta^{18}O$ represents the seasonal amplitude of SST (ΔT) and was taken to be the difference between the summer maximum and the winter minimum that preceded or followed it (Fig. 3). First or last data points were not used for the calculation of seasonal amplitudes unless the shell chronology showed a time difference with the closest minimum (maximum) larger than 12 months.

3.3. Estimation of uncertainties

Shell isotopic records converted to SST using a paleotemperature equation (Grossman and Ku, 1986; Carré et al., 2005) provide a statistical estimate of the average and variance of the seasonal amplitude of the SST (ΔT) for the late 20th century. The systematic and standard error associated to this estimate was quantified by a Monte Carlo simulation using the MoCo program, that simulates the uncertainty sources of mollusk- and coral-based SST reconstructions (Carré et al., 2012). MoCo was parameterized here to mimic the uncertainty sources specific to *M. donacium*, which includes a range of temperature from 6 to 22 °C for shell growth (temperatures over 22 °C are

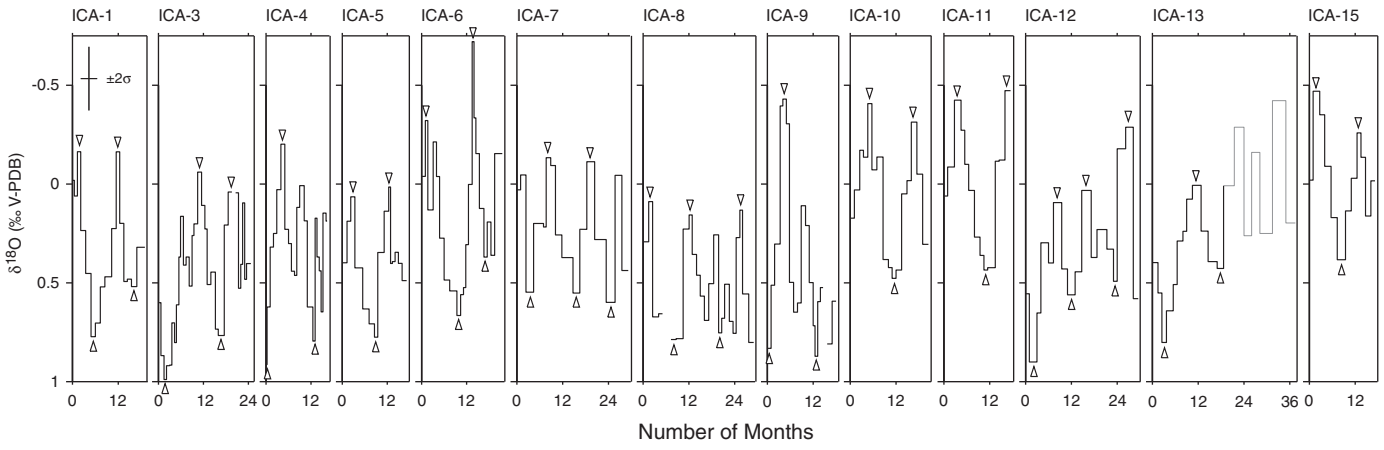

Fig. 3. $\delta^{18}O$ profiles of 13 modern *Mesodesma donacium* shells from the Rio Ica site, on monthly time axis. The length of horizontal segment represents the duration averaged by shell microsamples. Line interruptions are due to loss of samples. Gray line in Ica 13 indicates the part of the isotopic signal where the resolution was too low to accurately estimate seasonal amplitudes. Open triangles indicate seasonal extrema that were used for the calculation of ΔT values. These data points were averaged from at least 2 replicate analyses.

thus not recorded), random growth breaks, spatial heterogeneity of the coast, monthly variability of water $\delta^{18}O$, and analytical standard error for isotopic ratio. Temporal resolution variability in shell records is also a source of uncertainty for estimating ΔT, but is not included in MoCo simulations. The standard error was calculated as the standard deviation of the population of errors obtained by iterated reconstruction simulations. The instrumental temperature time series of Puerto Chicama was used for the simulation and error calculation. Extreme Niño years 1982–83 and 1997–98 were removed for an adequate assessment of uncertainties since the species does not record this part of ENSO variability. The uncertainty analysis is therefore assessing the ability of a shell sample to record the range of ENSO variability from La Niña anomalies to "normal" El Niño anomalies. The complete parameterization is available in the online Supplementary material.

4. Results and discussion

4.1. Variability of sea water $\delta^{18}O$

Sea water salinity and $\delta^{18}O$ are strongly correlated on monthly to decadal time scales since their variations are both dictated by freshwater input and evaporation (Epstein and Mayeda, 1953; Fairbanks et al., 1982). Salinity variability can therefore provide reliable indications about water $\delta^{18}O$ variability when direct isotopic data are not available. We compared monthly salinity time series for the period 2000–2007 from three IMARPE coastal laboratories, Huacho, Callao, and Ilo (Fig. 4). In the three sites, salinity variations were very small, with standard deviations of 0.11, 0.11, and 0.07 respectively (Fig. 4A). Although there was a slight tendency for higher salinity values during austral summer, the mean annual cycle was very weak, with amplitudes of 0.23, 0.09, and 0.06 respectively, which are similar to the monthly standard deviation. By extension we infer that coastal water $\delta^{18}O$ variations on intra- and inter-annual time scales are small on the central and southern coast of Peru. This result was confirmed by monthly time series of water $\delta^{18}O$ obtained in 2003 in Huacho and in 2003–2004 in Ilo (Fig. 4B). In these two short records, the standard deviation of sea water $\delta^{18}O$ was 0.2‰ and 0.14‰ respectively, but no seasonal signal could be discerned. These water isotopic values, however, do not faithfully reflect the monthly variability because they are instantaneous measurements and include thus a daily variability. The long series of monthly salinity data provide a better estimate of the isotopic monthly variability because they are averaged values of daily to weekly measurements. Based on Fairbanks' et al. (1982) relationship between salinity and water $\delta^{18}O$ in the eastern tropical Pacific, a standard deviation of 0.11 for salinity corresponds to a standard deviation of 0.03‰ for water $\delta^{18}O$, which translates into an uncertainty of ~0.1 °C for SST estimates. These data confirm that the intra-seasonal variations of water $\delta^{18}O$ do not significantly affect the reconstruction of seasonal SST variations. This result is also valid for the study site since the nearby Ica River has a small discharge that cannot significantly affect the sea water isotopic composition for a period as long as a month. In the exceptional case that the river flow was strong enough to affect the sea water $\delta^{18}O$, this type of event would be detected in the isotopic shell record by a simultaneous drop in both $\delta^{18}O$ and $\delta^{13}C$ values. This was not observed in modern Ica shells. A value of 0.05‰ was used for water $\delta^{18}O$ monthly variability in MoCo simulation. Sea water $\delta^{18}O$ also varies on millennial time scales with polar ice volume. This would affect the reconstruction of absolute temperatures but not of ΔT values which is used here to estimate ENSO activity as we will show in Section 4.3.

Mean sea water isotopic composition shows some geographical variations along the coast (Fig. 4C,D). A mean sea water $\delta^{18}O$ value of 0.24 ± 0.11‰ for the study area was estimated from 12 sea water samples taken along the coast between Callao (12°04′S) and Tanaka (15°43′S) at different times from 2001 to 2007. The sea water $\delta^{18}O$ values with the precise locations and dates of sampling are available in the online Supplementary material.

4.2. Shell $\delta^{18}O$ profiles

We obtained 13 isotopic records ($\delta^{18}O$) spanning one to two years with approximately 1-month resolution (Fig. 3). The cumulated timespan of the 13 shells is about 25 years assuming nonredundancy. The microsampling resolution ranged from 0.5 to 2 lunar months, except in the last part of shell Ica-13 which was not used for seasonality estimates because the timespan of microsamples was larger than 2 months. Single shell mean values ranged from −0.04‰ to 0.51‰ while the mean $\delta^{18}O$ value for the whole dataset was 0.25‰ (N = 249 data points).

Considering a sea water $\delta^{18}O$ value of 0.24‰ and using the paleotemperature equation calculated by Carré et al. (2005) for *M. donacium*, mean SST values calculated for single shells ranged from 16.5 °C to 18.5 °C, whereas the mean SST calculated for the full dataset was 17.4 °C. This value is in good agreement with the NODC (Levitus) World Ocean Atlas 1994 (Monterey and Levitus, 1997) (0.25° gridded dataset provided by the NOAA/OAR/ESRL PSD, Boulder, Colorado, USA, from their Web site at http://www.esrl.noaa.gov/psd/.) that indicates

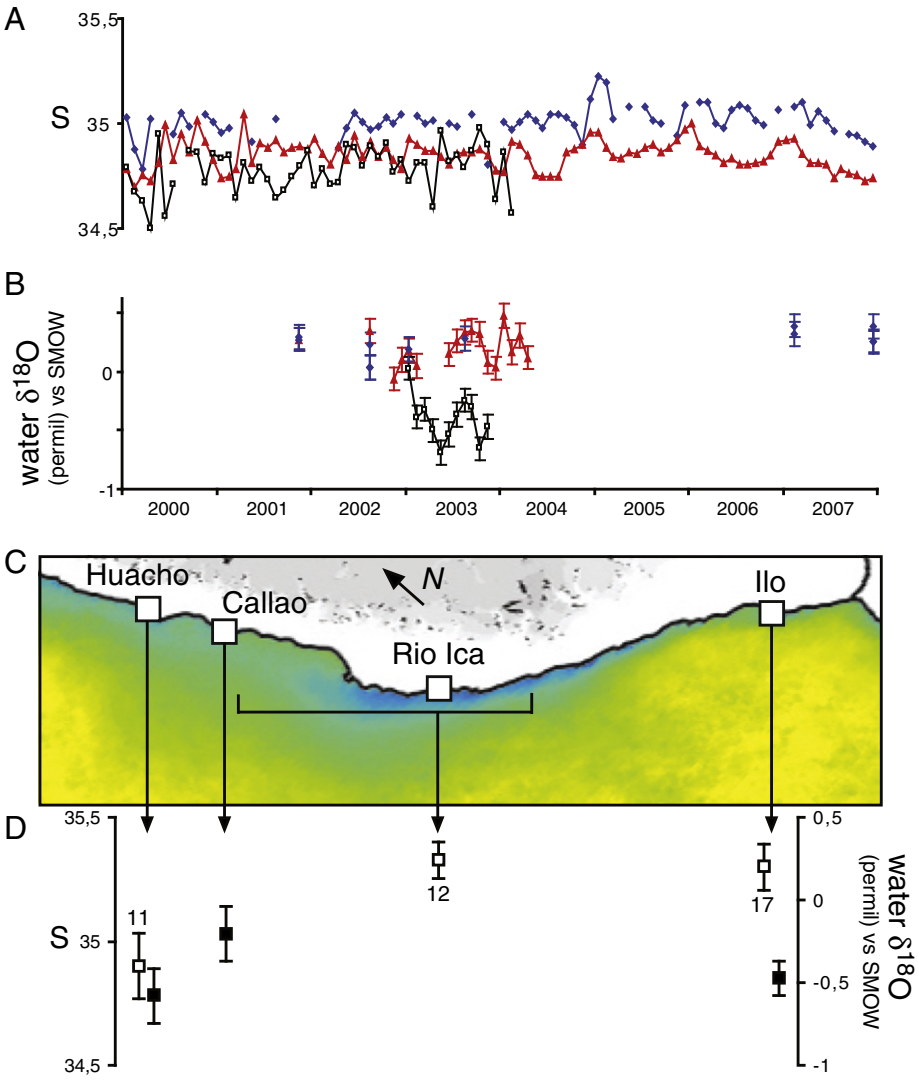

Fig. 4. A: Monthly time series of surface salinity in Huacho (open squares), Callao (blue diamonds), and Ilo (red triangles) measured by IMARPE. B: Sea water $\delta^{18}O$ data from Huacho (open squares), Ilo (red triangles), and coastal sites from the Rio Ica area (from Callao to Tanaka) (blue diamonds). Precise dates and locations were listed in Supplementary material. C: Legend as in Fig. 1. D: Mean values and standard deviation of salinity (black squares) and sea water $\delta^{18}O$ (open squares) for the locations indicated by arrows on the Peruvian southern coast.

mean annual SSTs from 17.2 to 17.7 °C along the Peruvian coast between 14°S and 16°S.

The seasonal amplitude of $\delta^{18}O$ was converted to a seasonal amplitude of SST and will be referred to as ΔT values thereafter. Each shell yielded between 2 and 4 ΔT values. 36 ΔT values were calculated from the full dataset with an average value of 3.0 °C using an aragonite temperature-fractionation slope of −3.66 °C/‰ (Carré et al., 2005) or 3.5 °C using a slope value of −4.34 °C/‰ (Grossman and Ku, 1986). These values are close to the mean seasonal amplitudes calculated from instrumental SST time series of Callao (3.5 °C) and Ilo (3.2 °C), implying that seasonal temperature variations are faithfully recorded by the shells. However, mollusk ΔT mean value calculated from Grossman and Ku's (1986) slope is closer to the Callao instrumental value while Carré et al.'s (2005) slope yields a value closer to Ilo instrumental value. Since our site is geographically closer to Callao and until further data from Rio Ica is available, we choose to use here Grossman and Ku's (1986) temperature-fractionation slope for the calculation of ΔT. The standard errors of the shell-derived mean SST (Tm) and mean ΔT value (<ΔT>) are ±0.36 °C and ±0.28 °C respectively for this sample size, based on Monte Carlo simulations with the MoCo program (Carré et al., 2012) (Fig. 5). These simulations also suggest that there is no systematic bias in the estimate of the annual mean temperature but a slight overestimation of 0.27 °C for <ΔT> (Fig. 5). This bias is due to the combined effect of monthly water $\delta^{18}O$ variability, carbonate microscale isotopic heterogeneity, and analytic uncertainty (Carré et al., 2012).

4.3. ENSO and the seasonal cycle of SST on the Peruvian coast

Coastal conditions may not be representative of the open ocean, especially where strong upwelling occurs, as in Peru. We aimed to test if paleoceanographic results from the Peruvian coast could be compared with results obtained from sediment cores or with climate model outputs. We thus examined how coastal SSTs in Peru correlate with the Niño1+2 index (0–10°S, 90–80°W) (Fig. 6). The direct month-to-month Pearson correlation coefficient between Niño1+2 index and *in situ* SST anomaly time series from Puerto Chicama (7°42′S), Callao (12°04′S), and Ilo (17°38′S) were respectively 0.85, 0.75, and 0.75 (Fig. 6A). Despite the long distance (~2000 km from Ilo to the center of Niño1+2 box) and the influence of the coastal upwelling, these high correlation coefficients imply that SST

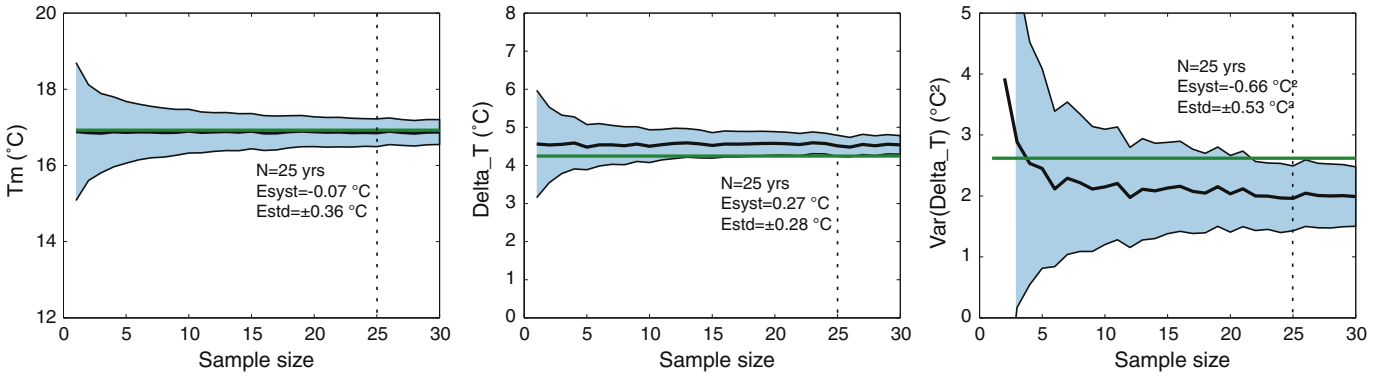

Fig. 5. Monte Carlo simulations of the reconstruction of the annual mean temperature Tm (left panel), the mean SST amplitude (central panel), and the ENSO activity indicated by the variance of the SST seasonal amplitude (right panel) using the MoCo program (Carré et al., 2012). Details about the program parameterization are given in online Supplementary material. Thick black lines indicate the reconstructed value *vs.* the cumulated number of years recorded by a shell sample (here the number of 1-year long shells). The green line shows the true value calculated from the 1925–2002 SST time series of Puerto Chicama, Peru. The blue area limited by thin black lines shows the standard error interval. The dotted line corresponds to the modern shell sample of Ica presented in this study which cumulates *ca.* 25 years. The systematic error values (Esyst) and the standard error values (Estd) obtained for N = 25 years are indicated.

anomalies along the Peruvian coast are likely influenced by the same factors that influence the Niño1 + 2 region. ENSO and warm (El Niño) events in particular are clearly captured by the coastal SST series and Niño1 + 2 (Fig. 6A).

However, absolute SST anomalies (which usually characterize ENSO) cannot be faithfully estimated in individual mollusk records because of the brevity of their lifespan and the local scale variability of mean conditions that prevent us from determining a reliable climate baseline for every single shell. We therefore examined further how the seasonal amplitude of SST on the Peruvian coast was related to ENSO. The correlation coefficients between Niño1 + 2 annual means and instrumental SST seasonal amplitudes in Puerto Chicama, Callao, and Ilo were respectively 0.87, 0.85, and 0.82 (Fig. 6B). This implies that ENSO strongly affects the seasonal amplitude of SST along the length of the Peruvian coast, with large amplitudes indicative of warm events and small amplitudes indicative of cold events. The cause of this relationship is the coastal upwelling that strongly depresses SST anomalies during austral winter so that coastal SSTs are mostly affected by ENSO events (warm or cold) during austral summer when coastal upwelling is lower. As a result, ENSO anomalies can be diagnosed by coastal ΔT anomalies. Since the relationship is linear (Fig. 6B) the variance of ΔT values should be related to the amplitude of ENSO variability in the Niño1 + 2 area. This was confirmed by the strong linear correlation between the variance of the Niño1 + 2 index annual mean and the variance of coastal ΔT values in Puerto Chicama, Callao, and Ilo over the 1950–2002 period (Fig. 6C).

As a result, the variance of ΔT values (Var(ΔT)) calculated from a sample of mollusk shells is a measure of ENSO-related SST variability in the Niño1 + 2 region. <ΔT> and Var(ΔT) (the mean and the variance) of the shell sample from Rio Ica can be used, respectively, as modern references to estimate changes in the SST seasonality and the amplitude of ENSO variability from fossil shell samples of the same species in the same region. Reconstructions of past conditions should be normalized by these modern values. This way, $<\Delta T>_{fossil}/<\Delta T>_{modern}$ and $Var(\Delta T)_{fossil}/Var(\Delta T)_{modern}$ are quantitative estimates of past changes in SST seasonality and ENSO activity, and are independent from the paleotemperature proxy model and its inherent uncertainties. This method could be applied with any Peruvian mollusk species that faithfully records the whole seasonal amplitude of SST, such as *Argopecten purpuratus* (Jones et al., 2009), *Trachycardium procerum* (Perrier et al., 1994; Andrus et al., 2005), and *Protothaca thaca* (Lazareth et al., 2006). Monte Carlo simulations indicate that the standard error for the reconstruction of var(ΔT) with our sample is ± 0.53 °C^2 (Fig. 5), which represents an uncertainty of ~19%. This uncertainty is much larger than for Tm and <ΔT> which was expected since capturing the variance is much more difficult than capturing average values. A systematic underestimation is also observed primarily due to the shell growth temperature threshold. These results show that reconstructions from fossil samples need to be compared to similar modern samples that will have similar biases.

Fossil shell samples may be collected from natural marine terraces or anthropogenic accumulations. A shell sample from a dated stratigraphical layer yields then a random sample of short-term windows producing together a statistical estimate of average conditions for the time period corresponding to the layer accumulation. Uncertainty related to statistical representativeness of the sample may be estimated using the MoCo program (Carré et al., 2012).

4.4. Characterizing and comparing ENSO records

ENSO activity is generally traced in long continuous proxy records by the interannual band of the frequency power spectra. The amplitude of its variability is then estimated by the variance of the filtered proxy record. We argue here that ENSO activity can also be usefully characterized by the frequency distribution of the ENSO-related anomalies. This simple representation allows better evaluation of changes in the intensity of events and in the distribution between El Niño and La Niña anomalies. The frequency distribution of Niño1 + 2 SST anomalies appears not to be symmetrical (Fig. 7A) as it is in the central equatorial Pacific (not shown). In the eastern Pacific, El Niño anomalies are larger than La Niña anomalies. On the Peruvian coast, Callao ΔT values and mollusk-derived ΔT values have similar asymmetric distributions that were most closely characterized by lognormal distributions (Fig. 7B,D). For better comparison with instrumental records, mollusk-derived ΔT values were calculated from $\Delta\delta^{18}O$ using the temperature calibration of Grossman and Ku (1986), which has a slope of 4.34 °C/‰, but using the slope from Carré et al. (2005) would not change the outcome and the ΔT distribution would still be lognormal.

Extreme El Niño warm events in 1983 and 1998 which represent the two warmest anomalies in the Niño1 + 2 series from 1950 to 2002 (Fig. 7A), were not included in the Callao distribution because *M. donacium* mortality is extremely high at these temperatures and they are therefore not expected to be observed in the fossil record of that species. However, the similarity of the mollusk ΔT distribution with the instrumental ΔT distributions is an additional confirmation that *M. donacium* is a reliable archive of ENSO variability, recording La Niña anomalies to "normal" El Niño anomalies. Given the lognormal form of the distributions, the mode and the threshold for La

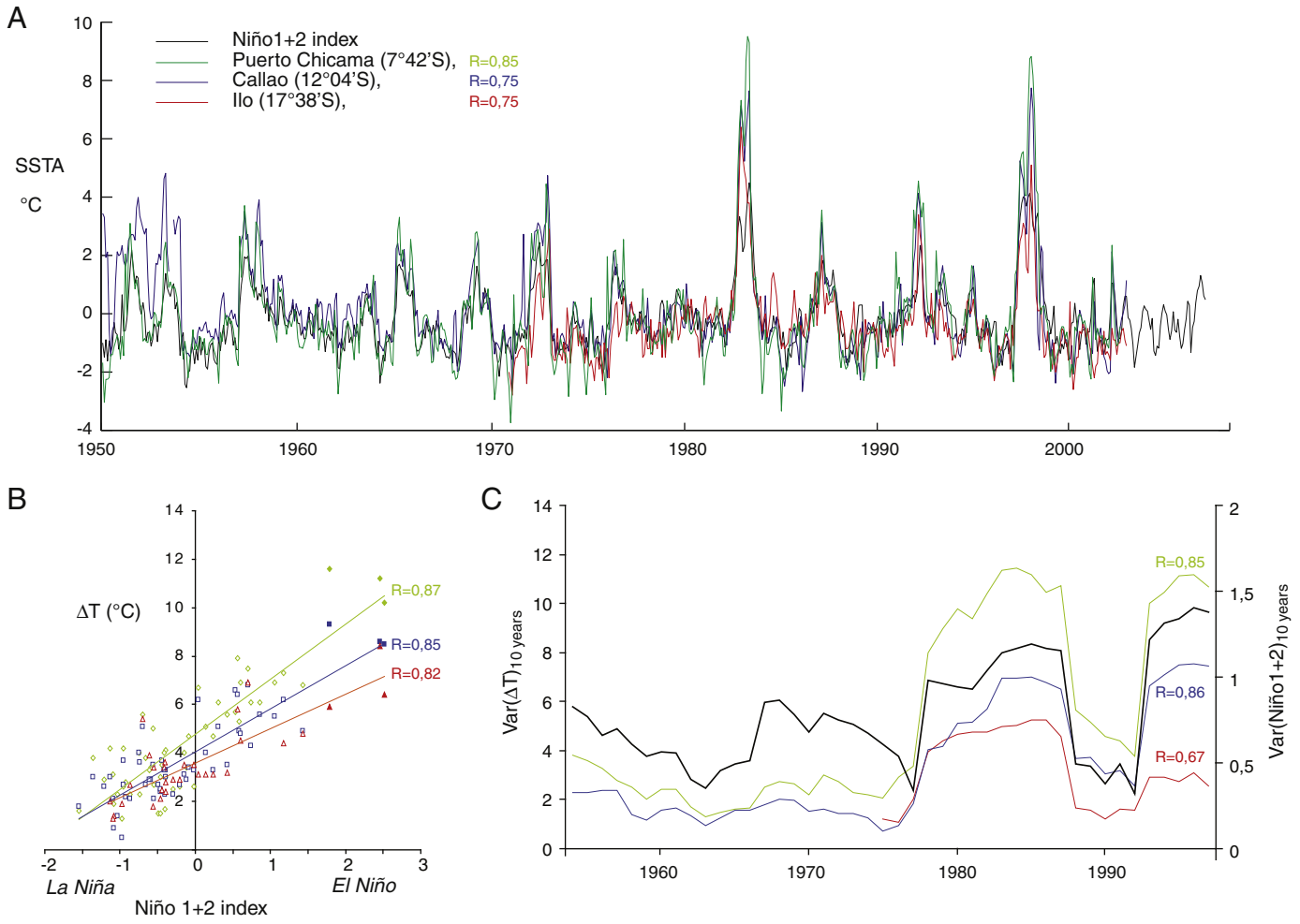

Fig. 6. A: Monthly SST anomalies from the Niño1 + 2 area (black), Puerto Chicama (green), Callao (blue) and Ilo (red). SSTs from Peru were measured *in situ* by IMARPE. Correlation coefficient of the coastal time series with the Niño 1 + 2 series are indicated. B: Linear correlations between Niño1 + 2 index annual mean and ΔT values from Puerto Chicama (green), Callao (blue), and Ilo (red). C: Variance of Niño1 + 2 index in 10-year running windows (black) compared to the variance of ΔT in 10-year running windows in Puerto Chicama (green), Callao (blue) and Ilo (red), with the corresponding correlation coefficients.

Niña and El Niño were defined by the mean and the standard deviation of the normal distributions of Ln(ΔT).

1982–83 and 1997–98 account for 25% of the variance in the Puerto Chicama time series, but this contribution is so dependent on a single event that it may vary significantly. These events were the most significant in terms of impact, and thus focused a lot of attention from the scientific community. However, they are so extraordinary in terms of timing and intensity that they are arguably not representative of the southern oscillation (Takahashi et al., 2011). Although these two events occurred in an interval of 15 years, they are unique in the instrumental record and may have been in the last centuries. Our proxy is thus complementary with rainfall-related proxies because it focuses on the southern oscillation itself while the latter record its occasional catastrophic extensions.

One of the most important results of this study is that a quantitative paleo-ENSO reconstruction method is now available for the eastern Pacific that allows direct comparisons with coral records from the central and western Pacific and with climate model outputs. To illustrate this, we plotted the distribution of the annual mean of Niño1 + 2 index from a 1000-year preindustrial control simulation of the IPSL_CM4v2 coupled ocean atmosphere general circulation model (GCM) (for details about the simulation, see Servonnat et al. (2010)), and the distribution of mean annual $\delta^{18}O$ values from the Punta Pitt coral studied by Shen et al. (1992) (Fig. 7C,E). The IPSL_CM4v2 model yielded a normal distribution and thus failed to capture the characteristics of the observed SST anomaly distribution in the Niño1 + 2 region, as most climate models do. The distribution from the Galapagos coral is slightly asymmetric but much less so than the Niño1 + 2 index distribution, which suggests that this coral may have stopped growing during the largest El Niño events.

5. Conclusions

Seasonal SST variations are faithfully reconstructed from $\delta^{18}O$ values in the shells of the mollusk *M. donacium*, especially because of low sea water $\delta^{18}O$ variability along the central and southern coasts of Peru. We analyzed a modern sample of 13 shells from the Peruvian southern coast (Rio Ica, Fig. 1) that represents a modern reference to estimate past oceanographic changes. The mean seasonal amplitude of SST is estimated by the mean of ΔT values (<ΔT>) calculated from the shell sample. The seasonal amplitude of SST, ΔT, along the length of the Peruvian coast is strongly correlated with the El Niño1 + 2 index from 1950 to 2002. Therefore, the variance, Var(ΔT), calculated from a shell sample yields a reliable estimate of the amplitude of ENSO variability at the regional scale. This variability includes the range of anomalies from La Niña to moderate El Niño events, but excludes extreme warm anomalies like the 1997–98 event because of high mortality of the shells. $<\Delta T>_{fossil}/<\Delta T>_{modern}$ and $Var(\Delta T)_{fossil}/Var(\Delta T)_{modern}$ would yield quantitative estimates of past changes in SST seasonality and ENSO activity, and are

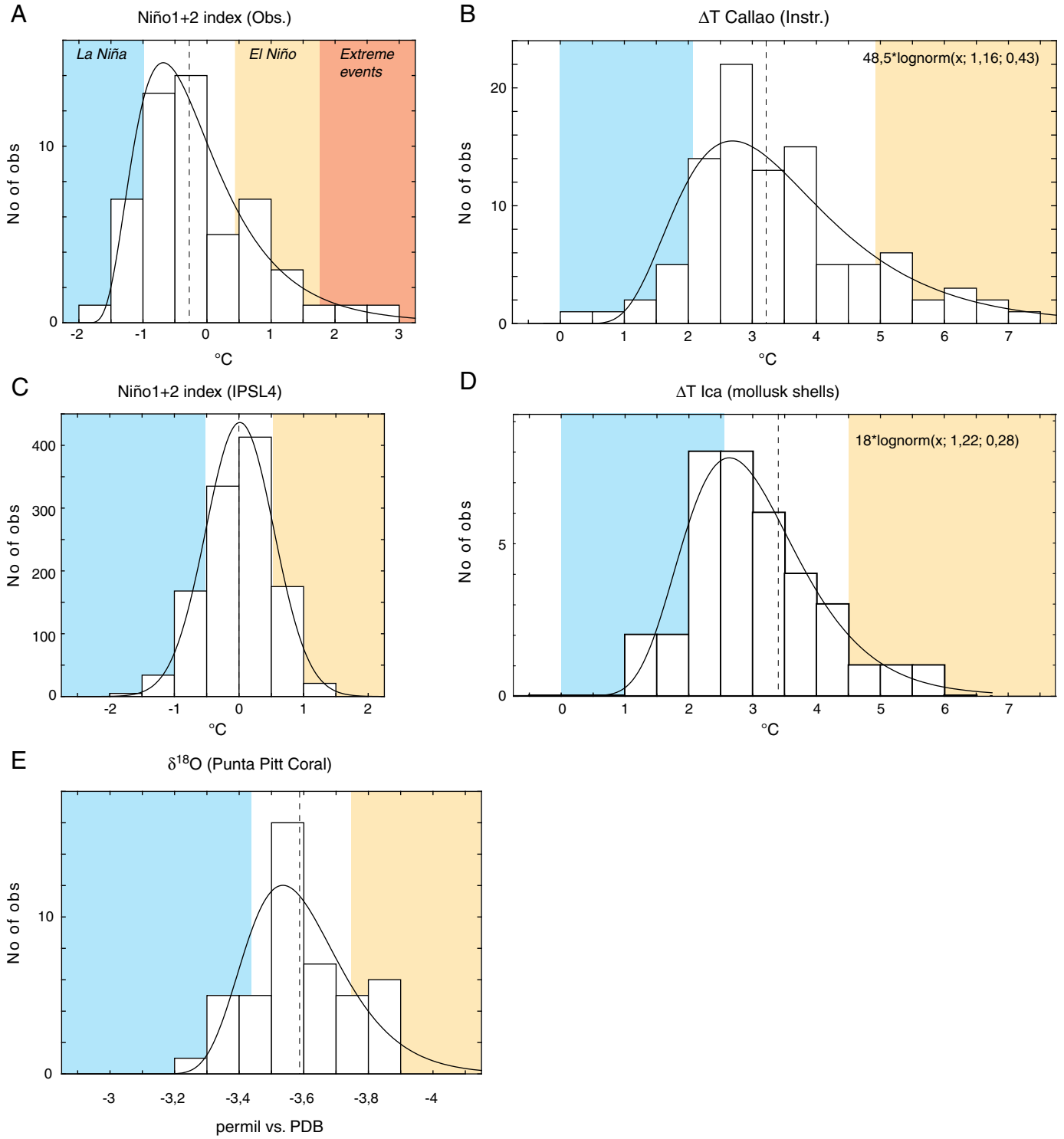

Fig. 7. Frequency distributions of (A) Niño1+2 index annual means from 1950 to 2002, (B) Callao ΔT values from 1950 to 2002, (C) Niño1+2 index annual means from IPSL_CM4v2 preindustrial control simulation, (D) ΔT values calculated from *M. donacium* shells from Rio Ica, (E) $\delta^{18}O$ annual means from the Punta Pitt coral recording the 1936–1982 period (Shen et al., 1992). Black curves represent the best lognormal fit, and the best normal fit for (C). Blue and yellow areas indicate La Niña and El Niño events respectively.

independent from the paleotemperature proxy model. The uncertainty of these reconstructions can be quantitatively estimated by the MoCo program (Carré et al., 2012). Changes in the event intensity and in the distribution of cold and warm ENSO events can be studied by the ΔT frequency distribution provided shell samples. The representation of ENSO activity as a frequency distribution of event intensity permits the comparison of shell records with coral records and with climate model simulations, which can give crucial insights into the variability of the spatial pattern of ENSO anomalies and the associated mechanisms. The method presented here may be used with any mollusk shell species that faithfully records the full annual cycle of SST. Well-preserved fossil mollusk shells are available in

abundance on the Peruvian coast for the Holocene period in anthropogenic shell middens or for the Pleistocene in marine terraces, and thus offer a unique opportunity to estimate quantitatively past ENSO activity in the eastern tropical Pacific.

Acknowledgments

This material is based upon work supported by the Joint Institute for the Study of Atmosphere and Ocean through a postdoctoral fellowship, the U.S. National Science Foundation under grant no. NSF-ATM-0811382 (J.P.S.), the U.S. National Oceanic and Atmospheric Administration under grant no. NOAA-NA08OAR4310685 (J.P.S.), and the ANR research project EL PASO (P.I. P. Braconnot). We are thankful to Catherine Pierre for water isotopic analyses. We thank 4 anonymous reviewers for helping improving the manuscript. This is ISEM contribution N° 2012-216.

Appendix A. Supplementary data

Supplementary data to this article can be found online at http://dx.doi.org/10.1016/j.palaeo.2012.12.014.

References

Andrus, C.F.T., Hodgins, G.W.L., Sandweiss, D.H., Crowe, D.E., 2005. Molluscan radiocarbon as a proxy for El Niño-related upwelling variation in Peru. In: Mora, G., Surge, D. (Eds.), Isotopic and Elemental Tracers of Cenozoic Climate Change. Geological Society of America, pp. 13–20.

Carré, M., 2007. El mes de recolección de la macha (Mesodesma donacium) determinado por sus líneas de crecimiento: aplicaciones arqueológicas. Bulletin de l'Institut Français d'Etudes Andines 36, 299–304.

Carré, M., Bentaleb, I., Blamart, D., Ogle, N., Cardenas, F., Zevallos, S., Kalin, R.M., Ortlieb, L., Fontugne, M., 2005. Stable isotopes and sclerochronology of the bivalve *Mesodesma donacium*: potential application to Peruvian paleoceanographic reconstructions. Palaeogeography, Palaeoclimatology, Palaeoecology 228, 4–25.

Carré, M., Klaric, L., Lavallée, D., Julien, M., Bentaleb, I., Fontugne, M., Kawka, O., 2009. Insights into early Holocene hunter-gatherer mobility on the Peruvian Southern Coast from mollusk gathering seasonality. Journal of Archaeological Science 36, 1173–1178.

Carré, M., Sachs, J.P., Wallace, J.M., Favier, C., 2012. Exploring errors in paleoclimate proxy reconstructions using Monte Carlo simulations: paleotemperature from mollusk and coral geochemistry. Climate of the Past 8, 433–450.

Cobb, K.M., Charles, C.D., Cheng, H., Edwards, R.L., 2003. El Niño/Southern Oscillation and tropical Pacific climate during the last millenium. Nature 424, 271–276.

Cohn, M., Urey, H.C., 1938. Oxygen exchange reactions of organic compounds with water. Journal of the American Chemical Society 60, 679–687.

Cole, J.E., Fairbanks, R.G., 1990. The southern oscillation recorded in the $\delta^{18}O$ of corals from Tarawa Atoll. Paleoceanography 5, 669–683.

Conroy, J.L., Overpeck, J.T., Cole, J.E., Shanahan, T.M., Steinitz-Kannan, M., 2008. Holocene changes in eastern Pacific climate inferred from a Galápagos lake sediment record. Quaternary Science Reviews 27, 1166–1180.

Coplen, T.B., 1996. New guidelines for reporting stable hydrogen, carbon, and oxygen isotope-ratio data. Geochimica et Cosmochimica Acta 60, 3359–3360.

Corrège, T., Delcroix, T., Rècy, J., Beck, W., Cabioch, G., Le Cornec, F., 2000. Evidence for stronger El Niño-Southern Oscillation (ENSO) events in a Mid-Holocene massive coral. Paleoceanography 15, 465–470.

D'Arrigo, R.D., Jacoby, G.C., 1992. A tree-ring reconstruction of New Mexico winter precipitation and its relation to El Niño/Southern Oscillation events. In: Diaz, H.F., Markgraf, V. (Eds.), El Niño, Historical and Paleoclimatic Aspects of the Southern Oscillation. Cambridge University Press, Cambridge, pp. 243–257.

D'Arrigo, R., Cook, E.R., Wilson, R.J., Allan, R., Mann, M.E., 2005. On the variability of ENSO over the past six centuries. Geophysical Research Letters 32.

Dunbar, R.B., Wellington, G.M., Colgan, M.W., Glynn, P.W., 1994. Eastern Pacific sea surface temperature since 1600 A.D.: the $\delta^{18}O$ record of climate variability in Galapagos corals. Paleoceanography 9, 291–315.

Epstein, S., Mayeda, T., 1953. Variation of ^{18}O content of waters from natural sources. Geochimica et Cosmochimica Acta 4, 213–224.

Evans, M.N., Kaplan, A., Cane, M.A., 2002. Pacific sea surface temperature field reconstruction from coral $\delta^{18}O$ data using reduced space objective analysis. Paleoceanography 17.

Fairbanks, R.G., Sverdlove, M., Free, R., Wiebe, P.H., Bé, A.W.H., 1982. Vertical distribution and isotopic fractionation of living planktonic foraminifera from the Panama basin. Nature 298, 841–844.

Garreaud, R.D., Vuille, M., Compagnucci, R., Marengo, J., 2009. Present-day South American climate. Palaeogeography, Palaeoclimatology, Palaeoecology 281, 180–195.

Grossman, E.L., Ku, Teh-Lung, 1986. Oxygen and carbon fractionation in biogenic aragonite: temperature effect. Chemical Geology 59, 59–74.

Hickson, J.A., Johnson, A.L.A., Heaton, T.H.E., Balson, P.S., 1999. The shell of the queen scallop *Aequipecten opercularis* as a promising tool for paleoenvironmental reconstruction: evidence and reasons for equilibrium stable-isotope incorporation. Palaeogeography, Palaeoclimatology, Palaeoecology 154, 325–337.

Jones, K.B., Hodgins, G.W.L., Etayo-Cadavid, M.F., Andrus, C.F.T., 2009. Upwelling signals in radiocarbon from early 20th-century Peruvian bay scallop (*Argopecten purpuratus*) shells. Quaternary Research 72, 452–456.

Kilbourne, K.H., Quinn, T.M., Taylor, F.W., Delcroix, T., Gouriou, Y., 2004. El Niño-Southern Oscillation-related salinity variations recorded in the skeletal geochemistry of a Porites coral from Espiritu Santo, Vanuatu. Paleoceanography 19, PA4002.

Kim, S.-T., Mucci, A., Taylor, B.E., 2007. Phosphoric acid fractionation factors for calcite and aragonite between 25 and 75 °C: revisited. Chemical Geology 246, 135–146.

Koutavas, A., deMenocal, P.B., Olive, G.C., Lynch-Stieglitz, J., 2006. Mid-Holocene El Niño-Southern Oscillation (ENSO) attenuation revealed by individual foraminifera in eastern tropical Pacific sediments. Geology 34, 993–996.

Lavallée, D., Julien, M., Béarez, P., Bolaños, A., Carré, M., Chevalier, A., Delabarde, T., Fontugne, M., Rodríguez-Loredo, C., Klaric, L., Usselmann, P., Vanhaeren, M., 2011. Quebrada de los burros. Los primeros pescadores del litoral Pacífico en el extremo sur peruano. Chungara, Revista de Antropología Chilena 43, 333–351.

Lazareth, C.E., Lasne, G., Ortlieb, L., 2006. Growth anomalies in *Protothaca thaca* (Mollusca, Veneridae) shells as markers of ENSO conditions. Climate Research 30, 263–269.

Leduc, G., Vidal, L., Cartapanis, O., Bard, E., 2009. Modes of eastern equatorial Pacific thermocline variability: implications for ENSO dynamics over the last glacial period. Paleoceanography 24. http://dx.doi.org/10.1029/2008PA001701.

McCulloch, M., Mortimer, G., Esat, T., Xianghua, L., Pillans, B., Chappell, J., 1996. High resolution windows into early Holocene climate: Sr/Ca coral records from the Huon Peninsula. Earth and Planetary Science Letters 138, 169–178.

McGregor, S., Timmermann, A., Timm, O., 2010. A unified proxy for ENSO and PDO variability since 1650. Climate of the Past 6, 1–17.

Monterey, G.I., Levitus, S., 1997. Climatological Cycle of Mixed Layer Depth in the World Ocean. U.S. Gov. Printing Office, NOAA NEDIS, p. 5.

Moy, C.M., Seltzer, G.O., Rodbell, D.T., Anderson, D.M., 2002. Variability of El Niño/Southern Oscillation activity at millennial timescales during the Holocene epoch. Nature 420, 162–165.

Perrier, C., Hillaire-Marcel, C., Ortlieb, L., 1994. Paléogéographie littorale et enregistrement isotopique (^{13}C, ^{18}O) d'évènements de type El Niño par les mollusques Holocènes et récents du Nord-Ouest Péruvien. Géographie Physique et Quaternaire 48, 23–38.

Rein, B., Lückge, A., Reinhardt, L., Sirocko, F., Wolf, A., Dullo, W.-C., 2005. El Niño variability off Peru during the last 20,000 years. Paleoceanography 20. http://dx.doi.org/10.1029/2004PA001099.

Riascos, J.M., Carstensen, D., Laudien, J., Arntz, W.E., Oliva, M.E., Güntner, A., Heilmayer, O., 2009. Thriving and declining: climate variability shaping life-history and population persistence of *Mesodesma donacium* in the Humboldt Upwelling System. Marine Ecology Progress Series 385, 151–163.

Riedinger, M.A., Steinitz-Kannan, M., Last, W.M., Brenner, M., 2002. A ~6100 ^{14}C yr record of El Niño activity from the Galapagos Islands. Journal of Paleolimnology 27, 1–7.

Rodbell, D.T., Seltzer, G.O., Anderson, D.M., Abbott, M.B., Enfield, D.B., Newman, J.H., 1999. An ~15,000-year record of El Niño driven alluviation in southwestern Ecuador. Science 283, 516–520.

Sandweiss, D.H., Richardson III, J.B., Reitz, E.J., Hsu, J.T., Feldman, R.A., 1989. Early maritime adaptations in the Andes: preliminary studies at the Ring Site, Peru. In: Rice, D., Stanish, C., Scarr, P.R. (Eds.), Ecology, Settlement and History in the Osmore Drainage, Peru: BAR International Series, 545 (i), pp. 35–84 (Oxford, I).

Sandweiss, D.H., McInnis, H., Burger, R.L., Cano, A., Ojeda, B., Paredes, R., Sandweiss, M.C., Glascock, M.D., 1998. Quebrada Jaguay: South American maritime adaptations. Science 281, 1830–1832.

Schöne, B.R., Freyre Castro, A.D., Fiebig, J., Houk, S.D., Oschmann, W., Kröncke, I., 2004. Sea surface water temperatures over the period 1884–1983 reconstructed from oxygen isotope ratios of a bivalve mollusk shell (*Arctica islandica*, southern North Sea). Palaeogeography, Palaeoclimatology, Palaeoecology 212, 215–232.

Servonnat, J., Yiou, P., Khodri, M., Swingedouw, D., Denvil, S., 2010. Influence of solar variability, CO2 and orbital forcing between 1000 and 1850 AD in the IPSLCM4 model. Climate of the Past 6, 445–460.

Shen, G.T., Cole, J.E., Lea, D.W., Linn, L.J., McConnaughey, T.A., Fairbanks, R.G., 1992. Surface ocean variability at Galapagos from 1936–1982: calibration of geochemical tracers in corals. Paleoceanography 7, 563–588.

Stahle, D.W., D'Arrigo, R.D., Krusic, P.J., Cleaveland, M.K., Cook, E.R., Allan, R.J., Cole, J.E., Dunbar, R.B., Therrell, M.D., Gay, D.A., Moore, M.D., Stokes, M.A., Burns, B.T., Villanueva-Diaz, J., Thompson, L.G., 1998. Experimental dendroclimatic reconstruction of the Southern Oscillation. Bulletin of the American Meteorological Society 79, 2137–2152.

Takahashi, K., Montecinos, A., Goubanova, K., Dewitte, B., 2011. ENSO regimes: reinterpreting the canonical and Modoki El Niño. Geophysical Research Letters 38.

Tarifeño, E., 1980. Studies on the Biology of Surf Clam *Mesodesma donacium* (Lamarck, 1818) (Bivalvia: Mesodesmatidae) from Chilean Sandy Beaches. University of California, Los Angeles, p. 229.

Tobin, T.S., Schauer, A.J., Lewarch, E., 2011. Alteration of micromilled carbonate $\delta^{18}O$ during Kiel Device analysis. Rapid Communications in Mass Spectrometry 25, 2149–2152.

Tudhope, A.W., Chilcott, C.P., McCulloch, M.T., Cook, E.R., Chappell, J., Ellam, R.M., Lea, D.W., Lough, J.M., Shimmield, G.B., 2001. Variability in the El-Niño Southern Oscillation through a Glacial–Interglacial Cycle. Science 291, 1511–1517.

PALEOCEANOGRAPHY

Holocene history of ENSO variance and asymmetry in the eastern tropical Pacific

Matthieu Carré,[1]* Julian P. Sachs,[2] Sara Purca,[3] Andrew J. Schauer,[4] Pascale Braconnot,[5] Rommel Angeles Falcón,[6] Michèle Julien,[7] Danièle Lavallée[8]

Understanding the response of the El Niño–Southern Oscillation (ENSO) to global warming requires quantitative data on ENSO under different climate regimes. Here, we present a reconstruction of ENSO in the eastern tropical Pacific spanning the past 10,000 years derived from oxygen isotopes in fossil mollusk shells from Peru. We found that ENSO variance was close to the modern level in the early Holocene and severely damped ~4000 to 5000 years ago. In addition, ENSO variability was skewed toward cold events along coastal Peru 6700 to 7500 years ago owing to a shift of warm anomalies toward the Central Pacific. The modern ENSO regime was established ~3000 to 4500 years ago. We conclude that ENSO was sensitive to changes in climate boundary conditions during the Holocene, including but not limited to insolation.

The El Niño–Southern Oscillation (ENSO) represents the largest natural perturbation to the global climate on an interannual time scale, affecting ecosystems and economies globally. Predicting how the amplitude and spatial pattern of ENSO will change in response to evolving radiative forcing from the buildup of greenhouse gases in the atmosphere is a scientific challenge (*1*) that requires knowledge of the character of ENSO under a range of climate boundary conditions as observed during the Holocene epoch.

A central paradigm of ENSO–mean state studies for the past decade has been that changes in insolation resulting from cyclical changes in Earth's orbital geometry exert a strong control on ENSO (*2*–*4*). This hypothesis was recently called into question by a series of coral oxygen isotope ($\delta^{18}O$) records from the Line Islands in the central Pacific showing large variability in the amplitude of ENSO variance over the past 7000 years, but no significant difference between the middle Holocene and the past millennium (*5*). Furthermore, no reconstructions of ENSO have yet been able to document changes in the spatial pattern of ENSO that are now recognized to account for an important component of its global teleconnections (*6*). We used a technique based on $\delta^{18}O$ variations in fossil mollusk shells from the coast of Peru (*7*) to quantify changes in the amplitude and spatial pattern of ENSO through the Holocene.

We reconstructed the distribution of ENSO-related sea surface temperature (SST) anomalies in the eastern tropical Pacific from monthly records of $\delta^{18}O$ values in fossil *Mesodesma donacium* shells on the coast of Peru. *M. donacium* is a fast-growing aragonitic bivalve that inhabits the surf zone of sandy beaches. Well-preserved shells were collected from radiocarbon-dated intervals at seven coastal archaeological sites (*8*) between 11.7 °S and 18.1 °S (Fig. 1, fig. S1, and table S1). *M. donacium* has been gathered and consumed by fishermen for more than 10,000 years (*9*), resulting in anthropogenic shell mounds up to 10 m in height along the Peruvian coastal desert (figs. S2 to S8). Shells were generally perfectly preserved owing to extremely arid conditions, ensuring the fidelity of $\delta^{18}O$ values (figs. S9 and S10) (*8*). Previous calibration work has demonstrated that *M. donacium* shells faithfully record 1 to 4 years of SST variability with ~1 month resolution (Fig. 1C), yielding quantitative estimates of the seasonal SST range (ΔT) in the coastal water (*10*). By analyzing a random sample of shells from a single depth interval that encompasses several decades or centuries of accumulation, the mean, variance, and skewness of coastal ΔT is obtained, as validated with modern specimens (*7*). A rigorous evaluation of the standard error for the mean, variance, and skewness of coastal ΔT was conducted with a series of pseudo-proxy Monte Carlo simulations that took into consideration the uncertainties associated with isotopic analyses, sampling within climate variability, mesoscale spatial variability, and shell growth, enabling the statistical significance of results to be ascertained (*11*).

Peruvian surf clams share similarities with corals as paleoclimate proxies in that the seasonality of SST can be resolved (*5*), and with individual foraminifera (*12*), because a sample of several specimens is required to statistically extract ENSO characteristics. *M. donacium* shells record ENSO variance resulting from La Niña anomalies and moderate El Niño anomalies but do not record extreme El Niño events. When coastal Peru SSTs warm dramatically (maximum anomaly of 7.7°C in January 1998 in Callao), mass mortality of *M. donacium* occurs. Nevertheless, the distribution of ΔT from a sample of modern shells, though truncated, accurately captures the positively skewed distribution of ENSO in the eastern Pacific (*7*). Our composite Holocene record from 180 mollusk shells and seven archaeological sites thus yields a quantitative reconstruction of mean annual SST, mean ΔT, as well as ENSO variance and skewness for coastal Peru. Because the variance of coastal Peruvian ΔT is highly correlated with the variance of SST anomalies in the Niño1+2 region [correlation coefficient (r) = 0.85], var(ΔT) in Peru can be used as a reliable indicator of ENSO variance in the eastern tropical Pacific (*7*).

Mean annual SST was significantly lower 4.5 thousand years ago (ka) to 9.6 ka than today, especially in southern Peru, where SSTs were ~3°C cooler (Fig. 2A). These cooler conditions imply an increase in the intensity of coastal upwelling (*13*, *14*). Although highly variable, the seasonal range of SST (ΔT) was significantly reduced compared with the late 20th century during most of the Holocene, with reductions up to ~30% (equivalent to ~1.1°C) 0.5, 4.7, 8.5, and

[1]UM2-CNRS–Institut pour la Recherche et le Développement (IRD), Institut des Sciences de l'Evolution de Montpellier, UMR 5554, Place Eugène Bataillon, 34095 Montpellier, France. [2]School of Oceanography, University of Washington, Post Office Box 355351, Seattle, WA 98195, USA. [3]Instituto del Mar del Perú (IMARPE), Esquina Gamarra y general Valle S/N, Callao, Perú. [4]Department of Earth and Space Sciences, University of Washington, Post Office Box 351310, Seattle, WA 98195, USA. [5]Institut Pierre-Simon Laplace/Laboratoire des Sciences du Climat et de l'Environnement, unité mixte CEA-CNRS–Université de Versailles Saint-Quentin-en-Yvelines, Orme des merisiers, Bâtiment 712, 91191 Gif sur Yvette, France. [6]Ministerio de Cultura, Museo de sitio de Pachacamac, Lurín, Lima, Perú. [7]Archéologies et Sciences de l'Antiquité, UMR 7041, Maison René Ginouvès, 21 Allée de l'Université, 92023 Nanterre, France. [8]Archéologie des Amériques, UMR 8096, Maison René Ginouvès, 21 Allée de l'Université, 92023 Nanterre, France.
*Corresponding author. E-mail: matthieu.carre@univ-montp2.fr

9.5 ka (Fig. 2B). Furthermore, ENSO variability, as derived from the variance of ΔT, was higher in the late 20th century than at any other sampled interval of the Holocene, even excluding the influence of the 1982–1983 and 1997–1998 extreme El Niño events (Fig. 3A). The lowest ENSO variance in the eastern tropical Pacific occurred at ~4.7 ka (55% reduction, 82% confidence level) (Fig. 3A).

A Holocene minimum in ENSO variance 4 to 5 ka is supported by a sedimentary record of $\delta^{18}O$ values in individual planktonic foraminifera from near the Galápagos that also indicates highly variable conditions throughout the Holocene, interrupted by a period of low foraminiferal $\delta^{18}O$ variance 4 to 5 ka (Fig. 3C) (*12*). In addition to interannual SST variability, however, the variance of foraminiferal $\delta^{18}O$ in marine sediments is influenced by decadal variability and changing precession-driven seasonality. In the central Pacific, coral $\delta^{18}O$ records indicate lower than modern ENSO variance during the Holocene, with large variations before 6 ka and after 3 ka and a minimum in ENSO variance 3 to 5 ka (*5*). Although the latter result is not statistically significant in light of the full data set (*5*), its robustness is now increased by the consistent variance reduction observed in our Peru mollusk record and the foraminiferal record from the Galapagos (*12*). Further support for low ENSO variance in the 4- to 5-ka time period comes from a 175-year coral $\delta^{18}O$ record from Christmas Island, which indicated a 79% reduction of ENSO variance in the central Pacific ~4.3 ka (*15*). A network of evidence thus supports the occurrence of a substantial multicentennial reduction of ENSO variance 4 to 5 ka across the Niño3.4 and Niño1+2 domains.

ENSO variance recorded by Peru mollusks 6 to 10 ka was variable but not statistically different from the Late Holocene. Our reconstruction combined with early Holocene dates of flood deposits in coastal Peru (*16*–*18*) challenge the hypothesis of little or no ENSO variance before ~5 ka (*19*–*21*)—a conclusion based largely on the analysis of clastic sediments in Lake Pallcacocha (*19*, *20*). However, clastic sediments in high Andean Lakes have recently been reinterpreted in terms of soil erosion from mountain glacier activity rather than from rainfall events associated with ENSO (*22*). The only reliable marine evidence for inactive ENSO in the early to middle Holocene is provided by corals from Papua New Guinea (*23*). Apparent disagreements between ENSO records from the Western and Eastern Pacific may in fact be indicative of changes in the spatial pattern of ENSO.

Two spatial modes of ENSO variability have been described, defined by maximum SST anomalies localized in the central Pacific (CP) or eastern Pacific (EP) (*24*, *25*). The EP mode tends to produce strong El Niño warming events in the East and moderate La Niña events. This well-known asymmetry between El Niño and La Niña events results in a positively skewed distribution of SST anomalies (Fig. 1A). The CP mode tends to produce moderate El Niño events centered in

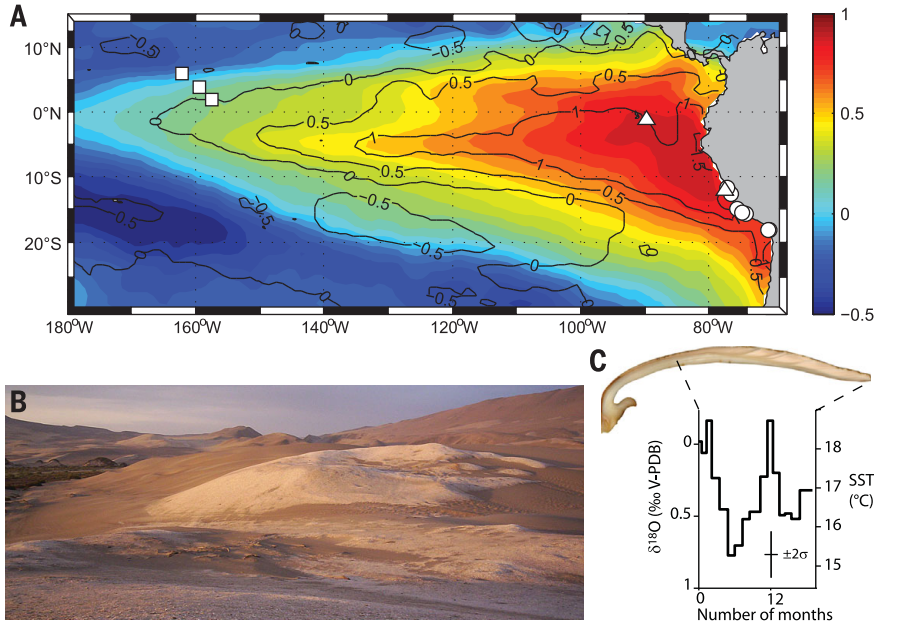

Fig. 1. The Peruvian archaeological shell middens. (**A**) Map of the central and eastern tropical Pacific indicating the location of shell middens (circles), sediment cores (triangles), and coral records (squares) discussed in the text. The skewness of monthly SST anomalies for the 1950–2010 period is represented by isolines, and the EP pattern of ENSO as defined in (*32*) is represented by color shades. For this analysis, the NOAA NCEP Global Reyn_SmithOIv2 product that merges satellite and station data (*33*) was used (NCEP, National Centers for Environmental Prediction). (**B**) Picture of the northern part of the Ica-IS2 archaeological shell midden in the lower Ica valley, Peru (*8*). (**C**) Illustrative example of a *M. donacium* cross section and its associated monthly isotopic record converted to SST (shell ICA-1) (*8*).

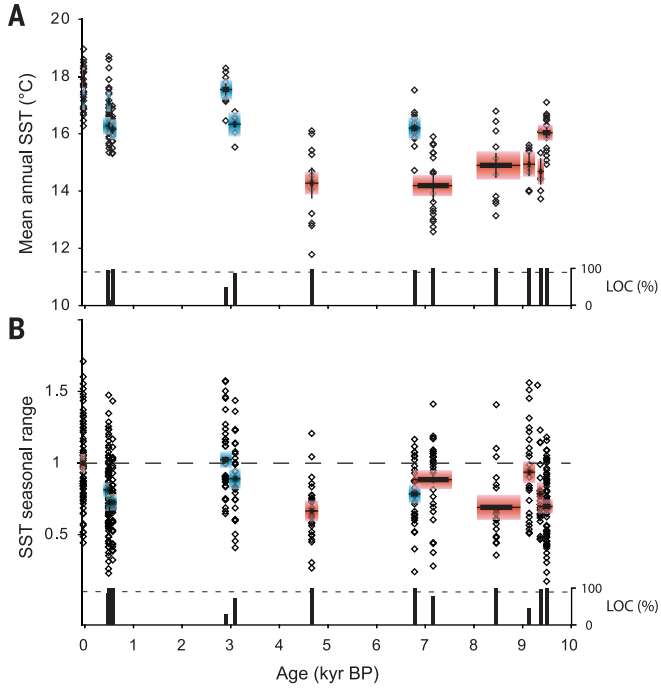

Fig. 2. Holocene reconstruction of mean annual SST and seasonal SST range from fossil mollusk $\delta^{18}O$ values on the Peru coast. (**A**) Mean SST values obtained from individual shells (open diamonds). For each shell midden, the average SST was represented over the occupation time span (thick horizontal line, prolonged by a thin line for the 1σ calibration interval). The standard error (±1σ) of reconstructed SSTs is represented by blue bars for the central coast and red bars for the southern coast of Peru (fig. S1). A second error bar (±1σ) incorporates any potential systematic error introduced by calibration of the mollusk $\delta^{18}O$ SST proxy plus uncertainty in the correction for ice volume effects on ocean $\delta^{18}O$ (*8*, *11*). The level of confidence (LOC) that reconstructed values of mean annual SST are significantly different from modern SSTs (Student's *t* test) is indicated by black bars in the bottom of both (A) and (B), with the dotted line indicating the 90% LOC. (**B**) Seasonal ranges of *M. donacium* shell $\delta^{18}O$ normalized to the modern mean value. Individual shells record one to eight successive ΔT values (open diamonds) (*8*). For each shell midden, average values and standard errors were represented as in (A). The horizontal dashed line represents modern conditions. LOC are indicated as in (A).

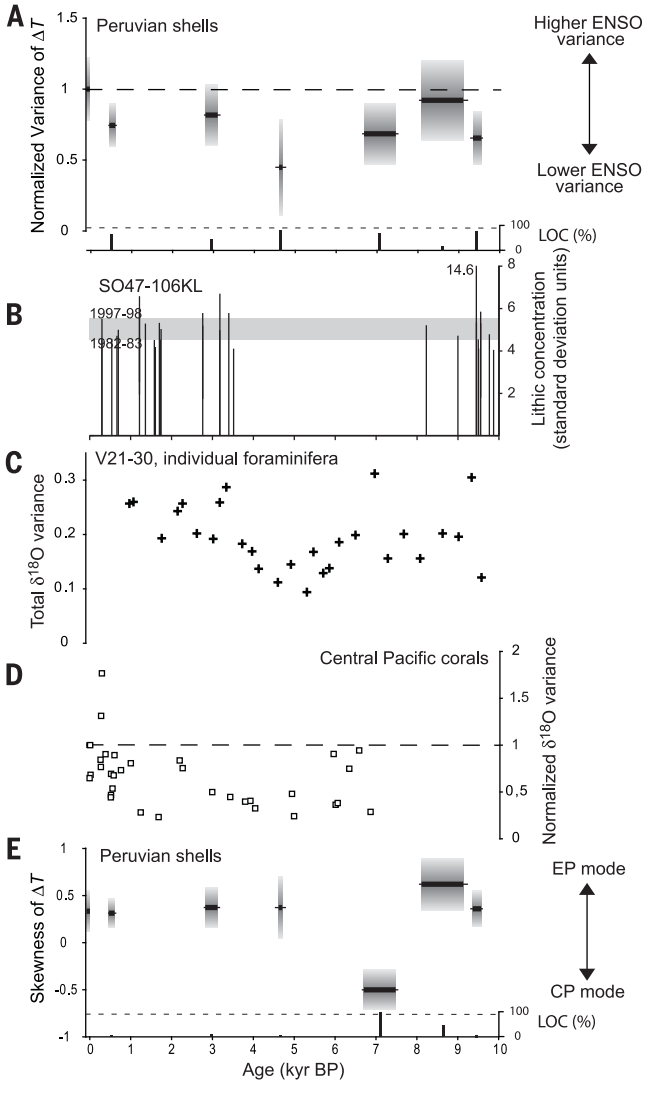

Fig. 3. Holocene records of ENSO from the eastern and central tropical Pacific Ocean. (**A**) Normalized variance of ΔT values in mollusk shell samples (this study) indicating ENSO variance in the Niño1+2 region, with ±1σ standard errors (gray boxes). LOC are indicated as in Fig. 2A. (**B**) Extreme flood events in coastal Peru inferred from lithic concentrations in excess of 4σ of the detrended signal in the SO147-106KL sediment core (*26*) (supplementary text). The level for the very stong El Niño events in 1982–1983 and 1997–1998 is indicated with gray shading for comparison. (**C**) $\delta^{18}O$ variance of individual *Globigerinoides ruber* planktonic foraminifera in core V21-30 from near the Galápagos (*12*). (**D**) ENSO variance inferred from $\delta^{18}O$ values of fossil corals from the Northern Line Islands of Palmyra, Fanning, and Christmas (*5*), normalized by the modern variance at each location (*8*). (**E**) Skewness of ΔT in *M. donacium* shell samples (this study) with standard errors (±1σ), indicating the relative contribution of CP and EP ENSO modes. LOC is shown as in Fig. 2A.

the CP and strong La Niña events, resulting in a negatively skewed distribution of SST anomalies in Peru as shown by instrumental data (*24*–*26*). The skewness of ENSO anomalies in fossil shell samples thus tracks past changes in the dominant spatial pattern of ENSO variability (*8*). Skewness values in the fossil record are positive and similar to modern conditions during most of the Holocene, except for the period 6.7 to 7.5 ka, when a significant shift (95% confidence level) toward negative skewness occurred (Fig. 3E). This result implies that the SST variability in the EP at that time was driven by cold anomalies, and that warm anomalies in the Niño1+2 region were less frequent and/or intense. A possible explanation for this pattern may be a predominantly CP mode of ENSO 6.7 to 7.5 ka.

This hypothesis is supported by a record of flood events from the Peru margin (Fig. 3B) (*27*). High lithic concentrations (exceeding 4σ of the signal) in a sediment core from the continental shelf off central Peru record coastal floods due to extreme El Niño events that are typical of the EP mode (*28*). By indicating extreme El Niño events, this proxy thus fills the gap of ENSO variance that is not recorded by Peruvian mollusk shells (supplementary text). That record clearly shows the occurrence of eight large flood events before 8 ka and 14 after 4 ka (Fig. 3B), which is also consistent with earlier studies of flood-related debris flow deposits in Peru (*16*, *17*, *29*). This is in agreement with the mollusk $\delta^{18}O$ data indicating strong ENSO activity dominated by the EP mode before 8 ka and after 4 ka. From 6.7 to 7.5 ka, on the other hand, the complete absence of flood events contrasts with the substantial though weaker ENSO variance reconstructed from mollusk shells. This apparent disagreement can be most simply explained by a predominance of the CP mode of ENSO at that time, as implied by the negative skewness of the ΔT distribution (Fig. 3E). CP El Niño events have a different teleconnection pattern and do not generate rainfall anomalies on the Peruvian coast.

A central question in climate science is the extent to which changes in the climatic mean state influence ENSO variability. Long unforced climate simulations exhibit multidecadal, internally generated changes in ENSO behavior (*30*). Our data indicate that changes in the character of ENSO during the Holocene persisted for centuries, exceeding the time scale of model-generated internal variability. We therefore surmise that ENSO is sensitive to external forcing. Climate models forced by 6- and 9.5-ka insolation produce a cooling and reduced ΔT in the eastern Pacific, along with reduced ENSO variance (*3*, *4*). The simulated impact of insolation is consistent with the mean annual and seasonal range of SST derived from Peru mollusks, but not for ENSO variance, which the mollusks indicate was high in the early Holocene. Climate simulations have demonstrated that a freshwater flux into the North Atlantic could offset the impact of insolation on ENSO in the early Holocene (*31*). Our data support this scenario and imply that any tendency toward lower ENSO variance during the mid-Holocene insolation regime may have been counteracted 6.7 to 10 ka by the influence of melting ice sheets (*31*). Although the low ENSO activity 4 to 5 ka is consistent with precessional forcing, the shift of ENSO asymmetry 6.7 to 7.5 ka points to factors within the climate system influencing changes in the spatial pattern of ENSO.

REFERENCES AND NOTES

1. A. Santoso *et al.*, *Nature* **504**, 126–130 (2013).
2. A. C. Clement, R. Seager, M. A. Cane, *Paleoceanography* **14**, 441–456 (1999).
3. W. Zheng, P. Braconnot, E. Guilyardi, U. Merkel, Y. Yu, *Clim. Dyn.* **30**, 745–762 (2008).
4. Y. Luan, P. Braconnot, Y. Yu, W. Zheng, O. Marti, *Clim. Past* **8**, 1093–1108 (2012).
5. K. M. Cobb *et al.*, *Science* **339**, 67–70 (2013).
6. T. Lee, M. J. McPhaden, *Geophys. Res. Lett.* **37**, L14603 (2010).
7. M. Carré, J. P. Sachs, A. J. Schauer, W. E. Rodríguez, F. C. Ramos, *Palaeogeogr. Palaeoclimatol. Palaeoecol.* **371**, 45 (2013).
8. Materials and methods are available as supplementary materials on *Science* Online.
9. D. H. Sandweiss *et al.*, *Science* **281**, 1830–1832 (1998).
10. M. Carré *et al.*, *Palaeogeogr. Palaeoclimatol. Palaeoecol.* **228**, 4–25 (2005).
11. M. Carré, J. P. Sachs, J. M. Wallace, C. Favier, *Clim. Past* **8**, 433–450 (2012).
12. A. Koutavas, S. Joanides, *Paleoceanography* **27**, PA4208 (2012).
13. M. Carré *et al.*, *Quat. Int.* **253**, 55–66 (2012).
14. J. Sadler *et al.*, *Geochem. Geophys. Geosyst.* **13**, Q01015 (2012).
15. H. V. McGregor *et al.*, *Nat. Geosci.* **6**, 949–953 (2013).
16. M. Fontugne, P. Usselmann, D. Lavallée, M. Julien, C. Hatté, *Quat. Res.* **52**, 171–179 (1999).
17. D. K. Keefer, M. E. Moseley, S. D. deFrance, *Palaeogeogr. Palaeoclimatol. Palaeoecol.* **194**, 41–77 (2003).
18. D. H. Sandweiss *et al.*, in *Climate Change and Cultural Dynamics: A Global Perspective on Mid-Holocene Transitions*, D. G. Anderson, K. A. Maasch, D. H. Sandweiss, Eds. (Academic Press, New York, 2007) pp. 25–50.
19. D. T. Rodbell *et al.*, *Science* **283**, 516–520 (1999).
20. C. M. Moy, G. O. Seltzer, D. T. Rodbell, D. M. Anderson, *Nature* **420**, 162–165 (2002).
21. J. L. Conroy, J. T. Overpeck, J. E. Cole, T. M. Shanahan, M. Steinitz-Kannan, *Quat. Sci. Rev.* **27**, 1166–1180 (2008).
22. D. T. Rodbell, G. O. Seltzer, B. G. Mark, J. A. Smith, M. B. Abbott, *Quat. Sci. Rev.* **27**, 1612–1626 (2008).
23. A. W. Tudhope *et al.*, *Science* **291**, 1511–1517 (2001).
24. H.-Y. Kao, J.-Y. Yu, *J. Clim.* **22**, 615–632 (2009).
25. S. I. An, F. F. Jin, *J. Clim.* **17**, 2399–2412 (2004).
26. B. Dewitte *et al.*, *Deep Sea Res. Part II Top. Stud. Oceanogr.* **77-80**, 143–156 (2012).
27. B. Rein *et al.*, *Paleoceanography* **20**, n/a (2005).
28. B. Rein, *Quat. Int.* **161**, 56–66 (2007).
29. L. E. Wells, *Geology* **18**, 1134 (1990).

30. A. T. Wittenberg, *Geophys. Res. Lett.* **36**, L12702 (2009).
31. P. Braconnot, Y. Luan, S. Brewer, W. Zheng, *Clim. Dyn.* **38**, 1081–1092 (2012).
32. K. Takahashi, A. Montecinos, K. Goubanova, B. Dewitte, *Geophys. Res. Lett.* **38**, L10704 (2011).
33. R. W. Reynolds, N. A. Rayner, T. M. Smith, D. C. Stokes, W. Wang, *J. Clim.* **15**, 1609–1625 (2002).

ACKNOWLEDGMENTS

This work was supported by the French Pérou-Sud archaeological project (D.L.), by the University of Washington–National Oceanic and Atmospheric Administration (NOAA) Joint Institute for the Study of Atmosphere and Ocean through a postdoctoral fellowship (M.C.), by the U.S. National Science Foundation under grant NSF-ATM-0811382 (J.P.S.), by NOAA under grant NOAANA080AR4310685 (J.P.S.), by the French National Research Agency under EL PASO grant 10-Blan-608-01 (P.B.), and by the French Institut National des Sciences de l'Univers with accelerator mass spectrometry dating (M.C.). We thank I. Bentaleb and H. Vonhof for their support in the early phase of this work, A. Portal for scanning electron microscopy observations at UM2, and M. Fontugne for his help and for providing the H4 shell sample. We are grateful to N. Mitma García, G. d'Herbes, J. Sadler, and M. Azzoug for technical assistance with sample preparation and to A. Mitma García for his help with fieldwork. The data reported in this paper are tabulated in the supplementary materials.

SUPPLEMENTARY MATERIALS

www.sciencemag.org/content/345/6200/1045/suppl/DC1
Materials and Methods
Figs. S1 to S11
Tables S1 to S3
Supplementary Text
References (*34*–*57*)
Data Tables S1 to S3

13 February 2014; accepted 14 July 2014
Published online 7 August 2014;
10.1126/science.1252220

nature geoscience

ARTICLES

PUBLISHED ONLINE: 14 DECEMBER 2015 | DOI: 10.1038/NGEO2608

Links between tropical Pacific seasonal, interannual and orbital variability during the Holocene

J. Emile-Geay[1]*, K. M. Cobb[2], M. Carré[3], P. Braconnot[4], J. Leloup[5], Y. Zhou[1], S. P. Harrison[6], T. Corrège[7], H. V. McGregor[8], M. Collins[9], R. Driscoll[10], M. Elliot[11], B. Schneider[12] and A. Tudhope[10]

The El Niño/Southern Oscillation (ENSO) is the leading mode of interannual climate variability. However, it is unclear how ENSO has responded to external forcing, particularly orbitally induced changes in the amplitude of the seasonal cycle during the Holocene. Here we present a reconstruction of seasonal and interannual surface conditions in the tropical Pacific Ocean from a network of high-resolution coral and mollusc records that span discrete intervals of the Holocene. We identify several intervals of reduced variance in the 2 to 7 yr ENSO band that are not in phase with orbital changes in equatorial insolation, with a notable 64% reduction between 5,000 and 3,000 years ago. We compare the reconstructed ENSO variance and seasonal cycle with that simulated by nine climate models that include orbital forcing, and find that the models do not capture the timing or amplitude of ENSO variability, nor the mid-Holocene increase in seasonality seen in the observations; moreover, a simulated inverse relationship between the amplitude of the seasonal cycle and ENSO-related variance in sea surface temperatures is not found in our reconstructions. We conclude that the tropical Pacific climate is highly variable and subject to millennial scale quiescent periods. These periods harbour no simple link to orbital forcing, and are not adequately simulated by the current generation of models.

ENSO, the oscillatory instability of the tropical Pacific ocean–atmosphere system, is the leading pattern of global interannual variability, with important physical, ecological and human impacts[1]. Yet, predicting its long-term behaviour in the face of continued anthropogenic forcing has proved elusive[2]. Whereas the predictive skill of climate models at interannual timescales can be tested using instrumental observations, such records are too short to evaluate the fidelity of model-simulated tropical Pacific variability on adaptation-relevant timescales. This motivates the use of palaeoclimate observations, which cover a much longer time span and predate the instrumental observations used to develop and tune climate models, hence providing an out-of-sample test of their predictive ability[3].

The mid-Holocene (MH, about 6,500 yr before present; 6.5 kyr BP) represents a key target for evaluating the simulated response of ENSO to external forcing. Whereas ice volume and greenhouse gas concentrations were essentially similar to today, the latitudinal and seasonal distribution of incoming solar radiation (insolation) was markedly different as a result of precession[4]: seasonal contrast was amplified in the Northern Hemisphere and reduced in the Southern Hemisphere. Thus, the MH provides an opportunity to explore the link between changes in the seasonal cycle, meridional asymmetry in the equatorial zone, and ENSO behaviour. Several circum-Pacific palaeoclimate records have been interpreted as implying a marked reduction in ENSO activity during the MH (refs 5–7), a reduction simulated by models of various complexity[8–13]. Furthermore, this reduction has been dynamically linked either to changes in the linear stability of ENSO (ref. 9), or to an insolation-driven increase in the amplitude of the annual cycle in near-equatorial sea surface temperature (SST; hereafter, AC; refs 9,10,12), in line with evidence for a negative correlation between ENSO and the AC documented in instrumental observations[14] and modelling studies of current and past climate states[8,15–19].

Several mechanisms have been proposed to account for the seasonal cycle influence on ENSO: frequency locking[15,20]; nonlinear resonance between annual and internal modes[21,22]; and combination tones of ENSO and the AC (ref. 23). We note, however, that the inverse link between ENSO variance and AC amplitude is not universal amongst models[4,10] nor in the various proposed mechanisms. Whereas some seasonally resolved palaeoclimate records suggest a strong dynamical link between precessional forcing and ENSO activity[24], reconstructions of central and eastern Pacific ENSO variance do not[25,26]. A synthesis of the available observations and simulations of ENSO and the annual cycle is timely, and would help constrain ENSO sensitivity to external forcing.

Here we synthesize high-resolution, well-dated palaeoclimate records from across the tropical Pacific spanning the Holocene

[1]Department of Earth Sciences, University of Southern California, Los Angeles, California 90089, USA. [2]School of Earth and Atmospheric Sciences, Georgia Institute of Technology, Atlanta, Georgia 30332, USA. [3]Institut des Sciences de l'Evolution, Université de Montpellier, CNRS, IRD, EPHE, Montpellier 34095, France. [4]IPSL/LSCE, unité mixte CEA-CNRS-UVSQ, Gif sur Yvette 91191, France. [5]Sorbonne Universités, UPMC Univ. Paris 6, LOCEAN/IPSL, UMR 7159, CNRS-IRD-MNHN, 75005 Paris, France. [6]Centre for Past Climate Change and School of Archaeology, Geography and Environmental Sciences (SAGES), University of Reading, Whiteknights, Reading RG6 6AB, UK. [7]Université Bordeaux, UMR CNRS 5805 EPOC, Allee Geoffroy St Hilaire, 33615 Pessac cedex, France. [8]School of Earth and Environmental Sciences, University of Wollongong, Wollongong, New South Wales 2522, Australia. [9]College of Engineering, Mathematics and Physical Sciences, University of Exeter, Laver Building, North Park Road, Exeter EX4 4QE, UK. [10]University of Edinburgh, School of GeoSciences, James Hutton Road, Edinburgh EH9 3FE, UK. [11]Paleoclimats Paleoenvironnements Bioindicateurs, Université de Nantes, LPGNantes, 2 rue de la Houssinière, Nantes 44300, France. [12]Institut für Geowissenschaften, Universität Kiel, D-24118 Kiel, Germany. *e-mail: julieneg@usc.edu

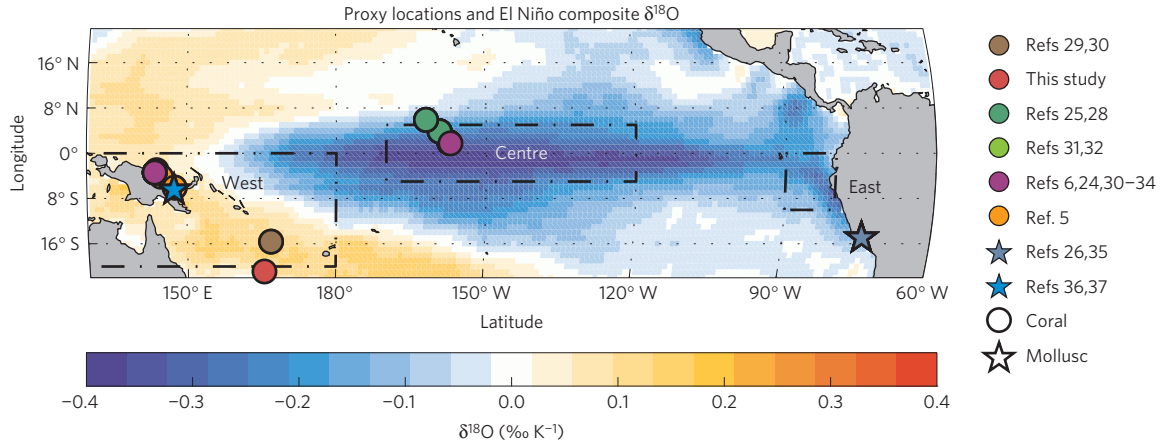

Figure 1 | Location and ENSO sensitivity of proxy archives. Circles denote corals; stars denote molluscs. Contours denote biocarbonate $\delta^{18}O$ composites (‰ per °C of NINO3.4 SST) derived from the model of ref. 39 driven by NCEP OI analysis v2 SST and SODA 2.2.4 SSS over 1981–2010 boreal winters (Supplementary Figs 8 and 9). $\delta^{18}O$ values were regressed onto NINO3.4 SST to highlight relationships to ENSO. The three equatorial study regions (west, centre and east) are delineated by rectangles. Note that refs 11,12,15,16,18–21 all use data from Kiritimati (1° 53′ N, 157° 24′ W).

(see Methods). We compare these observations with an ensemble of nine state-of-the-art global climate models (GCMs) from the Paleoclimate Modelling Intercomparison Project[27] (PMIP3), which include simulations of pre-industrial (PI; piControl) as well as industrial (historical) and MH (midHolocene) climate (Supplementary Table 2). This data set constitutes the most comprehensive collection of oxygen isotope measurements on Holocene corals[5,6,24,25,28–34] and molluscs[26,35–37] so far from the tropical Pacific (Fig. 1 and Supplementary Table 1 and Supplementary Figs 1–6). Such marine carbonates record the isotopic composition of oxygen ($\delta^{18}O$), which reflects changes in SST (Supplementary Fig. 10a) as well as the $\delta^{18}O$ of sea water (the latter linearly related to sea surface salinity (SSS, Supplementary Fig. 10b). The isotopic signal is generally dominated by the thermal component, except in the far western Pacific (Supplementary Fig. 11). All records have annual or finer resolution and collectively cover ~2,000 out of the past 10,000 years (Supplementary Table 1 and Supplementary Fig. 1). There are three clusters of sites in the western (WP, Papua New Guinea, New Caledonia, Vanuatu, Surprise Atoll), central (CP, the Line Islands of Palmyra, Fanning and Christmas) and eastern (EP, Peruvian coast) tropical Pacific.

Seasonal and interannual variability over the Holocene

The seasonal and interannual components of the tropical Pacific records show much irregularity in interannual (2–7 yr) variance—a measure of ENSO activity—as well as in AC amplitude. To enable comparisons between different records and sites, we show the ratio between fossil and modern (twentieth century) values of interannual variance and AC amplitude (Fig. 2), with uncertainties estimated with the block bootstrap (Methods). Most records of ENSO variance plot below unity, implying that twentieth-century ENSO was unusually active[25,38]. Those fossil samples exhibiting higher-than-modern ENSO variance have large uncertainties compatible with no change. Such uncertainties are usually the consequence of short fossil and/or modern sequences.

Despite appreciable differences between ENSO reconstructions from the three regions, some consistent patterns do emerge. In the WP (Fig. 2, top), the records show a significant decrease in ENSO variance during the early and mid-Holocene[5,6,29,36]; there are only a few records from the 6–2 kyr BP interval but these also show reduced ENSO variance. Low ENSO variance is present throughout the past 7 kyr in the CP (Fig. 2, centre), with the most consistent signal corresponding to a 64% reduction occurring between 3–5 kyr BP (Table 1) and a trend from extremely low variance to the present state from 2 kyr BP onwards[24,25]. Records from the EP show ENSO variance either similar to or lower than today, with the deepest reduction around 4.6 kyr BP (Fig. 2, bottom)[26]. Thus, our data set suggests that the MH reduction in ENSO variance identified in previous studies[5–7,32] is not an exceptional event, but rather that ENSO may have been less active than at present for much of the Holocene.

Reconstructions of the AC amplitude exhibit little coherence through time. Records from the WP show AC amplitudes similar to present before 7 kyr BP. However, records from the interval 7–4 kyr BP unequivocally exhibit a reduced AC amplitude, whereas after 3 kyr BP the records show a return to AC amplitudes similar to the present day. In contrast, records from the CP show considerable temporal structure in AC amplitude, although many of the individual records have high levels of uncertainty. In the EP, the records show slightly reduced AC amplitude throughout the past 10 kyr, except for a period with amplitude similar to the present day at 3 kyr BP.

Comparisons with simulated tropical Pacific climates

We now use this data set to constrain the behaviour of PMIP3 models. Although there are comparatively few records from precisely 6.5 kyr BP, we assume that the changes recorded during the window between about 7.5 and 5.5 kyr BP are representative of the MH and provide an indication of the average change to be expected in the MH simulations. To make quantitative model–data comparisons, we translate model output into oxygen isotope ratios using a forward modelling approach[39,40], in which the $\delta^{18}O$ of biocarbonates is parameterized as a function of SSS and SST (Methods). This approximates the isotopic variations that would have been recorded by the coral or mollusc in response to the simulated changes in climate produced by each climate model, which can then be directly compared with the observed variations at a site (Supplementary Figs 10 and 11). The forward model is a simplified representation of the incorporation of ^{18}O by mollusc and coral systems, in particular because it represents the relationship between seawater ^{18}O and SSS as time-invariant. However, it has been shown to reproduce the first-order basin-scale variability contained in modern corals from across the tropical Pacific[39]. Thus, this simple model provides a way of bridging GCMs and palaeo observations.

Most of our records are comparatively short: the average record length is around 50 years (Supplementary Fig. 1b) and very few are longer than 100 years. As ENSO variability is non-stationary,

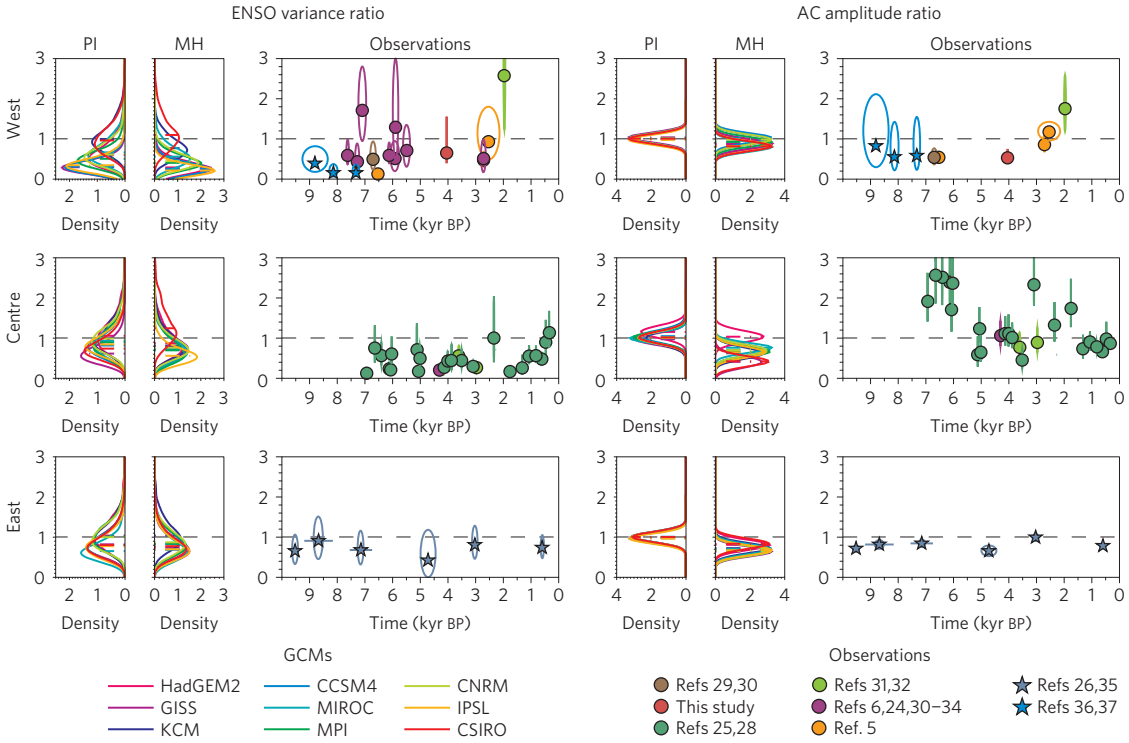

Figure 2 | Distribution of seasonal and interannual variability in models and observations. Top: changes in ENSO variance and AC amplitude over the Holocene. Left column: changes in ENSO-band (2–7 yr) variance between fossil and modern samples in the west (top), centre (middle) and east (bottom). Horizontals bars mark the period covered by each data set; except for molluscs from the Peruvian coast, these are narrower than the symbol width. Ellipses represent uncertainties about these ratios in both dimensions: the width represents a 95% CI for the central date of each sample, based on reported analytical uncertainty on radiometric ages; the vertical component is a 95% CI for the variance ratio, obtained through a block-bootstrap procedure (Methods). Unity (no change) is marked by a dashed grey line. Similar statistics derived from PMIP3 models on 50-yr windows are depicted on side panels for piControl and midHolocene experiments. Solid lines are kernel density estimates of those distributions (Methods), whereas dashed lines indicate their median. Right column: *idem* for AC amplitude.

quantifying ENSO variance over such short windows leads to a wide range of estimates[41,42]. Random sampling of multi-century model simulations under stationary boundary conditions shows that ENSO variance estimates on 50-year windows may vary by up to ±50% from sampling alone (Supplementary Fig. 13); these estimates converge as the observation window lengthens. Thus, the short length of most of the observations could make it difficult to discriminate between observed and simulated variability. Changes in the AC amplitude are much better constrained, although still sensitive to segment length (Supplementary Figs 12 and 13).

For each model, we estimate the statistical distributions of modelled ENSO and AC amplitude for 50-year periods using the block bootstrap for both the piControl and midHolocene simulations (Supplementary Table 2) and compare these distributions to the values obtained from the historical simulations (Supplementary Figs 14–22). The distributions of ENSO variance ratios are broad and positively skewed, whereas those of AC amplitude are narrow and symmetric (Fig. 2, coloured curves). ENSO variance ratios are clustered around unity in the piControl experiments, and fall below unity in most of the midHolocene experiments. The midHolocene reduction is small and, given the width of the distributions, only marginally significant at the 5% level. Nonetheless, it is qualitatively consistent with results from an intermediate complexity model[8] as well as many other GCM simulations[9–13], all of which show reduced ENSO variability during the MH compared with the PI climate.

Although the synthesis of existing palaeo-ENSO data presents a heterogeneous picture of ENSO variability through both space and time, there is evidence for a sustained reduction in ENSO variability from 3–5 kyr BP. This is especially true in the CP, where a deep reduction (64%) is accompanied by a relatively narrow 95% confidence interval (CI) of [28%, 84%] (Table 1). Reductions of similar magnitude are observed during the MH (5.5–7.5 kyr BP; 66% in the centre, 50% in the west, 33% in the east), albeit with CIs so wide that they cannot exclude increases in ENSO variance (Table 1). Thus, a salient feature of this data set is a robust, approximately two-thirds reduction in CP interannual variance, which seems to have persisted throughout much of the 3–5 kyr BP interval. This persistent reduction bears little resemblance to the model simulations of reduced MH ENSO (refs 4,8) followed by a gradual intensification to the present[13], and happened at a time when boreal summer/winter precessional forcing was weaker than during the MH (Supplementary Fig. 9).

Table 1 | Observed reductions in ENSO variance in the tropical Pacific during the MH (5.5–7.5 kyr BP) and the 3–5 kyr BP interval.

		Quantiles		
Period	**Region**	**2.5%**	**50%**	**97.5%**
5.5–7.5 kyr BP	West	−125%	50%	92%
	Centre	−5%	66%	92%
	East	−16%	33%	69%
3–5 kyr BP	West	−54%	35%	61%
	Centre	28%	64%	84%
	East	−18%	58%	109%

The numbers represent quantiles of the block-bootstrap ensembles. By convention, a negative reduction implies an increase.

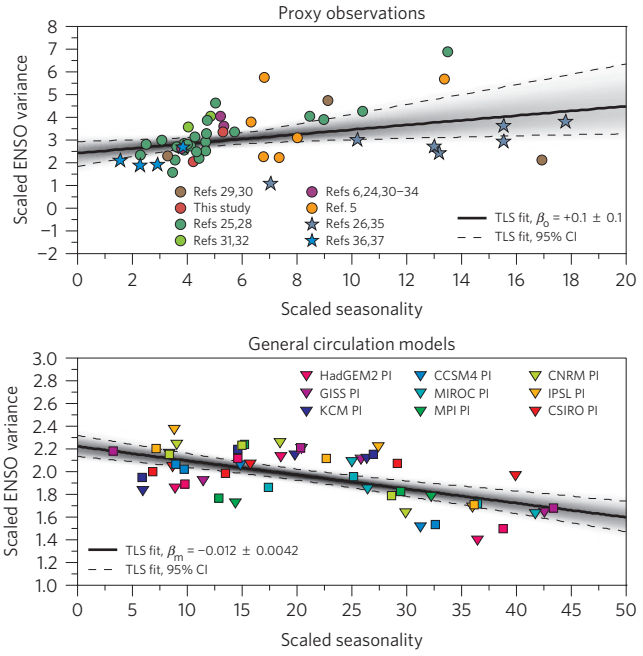

Figure 3 | Link between interannual and seasonal variability in models and observations. Link between ENSO variance and the seasonal cycle in proxy observations (top) and PMIP3 models (bottom). The observed values are for all seasonally resolved records from the Pacific during the whole of the past 10 kyr. The simulated values are based on 50-year segments from the midHolocene and piControl simulations. On top, symbology as in Fig. 1. On the bottom, triangles denote the median of piControl simulations, squares the median of midHolocene simulations. Data from the EP, CP and WP were pooled together, scaled by their interquartile range so their uncertainties on both axes are commensurate. An orthogonal regression (total least squares, TLS) fit is presented for both data sets, together with approximate 95% CIs (dashed lines) and probability density (grey contours) obtained through bootstrap resampling (Methods).

Can PMIP3 GCMs simulate the magnitude of such reductions, and if so, under which conditions? We answer this question by computing the probability of observing ENSO variance reductions of at least 64% on 50-year segments (Table 2). These probabilities are extremely low under PI conditions, ranging from 1 to 12%. Such occurrences are still rare under MH boundary conditions (probabilities ranging from 3 to 15%), although most (7 out of 9) of the models show an increased probability of ENSO reduction. Thus, whereas orbital forcing characteristic of the MH tends to drive simulated changes in ENSO variance in the right direction, the amplitude of simulated changes is too modest, and the response is not consistent among models. It is even harder to explain the larger, more sustained reductions that may have prevailed during the 3–5 kyr BP period, but the short length of the simulations (Supplementary Table 2) precludes an assessment of this question.

The models all show a reduction in the median amplitude of the AC in the midHolocene simulations, for all three regions. The reduction is between 10 and 50% (depending on the model) but is relatively uniform across the basin (Fig. 2, right). This uniformity contrasts strongly with the observed changes in the 7.5–5.5 kyr BP window, where AC amplitude is decreased in the WP but increased in the CP. However, the reduction in AC amplitude in the WP is ~50% larger than in the simulations.

Links between ENSO and the seasonal cycle amplitude

We investigate the link between changes in ENSO variance and in AC amplitude by plotting the fossil to modern ratio of ENSO-band variance against the same ratio of AC amplitude, in both Holocene observations and PMIP3 simulations (Fig. 3). Both axes are scaled by their uncertainty to make an orthogonal regression possible (Methods). The simulated relationship is significantly negative (Fig. 3, bottom), in agreement with previous work[17–20]. This contrasts with the observations, which reveal a weak positive relationship between ENSO variance and AC amplitude (Fig. 3, top). Moreover, the range of variations in AC amplitude is about 2–3 times larger in the observations than in the simulations (Supplementary Fig. 23). Similar results emerge if only data from the CP are considered (Supplementary Figs 24 and 25), or if wavelet analysis is used to diagnose the relationship between energy in the annual and interannual bands[19] (Methods and Supplementary Fig. 26). If our interpretation of the data is correct, the mismatch between the observed and simulated relationship between ENSO variance and AC amplitude has important dynamical implications. The frequency entrainment hypothesis[15,20] states that a self-exciting oscillator will give up its independent mode of oscillation and acquire the frequency of the applied forcing (in this case, the AC in insolation). It has long been invoked to explain the inverse relationship between ENSO and the AC in coupled GCMs (refs 12,13,17,18). Our results confirm that this link is strong in PMIP3 models, but suggest that it is opposite to that found in observations over the Holocene.

In comparing the ENSO–AC relationship across models and data, it is important to note the limitations associated with using a sparse set of observations to constrain tropical Pacific dynamics. One possible explanation for the model–data mismatch in the ENSO–AC relationship is that uncertainties in AC amplitude estimates from corals are more uncertain than depicted by the bootstrap intervals, as documented by discrepancies of up to 30% in AC estimates from overlapping coral $\delta^{18}O$ records from the CP (Supplementary Fig. 12). The relationship between $\delta^{18}O$ and SSS is poorly constrained on subannual scales, and may vary across a given reef environment, further confounding estimates of AC amplitude changes from high-resolution archives. Results are, however, insensitive to the choice of ENSO metric as long as fossil/modern ratios are used (Supplementary Fig. 27).

Changes in the spatial characteristics of ENSO represent another source of uncertainty, as different flavours of ENSO have different impacts on SST and SSS across the study domain. Canonical El Niño events involve temperature changes in the EP. However, many events peak in the CP (ref. 43). Indeed, changes in the prevalence of ENSO flavours in the Holocene have been suggested by changes in the asymmetry of ENSO anomalies in the EP (ref. 26) as well as analysis of PMIP3 midHolocene simulations[12,44]. Thus, some of the observed variations in ENSO intensity/frequency over the Holocene could reflect changes in the spatial pattern of ENSO and differences between individual records could reflect a dominance of one expression of ENSO over another[26]. However, an empirical

Table 2 | Probability of observing periods of reduced ENSO activity in the CP in nine GCMs.

H_0	HadGEM2	GISS	KCM	CCSM4	MIROC	MPI	CNRM	IPSL	CSIRO
PI null	1.37%	11.98%	1.62%	3.66%	2.82%	3.55%	0.88%	2.06%	5.00%
MH null	3.12%	3.16%	3.35%	5.60%	7.36%	9.78%	3.81%	15.50%	0.21%

Top row: frequency of occurrence of 50-year-long periods for which the ENSO variance ratio is as low as the 3–5 kyr BP average inferred from palaeoclimate observations (0.36—a 64% reduction) in pre-industrial (piControl) simulations. Bottom row: same for midHolocene simulations.

ENSO model suggests that modern changes in the prevalence of ENSO flavours may arise internally[45]. Our data set is too sparse to resolve spatial features of ENSO or the AC structure, but it is hoped that denser proxy networks will shed light on these questions in the future.

Implications for ENSO dynamics

It has been suggested that boreal autumn insolation, which peaks at ~5 kyr BP (Supplementary Fig. 8), modulates ENSO variability through air/sea coupling strength[8]. Our analyses reveal that changes in ENSO variance and AC amplitude over the Holocene bear no simple relation to orbital forcing, excluding a linear mechanism. It is possible that millennial-scale changes in ENSO variability arose: internally; or as a nonlinear response to orbital forcing; or because of other factors, such as the presence of a remnant Laurentide ice sheet, which modulated the response to orbital forcing[46]. Our observations suggest persistent changes in ENSO variance and AC amplitude that fall well outside the range shown by both piControl and midHolocene PMIP3 simulations, particularly during the 3–5 kyr BP interval. The PMIP3 ensemble does not capture the potential range of ENSO variability over this interval, which should become a key target for climate models of varying complexity to simulate and explain. One challenge in simulating such changes with GCMs is that computational requirements restrict simulations to 200–500 yr, on average. Additional long transient runs, both forced[13] and unforced[41], would help distinguish endogenous from exogenous sources of ENSO variability. Furthermore, the simulated relationship between ENSO variance and AC amplitude is incompatible with observations. GCMs where an inverse relationship to AC amplitude dominates the ENSO response to orbital forcing may therefore not be representative of the real world. Given that the mean state, AC and ENSO are so tightly connected[16,47], the substantial climatological biases in the fifth phase of the Coupled Modelling Intercomparison Project (CMIP5) models[48] are a logical suspect for this exaggerated relationship. Of particular relevance is the SST–shortwave feedback[49], the asymmetric nature of which is not captured by many state-of-the-art GCMs (ref. 48). Even those GCMs that qualitatively simulate the feedback may do so through error compensation, so we speculate that large improvements in ENSO simulations would result from a correct representation of the underlying processes.

Whereas precessional and greenhouse gas forcing are fundamentally different in character, our work demonstrates the ability of high-resolution palaeoclimate records to provide fundamental constraints on tropical climate dynamics, as represented in models used to project twenty-first-century climate trends. In that context, the fact that ENSO seemed relatively impervious to a large external forcing suggests that processes internal to the climate system could dominate external influences. Understanding internal processes of low-frequency ENSO modulation, and the extent to which they are captured by climate models, is therefore of utmost importance to improving climate projections.

Methods

Methods and any associated references are available in the online version of the paper.

Received 9 April 2015; accepted 29 October 2015; published online 14 December 2015

References

1. Sarachik, E. S. & Cane, M. A. *The El Niño-Southern Oscillation Phenomenon* 336–384 (Cambridge Univ. Press, 2010).
2. Collins, M. *et al.* The impact of global warming on the tropical Pacific Ocean and El Niño. *Nature Geosci.* **3,** 391–397 (2010).
3. Schmidt, G. A. Enhancing the relevance of palaeoclimate model/data comparisons for assessments of future climate change. *J. Quat. Sci.* **25,** 79–87 (2010).
4. Braconnot, P., Luan, Y., Brewer, S. & Zheng, W. Impact of Earth's orbit and freshwater fluxes on Holocene climate mean seasonal cycle and ENSO characteristics. *Clim. Dynam.* **38,** 1081–1092 (2012).
5. Tudhope, A. W. *et al.* Variability in the El Niño-Southern Oscillation through a glacial-interglacial cycle. *Science* **291,** 1511–1517 (2001).
6. McGregor, H. V. & Gagan, M. K. Western Pacific coral δ^{18}O records of anomalous Holocene variability in the El Niño-Southern Oscillation. *Geophys. Res. Lett.* **31,** L11204 (2004).
7. Koutavas, A. & Joanides, S. El Niño-Southern Oscillation extrema in the Holocene and Last Glacial Maximum. *Paleoceanography* **27,** PA4208 (2012).
8. Clement, A. C., Seager, R. & Cane, M. A. Suppression of El Niño during the mid-Holocene by changes in the Earth's orbit. *Paleoceanography* **15,** 731–737 (2000).
9. Liu, Z., Kutzbach, J. & Wu, L. Modeling climate shift of El Niño variability in the Holocene. *Geophys. Res. Lett.* **27,** 2265–2268 (2000).
10. Zheng, W., Braconnot, P., Guilyardi, E., Merkel, U. & Yu, Y. ENSO at 6 ka and 21 ka from ocean–atmosphere coupled model simulations. *Clim. Dynam.* **30,** 745–762 (2008).
11. Chiang, J. C. H., Fang, Y. & Chang, P. Pacific climate change and ENSO activity in the mid-Holocene. *J. Clim.* **22,** 923–939 (2009).
12. An, S.-I. & Choi, J. Mid-Holocene tropical Pacific climate state, annual cycle, and ENSO in PMIP2 and PMIP3. *Clim. Dynam.* **43,** 957–970 (2014).
13. Liu, Z. *et al.* Evolution and forcing mechanisms of El Niño over the past 21,000 years. *Nature* **515,** 550–553 (2014).
14. Wang, X. L. The coupling of the annual cycle and ENSO over the tropical Pacific. *J. Atmos. Sci.* **51,** 1115–1136 (1994).
15. Chang, P., Wang, B., Li, T. & Ji, L. Interactions between the seasonal cycle and the Southern Oscillation—frequency entrainment and chaos in a coupled ocean-atmosphere model. *Geophys. Res. Lett.* **21,** 2817–2820 (1994).
16. Guilyardi, E. El Niño mean state seasonal cycle interactions in a multi-model ensemble. *Clim. Dynam.* **26,** 329–348 (2006).
17. Timmermann, A., Lorenz, S. J., An, S.-I., Clement, A. & Xie, S.-P. The effect of orbital forcing on the mean climate and variability of the tropical Pacific. *J. Clim.* **20,** 4147–4159 (2007).
18. An, S.-I. *et al.* The inverse effect of annual-mean state and annual-cycle changes on ENSO. *J. Clim.* **23,** 1095–1110 (2010).
19. An, S.-I. & Choi, J. Inverse relationship between the equatorial eastern Pacific annual-cycle and ENSO amplitudes in a coupled general circulation model. *Clim. Dynam.* **40,** 663–675 (2013).
20. Liu, Z. A simple model study of ENSO suppression by external periodic forcing. *J. Clim.* **15,** 1088–1098 (2002).
21. Tziperman, E., Stone, L., Cane, M. A. & Jarosh, H. El Niño chaos: overlapping of resonances between the seasonal cycle and the Pacific ocean-atmosphere oscillator. *Science* **264,** 72–74 (1994).
22. Jin, F.-F., Neelin, J. D. & Ghil, M. El Niño on the Devil's staircase: annual subharmonic steps to chaos. *Science* **264,** 70–72 (1994).
23. Stuecker, M. F., Timmermann, A., Jin, F.-F., McGregor, S. & Ren, H.-L. A combination mode of the annual cycle and the El Niño-Southern Oscillation. *Nature Geosci.* **6,** 540–544 (2013).
24. McGregor, H. V. *et al.* A weak El Niño-Southern Oscillation with delayed seasonal growth around 4,300 years ago. *Nature Geosci.* **6,** 949–953 (2013).
25. Cobb, K. M. *et al.* Highly variable El Niño-Southern Oscillation throughout the Holocene. *Science* **339,** 67–70 (2013).
26. Carré, M. *et al.* Holocene history of ENSO variance and asymmetry in the eastern tropical Pacific. *Science* **345,** 1045–1048 (2014).
27. Braconnot, P. *et al.* Evaluation of climate models using palaeoclimatic data. *Nature Clim. Change* **2,** 417–424 (2012).
28. Cobb, K. M., Charles, C. D., Cheng, H. & Edwards, R. L. El Niño/Southern Oscillation and tropical Pacific climate during the last millennium. *Nature* **424,** 271–276 (2003).
29. Duprey, N. *et al.* Early mid-Holocene SST variability and surface-ocean water balance in the southwest Pacific. *Paleoceanography* **27,** PA4207 (2012).
30. Kilbourne, K. H., Quinn, T. M., Taylor, F. W., Delcroix, T. & Gouriou, Y. El Niño-Southern Oscillation-related salinity variations recorded in the skeletal geochemistry of a *Porites* coral from Espiritu Santo, Vanuatu. *Paleoceanography* **19,** PA4002 (2004).
31. Woodroffe, C. D. & Gagan, M. K. Coral microatolls from the central Pacific record Late Holocene El Niño. *Geophys. Res. Lett.* **27,** 1511–1514 (2000).
32. Woodroffe, C. D., Beech, M. R. & Gagan, M. K. Mid-late Holocene El Niño variability in the equatorial Pacific from coral microatolls. *Geophys. Res. Lett.* **30,** 1358 (2003).
33. Evans, M., Fairbanks, R. & Rubenstone, J. A proxy index of ENSO teleconnections. *Nature* **394,** 732–733 (1998).

34. McGregor, H. V., Fischer, M. J., Gagan, M. K., Fink, D. & Woodroffe, C. D. Environmental control of the oxygen isotope composition of *Porites* coral microatolls. *Geochim. Cosmochim. Acta* **75,** 3930–3944 (2011).
35. Carré, M., Sachs, J. P., Schauer, A. J., Rodríguez, W. E. & Ramos, F. C. Reconstructing El Niño-Southern Oscillation activity and ocean temperature seasonality from short-lived marine mollusk shells from Peru. *Palaeogeogr. Palaeoclimatol. Palaeoecol.* **371,** 45–53 (2013).
36. Driscoll, R. *et al.* ENSO reconstructions over the past 60 ka using giant clams (*Tridacna* sp.) from Papua New Guinea. *Geophys. Res. Lett.* **41,** 6819–6825 (2014).
37. Welsh, K., Elliot, M., Tudhope, A., Ayling, B. & Chappell, J. Giant bivalves (*Tridacna gigas*) as recorders of ENSO variability. *Earth Planet. Sci. Lett.* **307,** 266–270 (2011).
38. McGregor, S., Timmermann, A., England, M. H., Elison Timm, O. & Wittenberg, A. T. Inferred changes in El Niño-Southern Oscillation variance over the past six centuries. *Clim. Past* **9,** 2269–2284 (2013).
39. Thompson, D. M., Ault, T. R., Evans, M. N., Cole, J. E. & Emile-Geay, J. Comparison of observed and simulated tropical climate trends using a forward model of coral $\delta^{18}O$. *Geophys. Res. Lett.* **38,** L14706 (2011).
40. Dee, S. G. *et al.* PRYSM: an open-source framework for proxy system modeling, with applications to oxygen-isotope systems. *J. Adv. Mod. Earth Syst.* **7,** 1220–1247 (2015).
41. Wittenberg, A. T. Are historical records sufficient to constrain ENSO simulations? *Geophys. Res. Lett.* **36,** L12702 (2009).
42. Russon, T., Tudhope, A. W., Hegerl, G. C., Schurer, A. & Collins, M. Assessing the significance of changes in ENSO amplitude using variance metrics. *J. Clim.* **27,** 4911–4922 (2014).
43. Kug, J.-S., Jin, F.-F. & An, S.-I. Two types of El Niño events: cold tongue El Niño and warm pool El Niño. *J. Clim.* **22,** 1499–1515 (2009).
44. Karamperidou, C., Di Nezio, P. N., Timmermann, A., Jin, F.-F. & Cobb, K. M. The response of ENSO flavors to mid-Holocene climate: implications for proxy interpretation. *Paleoceanography* **30,** 527–547 (2015).
45. Newman, M., Shin, S.-I. & Alexander, M. A. Natural variation in ENSO flavors. *Geophys. Res. Lett.* **38,** L14705 (2011).
46. Luan, Y., Braconnot, P., Yu, Y. & Zheng, W. Tropical Pacific mean state and ENSO changes: sensitivity to freshwater flux and remnant ice sheets at 9.5 ka BP. *Clim. Dynam.* **44,** 661–678 (2015).
47. Roberts, W. H. G., Battisti, D. S. & Tudhope, A. W. ENSO in the mid-Holocene according to CSM and HadCM3. *J. Clim.* **27,** 1223–1242 (2013).
48. Bellenger, H., Guilyardi, E., Leloup, J., Lengaigne, M. & Vialard, J. ENSO representation in climate models: from CMIP3 to CMIP5. *Clim. Dynam.* **42,** 1999–2018 (2014).
49. Lloyd, J., Guilyardi, E. & Weller, H. The role of atmosphere feedbacks during ENSO in the CMIP3 models. Part III: the shortwave flux feedback. *J. Clim.* **25,** 4275–4293 (2012).

Acknowledgements

We acknowledge the World Climate Research Program's Working Group on Coupled Modelling, which is responsible for CMIP, and we thank the PMIP3 modelling groups for producing and making available their model output. The US Department of Energy's Program for Climate Model Diagnosis and Intercomparison provides coordinating support for CMIP, and led development of software infrastructure in partnership with the Global Organization for Earth System Science Portals. J.E.-G. acknowledges support from US NSF grant DMS 1025465. K.M.C. acknowledges support from NOAA award NA11OAR4310166 and NSF award OCE-0752091. M.Collins acknowledges support from UK NERC grant NE/H009957/1. H.V.M. and A.T. acknowledge support from Australian Research Council (ARC) Discovery Project grant DP1092945. H.V.M. is supported by an ARC Future Fellowship FT140100286 grant. A.T. acknowledges support from UK NERC grant NE/H009957/1. T.C. thanks M. McCulloch (formerly at ANU) for dating the Bayes coral, and M. Gagan's team at ANU for help with isotopic measurements. The Bayes 1 core was collected with funds from the Institut de Recherche pour le Développement. B.S. was supported by the DFG Cluster of Excellence 'The Future Ocean' (EXC 80/2). P.B., M.Carré, T.C., J.L., M.E. and A.T. were supported by the French National Research Agency under EL PASO grant (no. 2010 298 BLANC 608 01). This project also serves for coordination and implementation of the PMIP3/CMIP5 simulations on the ESGF distributed database. We thank J.-Y. Peterschmitt for his help with the PMIP database. This work was initiated in a workshop co-sponsored by WCRP/CLIVAR, IGBP/PAGES, INQUA and IPSL in 2011.

Author contributions

J.E.G. designed the study, performed the analysis, led the writing, and prepared the manuscript. P.B. coordinated the synthesis. M.Carré, K.M.C., T.C., M.E. and R.D. contributed data and/or analysis. P.B. and J.L. analysed simulations and contributed to writing. Y.Z. processed PMIP3 output and generated some of the supplementary figures. A.T., B.S. and M.Collins provided input in the analysis and interpretation. J.E.G., K.M.C., M.Carré, S.P.H., H.V.M., T.C., P.B. and A.T. wrote the paper. All authors reviewed the manuscript.

Additional information

Supplementary information is available in the online version of the paper. Reprints and permissions information is available online at www.nature.com/reprints. Correspondence and requests for materials should be addressed to J.E.-G.

Competing financial interests

The authors declare no competing financial interests.

Methods

Observational synthesis. We compiled oxygen isotopic records ($\delta^{18}O$) obtained from coral or mollusc aragonitic skeletons from 65 sites in the Pacific (Supplementary Table 1). Most of the records have been published[5,6,24–26,28–37], but some are published for the first time here (Supplementary Information). Most of the individual records are comparatively short (50 years or less, Supplementary Fig. 1). The records sample 2,162 years out of the past 10,000 years (Supplementary Fig. 1 and Supplementary Table 1).

For analytical purposes, we group the individual sites into three separate regions: west [120°, 180°, 20° S, 0°], including Papua New Guinea and New Caledonia; centre [170° W, 120° W, 5° S, 5° N], corresponding to the NINO3.4 region (for which the SST average is a key ENSO indicator) and encompassing part of the Line Islands; east [90° W, 80° W, 5° S, 5° N], corresponding to the NINO1+2 regions, a primary region to monitor coastal warming.

Figure 1 shows that these three climatically meaningful regions encompass most of the sites. Note that the sites of ref. 26, although formally outside the NINO1+2 region (eastern box), are interpreted as recording NINO1+2 SST (ref. 35).

Analysis of observations. Changes in ENSO variance were quantified by computing the ratio of fossil to modern variance in the 2–7 yr band. In continuous records, the latter was isolated by means of a (Morlet) wavelet filter (Supplementary Fig. 7), whereas for Peruvian molluscs we used the ratio of fossil to modern variance of the distribution of the annual cycle $\delta^{18}O$ amplitude[35], a proxy for interannual variance in NINO1+2 SST. Results are not sensitive to the filter type or exact metric (Supplementary Information). AC amplitude was quantified as the range (maximum minus minimum) of a monthly mean seasonal cycle evaluated over each record's time span after high-pass filtering the data with a 10-year smoothing spline[50,51] to avoid the biasing effect of trends. Changes in this quantity were, likewise, computed as a ratio between fossil and modern samples.

Uncertainties in ENSO variance and AC amplitude ratios were estimated using a block-bootstrap procedure[52,53] with 1,000 draws. For interannual variance, the block length was set at 2 years, and for seasonal amplitude the block length was set to the number of samples per year. Both choices reflect a compromise between the approximate decorrelation time of the records and the shortness of some proxy records. For Peruvian molluscs, uncertainties were estimated through Monte Carlo simulations as described in ref. 54. The procedure is similar to a block-bootstrap analysis with 5,000 draws and block lengths of 1 year using an instrumental time series sampled and disturbed by simulated proxy-related noise sources.

Climate models and simulations. We consider the simulations that have been run as part of the fifth phase of the Coupled Modelling Intercomparison Project[55] (CMIP5) and analysed in the third phase of the Palaeoclimate Modelling Intercomparison Project[27] (PMIP3). This set of simulations is usually referred to as the CMIP5/PMIP3 experiments, although here we simply refer to them as PMIP3 experiments. The models used (Supplementary Table 2) are state-of-the-art coupled ocean–atmosphere general circulation models (GCMs), or Earth system models with different levels of complexity in the forcing used or in the interactions between climate and the carbon cycle[56]. We consider three experimental designs, following PMIP3 nomenclature.

piControl: the reference is pre-industrial simulations for which Earth's orbit and solar constant are representative of modern conditions. Trace gases concentrations, land use and aerosol loadings are prescribed to their AD 1850 values. The prescribed values vary slightly from one model to the other. Details are given in https://wiki.lsce.ipsl.fr/pmip3/doku.php/pmip3:design:pi:final.

midHolocene: for the mid-Holocene we use simulations in which Earth's orbital parameters and trace gases have been prescribed to those valid for 6 kyr BP (ref. 27). In all of the simulations the date of the vernal equinox is fixed to 21 March at noon. The insolation forcing at the Equator is shown in Supplementary Fig. 9 (see also ref. 57 and Fig. 3). Details are given in https://wiki.lsce.ipsl.fr/pmip3/doku.php/pmip3:design:6k:final.

Historical: to test the impact of the reference period on the analyses of the simulated change in the different climates we also consider historical simulations[55] forced with time evolution of trace gases, volcanic forcing and land use over the period 1860–2005. We sampled from the full ensemble of HIST simulations, including several runs with slightly different initial conditions for each model. In general, their ENSO statistics were indistinguishable from PI within uncertainties.

Forward modelling of marine bicarbonates. Although $\delta^{18}O$ in marine biocarbonates predominantly reflects either SST (refs 58–60) or seawater $\delta^{18}O$ variations resulting from net surface freshwater balance[61,62], most corals and molluscs are affected by both variables. This problem may be directly addressed by explicitly modelling the relationship between the environmental variables and the observed $\delta^{18}O$ (that is, forward modelling[40,63]). Unlike empirical calibration, forward models do not require assumptions to be made about linearity, the independence of predictors, or the normality of residuals.

A reasonably complete model of the incorporation of ^{18}O in coral aragonite requires information on local ocean temperature, seawater ^{18}O, pH, insolation and nutrients. However, ref. 39 developed a simple bivariate model to predict the ^{18}O of coral aragonite using SST and SSS as sole inputs. SSS acts as a proxy for seawater ^{18}O, with regionally dependent coefficients calibrated over the instrumental era. The thermal dependence is set at $-0.22‰\,°C^{-1}$, close to the expected slope for inorganic equilibrium fractionation[64]. This model has been shown to capture first-order variations in the hydrologic response of coral oxygen isotopic composition[39,65]. There are known limitations to the use of such a simple model[65–67]. Specifically, it ignores coral biology and non-equilibrium effects, which are thought to explain some low-frequency trends in corals[68]. Further, the SSS–$^{18}O_{sw}$ slope may not be constant on millennial timescales[69], and its spatial variations may severely bias the estimation of palaeo-ENSO variability, particularly in the WP (ref. 65). Nevertheless, we use this model to translate climate model outputs into a ^{18}O signal for comparison with the observations because very few of the climate models explicitly simulate water isotopes. The same model may be applied to simulate $\delta^{18}O$ values in the shells of *Tridacna* sp. and *Mesodesma donacium*[26,36,37] because they precipitate aragonite like corals. The slope of the SST–$\delta^{18}O$ relationship generally used for aragonitic molluscs ranges from -0.21 to $-0.27‰\,°C^{-1}$ (refs 70,71), compatible with the slope of $-0.22‰\,°C^{-1}$ used by ref. 39.

We note that recent studies have attempted to quantify uncertainties in inferring changes in ENSO variance from calibrated proxy observations[42,72]. By using a process model, we eschew some of the difficulties associated with calibration, but this passes the uncertainties on to the process model. Additionally, ref. 72 neglected sampling uncertainties, which are central to our analysis. The existence of non-climatic noise is a problem in every palaeoclimate data set, and the reader is referred to the original studies for an appraisal of the strength of each climate signal.

Analysis of GCM simulations. GCM-simulated SST and SSS were translated to $\delta^{18}O$ values using the forward model described above. The ensuing 'pseudocoral' fields were averaged over the three main regions (WP, CP, EP), and then resampled using the above-mentioned block-bootstrap procedure with $N = 1{,}000$ draws, before being subsampled on contiguous 50-year blocks to emulate short observational windows (Supplementary Information and Supplementary Figs 13–22). We then computed ENSO variance and AC amplitude, as well as their ratios, for each ensemble member. Probability distributions from these 1,000 member ensembles were then obtained using kernel density estimation with a bandwidth $h = 0.15$ (Fig. 2).

Regression analysis. We used total least-squares (TLS) regression (a form of error-in-variables modelling, closely connected to orthogonal regression[73]), to account for uncertainties in the ENSO–AC amplitude relationship. TLS steepens regression slopes by taking the potentially biasing effects of observational noise into account[74]. ENSO variance and AC amplitude ratios were scaled by their uncertainty (measured by the interquartile range of their block-bootstrap distributions) before TLS regression, to ensure homogeneous error magnitudes on both axes of Fig. 3. Uncertainties in regression parameters are estimated through a bootstrap approach[75], with 2,000 draws.

Wavelet analysis. The relationship between ENSO and the AC is also probed through Morlet wavelet analysis[76]. As in ref. 19, we sum the energies corresponding to the 2–7 yr and 0.8–1.2 yr bands and report linear correlations between the resulting series. We do so for all seasonally resolved, continuous records in the database (that is, all except those of refs 26,35) and for the PMIP3 piControl and midHolocene model outputs, separately for each of the three geographic regions. Statistical significance is established by means of a non-parametric, isospectral test[77], which accounts for the loss of degrees of freedom imparted by smoothing by low-frequency wavelets.

Data. Data for the palaeo observations and model output for the three areas outlined in Fig. 1 are available at https://github.com/CommonClimate/EmileGeay_NatGeo2015. The original model data were obtained via the CMIP5/PMIP3 portal (http://cmip-pcmdi.llnl.gov/cmip5), and the published palaeo data were obtained from the National Climatic Data Center (https://www.ncdc.noaa.gov/data-access/paleoclimatology-data).

Code availability. The code to reproduce all of the figures and tables in this manuscript is publicly available. Specifically, Matlab/Python code to reproduce the block-bootstrap, wavelet and regression analysis is available at https://github.com/CommonClimate/EmileGeay_NatGeo2015. These codes generate the probability distributions for all of the ratios plotted in Fig. 2, except those associated with ref. 26. The Matlab code to generate the latter distributions is available at http://www.isem.univ-montp2.fr/carre_matthieu, using the parameter

values published in ref. 54 (SOM). See the ReadMe.md file at https://github.com/CommonClimate/EmileGeay_NatGeo2015 for more detailed instructions.

References

50. Cook, E. R. & Peters, K. The smoothing spline: a new approach to standardizing forest interior tree-ring width series for dendroclimatic studies. *Tree-Ring Bull.* **41,** 45–53 (1981).
51. Weinert, H. L. A fast compact algorithm for cubic spline smoothing. *Comput. Stat. Data Anal.* **53,** 932–940 (2009).
52. Efron, B. & Tibshirani, R. J. *An Introduction to the Bootstrap* (Chapman & Hall, 1993).
53. Kunsch, H. R. The jackknife and the bootstrap for general stationary observations. *Ann. Stat.* **17,** 1217–1241 (1989).
54. Carré, M., Sachs, J. P., Wallace, J. M. & Favier, C. Exploring errors in paleoclimate proxy reconstructions using Monte Carlo simulations: paleotemperature from mollusk and coral geochemistry. *Clim. Past* **8,** 433–450 (2012).
55. Taylor, K. E., Stouffer, R. J. & Meehl, G. A. An overview of CMIP5 and the experiment design. *Bull. Am. Meteorol. Soc.* **93,** 485–498 (2011).
56. Flato, G. *et al.* in *Climate Change 2013: The Physical Science Basis* (eds Stocker, T. F. *et al.*) 741–866 (IPCC, Cambridge Univ. Press, 2013).
57. Luan, Y., Braconnot, P., Yu, Y., Zheng, W. & Marti, O. Early and mid-Holocene climate in the tropical Pacific: seasonal cycle and interannual variability induced by insolation changes. *Clim. Past* **8,** 1093–1108 (2012).
58. Dunbar, R. B., Wellington, G. M., Colgan, M. W. & Glynn, P. W. Eastern Pacific sea surface temperature since 1600 A.D.: the $\delta^{18}O$ record or climate variability in Galápagos corals. *Paleoceanography* **9,** 291–316 (1994).
59. Evans, M., Fairbanks, R. & Rubenstone, J. The thermal oceanographic signal of El Niño reconstructed from a Kiritimati Island coral. *J. Geophys. Res.* **104,** 13409–13422 (1999).
60. Cobb, K. M., Charles, C. D. & Hunter, D. E. A central tropical Pacific coral demonstrates Pacific, Indian, and Atlantic decadal climate connections. *Geophys. Res. Lett.* **28,** 2209–2212 (2001).
61. Fairbanks, R. G. *et al.* Evaluating climate indices and their geochemical proxies measured in corals. *Coral Reefs* **16,** S93–S100 (1997).
62. Conroy, J. L., Cobb, K. M., Lynch-Stieglitz, J. & Polissar, P. J. Constraints on the salinity–oxygen isotope relationship in the central tropical Pacific Ocean. *Mar. Chem.* **161,** 26–33 (2014).
63. Evans, M. N., Tolwinski-Ward, S. E., Thompson, D. M. & Anchukaitis, K. J. Applications of proxy system modeling in high resolution paleoclimatology. *Quat. Sci. Rev.* **76,** 16–28 (2013).
64. McConnaughey, T. ^{13}C and ^{18}O isotopic disequilibrium in biological carbonates: I. Patterns. *Geochim. Cosmochim. Acta* **53,** 151–162 (1989).
65. Russon, T., Tudhope, A. W., Hegerl, G. C., Collins, M. & Tindall, J. Inter-annual tropical Pacific climate variability in an isotope-enabled CGCM: implications for interpreting coral stable oxygen isotope records of ENSO. *Clim. Past* **9,** 1543–1557 (2013).
66. Stevenson, S., McGregor, H. V., Phipps, S. J. & Fox-Kemper, B. Quantifying errors in coral-based ENSO estimates: toward improved forward modeling of $\delta^{18}O$. *Paleoceanography* **28,** 633–649 (2013).
67. Thompson, D. M. *et al.* Coral-model comparison highlighting the role of salinity in long-term trends. *PAGES Newsl.* **21,** 60–61 (2013).
68. Lough, J. A strategy to improve the contribution of coral data to high-resolution paleoclimatology. *Palaeogeogr. Palaeoclimatol. Palaeoecol.* **204,** 115–143 (2004).
69. LeGrande, A. N. & Schmidt, G. A. Water isotopologues as a quantitative paleosalinity proxy. *Paleoceanography* **26,** PA3225 (2011).
70. Grossman, E. L. & Ku, T.-L. Oxygen and carbon isotope fractionation in biogenic aragonite: temperature effects. *Chem. Geol.* **59,** 59–74 (1986).
71. Carré, M. *et al.* Stable isotopes and sclerochronology of the bivalve *Mesodesma donacium*: potential application to Peruvian paleoceanographic reconstructions. *Palaeogeogr. Palaeoclimatol. Palaeoecol.* **228,** 4–25 (2005).
72. Russon, T., Tudhope, A. W., Collins, M. & Hegerl, G. C. Inferring changes in ENSO amplitude from the variance of proxy records. *Geophys. Res. Lett.* **42,** 1197–1204 (2015).
73. Van Huffel, S. *Total Least Squares and Errors-in-Variables Modeling: Bridging the Gap between Statistics, Computational Mathematics and Engineering* 539–555 (Physica-Verlag, 2004).
74. Markovsky, I., Sima, D. M. & Van Huffel, S. Total least squares methods. *Wiley Interdiscip. Rev.* **2,** 212–217 (2010).
75. Pešta, M. Total least squares and bootstrapping with applications in calibration. *Statistics* **47,** 966–991 (2013).
76. Torrence, C. & Compo, G. P. A practical guide to wavelet analysis. *Bull. Am. Meteorol. Soc.* **79,** 61–78 (1998).
77. Ebisuzaki, W. A method to estimate the statistical significance of a correlation when the data are serially correlated. *J. Clim.* **10,** 2147–2153 (1997).

Quaternary Research 85 (2016) 87–93

Contents lists available at ScienceDirect

Quaternary Research

journal homepage: www.elsevier.com/locate/yqres

Variability of ^{14}C reservoir age and air–sea flux of CO_2 in the Peru–Chile upwelling region during the past 12,000 years

Matthieu Carré [a,*], Donald Jackson [b], Antonio Maldonado [c], Brian M. Chase [a], Julian P. Sachs [d]

[a] Institut des Sciences de l'Evolution, Université de Montpellier, CNRS, IRD, EPHE, place Eugène Bataillon, 34095 Montpellier, France
[b] Departamento de Antropología, FACSO, Universidad de Chile, Ignacio Carrera Pinto 1045, Ñuñoa, Santiago, Chile
[c] Centro de Estudios Avanzados en Zonas Aridas (CEAZA), Universidad de La Serena, Casilla 599, La Serena, Chile
[d] School of Oceanography, University of Washington, Box 355351, Seattle, WA 98195, USA

ARTICLE INFO

Article history:
Received 6 May 2015
Available online 9 January 2016

Keywords:
Humboldt system
Reservoir age
Shell middens
Deglaciation
Radiocarbon
CO_2

ABSTRACT

The variability of radiocarbon marine reservoir age through time and space limits the accuracy of chronologies in marine paleo-environmental archives. We report here new radiocarbon reservoir ages (ΔR) from the central coast of Chile (~32°S) for the Holocene period and compare these values to existing reservoir age reconstructions from southern Peru and northern Chile. Late Holocene ΔR values show little variability from central Chile to Peru. Prior to 6000 cal yr BP, however, ΔR values were markedly increased in southern Peru and northern Chile, while similar or slightly lower-than-modern ΔR values were observed in central Chile. This extended dataset suggests that the early Holocene was characterized by a substantial increase in the latitudinal gradient of marine reservoir age between central and northern Chile. This change in the marine reservoir ages indicates that the early Holocene air–sea flux of CO_2 could have been up to five times more intense than in the late Holocene in the Peruvian upwelling, while slightly reduced in central Chile. Our results show that oceanic circulation changes in the Humboldt system during the Holocene have substantially modified the air–sea carbon flux in this region.

Introduction

Extending over 5000 km from the equator to ~50°S, the Peru–Chile coastal upwelling region is the longest eastern boundary upwelling system in the world. The Peru–Chile coastal upwelling plays a significant role in the global carbon cycle, being a highly productive area (Chavez et al., 2008) as well as one of the most intense carbon sources of the global coastal ocean (Laruelle et al., 2010). There is growing evidence that eastern boundary upwelling systems are intensifying with global warming (Bakun, 1990; McGregor et al., 2007; García-Reyes and Largier, 2010; Narayan et al., 2010; Gutiérrez et al., 2011). In addition, climate model simulations recently projected a change in upwelling spatial structure with future intensification being larger at high latitudes than at low latitudes (Wang et al., 2015). Assessing current changes in upwelling systems requires knowledge of their natural temporal and spatial variability.

The Humboldt Current system is complex, involving water masses from the Pacific Equatorial undercurrent in the north and subantarctic surface and intermediate waters in the South, which are characterized by different $\Delta^{14}C$ values (Toggweiler et al., 1991; Strub et al., 1998). The difference in the ^{14}C age of dissolved inorganic carbon (DIC) in marine surface waters relative to the ^{14}C age of contemporaneous terrestrial carbon in equilibrium with the atmosphere is referred to as the marine radiocarbon reservoir age (R) and is due to the residence time of carbon in the ocean. Today, the average marine radiocarbon reservoir age in the ocean mix layer is assumed to be 400 yr by convention. For the past 10,500 years, the Marine13 radiocarbon calibration dataset (Reimer et al., 2013) includes a radiocarbon reservoir age calculated using the atmospheric ^{14}C calibration curve IntCal13 and an ocean–atmosphere box diffusion model (Reimer et al., 2013). Although the model is simplified, the calculated marine radiocarbon curve is consistent with independent estimates from marine archives (Reimer et al., 2013). From 10.5 to 13.9 cal ka BP, the marine radiocarbon calibration includes data from Cariaco Basin varved sediments and from corals (Reimer et al., 2013). Local deviations from the global reservoir age (ΔR), however, vary in space and time with oceanic circulation.

Surface waters off Peru and northern Chile are typically characterized by large marine reservoir ages owing to the upwelling of ^{14}C-depleted deep waters. ΔR values may change on seasonal (Jones et al., 2007, 2010) to multi-millennial time scales as a function of variations in upwelling intensity and/or the origin of the upwelled waters (Toggweiler et al., 1991; Fontugne et al., 2004; Ortlieb et al., 2011). Modern and past ΔR estimates are scarce in the southeast Pacific. On the Chilean coast south of 24°S, only two estimates of pre-bomb ΔR are available today in the 14CHRONO marine reservoir database (http:// http://calib.qub.ac.uk/marine/). A few estimates of Holocene ΔR are available from sediment cores collected off southern Chile

* Corresponding author.
E-mail address: matthieu.carre@umontpellier.fr (M. Carré).

http://dx.doi.org/10.1016/j.yqres.2015.12.002
0033-5894/

(De Pol-Holz et al., 2010, Van Beek et al., 2002; Siani et al., 2013) and none from the coast. Therefore, the uncertainty in ΔR is considerable along ~3600 km of coast, which is a significant limitation on the accurate ^{14}C-dating of ancient sedimentological, biological, or archeological materials of marine origin.

Here we provide new estimates of ΔR over the past 12,000 years in central Chile (31°S–33°S) from paired charcoal and mollusk shells collected in archeological shell middens in the area of Los Vilos. The coast in this area is open to the ocean and does not show any local oceanographic feature or any large river system, so we can consider it as representative of the coastal Humboldt system at this latitude. A comparison with reconstructions from southern Peru and northern Chile compiled by Ortlieb et al. (2011) provides new insights into the spatial structure variability of the globally significant Peru–Chile coastal upwelling system. Based on an empirical relationship between ^{14}C reservoir age and pCO_2 in the southeast Pacific, we discuss the implications for past variability of air–sea CO_2 exchange in this region.

Material and methods

A pre-bomb radiocarbon reservoir age value was estimated from a *Mesodesma donacium* shell collected in Valparaiso and deposited in Paris at the National Museum of Natural History in 1837. This modern reservoir age value might be slightly overestimated since this shell had probably been collected a few years earlier. Holocene ΔR values were estimated from ^{14}C dates of paired mollusk shells and charcoal fragments collected in seven archeological shell middens close to Los Vilos (31.9°S, 71.5°W), on the central coast of Chile (Fig. 1, Table 1). Details on hunter-gatherer archeological occupations around Los Vilos can be found in Jackson (2002) and Méndez and Jackson (2004, 2006). Some authors recommend dating multiple pairs so that contemporaneity of samples can be statistically tested (Russell et al., 2011), which was not possible here. However, the risk of non-contemporaneity was here minimized by a careful control of the archeological context and the stratigraphy. Shell middens used in this study, except for one site (Ñague, Table 1), were thin lenses resulting from ephemeral occupations lasting approximately one season. We selected these sites to ensure a contemporaneous deposition of charcoal and shells. In the Ñague middens, contemporaneity was ensured by selecting shells that were collected in the stratigraphy between two charcoal fragments that yielded statistically undistinguishable radiocarbon dates (Table 1).

The estimate of a marine reservoir age can be biased if the charcoal fragment comes from a tree that died centuries before being used as fuel. This issue, referred to as the "old wood" effect, can be relatively common in the hyper arid coast of Peru (Kennett et al., 2002). While charcoal fragments are sometimes older than associated shells in northern Chile due to the old wood effect and must thus be discarded (Ortlieb et al., 2011), this was not observed in any pair analyzed in central Chile. This risk is mitigated in the central coast as compared to the Atacama desert because central Chile is much less arid, and so dead trees are not as well preserved as in the Atacama desert. Plant species could not be determined from charcoal fragments. However, we minimized the risk of old wood bias by analyzing two charcoal fragments when possible.

We used shell fragments from the same species, *M. donacium*, to minimize variability related to microhabitat or to biological effects. *M. donacium* is a filter-feeder bivalve living in the intertidal to subtidal zone of high energy sand beaches of Peru and Chile (Tarifeño, 1980). Filter feeders are considered to be in equilibrium with dissolved inorganic carbon and thus well suited for ΔR reconstructions (Petchey and Ulm, 2012). Seasonal changes in coastal upwelling can result in substantial

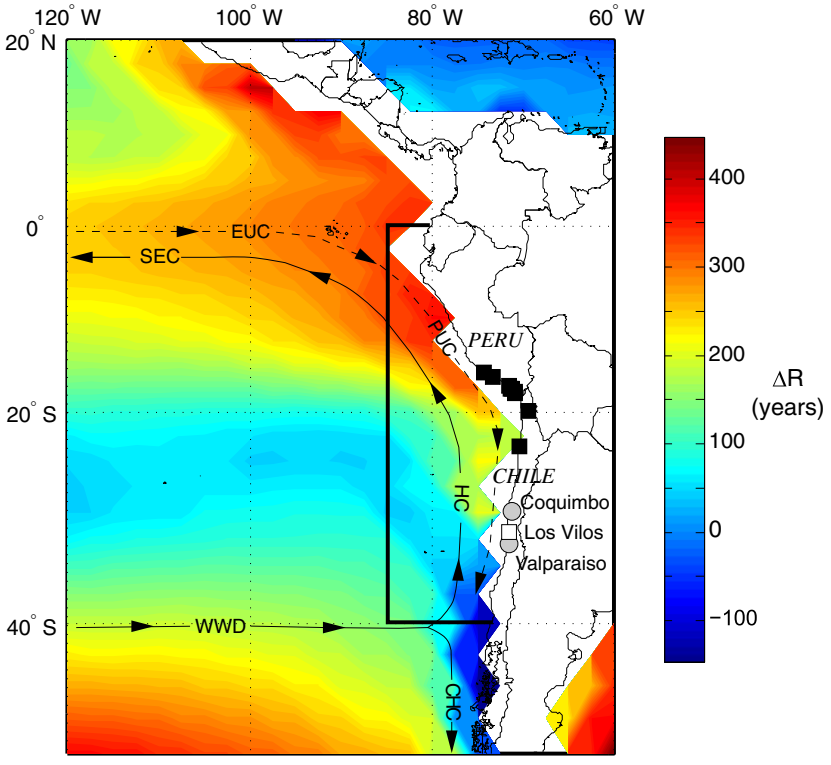

Figure 1. Map of the study region showing simulated marine reservoir age deviations (ΔR, years) of surface water (Butzin et al., 2012) in modern pre-bomb conditions. A simplified representation of ocean circulation (continuous arrows for surface currents and dashed arrows for undercurrents) based on Strub et al. (1998) indicates the South Equatorial current (SEC), the Equatorial undercurrent (EUC), the Peruvian undercurrent (PUC) (which feeds coastal upwelling), the Humboldt current (HC) (also called the Peruvian current), the West Wind drift (WWD), and the Cape Horn current (CHC). We show the sites for modern pre-bomb reservoir age estimates (gray circles), published Holocene reservoir age estimates in southern Peru and northern Chile (black squares) (Southon et al., 1995; Kennett et al., 2002; Owen, 2002; Fontugne et al., 2004; Ortlieb et al., 2011), and Los Vilos, the site for Holocene reservoir age estimates in central Chile (this study, open square). The thick black line shows the area considered for the calculation of the relationship between pCO_2 and ΔR (Fig. 3).

Table 1
Radiocarbon dates, reservoir ages, and $\Delta^{14}C$ of surface water in central Chile.

Sample	Material	Lab Ref.	$\delta^{13}C$ (‰ V-PDB)	^{14}C age (yr BP)	Mean ^{14}C age (yr BP)	1σ range (Cal yr BP)	ΔR (yr)	$\Delta^{14}C$ (‰)
Modern pre-bomb samples								
Coquimbo (29.9°S) collection: AD 1837	Marine shell	UCIAMS-142533	[a]	605 ± 25		113–133	146 ± 25	−58.6 ± 4.1
Valparaiso (33.1°S) collection: AD 1939 (Ingram and Southon, 1996)	Marine shell	CAMS-17919/1	2.0	520 ± 50		11	43 ± 52	−61.4 ± 5.8
Valparaiso (33.1°S) collection: AD 1935 (Taylor and Berger, 1967)	Marine shell	UCLA-1278	1.3	770 ± 76		15	303 ± 77	−89.8 ± 8.6
Holocene samples from Los Vilos (31.9°S)								
LV007-N2	Marine shell	OS-63180	1.3	3560 ± 35				
LV007 U3 Capa2	Charcoal	OS-60569	−25.3	3090 ± 40		3182–3339	168 ± 69	−48.4 ± 13.2
Huentelauquen2-N1	Marine shell	Beta-281204	−0.7	6350 ± 40				
Huentelauquen2-N1	Charcoal	Beta-292185	−25.4	6000 ± 40		6732–6857	18 ± 57	31.1 ± 12.9
LV 531 U1 m	Marine shell	CAMS-144653	(0)[b]	8125 ± 30				
LV531 U1 ch	Charcoal	CAMS-144812	(−25)	7780 ± 35*	7830 ± 50	8479–8627		
LV531 U1 ch-rep	Charcoal	CAMS-144818	(−25)	7880 ± 25*			9 ± 45	25.3 ± 13.0
NagueB-N8	Marine shell	OS-63176	0.5	9100 ± 40				
NagueB-N7	Charcoal	OS-60542	−24.2	8690 ± 50	8655 ± 59	9527–9631		
NagueB-N10	Charcoal	OS-61907	−24.2	8620 ± 110			169 ± 54	27.2 ± 12.8
NagueB-N14	Marine shell	OS-63177	1.0	9310 ± 50				
NagueB-N13	Charcoal	OS-61906	−23.3	9190 ± 45*	9190 ± 69	10233–10397		
NagueB-N17	Charcoal	OS-61450	−24.9	9190 ± 130*			−166 ± 73	94.9 ± 17.6
LV079-U2-N1	Marine shell	Beta-293612	−0.9	10,360 ± 50*	10,500 ± 140			
LV079-U2-N9	Marine shell	Beta-293613	0.7	10,640 ± 60*				
LV079-U2-N6	Charcoal	Beta-342528	−24.6	9790 ± 40		11,165–11,228	295 ± 143	47.6 ± 22.3
LV080-U1-N8	Marine shell	Beta-158699	0.4	10,180 ± 70				
LV080-U1-N9	Terr. shell	UGAMS-8849	−10.9	9890 ± 30		11,218–11,263	−95 ± 72	97.3 ± 12.5
PPLV80-N7	Marine shell	OS-63181	0.7	10,400 ± 50				
PPLV80-N6	Charcoal	OS-60566	−24.4	10,050 ± 50*	10,050 ± 37	11,355–11,608		
PPLV80-N9	Charcoal	OS-60559	−24.7	10,050 ± 55*			−12 ± 61	99.4 ± 24.7

* Pooled ages
[a] Value measured on graphite, not shown by lab.
[b] $\delta^{13}C$ values in parenthesis were assumed, not measured.

variations of ^{14}C activity within shells (Jones et al., 2007, 2010). This variability was here averaged out by dating fragments of the shell hinge that integrate most of the mollusk life span (one to four years). The shell hinge is the thickest and best-preserved part of the shell so that original isotopic value is well preserved. Shell recrystalization in *M. donacium* can be diagnosed by direct microscope observation (Carré, 2005; Carré et al., 2014). The dense white and opaque structure and the apparent growth lines observed in the cross-section support the absence of recrystallization in our samples. Shell hinge fragments were mechanically and chemically cleaned to eliminate potentially contaminated surface material. Shell and charcoal fragments were sent to accelerator mass spectrometry (AMS) facilities for radiocarbon dating (Table 1).

^{14}C reservoir age deviations ΔR were calculated from the conventional radiocarbon dates of paired shell and charcoal samples according to the procedure described in Southon et al. (1995), using the SH13 (Hogg et al., 2013) and Marine13 (Reimer et al., 2013) ^{14}C calibration datasets. When two charcoal or two shell ^{14}C dates were available, dates were pooled and the average conventional ^{14}C dates were used for ΔR calculation (Table 1). Pooled dates were statistically identical at 95% confidence level based on Ward and Wilson (1978) chi-square test, except for two cases. First, at the LV079 site, two shells were dated and yielded statistically different ages (Table 1). The archeological context based on excavation observation clearly shows an ephemeral occupation so that shells are likely contemporaneous. Their age difference is thus thought to be a result of seasonal to interannual variability of the coastal upwelling, which justifies their pooling to estimate an average reservoir age. Second, two charcoal dates are statistically different at the LV531-U1 site (Table 1), but these dates are replicates from the same charcoal sample. Since the difference is in this case necessarily due to uncertainties in the analytic procedure, these dates were also pooled. Uncertainty of pooled dates was estimated by the larger of the propagated error or half the difference between the two ages. Propagated uncertainty of ΔR was calculated as described in Russell et al. (2011). Decay-corrected $\Delta^{14}C$ values of marine dissolved inorganic carbon (DIC) were calculated following Stuiver and Polach (1977) and using the 5730 yr ^{14}C half-life.

Deep water masses usually have higher pCO_2 because of the cumulated effect of organic matter mineralization, and lower $\Delta^{14}C$ values (i.e., higher ΔR values) because of limited exchange with atmospheric CO_2. We propose to use this indirect link between ΔR and pCO_2 in our study region to evaluate past changes in surface water pCO_2 associated with changes in ΔR. We thus estimated the modern pre-bomb relationship between pCO_2 and ΔR in the southeast Pacific from the coast to 85°W and from 0 to 40°S (Fig. 1). ΔR was obtained from pre-bomb $\Delta^{14}C$ estimated from total alkalinity by Key et al. (2004). Ocean pCO_2 was calculated from alkalinity and total CO_2 from the Global Data Analysis Project (GLODAP) 1° gridded dataset using equilibrium constants K0 as defined by Weiss (1974), and K1 and K2 as defined by Lueker et al. (2000). Those constants were calculated using a constant salinity value of 35 and water temperature from the World Ocean Atlas (WOA09). Linearly interpolated relationships between pCO_2 and ΔR

were obtained in every grid cell along the depth profiles (0 to 100 m, and 0–600 m), and then averaged to obtain a regional model. We used the depth profiles of pCO_2 and ΔR instead of the surface relationship because water chemistry changes in coastal upwelling areas are expected to occur primarily because of changes in the vertical advection (upwelling intensity) rather than horizontal advection.

The pCO_2–ΔR relationship was calculated first using local temperature (at the depth where alkalinity and total CO_2 were measured), and second using sea–surface temperature to account for the change in carbonate chemistry with temperature when deep waters are upwelled to the surface. We use this latter model for a first-order estimate of past pCO_2 changes in our study area, assuming that the pCO_2–ΔR relationship remained similar throughout the Holocene, which will be discussed later. The pCO_2–ΔR relationship was calculated over a region that was limited, so it is relevant to this oceanographic context while being large enough to account for regional variability and get robust statistics.

Results

A pre-bomb (AD 1837) ΔR value of 146 ± 25 yr was obtained at Coquimbo, which lies between previous estimates of 303 ± 77 yr (Taylor and Berger, 1967) and 43 ± 52 yr (Ingram and Southon, 1996), both from Valparaiso. The average modern pre-bomb ΔR value for central Chile is thus 164 ± 131 yr. At 3.2 cal ka BP, a ΔR value of 168 ± 69 yr was obtained in Los Vilos, very close to the modern pre-bomb value (Fig. 2A). The average value obtained for the whole pre-bomb late Holocene is 165 ± 50 yr. In the early to middle Holocene (from 12 to 6 cal ka BP), ΔR values at Los Vilos ranged from −166 ± 73 to 295 ± 143 yr with an average value of 31 ± 156 yr, but they were particularly variable from 11.5 to 9.5 cal ka BP (Fig. 2A). The average ΔR value for the early to middle Holocene is slightly lower compared to the late Holocene, although the difference is not statistically significant at the 95% confidence level.

Surface DIC $\Delta^{14}C$ values calculated in Los Vilos dropped by ~150‰ during the Holocene: from ~85‰ before 10 cal ka BP to ~−65‰ in the late Holocene (Fig. 2B). The reconstructed $\Delta^{14}C$ values closely follow the global trend of decreasing atmospheric radiocarbon activity that began during the deglaciation and continued through the Holocene (Reimer et al., 2013).

We compare here the new ΔR values from central Chile with Holocene ΔR values estimated and compiled by Ortlieb et al. (2011) for southern Peru and northern Chile (from 15°50′S to 23°34′S). Here, ΔR values were recalculated for consistency using SH13 and Marine13 calibration curves, as in Hua et al., (2015). The average ΔR value for the late Holocene, including modern pre-bomb values, is 225 ± 117 yr (Fig. 2), which is slightly higher than the late Holocene value in central Chile. Although this difference is not statistically significant, it is in agreement with simulations (Butzin et al., 2012) (Fig. 1) and with GLODAP estimates based on water alkalinity (Key et al., 2004). On the other hand, the mean ΔR value in the early Holocene is 528 ± 301 yr for southern Peru and northern Chile, which is much higher (statistically significant at 95% confidence level) than the mean ΔR value of 31 ± 156 yr that we obtained in central Chile at 32°S for the same period (Fig. 2).

The modern pre-bomb relationship between pCO_2 and ΔR in the southeast Pacific shows an increasing trend of pCO_2 with ΔR (Fig. 3), that is essentially due to pCO_2 and ΔR increasing in parallel with depth. Based on the model calculated with SST on a 600-m water column, we estimated the surface water pCO_2 in central Chile and southern Peru in modern pre-bomb conditions and in the early Holocene using estimated average ΔR values for these regions and periods. Reconstructed values of past pCO_2 were then compared to pre-industrial atmospheric pCO_2, which remained between 250 and 290 ppm during the Holocene based on ice-core measurements (Monnin et al., 2004). In central Chile, a late Holocene pre-bomb pCO_2 value of 305 ± 59 ppm was estimated, very close to atmospheric CO_2 concentration. A pCO_2 value could not be estimated for this region for the early Holocene because the ΔR value of 31 yr is beyond the range of this model. In Southern Peru and northern Chile, we obtain a late Holocene pCO_2 value of 516 ± 125 ppm and an early Holocene pCO_2 value of 1576 ± 208 ppm. The error bar here only includes the uncertainty related to the pCO_2–ΔR relationship.

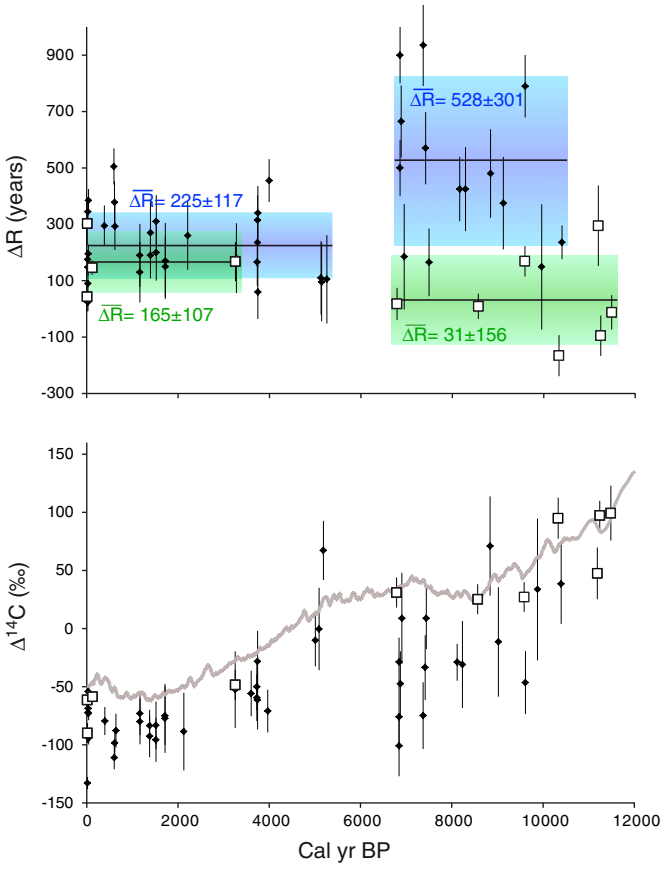

Figure 2. Holocene changes of surface water radiocarbon content in central Chile (green) and in southern Peru/northern Chile (blue). (A) Reservoir age deviation (ΔR) calculated from 12,000 cal yr BP to the modern pre-bomb period in central Chile (32°S) (open squares) compared to values from northern Chile–southern Peru (14–24°S) (black diamonds) compiled by Ortlieb et al. (2011). For consistency with the new data, ΔR values were here recalculated using Marine13 and SH13 calibration curves as in Hua et al. (2015). Mean values and ±1σ intervals are shown for the early Holocene and for the late Holocene in central Chile (green box) and northern Chile–southern Peru (blue box). (B) DIC decay-corrected $\Delta^{14}C$ calculated values from central Chile and northern Chile–southern Peru. The Marine13 calibration curve (Reimer et al., 2013) is shown in gray.

Discussion

These ΔR values from Los Vilos archeological sites are the first estimates of Holocene radiocarbon reservoir age in central Chile. They will help in improving radiocarbon-based chronologies of coastal archeological sites and paleoenvironmental marine archives in this region. Early Holocene ΔR values from central Chile imply a similar or weaker influence of ^{14}C-impoverished deep water, caused by either decreased upwelling or the upwelling of better ventilated water. Sea–surface temperature (SST) reconstructions from the region indicate that temperatures were warmer than today offshore (Kim et al., 2002) and similar along the coast (Carré et al., 2012), suggesting that coastal upwelling in central Chile occurred in a narrower band close to the coast in the early Holocene.

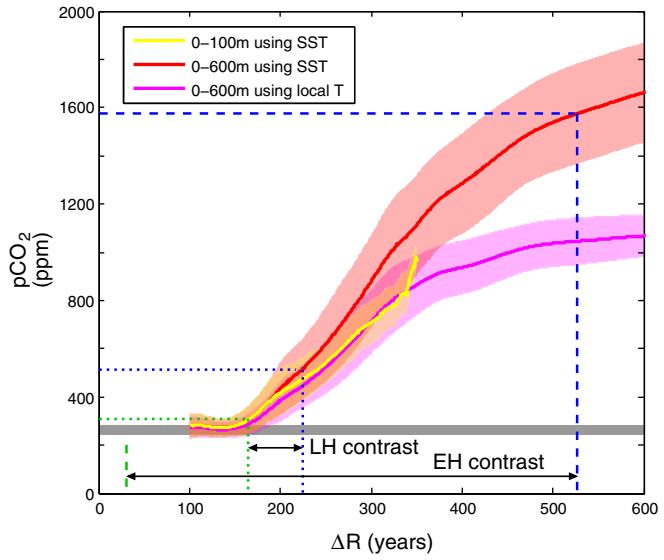

Figure 3. Average relationship between pCO_2 and ΔR (with $\pm 1\sigma$ interval) in the southeast Pacific (area indicated by the thick line in Fig. 1) calculated from GLODAP data (Key et al., 2004) from 0 to 100 m depth using annual SST values (yellow), from 0 to 600 m depth using SST values (red), and from 0 to 600 m depth using local temperature (pink). The Holocene range of atmospheric pCO_2 in Dome C ice core (Monnin et al., 2004) is indicated for comparison by a dark gray band. Late Holocene (dotted lines) and early Holocene (continuous lines) pCO_2 and ΔR are indicated for central Chile (green) and southern Peru (blue). Arrows show the latitudinal contrast in the late Holocene (LH) and early Holocene (EH).

Our new ΔR estimates from central Chile contrast with those obtained in southern Peru and northern Chile, showing high ΔR values of 528 ± 301 yr in the early Holocene (Fontugne et al., 2004; Ortlieb et al., 2011) (Fig. 2A). These high reservoir age values in southern Peru were attributed to vigorous coastal upwelling, an interpretation supported by low $\delta^{13}C$ values in mollusk shells (Sadler et al., 2012) and lower SSTs (Carré et al., 2005, 2014).

The latitudinal contrast in ΔR was much stronger in the early Holocene, which implies a change in the character of the Humboldt system. Today, the waters upwelled off Peru and Chile are transported from the north by the Peru–Chile Undercurrent, which is fed by Equatorial Subsurface Water (ESSW) that has its origins in the lower part of the Equatorial Undercurrent fed by subantarctic mode waters (SAMW) (Toggweiler et al., 1991). These waters are characterized by low $\Delta^{14}C$, low oxygen content and high pCO_2. Fontugne et al. (2004) suggested that the early Holocene increase in coastal ΔR in Peru was too large to result from upwelling enhancement alone and required that upwelled waters were more ^{14}C-depleted. Lower $\Delta^{14}C$ values of upwelled waters could have resulted from a longer residence time, or from a larger contribution of SAMW in the Equatorial undercurrent. This hypothesis was discussed by Hua et al. (2015), who observed that the ^{14}C marine reservoir age increased during the early Holocene in the Western and in the eastern tropical Pacific. It is supported by a comparison between ocean model simulations and a coral $\Delta^{14}C$ record in the Galapagos, which showed that $\Delta^{14}C$ modern variability in the eastern tropical Pacific is primarily controlled by changes in the SAMW component in the upwelling water (Rodgers et al., 2004).

Another hypothesis is that the geographic origin of upwelled waters changed, potentially to Antarctic intermediate waters (AAIW) that are even more ^{14}C-depleted than SAMW. This effect was not observed in central Chile. The influence of the Peru–Chile undercurrent decreases southward as its water mixes with the Humboldt Current that transports oxygen-rich Subantarctic Surface Water (SSW) northward (Silva et al., 2009). Today, this front is observed at 36.5°S and is characterized by an abrupt transition of the air–sea CO_2 flux (Torres et al., 2011). In the early Holocene, the slightly lower ΔR values at 32°S and the stronger latitudinal gradient between northern and central Chile implies that the front between ESSW and SSW was likely located north of its modern position.

In a marine sediment core collected at ~1000 m depth at 46°S, a sea-surface ^{14}C reservoir age increase of ~100 yr was estimated at ca. 11.5 cal ka BP compared to late Holocene conditions (Siani et al., 2013). In a sediment core located farther south at 53°S, within the influence of the Antarctic Circumpolar Current, Van Beek et al. (2002) estimated a ^{14}C reservoir age increase of ~900 yr at ca. 9.5-cal ka BP compared to the middle and late Holocene, which was interpreted as evidence for a stronger influence of AAIW. Similar trends are thus observed in the southern coast of Chile and in southern Peru, while at the same time ΔR along the central coast seemed unaffected. This suggests that changes in southern Peru and southern Chile were not connected through the Humboldt system.

The Humboldt system, from the equator to ~36°S, is the most intense carbon source of the global coastal ocean (Laruelle et al., 2010); whereas south of 36.5°S, Chilean coastal waters become a carbon sink (Torres et al., 2011). Changes in the gradient of ΔR in the Peru–Chile upwelling region therefore imply changes in the latitudinal character of air–sea CO_2 exchange. Air–sea CO_2 flux is proportional to ΔpCO_2, the difference between surface-water pCO_2 and atmospheric pCO_2. Past ΔpCO_2 can be estimated from atmospheric pCO_2 reconstructed from ice cores, and from marine pCO_2 reconstructed here from ΔR values using the pCO_2–ΔR relationship calculated for the southeast Pacific (Fig. 3).

In central Chile, the late Holocene ΔR value (165 ± 107 yr) indicates a seawater ΔpCO_2 of about 30 ppm, which is lower than recent measurements (Torres et al., 2011). However, the late Holocene pCO_2 of 516 ± 125 ppm estimated for southern Peru and northern Chile (Fig. 3) is within the range of pCO_2 values measured in Peru (~400 to 1000 ppm) and close to the average value of about 600 ppm (Friederich et al., 2008). This result supports the accuracy of the model for the Peruvian area and suggests that average ΔR values estimated from shell hinges integrate and average out the high temporal and spatial variability. ΔpCO_2 was thus about 250 ppm in southern Peru in the late Holocene, which means that waters in Peru were a very intense carbon source. Assuming that the model was still valid in the early Holocene, ΔpCO_2 was about 1300 ppm in Peru during that period, which suggests that CO_2 outgassing might have been five times more intense in average. Based on the relationship between pCO_2 and SST observed in Peru (Friederich et al., 2008) and Holocene SST reconstructions in southern Peru (Carré et al., 2014), we can independently estimate that the sea-to-air CO_2 flux in southern Peru during the early Holocene was twice the modern value. Today that flux is 5.1 mol/m^2/yr in Peru (Friederich et al., 2008) and 2.7 mol/m^2/yr in Chile from Iquique (21°S) to Concepcion (36°S) (Paulmier et al., 2008). The CO_2 flux may have reached ~10 to 25 mol/m^2/yr in Peru during the early Holocene, while it was unchanged or slightly lower than today in central Chile.

These estimates only yield indications about the order of magnitude of past air–sea flux changes in the Peru–Chile upwelling system. Their accuracy is limited (1) by the fact that the water $\Delta^{14}C$ and pCO_2 depth profiles were likely different in the early Holocene, and (2) by the large variability of reconstructed ΔR values. It is interesting to note that early Holocene ΔR values in central Chile and in southern Peru are, respectively, below and above the range of values observed today in the region in the 0–100 m water column (Fig. 3). This strongly supports the hypothesis of Fontugne et al. (2004) that upwelling alone cannot account for these changes, and so which must also involve a change in the origin of the upwelled water.

Conclusions

Radiocarbon dates of contemporaneous marine shells and charcoal fragments collected in coastal archeological deposits near Los Vilos, Chile (31.9°S, 71.5°W) provided estimates of marine reservoir ages

during the past 12,000 years. A mean ΔR value of 165 ± 107 yr was obtained for the late Holocene conditions, while a value of 31 ± 156 was obtained for the early to middle Holocene (12 to 6 cal ka BP). Farther north on the southern Peru and northern Chile coast, higher ΔR values in the early Holocene imply an increase in upwelling intensity combined with the upwelling of poorly ventilated water (Fontugne et al., 2004; Carré et al., 2005, 2014; Ortlieb et al., 2011; Hua et al., 2015). A similar trend was also observed off the southern coast of Chile (Van Beek et al., 2002; Siani et al., 2013). The early Holocene is thus characterized by a large latitudinal gradient in $\Delta^{14}C$ of DIC, which indicates a substantial difference in the structure of the Humboldt system in the early, as compared to the late, Holocene. While southern Peru and southern Chile seemed to be more influenced in the early Holocene by SAMW and AAIW respectively, these influences may have been disconnected since they did not reach our study area at ~32°S. Based on the modern relationship between ΔR and seawater pCO_2 in the southeast Pacific, we project that the Peruvian upwelling CO_2 emission to the atmosphere was two to five times more intense in the early Holocene as upwelling was intensified and brought a more CO_2-rich (and ^{14}C-depleted) water mass to the surface. At the same period, the air–sea CO_2 flux in central Chile was similar to modern conditions or slightly weaker.

These results, while allowing for better radiocarbon chronologies of marine material in central Chile, show profound changes in the oceanic circulation within the Humboldt system during the Holocene, which were associated with large changes in the air–sea CO_2 flux in this area.

Acknowledgments

This research was supported by the National Geographic Society under grant no. 8122-06 (M.C.), the U.S. National Science Foundation under grant no. NSF-ATM-0811382 (J.P.S.), and the Chilean FONDECYT under grant no. 1140824 (D.J.). We are thankful to Robert M. Key for providing the GLODAP data, to Martin Butzin for providing the simulated radiocarbon data. We thank Rachid Cheddadi, Associate Editor Tom Marchitto, Senior Editor Derek Booth, and two anonymous reviewers for their constructive comments.

References

Bakun, A., 1990. Global warming change and intensification of coastal ocean upwelling. Science 247, 198–201.
Butzin, M., Prange, M., Lohmann, G., 2012. Readjustment of glacial radiocarbon chronologies by self-consistent three-dimensional ocean circulation modeling. Earth and Planetary Science Letters 317–318, 177–184.
Carré, M. (2005). "Etude géochimique et sclérochronologique de coquilles de bivalves marins: paléocéanographie de la côte sud du Pérou à l'Holocène inférieur et implications archéologiques." Unpublished PhD thesis, Université Montpellier 2.
Carré, M., Bentaleb, I., Fontugne, M., Lavallée, D., 2005. Strong El Niño events during the early Holocene: stable isotope evidence from Peruvian sea-shells. The Holocene 15, 42–47.
Carré, M., Azzoug, M., Bentaleb, I., Chase, B.M., Fontugne, M., Jackson, D., Ledru, M.-P., Maldonado, A., Sachs, J.P., Schauer, A.J., 2012. Mid-Holocene mean climate in the south-eastern Pacific and its influence on South America. Quaternary International 253, 55–66.
Carré, M., Sachs, J.P., Purca, S., Schauer, A.J., Braconnot, P., Angeles Falcón, R., Julien, M., Lavallée, D., 2014. Holocene history of ENSO variance and asymmetry in the eastern tropical Pacific. Science 345, 1045–1048.
Chavez, F.P., Bertrand, A., Guevara-Carrasco, R., Soler, P., Csirke, J., 2008. The northern Humboldt Current System: Brief history, present status and a view towards the future. Progress In Oceanography 79, 95–105.
De Pol-Holz, R., Keigwin, L., Southon, J., Hebbeln, D., Mohtadi, M., 2010. No signature of abyssal carbon in intermediate waters off Chile during deglaciation. Nature Geoscience 3, 192–195.
Fontugne, M., Carré, M., Bentaleb, I., Julien, M., Lavallée, D., 2004. Radiocarbon reservoir age variations in the south Peruvian upwelling during the Holocene. Radiocarbon 46, 531–537.
Friederich, G.E., Ledesma, J., Ulloa, O., Chavez, F.P., 2008. Air–sea carbon dioxide fluxes in the coastal southeastern tropical Pacific. Progress in Oceanography 79, 156–166.
García-Reyes, M., Largier, J., 2010. Observations of increased wind-driven coastal upwelling off central California. Journal of Geophysical Research, Oceans 115, C04011.
Gutiérrez, D., Bouloubassi, I., Sifeddine, A., Purca, S., Goubanova, K., Graco, M., Field, D., Méjanelle, L., Velazco, F., Lorre, A., Salvatecci, R., Quispe, D., Vargas, G., Dewitte, B., Ortlieb, L., 2011. Coastal cooling and increased productivity in the main upwelling zone off Peru since the mid-twentieth century. Geophysical Research Letters 38.
Hogg, A.G., Hua, Q., Blackwell, P.G., Niu, M., Buck, C.E., Guilderson, T.P., Heaton, T.J., Palmer, J.G., Reimer, P.J., Reimer, R.W., Turney, C.S.M., Zimmerman, S.R.H., 2013. SHCal13 Southern Hemisphere Calibration, 0–50,000 years cal BP. Radiocarbon 55, 1–15.
Hua, Q., Webb, G.E., Zhao, J.X., Nothdurft, L.D., Lybolt, M., Price, G.J., Opdyke, B.N., 2015. Large variations in the Holocene marine radiocarbon reservoir effect reflect ocean circulation and climatic changes. Earth and Planetary Science Letters 422, 33–44.
Ingram, B.L., Southon, J.R., 1996. Reservoir ages in eastern Pacific coastal and estuarine waters. Radiocarbon 38, 573–582.
Jackson, D., 2002. Cazadores y recolectores del holoceno medio del norte semiárido de Chile. Universidad de Chile (Tesis para optar el grado de Magíster en Arqueología).
Jones, K.B., Hodgins, G.W.L., Dettman, D.L., Andrus, C.F.T., Nelson, A., Etayo-Cadavid, M.F., 2007. Seasonal variations in Peruvian marine reservoir age from pre-bomb *Argopecten purpuratus* shell carbonate. Radiocarbon 49, 877–888.
Jones, K.B., Hodgins, G.W.L., Etayo-Cadavid, M.F., Andrus, C.F.T., Sandweiss, D.H., 2010. Centuries of marine radiocarbon reservoir age variation within archaeological *Mesodesma donacium* shells from southern Peru. Radiocarbon 52, 1207–1214.
Kennett, D.J., Ingram, B.L., Southon, J.R., Wise, K., 2002. Differences in ^{14}C age between stratigraphically associated charcoal and marine shell from the archaic period site of kilometer 4, southern Peru: old wood or old water? Radiocarbon 44, 53–58.
Key, R.M., Kozyr, A., Sabine, C.L., Lee, K., Wanninkhof, R., Bullister, J.L., Feely, R.A., Millero, F.J., Mordy, C., Peng, T.H., 2004. A global ocean carbon climatology: results from Global Data Analysis Project (GLODAP). Global Biogeochemical Cycles 18, GB4031.
Kim, J.-H., Schneider, R.R., Hebbeln, D., Müller, P.J., Wefer, G., 2002. Last deglacial sea–surface temperature evolution in the Southeast Pacific the South American continent. Quaternary Science Reviews 21, 2085–2097.
Laruelle, G.G., Dürr, H.H., Slomp, C.P., Borges, A.V., 2010. Evaluation of sinks and sources of CO2 in the global coastal ocean using a spatially-explicit typology of estuaries and continental shelves. Geophysical Research Letters 37, L15607.
Lueker, T.J., Dickson, A.G., Keeling, C.D., 2000. Ocean pCO2 calculated from dissolved inorganic carbon, alkalinity, and equations for K1 and K2: validation based on laboratory measurements of CO2 in gas and seawater at equilibrium. Marine Chemistry 70, 105–119.
McGregor, H.V., Dima, M., Fischer, H.W., Mulitza, S., 2007. Rapid 20th-Century Increase in Coastal Upwelling off Northwest Africa. pp. 637–639.
Méndez, C.A., Jackson, D.G., 2004. Ocupaciones humanas del Holoceno tardío en Los Vilos (IV Región, Chile): origen y características conductuales de la población local de cazadores recolectores de litoral. Chungará Revista de Antropología Chilena 36, 279–293.
Méndez, C.A., Jackson, D.G., 2006. Causalidad o concurrencia, relaciones entre cambios ambientales y sociales en los cazadores recolectores durante la transición entre el Holoceno medioy tardío (coasta del semiárido de Chile). Chungará Revista de Antropología Chilena 38, 172–184.
Monnin, E., Steig, E.J., Siegenthaler, U., Kawamura, K., Schwander, J., Stauffer, B., Stocker, T.F., Morse, D.L., Barnola, J.-M., Bellier, B., Raynaud, D., Fischer, H., 2004. Evidence for substantial accumulation rate variability in Antarctica during the Holocene, through synchronization of CO2 in the Taylor Dome, Dome C and DML ice cores. Earth and Planetary Science Letters 224, 45–54.
Narayan, N., Paul, A., Mulitza, S., Schulz, M., 2010. Trends in coastal upwelling intensity during the late 20th century. Ocean Science 6, 815–823.
Ortlieb, L., Vargas, G., Saliège, J.-F., 2011. Marine radiocarbon reservoir effect along the northern Chile-southern Peru coast (14–24°S) throughout the Holocene. Quaternary Research 75, 91–103.
Owen, B.D., 2002. Marine carbon reservoir age estimates for the far south coast of Peru. Radiocarbon 44, 701–708.
Paulmier, A., Ruiz-Pino, D., Garcon, V., 2008. The oxygen minimum zone (OMZ) off Chile as intense source of CO2 and N2O. Continental Shelf Research 28, 2746–2756.
Petchey, F., Ulm, S., 2012. Marine reservoir variation in the Bismarck region: an evaluation of spatial and temporal change in ΔR and R over the last 3000 years. 54 pp. 45–58.
Reimer, P.J., Bard, E., Bayliss, A., Beck, J.W., Blackwell, P.G., Bronk Ramsey, C., Buck, C.E., Cheng, H., Edwards, R.L., Friedrich, M., Grootes, P.M., Guilderson, T.P., Haflidason, H., Hajdas, I., Hatté, C., Heaton, T.J., Hoffmann, D.L., Hogg, A.G., Hughen, K.A., Kaiser, K.F., Kromer, B., Manning, S.W., Niu, M., Reimer, R.W., Richards, D.A., Scott, E.M., Southon, J.R., Staff, R.A., Turney, C.S.M., van der Plicht, J., 2013. IntCal13 and Marine13 radiocarbon age calibration curves 0–50,000 years cal BP. Radiocarbon 55, 1869–1887.
Rodgers, K.B., Aumont, O., Madec, G., Menkes, C., Blanke, B., Monfray, P., Orr, J.C., Schrag, D.P., 2004. Radiocarbon as a thermocline proxy for the eastern equatorial Pacific. Geophysical Research Letters 31, L14314.
Russell, N., Cook, G.T., Ascough, P.L., Scott, E.M., Dugmore, A.J., 2011. Examining the inherent variability in ΔR: new methods of presenting ΔR values and implications for MRE studies. Radiocarbon 53.
Sadler, J., Carré, M., Azzoug, M., Schauer, A.J., Ledesma, J., Cardenas, F., Chase, B.M., Bentaleb, I., Muller, S.D., Mandeng, M., Rohling, E.J., Sachs, J.P., 2012. Reconstructing past upwelling intensity and the seasonal dynamics of primary productivity along the Peruvian coastline from mollusk shell stable isotopes. Geochemistry, Geophysics, Geosystems 13, Q01015.
Siani, G., Michel, E., De Pol-Holz, R., DeVries, T., Lamy, F., Carel, M., Isguder, G., Dewilde, F., Lourantou, A., 2013. Carbon isotope records reveal precise timing of enhanced Southern Ocean upwelling during the last deglaciation. Nature Communications 4.
Silva, N., Rojas, N., Fedele, A., 2009. Water masses in the Humboldt Current System: properties, distribution, and the nitrate deficit as a chemical water mass tracer for equatorial subsurface water off Chile. Deep Sea Research Part II: Topical Studies in Oceanography 56, 1004–1020.
Southon, J.R., Oakland Rodman, A., True, D., 1995. A comparison of marine and terrestrial radiocarbon ages from northern Chile. Radiocarbon 37, 389–393.
Strub, P.T., Mesias, J.M., Montecino, V., Rutllant, J., Salinas, S., 1998. Coastal ocean circulation off western South America. In: Robinson, A.R., Brink, K.H. (Eds.), The Global Coastal Ocean. Regional Studies and Syntheses. Wiley, New York, pp. 273–315.

Stuiver, M., Polach, H.A., 1977. Discussion; reporting of C-14 data. Radiocarbon 19, 355–363.
Tarifeño, E. (1980). "Studies on the Blology of Surf Clam *Mesodesma donacium* (Lamarck, 1818) (Bivalvia: Mesodesmatidae) from Chilean Sandy Beaches." Unpublished PhD thesis, University of California.
Taylor, R.E., Berger, R., 1967. Radiocarbon content of marine shells from the Pacific coasts of Central and South America. Science 158, 1180–1182.
Toggweiler, J.R., Dixon, K., Broecker, W.S., 1991. The Peru upwelling and the ventilation of the South Pacific thermocline. Journal of Geophysical Research 96, 20,467–20,497.
Torres, R., Pantoja, S., Harada, N., González, H.E., Daneri, G., Frangopulos, M., Rutllant, J.A., Duarte, C.M., Rúiz-Halpern, S., Mayol, E., Fukasawa, M., 2011. Air–sea CO2 fluxes along the coast of Chile: from CO2 outgassing in central northern upwelling waters to CO2 uptake in southern Patagonian fjords. Journal of Geophysical Research, Oceans 116, C09006.
van Beek, P., Reyss, J.-L., Paterne, M., Gersonde, R., van der Loeff, M.R., Kuhn, G., 2002. 226Ra in barite: absolute dating of Holocene Southern Ocean sediments and reconstruction of sea–surface reservoir ages. Geology 30, 731–734.
Wang, D., Gouhier, T.C., Menge, B.A., Ganguly, A.R., 2015. Intensification and spatial homogenization of coastal upwelling under climate change. Nature 518, 390–394.
Ward, G.K., Wilson, S.R., 1978. Procedures for comparing and combining radiocarbon age determinations: a critique. Archaeometry 20, 19–31.
Weiss, R.F., 1974. Carbon dioxide in water and seawater: the solubility of a non-ideal gas. Marine Chemistry 2, 203–215.

Modern drought conditions in western Sahel unprecedented in the past 1600 years

Authors:

Matthieu Carré[1,2*] (ORCID ID: 0000-0001-8178-7316), Moufok Azzoug[3], Paul Zaharias[4], Abdoulaye Camara[5] , Rachid Cheddadi[6] , Manuel Chevalier[7], Denis Fiorillo[8], Amadou T. Gaye[9], Serge Janicot[1], Myriam Khodri[1], Alban Lazar[1], Claire E. Lazareth[1], Juliette Mignot[1], Nancy Mitma Garcia[6], Nicolas Patris[10], Océane Perrot[6], Malick Wade[11].

Affiliations:

[1] *Sorbonne Universités (UPMC, Univ Paris 06)-CNRS-IRD-MNHN, LOCEAN Laboratory, Paris, France.*

[2] *CIDIS-LID-Facultad de Ciencias y Filosofía-Universidad Peruana Cayetano Heredia, Lima, Perú.*

[3] *Département de génie des procédés, faculté de technologie, Université de Bejaia, 06000 Bejaia, Algeria.*

[4] *ISYEB – UMR 7205 – CNRS, MNHN, UPMC (Université Paris 6), EPHE – Muséum national d'Histoire naturelle, Sorbonne Universités, Paris, France.*

[5] *Institut Fondamental d'Afrique Noire, Université Cheikh Anta Diop, Dakar, Senegal.*

[6] *CNRS-UM-IRD-EPHE, Institut des Sciences de l'Evolution de Montpellier, Montpellier, France.*

[7] *Institut des Dynamiques de la Surface Terrestre, University of Lausanne, Switzerland.*

[8] *CNRS-MNHN, Archéozoologie, archéobotanique: sociétés, pratiques et environnements, Paris, France.*

[9] *Institut polytechnique, Université Cheikh Anta Diop, Dakar, Senegal.*

[10] *IRD-CNRS-UM, Hydrosciences Montpellier, Montpellier, France.*

[11] *Laboratoire de Physique de l'Atmosphere et de l'Ocean Simeon Fongang, Université Cheikh Anta Diop, Dakar, Senegal.*

*Correspondence to: matthieu.carre@locean-ipsl.upmc.fr;

Tel.: +33 629 10 43 84 / +51 938 818 475

Abstract

As climate model uncertainties remain very large for future rainfall in the Sahel, a multi-centennial perspective is required to assess the situation of current Sahel climate in the context of global warming. We present here the first record of hydroclimatic variability over the past 1600 years in Senegal, obtained from stable oxygen isotope analyses ($\delta^{18}O$) in archaeological shell middens from the Saloum Delta. During the preindustrial period, the region was relatively humid, with maximum humidity reached during the period from AD 1500 to AD 1800, referred to as the Little Ice Age. A significant negative link is observed at the centennial scale between global temperature and humidity in the Sahel that is at odds with the expected effects of latitudinal shifts of the intertropical convergence zone during the last millennium. In the context of the past 1600 years, the Western Sahel appears to be experiencing today unprecedented drought conditions. The rapid aridification that started *ca*. AD 1800 and the recent emergence of Sahel drought from the natural variability point to an anthropogenic forcing of Sahel drying trend. This new long-term perspective suggests that the recovery of Sahel rainfall in the last decade may only result from short-term internal variability, and supports climate models that predict an increase of Sahel drought under future greenhouse climate.

Keywords: West African Monsoon, Climate Change, Paleoclimate, Shell middens

1. Introduction

Precipitation in the Sahel declined by ~30% in the 1960s, initiating a severe multi-decadal drought that represents one of the most significant climate change episodes in the global instrumental record (Christensen et al. 2013), with devastating socio-economic impacts. The contributions of global warming and land use to this event, however, are still not clearly understood, partly because of the underperformance of climate models in the simulation of the West African Monsoon (WAM), and partly because of the shortness of the instrumental record (Biasutti 2013). Rain gauge data in the Sahel start in AD 1851 in Saint Louis, Senegal, but regional data is generally considered robust only after AD 1900 (Nicholson et al. 2012). In the instrumental record, the Sahel climate has been dominated by multidecadal variability which may mask longer-term trends. Assessing current trends in Sahel rainfall and determining the potential role of anthropogenic activities in this climatically vulnerable region requires a multi-centennial perspective of natural variability, which is so far lacking in this region (Nash et al. 2016). The closest continuous record documenting hydroclimate change in the past two millennia comes from Lake Bosumtwi, Ghana (Shanahan et al. 2009), which is not located in the Sahel but in the convection area of the WAM.

In this study, we use oxygen isotope ratios ($\delta^{18}O$) of *Senilia senilis* shells from the Saloum Delta in Senegal, to construct the first record of centennial variability of the hydrologic balance of the Western Sahel, spanning the last 1600 years. The people of the region have long depended on *S. senilis* as a staple food, as evidenced by the massive archaeological shell middens (up to 15 m high) that have been accumulated throughout the Delta (Thilmans and Descamps 1982; Hardy et al. 2016). By virtue of their size and antiquity, these middens present a unique opportunity to obtain diachronic records of hydrological change.

The Saloum Delta is a mangrove estuary with a small catchment basin, disconnected from the Senegal River or the Gambia River catchment basins. The extremely steep latitudinal precipitation gradient at this location makes the Saloum estuary highly sensitive to changes in the WAM (Fig. 1). Although a contrasted evolution of rainfall in central and western Sahel has been described in the past decade, and projected in the future (Biasutti 2013), instrumental observations show a remarkable coherence of precipitation for the whole of the Sahel (Nicholson 2014) and in particular a strong correlation between precipitation in the Saloum Delta and the Sahel (Wade et al. 2015) (Fig. 1). Assuming the stationarity of this spatial coherence, we consider that our record is largely representative of conditions in at least the western Sahel region and potentially the whole Sahel band.

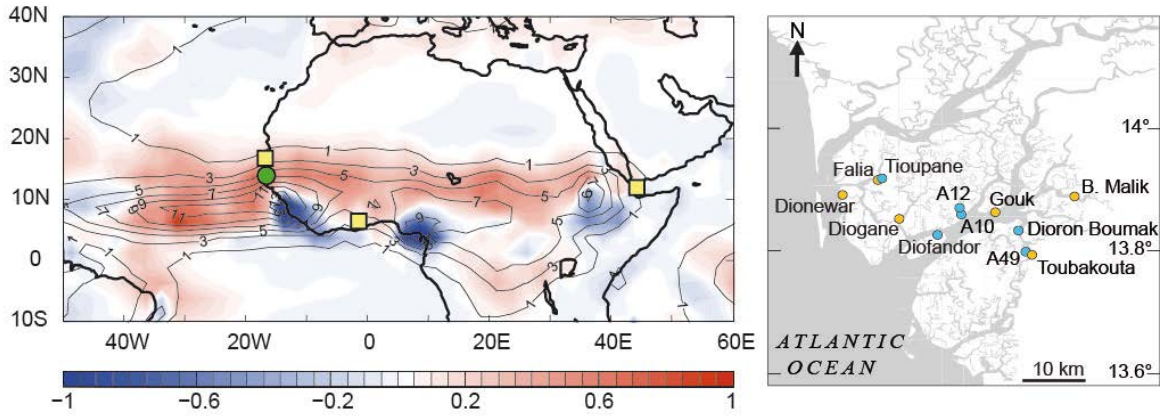

Fig. 1. (Left) Regional representativeness of summer precipitation in the Saloum study site. Linear regression (color shades) of summer rainfall (JAS) decadal variability in the Saloum Delta (green circle) with summer rainfall in the rest of the domain, using GPCP data (Pendergrass et al. 2016). Mean summer (JAS) rainfall is shown by black contours (mm/d). Yellow squares indicate the location, from west to east, of core GeoB9501 (Mulitza et al. 2010), Lake Bosumtwi (Shanahan et al. 2009), and core P178-15 (Tierney et al. 2015). (Right) Map of the Saloum mangrove Delta showing the location of water and modern shell sampling sites (orange circles) and fossil (blue circles) shell sampling.

2. Material and methods

2.1. Bivalve shells

Modern shells of *Senilia senilis* were collected live on intertidal mud flats in five locations distributed across the mangrove delta close to the archaeological sites (Fig. 1). Fossil shells from sites A10, A12, and A49 were collected on the surface of those shell middens. In Dioron Boumak shell midden, the full stratigraphy of the shell accumulation could be sampled in the outcrop produced by tidal erosion (Fig. 2). In Tioupane and Diofandor, we sampled the middens from the surface to depths of 5.50 and 1.15m respectively, in outcrops produced by ancient exploitation for lime production. The shell middens were almost exclusively composed of *S. senilis* shells, with infilling composed of sand, silts, and ashes, and had therefore a very poor cohesive structure (Fig. 2). After cleaning the outcrops, the accumulations were divided into a continuous vertical sequence of stratigraphic sections. About 30 shells were collected on the field in each section from the surface to the bottom. Subsequently, subsamples of 1 to 7 shells per section were selected in the lab based on shell size and preservation. Therefore, each shell comes from a depth interval and as such, it represents a short ~2-10-yr window (~5 years in average) randomly drawn from the time period when the section was accumulated. The depth, thickness and the number of shells analyzed are indicated for each stratigraphic layer in the depth-age model plots (Fig. 3).

Shell preservation was tested by observing the aragonite microstructure in the hinge of a subsample of shells from Dioron Boumak using a Scanning Electronic Microscope (SEM). Images revealed a perfectly preserved cross-lamellar structure (Fig. 4C). To guarantee a well preserved isotopic signal, aragonite powder samples for isotopic analyses were collected in

cross section to avoid surface alteration, in the hinge, which is the thickest and best preserved part (Fig. 4A). For shells that were not observed by SEM, preservation was evaluated by optical microscope observation of the polished cross sections. Aragonite opacity and the fact that growth lines could be observed in every part of the shells are complementary evidence that shells and their original isotopic composition were well preserved.

Fig. 2. The Dioron Boumak shell midden. The shell midden is about 11m high, 300m long and topped by a baobab forest (left). It was accumulated by ancient mollusk shell gatherers during at least 600 years, and is one of the largest and best preserved archaeological shell middens of the Saloum Delta. The beach in the front is exclusively composed of *S.senilis* shells from the tidal erosion of the shell accumulation. (Center) Dioron Boumak stratigraphic profile sampled for charcoal fragments and fossil shells. (Right) Close up view of the shell midden showing the extreme density of the shell accumulation.

Table 1. Radiocarbon dates and calibration

Site	Material	Lab. Ref.	Depth (cm)	$\delta^{13}C$ (‰ VPDB)	^{14}C age / $F^{14}C$	Calibration dataset	%mar. carbon	Cal. median (AD)	2σ range
Diofandour	charcoal	UBA-29457	20	-25*	1.0921 ±0.0044	NHZ2		1957	1957-1958***
	charcoal	SacA 25602	40	-25.3	35±30	IntCal13		1893	1695-1955
	charcoal	UBA-29458	80	-25*	363±26	IntCal13		1519	1451-1633
	charcoal	SacA 25603	115	-25.9	415±30	IntCal13		1463	1429-1618
Tioupane	charcoal	SacA 25604	20	-31.4	690±35	IntCal13		1294	1262-1390
	charcoal	SacA37940	140	-26.6	840±30	IntCal13		1203	1059-1264
	charcoal	SacA25605	300	-24.1	985±30	IntCal13		1047	991-1154
	charcoal	SacA 25606	500	-24.4	970±30	IntCal13		1089	1017-1155
	charcoal	SacA 25607	540	-22.9	995±30	IntCal13		1031	986-1153
Dioron Boumak	charcoal	UBA 19943	50	-25*	817±23	IntCal13		1229	1179-1265
	charcoal	UBA 19944	150	-25*	1083±38	IntCal13		957	890-1019
	charcoal	SacA 25596	240	-24.2	1195±35	IntCal13		829	694-947
	charcoal	SacA 25597	360	-25.9	1260±30	IntCal13		736	669-862
	charcoal	SacA 25598	480	-19.8	1270±30	IntCal13		729	664-856
	charcoal	SacA 25599	670	-23	1370±30	IntCal13		655	608-688
	charcoal	SacA 25600	850	-24.8	1480±30	IntCal13		587	541-642
	charcoal	SacA 25601	925	-20.8	1530±30	IntCal13		537	432-600
A-10	shell	SacA37929	0	-7.1	340±30	Mixed **	72	1890	1718-1955
A-12	shell	SacA37930	0	-9.1	950±30	Mixed **	64	1296	1245-1387
A-49	shell	SacA37922	0	-2.1	1885±30	Mixed **	92	494	411-577

*assumed value

**mixed using IntCal13 and Marine13 with ΔR=0. Marine carbon percentage was estimated from $\delta^{13}C$ value assuming a 0‰ value for the marine endmember and a -25‰ value for the terrestrial carbon endmember.

***the 1997-2002 interval was excluded from the calibration because the site was abandoned in 1982.

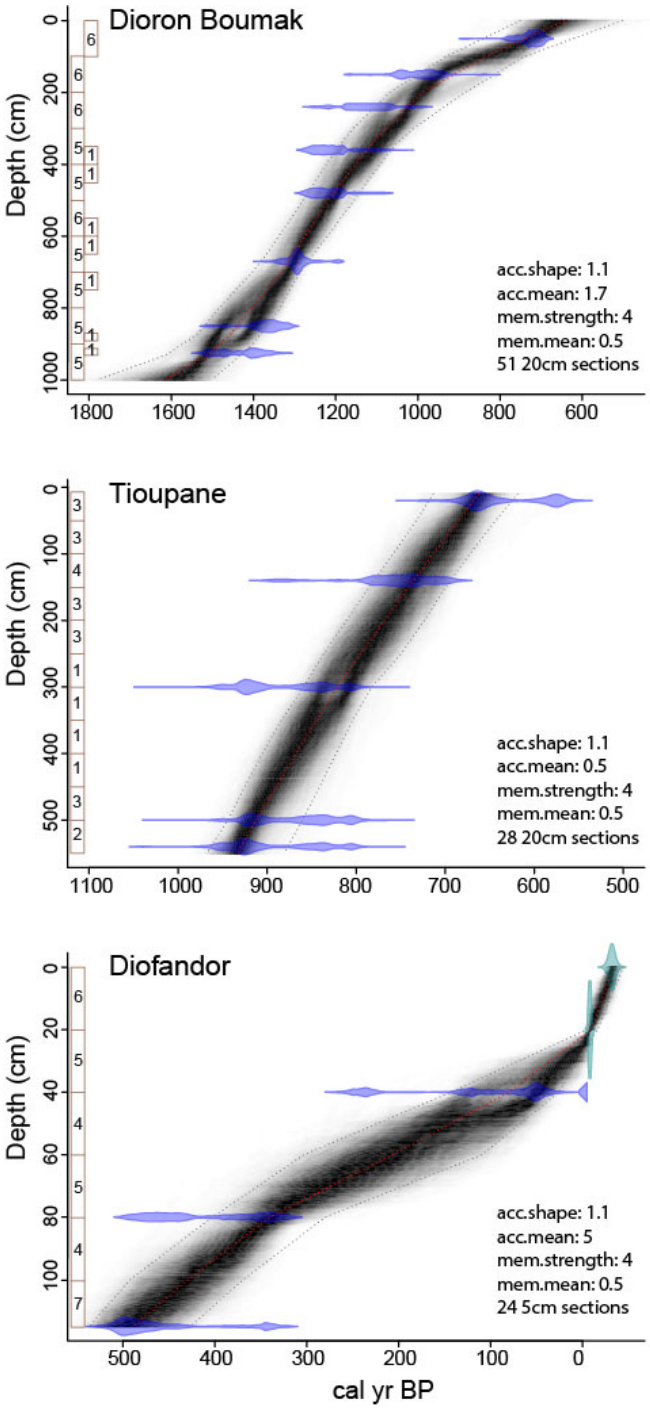

Fig. 3. Bayesian age-depth models of Dioron Boumak, Tioupane and Diofandor shell middens. Models were calculated from charcoal radiocarbon dates using the Bacon R software (*34*). Parameter values used for Bacon are indicated for each site. Two calendar dates were assigned for Diofandor (gray): 1982±3 for the top, which corresponds to the site abandonment estimated by local witnesses, and 1957±1 at 20 cm. This latter date is the only possible calibrated date for this radiocarbon measurement (Table S1), after excluding the 1997-2002 interval which is inconsistent with the site abandonment date. The depth of the stratigraphic layers and the number of shells analyzed are indicated along the vertical axis. For Dioron Boumak, two columns are shown corresponding to two field campaigns in 2010 (left) and 2011 (right) (Azzoug et al. 2012b).

2.2. Chronology

For Dioron Boumak, Tioupane, and Diofandor, depth-age models were calculated from radiocarbon dates obtained on charcoal fragments collected along the middens' stratigraphy (Table 1). Radiocarbon date series were all stratigraphically consistent. Bayesian depth-age models were calculated using the Bacon program (Blaauw and Christen 2011) with a broad distribution of accumulation rate and a low memory strength parameter to allow for large flexibility in the accumulation rate (Fig. 3). Default values of *t.a* and *t.b* (3 and 4 respectively) parameters of the student'st-distribution were used. Based on these models, calibrated dates and their 95% confidence interval were calculated for the depth boundaries of the stratigraphic sections. Three shells (from A10, A12, and A49) were directly radiocarbon dated from a shell hinge fragment. Calibration of these dates was performed using mixed terrestrial and marine radiocarbon calibration curves (Reimer et al. 2013). We used the marine reservoir age (R=511±50 yrs) estimated for Senegal by Ndeye (2008), and a percentage of marine carbon calculated from the shell $\delta^{13}C$ value, considering two end members of 0‰ for marine carbon and -25‰ for terrestrial carbon (72% of marine carbon for A10, 64% for A12, and 92% for A49, see Table 1).

2.3. Shell analysis

45 modern shells and 120 archaeological shells were analyzed. Shells were embedded in polyester resin and radially cut with a low-speed diamond saw to extract a 1mm thick lamina that was then mounted on a microscope slide and polished. A sample of aragonite powder was collected by drilling a thin groove across the hinge cross section using an automated microsampler Micromill®. Each groove crossed the most part of the hinge growth, so that the

aragonite sample integrates most of the shell lifetime, ~5 years in average (Fig. 4A). One fossil shell and 16 modern shells were serially microsampled in the outer shell layer with a time resolution corresponding to approximately one month following the procedure described by Azzoug et al. (2012a). Aragonite powder samples of typically 50-100µg were analyzed for their isotopic composition ($\delta^{13}C$ and $\delta^{18}O$) using a Thermo Finnigan Delta V isotope ratio mass spectrometer coupled to a Kiel IV carbonate device. Long-term reproducibility for $\delta^{13}C$ and $\delta^{18}O$ was better than 0.05‰ and 0.08‰ respectively based on repeated internal lab standard analyses. Isotopic analyses of aragonite samples from Tioupane and Diofandor were replicated 2 to 5 times. Shell isotopic ratios ($\delta^{13}C$ and $\delta^{18}O$) were reported as relative deviation from the V-PDB international reference. Since isotopic standards for calcium carbonates are all calcitic and because aragonite and calcite have different acid fractionation factors, a correction of -0.38‰ (at 70°C) was applied to aragonite isotopic values following Kim et al. (2007).

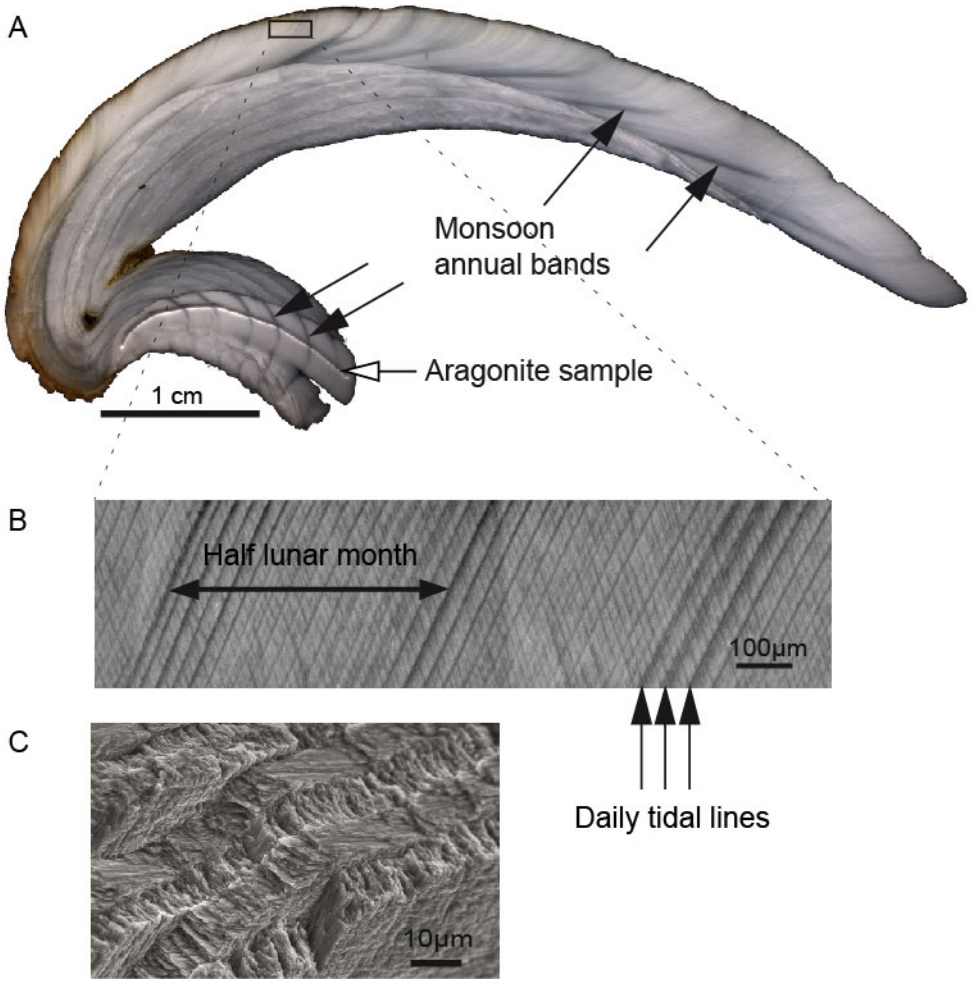

Fig. 4. *Senilia senilis* sclerochronology. A: polished cross section of a fossil shell from the Saloum Delta. Dark bands can be seen in the outer layer and in the hinge (two of them are indicated by black arrows), that correspond to monsoon season growth. The lifespan of the shell can thus be estimated at about 8 years from the number of annual bands. Isotopic values presented in this study were obtained from the analysis of aragonite powder collected in the hinge along a transect that integrates most of the mollusk life. The sampling groove is here indicated by the white arrow. B: Microscope view of tidal growth lines. Clusters of darker and thicker tidal lines can be observed during spring tides every half lunar month (*6*). C: Scanning electronic microscope image of a perfectly preserved aragonite cross lamellar structure observed in a fossil shell hinge.

2.4. Environmental monitoring and calibration

As a function of the region's highly seasonal rainfall regime, the salinity (and the water oxygen isotopes) of the estuary varies seasonally from brackish in the monsoon season to hypersaline in the dry season. The relationship between shell $\delta^{18}O$ and local climate was

determined by an *in situ* environmental monitoring in Toubakouta and isotopic analysis of modern shells collected live in Toubakouta and in 4 other sites from across the estuary (Fig. 1). In Toubakouta, sea surface temperature was measured hourly with an Onset Tidbit.v2 datalogger since 2011. Rainfall was measured with an Onset RG-3 rain gauge datalogger since 2011. Sea water samples were collected weekly for $\delta^{18}O_w$ since November 2010. The oxygen isotopic composition of water samples was measured using a dual inlet Isoprime IRMS with the conventional CO_2-H_2O equilibration method (Cohn and Urey 1938). The standard error estimated from repeated standard measurement was 0.07‰. Water $\delta^{18}O$ values were reported as relative deviations from the V-SMOW international standard. High-resolution isotopic records of modern shells from Toubakouta allowed us to study seasonal scale variability of shell isotopic ratios and their relationship with local climate (Fig. 5).

The first observation is that high resolution shell $\delta^{18}O$ records from Toubakouta show a good reproducibility (Fig. 5A). Then, we calculated $\delta^{18}O_w$ from modern shell $\delta^{18}O$ using the Grossman and Ku's third paleotemperature equation (Grossman and Ku 1986) and the local mean SST annual cycle. Since calculated values faithfully reproduce measured water $\delta^{18}O_w$ (Fig. 5D), we conclude that *S. senilis* shells precipitate in isotopic equilibrium. At the seasonal scale, $\delta^{18}O_w$ accounts for ~3‰ in aragonite $\delta^{18}O$ variations while the 8°C range of temperature may account for 1.7‰ change in shell aragonite. However, because the temperature cycle is not in phase with $\delta^{18}O_w$ ($\delta^{18}O_w$ lags by ~3 months), it contributes positively to the shell $\delta^{18}O$ range only during the rainy season which represents a temperature variation of 2-3°C. The temperature contribution to the shell isotopic variations is thus only 0.4 to 0.6‰. $\delta^{18}O_w$ is the primary driver (85%) of shell $\delta^{18}O$ variations at the seasonal time scale. On longer time scales, this predominance of $\delta^{18}O_w$ influence is expected to be even larger since rainfall long-term variability is much larger than temperature variability.

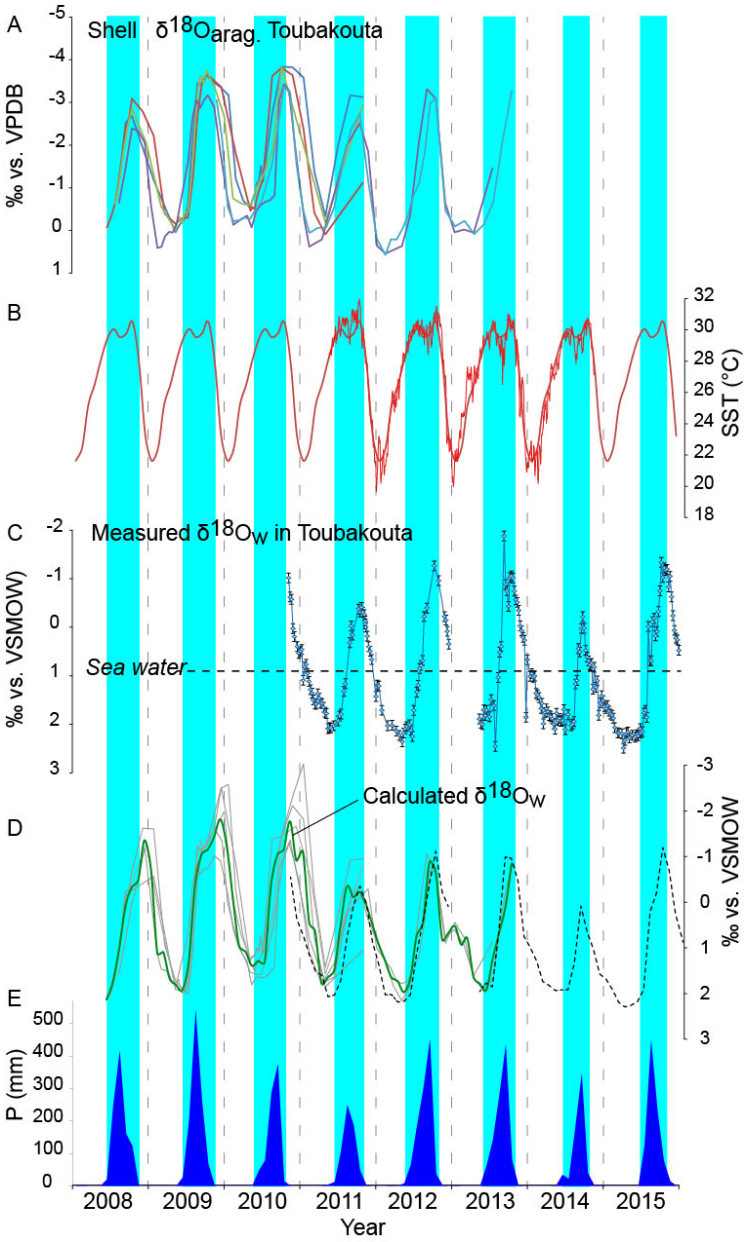

Fig. 5. Environmental monitoring and isotopic calibration in Toubakouta. (A) High resolution profiles of aragonite $\delta^{18}O$ (reversed scale) measured along five modern shells of *S. senilis* collected live in Toubakouta (three in 2011 and two in 2013). The chronology was determined using tidal fortnightly growth lines and assigning minimum values to the average date of minimum water $\delta^{18}O_w$. (B) Daily sea surface temperature (SST) measured in Toubakouta (thin red line), and average monthly SST annual cycle (thick red line). (C) Weekly estuary water $\delta^{18}O_w$ measured in Toubakouta from 2010 to 2015. Samples of early 2013 were lost. (D) Water $\delta^{18}O_w$ calculated from shell aragonite $\delta^{18}O$ (individual shells in grey, averaged shell profile in green) using Grossman and Ku third equation (Grossman and Ku 1986) and the mean annual cycle of SST. Calculated $\delta^{18}O_w$ is compared with measured monthly $\delta^{18}O_w$ (black dotted line). (E) Monthly rainfall (mm) measured in Toubakouta. Light blue vertical bands indicate the rainy seasons.

The Toubakouta rainfall record (Fig. 5E) shows that the rainy seasons correspond exactly to the periods of decreasing $\delta^{18}O_w$ values (reversed scale), while dry seasons correspond to periods of increasing $\delta^{18}O_w$ values, a pattern that is also clear in shell $\delta^{18}O$ records. The estuary water isotopic values, closely linked to salinity (Fig. 6), become lower than sea water values in the rainy season and higher than the sea water values in the dry season (Fig 5C). The sea water $\delta^{18}O_w$ measured at the mouth of the Delta in the dry season is close to 1‰. This *in situ* calibration dataset demonstrates that shell $\delta^{18}O$ faithfully reflect $\delta^{18}O_w$ which is closely linked to precipitation.

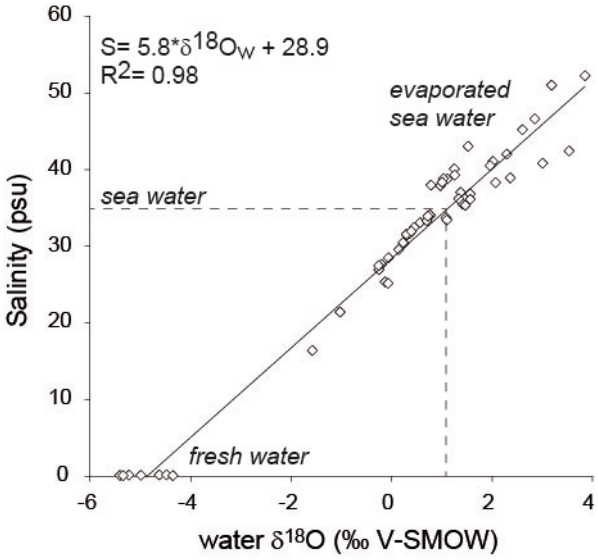

Fig. 6. Relationship between water isotopic ratio ($\delta^{18}O_w$) and salinity in the Saloum estuary. Water samples were collected across the estuary from Dionewar to Bombugar Malik (Fig. 1) at different seasons between 2011 and 2016. The least square linear regression is shown as well as the determination coefficient R^2. Sea water (~35 psu) corresponds to an isotopic ratio of ~1‰. Higher values are observed in the dry season and indicate evaporated sea water, while lower values correspond to a mix between sea water and rain water.

2.5. Spatial variability across the Delta

Since fossil shells were collected in different sites within the Saloum Delta, we studied the spatial variability of isotopic values in modern shells from across the Delta. First, modern

shell $\delta^{18}O$ values show no statistically significant difference between the five collection sites (Fig. 7). This means that the variability within the fossil $\delta^{18}O$ record cannot be explained by changes in their origin. In contrast, there is a clear negative trend for shell $\delta^{13}C$ toward the continent (Fig. 7). This gradient can be explained by the mixing of two carbon sources: dissolved inorganic carbon from the ocean (~0‰) and terrestrial carbon, primarily from mangrove litter (~-25‰). Since this gradient is also observed during the dry season when the Saloum Delta is an inverse estuary, the mixing of carbon is not due to the mixing of marine *vs* runoff water but to tidal mixing. In estuaries where DIC $\delta^{13}C$ has very large variations, mollusk shell $\delta^{13}C$ variability primarily reflects DIC $\delta^{13}C$ (Gillikin et al. 2006). In this setting, shell $\delta^{13}C$ can thus be used to estimate the ratio of terrestrial *vs* marine carbon 1) for calibration of shell radiocarbon dates, and 2) to estimate past changes in the tidal mixing due to the estuary geomorphology. $\delta^{13}C$ values of fossil shells from Diofandor and Tioupane fall on the trend defined by modern shells (Fig. 7) suggesting that despite the strong dynamicity of delta environments, the general morphology of the estuary remained similar to the current one during the studied period. $\delta^{13}C$ values from Dioron Boumak shells are more positive than the prediction of the modern trend, suggesting a stronger connection with the sea, but still within the range of modern Saloum shells. The last marine transgression has been dated by Faure et al. (1980) at 1545±120 ^{14}C BP and was approximately 0.5m high. This would correspond to the very beginning of our record and could partly explain Dioron Boumak $\delta^{13}C$ values, but could not account for the more negative $\delta^{18}O$ values at Dioron Boumak compared to modern values. The general consistency of past $\delta^{13}C$ values with the modern estuary geomorphology, and the fact mean shell $\delta^{18}O$ values are constant across the estuary show that the estuary morphology cannot account for the long-term oxygen isotope variability. This result confirms geomorphological studies which suggested that the geometry of the Saloum Delta 1500 years

ago was already similar to the modern conditions (Barusseau et al. 1995; Diara and Barusseau 2006).

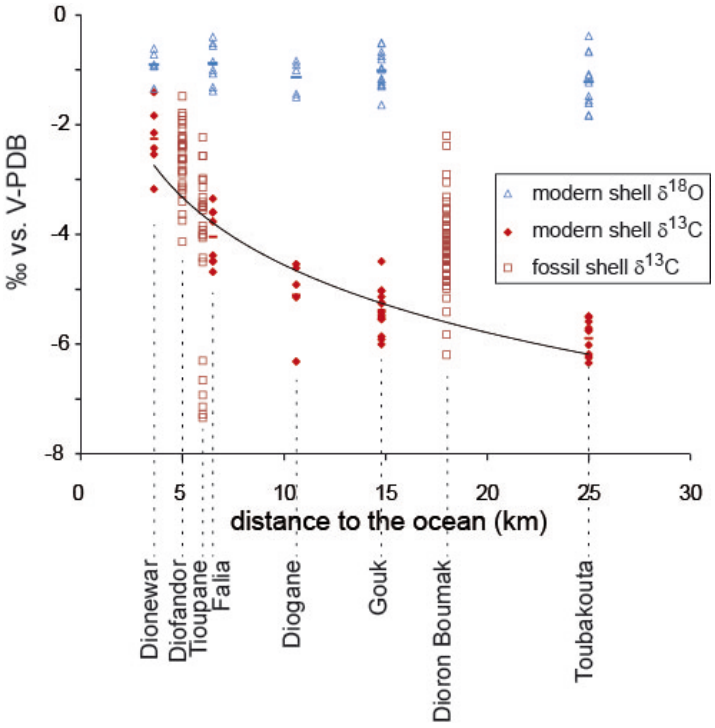

Fig. 7. Gradients of shell isotopic values across the Saloum Delta. Modern shell $\delta^{18}O$ (blue triangles) and $\delta^{13}C$ values (red diamonds) from the 5 collection sites *versus* their distance to the open ocean. The black curve shows the decreasing trend of $\delta^{13}C$ from the sea towards the land, as a result of the increasing contribution of mangrove carbon. Fossil shell $\delta^{13}C$ (open red squares) *versus* the distance to the open ocean. Distances were estimated from satellite pictures.

2.6. Accuracy of bulk isotopic analyses in *Senilia senilis* shells

Most shell isotopic values in this study were obtained from bulk sampling in the hinge part of the shell. Isotopic values obtained from bulk samples could potentially be biased because bivalve shell growth can stop or change because of physiological factors (age, reproduction) or environmental factors (Goodwin et al. 2003). We discuss here the causes of shell growth variations, their potential effect on bulk isotopic values, and eventually evaluate the accuracy of bulk isotopic analyses in this study. *S. senilis* is a euryhaline species that has

been observed live in salinities ranging from 0 to 60 psu, on intertidal mudflats in coastal lagoons from Mauritania to Angola (Elouard and Rosso 1977; Debenay et al. 1994; Azzoug 2012; Lavaud et al. 2013) . *S. senilis* can thus support and record large salinity changes. Seasonal salinity variations in our study sites are clearly within this tolerance range.

The study of growth increment thickness and periodic growth lines (sclerochronology) related to lunar tidal cycles observed in *S. senilis* shells (Fig. 4) allows for a detailed control of growth rate changes or stops through the shell's life (Azzoug et al. 2012a; Debenay et al. 1994; Lavaud et al. 2013). In Mauritania, shell growth rate is lower in the cool season (November-February) (Lavaud et al. 2013), while in the Saloum Delta, it is lower during the rainy season (July-September) (Azzoug et al. 2012a). The number of periodic growth lines per year observed in shells indicates that shells grow continuously throughout the year so that the full annual cycle is recorded (Azzoug et al. 2012a). In some bivalve species, mainly from mid-to high latitudes, the length of the seasonal slowdown or shutdown increases with age which produces a progressive decrease in the seasonal isotopic range and an overall systematic trend in high resolution isotopic shell records (Goodwin et al. 2003). Such a systematic trend was not observed in modern or fossil shells of *S. senilis* (Azzoug 2012).

Nevertheless, growth slowdown in the rainy season may bias bulk analyses toward dry season conditions characterized by less negative $\delta^{18}O$ values. We estimated the effect of bulk sampling on isotopic values by comparing bulk values with average values obtained from high-resolution isotopic records in 15 modern shells from 3 locations in the Saloum Delta. Shell high-resolution isotopic records were resampled at a constant monthly resolution to avoid biases due to variations in temporal resolution. The difference between bulk isotopic values and averaged monthly values ranged from -0.57‰ to 0.83‰. The average difference is 0.22±0.44‰ (1σ). A student t-test shows that the bias due to bulk sampling is not different from zero at the 0.05 significance level. This demonstrates that bulk sampling does not

significantly affect the accuracy of isotopic data in this study. It does introduce noise to the signal ($\sigma \approx 0.44‰$), that we interpret as primarily related to variations in the relative contribution of rainy and dry seasons in the shell life span. For serially sampled shells, we used the average of the hinge bulk value and of the high-resolution record mean.

2.7. A composite record of shell $\delta^{18}O$ centennial variability

The record is composed of 164 isotopic values including 120 archaeological shell values (Fig. 8). Except for the three shells that were directly radiocarbon dated, each of these archaeological shell values is floating in a time interval defined by the ages of the upper and lower depths of the stratigraphic section where the shell was collected (see section 2.1). Since these shells do not have an assigned depth, their age cannot be directly estimated from the age model. Only the upper and lower boundaries of stratigraphic sections can be dated using the age model. From this floating discontinuous dataset, we built a continuous record of the probability distribution of the average shell aragonite $\delta^{18}O$ value. This was achieved through a Monte Carlo (MC) sampling where iterations represent random possibilities of the floating chronology. In every iterations, the first step is a random sampling of the age of the stratigraphic sections' limits from their respective probability density function determined by the Bayesian depth-age model (Fig. 3). Once the time boundaries of stratigraphic sections have been fixed, the second step assigns a random age for each shell within the time interval represented by its stratigraphic section. In addition to the chronology uncertainty, the uncertainty on $\delta^{18}O$ values related to bulk sampling was also sampled from a normal distribution ($\mu=0$, $\sigma=0.44‰$). A 7 point moving average is then calculated and annually interpolated. 10 000 iterations provide us with an ensemble of potential moving average curves. Moving average curves smooth out the high frequency variability and most of the data

scattering related to shell sampling. This ensemble yields the probability distribution through time of the centennial scale average shell $\delta^{18}O$ value, represented by the gray scale in Fig. 8, a median value and a 95% confidence interval. The procedure was tested with running windows of 5, 7, and 10 points. The running window size slightly affects the size of the confidence interval but not the main features of our results, which shows that the method is robust to different window widths. The statistical representativeness of the dataset through time was estimated by the average number of shells per century in the MC experiment (Fig. 8B). The least robust period is the 14th century with an average number of only 1.5 shells, while the most robust (apart from the modern sample) is the 13th century with 12.8 shells. We have 7.1 shells per century in average (excluding the modern period). Considering that each shell integrates in average ~5 years, and assuming no significant overlap, this means that the record was built with ~35 years per century in average, which is statistically robust to estimate centennial mean conditions ($CI = \pm 1.96 \cdot \sigma / \sqrt{N} = \pm 0.17‰$) even considering all possible uncertainty sources related to mollusk shells (Carré et al. 2012). The raw dataset, the reconstructed annual isotopic time series and the Matlab code of the MC procedure are available in the electronic supplementary materials (Online Resource 1, 2, 3).

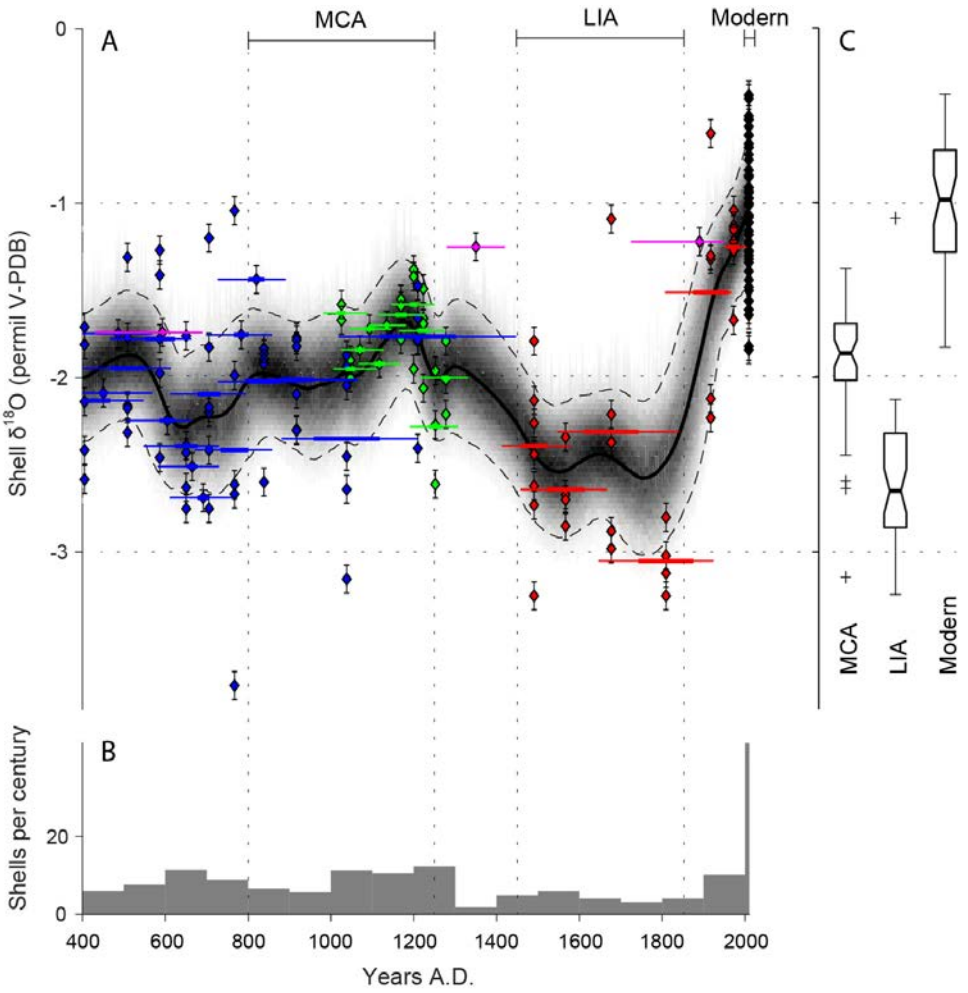

Fig. 8. Variability of shell $\delta^{18}O$ values in the past 1600 years in the Saloum Delta. (a) Isotopic values of individual shells (diamonds) are represented with 2σ analytical error. Modern shells (black) were collected live in 5 locations across the estuary between 2011 and 2014. Fossil shells from the stratified shell middens of Diofandor (red), Tioupane (green), Dioron Boumak (blue) were dated using Bayesian age-depth models (Fig. 3). Fossil shells from sites A10, A12, and A49 (pink) were directly ^{14}C dated (Table 1). Average $\delta^{18}O$ values for successive stratigraphic levels are indicated by horizontal bars. The length of thick bars indicates the most likely occupation period, and the thinner bars the 2σ intervals. Gray scale shading represents the probability distribution of the shell $\delta^{18}O$ moving average considering chronological uncertainty. The thick black lines represent the median probability and the dashed lines the 95% confidence interval. (b) Histogram of the average number of shells per century in the Monte Carlo sampling analysis. The average timespan integrated by a shell value is approximately 5 years. (c) Box plots of isotopic values for modern shells, and fossil shells of the MCA and LIA periods. MCA and LIA are here defined by the AD 800-1250 and AD 1450-1850 periods respectively. Box plots represent the full range of values (whiskers) excluding statistical outliers, the 25th and 75th percentiles (box edges), the median (central mark), and the confidence interval (95% confidence level) of the median (box notch).

3. Results

Significant centennial variations of shell $\delta^{18}O$ show values depleted relative to the present day during the whole preindustrial part of the record. The record can be divided into three broad periods that roughly correspond to the Medieval Climate Anomaly (MCA; AD 800-1250), the Little Ice Age (AD 1400-1850) and the industrial period (1850-today) (Fig. 8). The MCA period shows a slight increasing trend of aridity until a maximum at *ca*. -1.7±0.2‰ in the 12th century. The transition into the LIA is characterized by decreasing isotopic values from AD 1200 to AD 1500, to reach a minimum value of *ca*. -2.6±0.3‰ from *ca*. AD 1500 to AD 1800, corresponding to the coolest period of the LIA. An abrupt increasing trend started in the late 18th century and has continued through to the present day, which has clearly the most positive isotopic values (-1±0.15‰) of the last 1600 years. The values of the modern period are significantly enriched compared to the LIA, the MCA, or the whole preindustrial period (t-test, 0.01 significance level) (Fig. 8, Fig. 9). The difference between MCA and LIA values is also statistically significant (t-test, 0.01 significance level).

The isotopic pattern in Senegal is strikingly similar to the pattern of temperature change in the northern hemisphere (Fig. 10). We thus tested the correlation of the shell isotopic record with a global temperature reconstruction (Pages2k 2013) and two north hemisphere reconstructions (Moberg et al. 2005; Mann et al. 2009). To account for the degrees of freedom of our dataset (163) and the chronology uncertainty, we calculated the Pearson correlation coefficients using the 163 raw isotopic values coupled to the temperature reconstruction values taken at the dates of the Monte Carlo chronologies, which provides an ensemble of correlation coefficients with each temperature reconstruction. The average correlation coefficients obtained with Pages2k, Moberg and Mann's reconstructions are R=0.28 (p=0.019), R=0.27 (p=0.022), and R=0.20 (p=0.092) respectively. The correlation between

the Saloum isotopic record and temperature reconstruction is thus statistically significant at the 0.05 significance level for Pages2k global reconstruction and Moberg north hemisphere reconstruction.

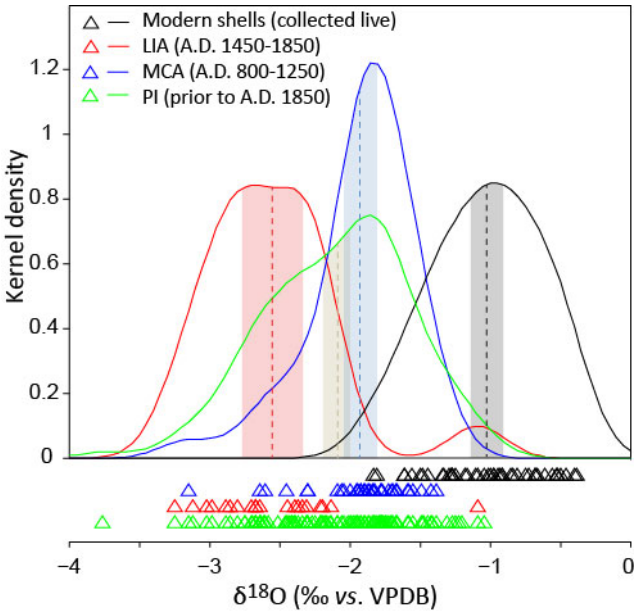

Fig. 9. Distributions of shell $\delta^{18}O$ values per time period. Modern= all modern values from live-collected shells (N=44) (black). PI= all values with median date prior to A.D. 1850 (N=109) (green). LIA= all values with median dates between 1450 and 1850 (N=20) (red). MCA= all values with median dates between 800 and 1250 (N=36) (blue). For each shell sample, isotopic values are plotted as triangles at the bottom, and the corresponding normal Kernel probability density curves are plotted (n=50, bandwidth=0.2). Mean values and the 95% confidence intervals of the estimated mean values are represented by dashed lines and shaded areas.

We compared the monthly resolved isotopic signals of a LIA shell from Diofandor and a modern shell collected live in the same location. Both shells exhibit a perfectly regular seasonal $\delta^{18}O$ signal, recording 4 monsoon seasons for the modern shell and 5 monsoon seasons in the fossil shell (Fig. 11). The LIA shell $\delta^{18}O$ values are significantly more negative than modern shell values by 1.18‰ on average (t-test, p-value<0.001), in agreement with centennial scale variations. Rainy season conditions in the modern shell correspond to average conditions in the fossil shells. Growth slowdowns observed in shell growth lines were similar in the modern and the fossil shell. They occurred in both cases during the rainy season and were similar in length. These observations combined with the consistency of high resolution

and bulk isotopic values confirm (1) that fossil shells are well preserved, (2) that growth was continuous year-round and not significantly different in fossil shells, including those that lived in the most different conditions from today. The amplitude of seasonal variations was 40% larger in the LIA shell compared to the modern shell.

4. Discussion

4.1. Interpretation of the isotopic record

Since *S. senilis* aragonite was showed to precipitates in isotopic equilibrium with the ambient water (Fig. 5), shell $\delta^{18}O$ values are determined by water temperature and $\delta^{18}O_w$ only (Grossman and Ku 1986). We find that temperature cannot account for the shell $\delta^{18}O$ centennial variability, as shown by the sign and amplitude of the centennial isotopic signal: if temperature were here the primary influence, the ~1.5‰ increase observed in aragonite $\delta^{18}O$ in the past 200 years would represent a 6.5°C *cooling*, which is unrealistic and opposed to observations (Kuhnert and Mulitza 2011; Nicholson, 2013) (Fig. 10b). Hence, our signal must result from centennial changes in the estuary $\delta^{18}O_w$. $\delta^{18}O_w$ in the Saloum Delta is determined by 1) the relative contribution of sea water ($\delta^{18}O_w$ ~1‰ in this area) *versus* monsoon rainfall water ($\delta^{18}O$ ~ -4.9±0.4‰), and 2) evaporation (Fig. 6). We showed that the relative contribution of both end members was not significantly affected through time by changes in the sea level or in the estuary connection to the sea (see section 2.5). On the other hand, the strong increasing trend observed in the Saloum salinity from 1960 to 1990 shows the sensitivity of water chemistry to changes in the P-E budget (Pagès and Citeau, 1990; Savenije and Pagès, 1992; Mikhailov and Isupova, 2008). The estuary $\delta^{18}O_w$ could additionally be affected by changes in the rain water isotopic composition, which could result from a change

in the moisture source or by a change in rainfall intensity (amount effect). Isotopic changes due to the rainfall amount effect would strengthen this pattern. A change in the moisture source cannot be ruled out, but we don't expect it to have a major quantitative effect since it would only affect one of both end members. Therefore, we suggest that $\delta^{18}O$ variations in the Saloum water and shells reflect changes in the P-E budget, with more positive (negative) values indicating arid (humid) conditions.

We discuss now whether P-E changes observed in the past 1600 years are primarily due to changes in evaporation or in the precipitation regime. Before AD 1850, the magnitude of temperature changes in Senegal sea water (Kuhnert and Mulitza 2011) and in global reconstructions (Moberg et al. 2005; Mann et al. 2009; Pages2k 2013) seems too small (<0.5°C) to induce significant changes in evaporation (Fig. 10), which suggests that the pre-industrial P-E centennial variability is likely primarily related to precipitation changes. Since AD 1880, a warming of ~1°C has been measured in the ocean (ERSST 3b) (Smith et al. 2008) and ~1-2°C on the continent (Nicholson 2013) that must have induced an increased evaporation. An important indication, however, is given by the African Southwesterly Index (ASWI), reconstructed from historical wind direction measurements, which indicates a clear decreasing trend of rainfall in western Sahel since at least AD 1840 (Gallego et al. 2015). This rainfall record, in agreement with our data, suggests that the aridification trend observed in our isotopic record for the past 200 years is not only due to an increased evaporation but largely to a rainfall deficit. Finally, more intense monsoon precipitation during the LIA is indicated in the LIA shell isotopic record by ~40% larger seasonal peaks compared to the modern shell (Fig. 11). During the monsoon season, calculated water isotopic values reached ~-2.8‰ (-3.1‰ when considering 1.5°C lower temperature in the LIA) which corresponds to a salinity of ~13 psu (11 psu considering LIA temperature change). Such a low value close to the estuary mouth requires a strong freshwater flow that is never observed today.

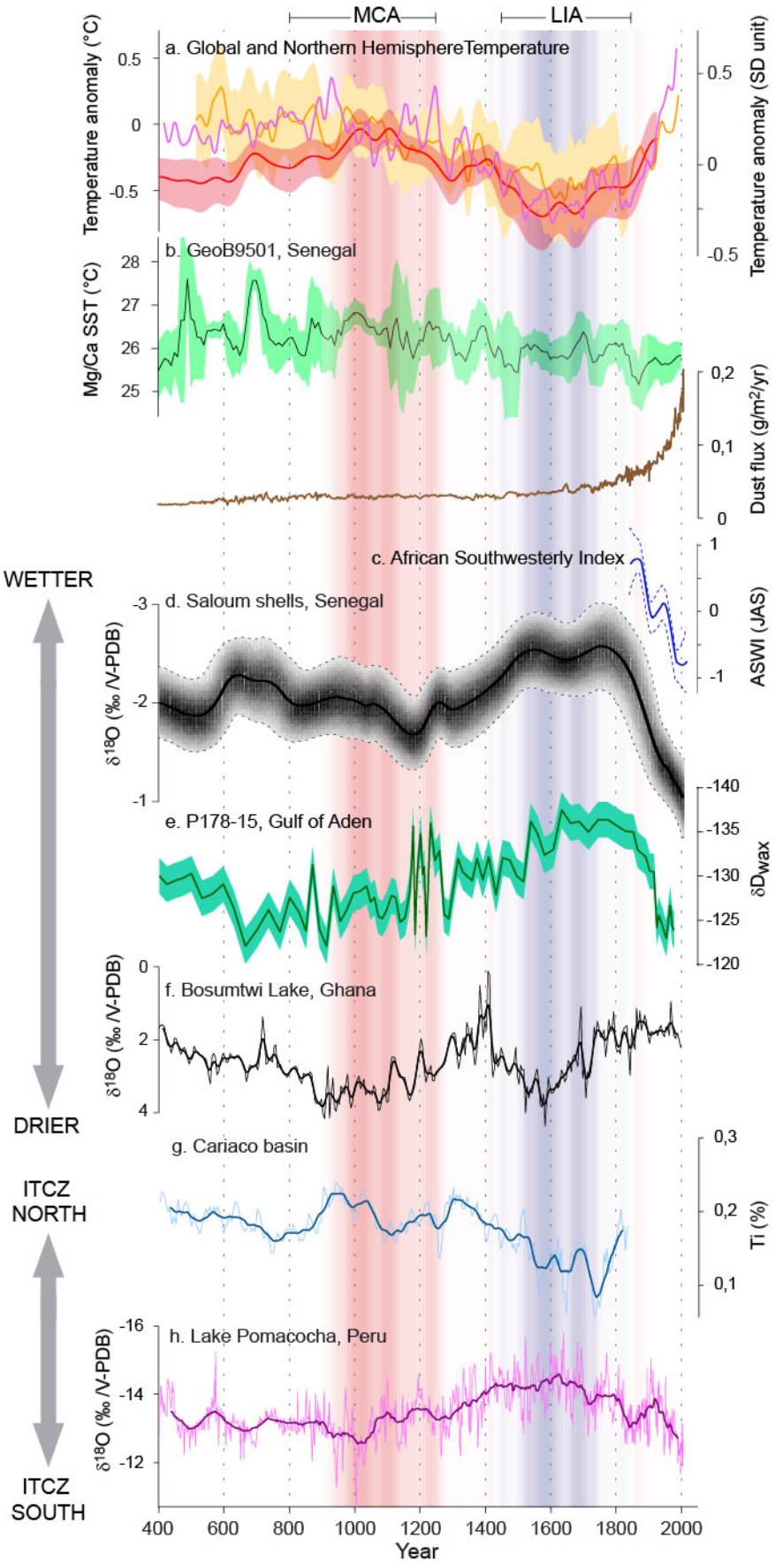
MCA
LIA
a. Global and Northern HemisphereTemperature
Temperature anomaly (°C)
Temperature anomaly (SD unit)
b. GeoB9501, Senegal
Mg/Ca SST (°C)
Dust flux (g/m²/yr)
c. African Southwesterly Index
ASWI (JAS)
WETTER
d. Saloum shells, Senegal
δ18O (‰ /V-PDB)
e. P178-15, Gulf of Aden
δDwax
f. Bosumtwi Lake, Ghana
DRIER
g. Cariaco basin
Ti (%)
ITCZ NORTH
h. Lake Pomacocha, Peru
ITCZ SOUTH
Year

Fig. 10. Comparison of the Saloum hydroclimate record with regional and global climate records. The time scale is in calendar years AD. (a) Temperature variability: northern Hemisphere temperature reconstructed by Mann et al. (2009) and smoothed with a 30-yr triangular filter (orange curve and shading), low frequency northern hemisphere temperature variability calculated by Moberg et al. (2005) (red curve and shading), global temperature anomaly (SD unit) as the area-weighted average of continent scale reconstructions by Pages-2k consortium (2013) (pink). Vertical red and blue shading was calculated from the temperature anomaly in Moberg et al.'s (2005) record. MCA and LIA periods are indicated above. (b) Records from marine sediment core GeoB9501: SST calculated from foraminifera Mg/Ca (Kuhnert and Mulitza 2011) (green), and Aeolian dust flux (Mulitza et al. 2010) (brown). (c) African Southwesterly Index (ASWI) of JAS, from 1840 to 2013, with 30-yr LOESS smoothed curve (Gallego et al. 2015). (d) Shell $\delta^{18}O$ density of probability (gray shading), median probability (black line) and confidence interval (dashed lines) in the Saloum estuary as an indicator of the precipitation-evaporation budget in the Western Sahel (this study). (e) Leaf wax hydrogen isotopic ratios (δD_{wax}) in the marine sediment core P178-15 from the Gulf of Aden (Tierney et al. 2015). The error bar is the ±1sigma analytical precision. (f) Calcite $\delta^{18}O$ in Lake Bosumtwi, Ghana, and 30-yr triangular filter smooth (Shanahan et al. 2009). (g) Ti content in ODP1002 sediment core indicating continental freshwater runoff into the Cariaco Basin, off Venezuela (Haug et al. 2001), and 10-point moving average curve (dark blue). (h) Calcite $\delta^{18}O$ in Lake Pomacocha, Central Peruvian Andes (Bird et al. 2011), and 30-yr moving average (purple).

In conclusion, the Saloum isotopic variations reflect hydroclimate changes primarily due to changes in local precipitation, which come almost entirely from the West African Monsoon system. This means that (1) the AD 1500-1800 period in LIA was the most humid period in the past 1600 years, (2) an abrupt aridification occurred in the past 200 years, (3) in the context of the past 1600 years, drought conditions in western Sahel have emerged in the 20th century from the range of natural climate variability.

4.2. The regional context

Records of hydroclimate in the past 1600 years are extremely scarce in the Sahel region. Some documentary and archaeological evidence indicate moister conditions in the medieval period. In Mauritania, the Ghana empire thrived in the 11th century suggesting a more prosperous agriculture (El-Bekri 1859). Awdaghust was an active trade city in the 8th to 14th century in what is today an extreme desert (Robert 1970). In the 16th century, Portuguese

explorer Fernandes reports that farmers did two crop yields per year in the Saloum region while rainfall today only allows for one *(*Fernandes et al. 1951; Daveau 1969). Documentary sources were used to reconstruct rainfall variability in Africa since AD 1800 (Nicholson et al. 2012). These sources indicate a very strong drought in the Sahel from AD 1800 to AD 1850, also supported by evidence of a drop in the Lake Chad level approximately at this time (Maley 1981). Considering the response time of the Saloum mean salinity, the drought reported in historical documents is consistent with the onset of the abrupt isotopic trend recorded by shells in the Senegal *ca*. AD 1800. West of Lake Chad, dust and ostracod $\delta^{18}O$ records were obtained from two oasis (Street-Perrott et al., 2000; Cockerton et al., 2014). While dust flux increased through the past 2000 years possibly in relation to the changing volume of Lake Chad and to human activities, ostracod $\delta^{18}O$ show slightly more negative values in the LIA than in the MCA, suggesting more humid conditions in the LIA in agreement with our record. No recent increase of $\delta^{18}O$ values was observed in these sites, either because of different local conditions or because of a truncation of the core top.

A continuous record of WAM variability was provided by calcite $\delta^{18}O$ measured in Lake Bosumtwi, Ghana (Shanahan et al. 2009). Interestingly, the Saloum hydrological changes are very different from those recorded at Lake Bosumtwi (Fig. 10), which is located in the convective zone of the monsoon. On the other hand, the Saloum isotopic record shows similarity over the past 700 years with the first EOF of eastern Africa Lake records (Tierney et al. 2013) and with a record of past precipitation located at the same latitude in the Gulf of Aden (Tierney et al. 2015) (Fig. 10). These results suggest that the spatial coherence of rainfall across the Sahel, as well as the weak correlation between the Sahel and the Gulf of Guinea observed in the instrumental data at the decadal scale (Fig. 1) applies also at the centennial time scale.

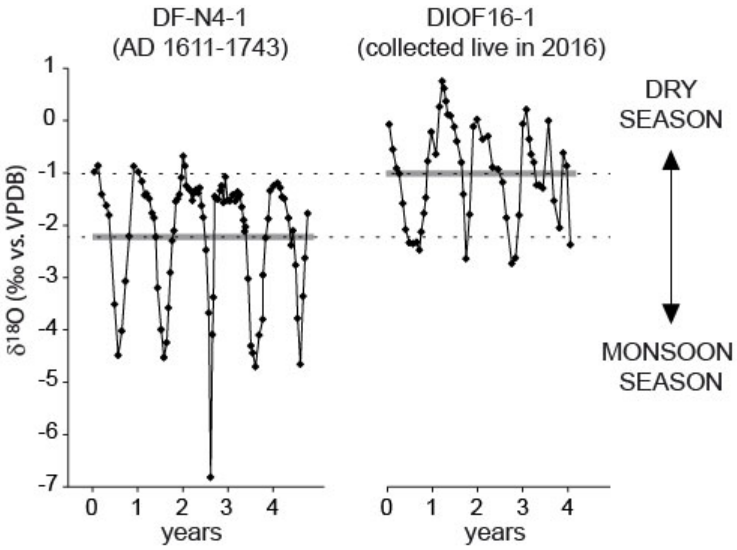

Fig. 11. Monthly resolved $\delta^{18}O$ records of a modern and a fossil shell from Diofandor (Fig. 1). Average values are indicated by gray lines. Negative values reflect lower salinity. Time axes represent the shell ontogenic age.

4.3. Sahel rainfall and global climate change

Explanations of millennial to centennial scale rainfall variability in the tropics have been often related to latitudinal shifts of the mean position of the ITCZ in response to inter-hemispheric temperature contrasts (Street-Perrott and Perrot, 1990; Mulitza and Rühlemann, 2000; Haug et al. 2001; Yancheva et al., 2007). Following this model, and according to paleoclimate records from the Pacific (Sachs et al. 2009), South America (Haug et al. 2001, Bird et al., 2011), Asia (Yan et al. 2015), and East Africa (Brown and Johnson 2005), the LIA is characterized by a relatively southern position of the July ITCZ (Fig. 10), which is in apparent contradiction with increased humidity over the Sahel during this period. The centennial variability of conditions in the Sahel must therefore be governed by processes more complex than the simple shift of the rain belt driven by the position of the July ITCZ.

Sea-surface temperature and the Atlantic multidecadal oscillation have been identified in the instrumental record as one of the main drivers of Sahel rainfall (Folland et al. 1986; Giannini et al. 2003; Zhang and Delworth 2006; Mohino et al. 2011). During positive AMO

phases, increased summer precipitation is observed in the Sahel in response to a strengthening of the Sahara heat convection and increased moisture flux from the Mediterranean Sea (Martin and Thorncroft 2014). However, past temperature reconstructions suggest that the LIA period corresponds to a negative AMO-like phase (Mann et al. 2009) which, if the same type of mechanism can be invoked at a longer time-scale, would therefore tend to induce dry conditions in the Sahel, in opposition with our observations. Our multicentennial perspective shows thus that western Sahel hydroclimate centennial variability responds to remote forcings through processes that are different from those identified at multidecadal timescales (AMO) or millennial time scales (ITCZ shifts).

The most prominent characteristics of the Saloum hydroclimate record is the significant correlation with global or hemispheric temperature reconstructions, while no correlation is observed with local SSTs (Fig. 10), suggesting that low frequency variability of Sahel rainfall primarily depends on changes in the global atmospheric circulation. Although determining the mechanisms responsible for the observed negative relationship between western Sahel rainfall and global temperature is beyond the scope of this study, our results bring new constraints to understand the processes that affect Sahel rainfall in the context of the on-going long-term global warming trend.

First, the facts that (1) over the past 200 years, the strong aridification in the Western Sahel coincides with rapid global warming, and (2) that drought conditions in western Sahel are today beyond the range of the pre-industrial climatic variability of the past 1600 years, point to an anthropogenic forcing of the Sahel drying trend. The last 200 years have also seen the development and expansion of commercial agriculture in the Sahel, corresponding to an increase of Saharan aeolian dust flux (Fig. 10) as a result of an increased erosion due to increased agricultural land use (Mulitza et al. 2010). This human-induced change in vegetation cover is likely to have contributed to the decrease in rainfall of the past 200 years

through the positive local vegetation-precipitation feedback. This local effect was probably combined with the global effect of anthropogenic warming that modified the tropical atmospheric circulation.

Second, the negative relationship between western Sahel rainfall and global temperature revealed by our reconstruction is in agreement with model and instrumental data analyses that showed a decreasing trend of rainfall in the margin of the convective regions (Allan and Soden 2007) and a narrowing of the ITCZ as a result of global warming (Lau and Kim, 2015; Byrne and Schneider 2016; Wodzicki and Rapp 2016; Su et al., 2017). The result is an enhancement of the Precipitation-Evaporation pattern (Held and Soden, 2006). This trend has been attributed to the "upped-ante mechanism" (Neelin et al. 2003), which describes changes in horizontal moisture advection, and to a strengthening of the meridional gradient of moist static energy with warming of the troposphere (Byrne and Schneider 2016). Our reconstruction supports climate models predicting increasing drought in the Sahel with future global warming (Held et al. 2005), although a majority of climate models tend now to predict wetter future climate (Biasutti 2013). It also suggest that the rainfall "recovery" of the past 15 years in the Sahel is likely related to short-term multidecadal internal climate variability. In the context of the past 1600 years, the modern conditions in western Sahel should be considered as an extreme drought likely caused by human activities. Although the nature of external forcings in the 21st century is different from the pre-industrial period, the long-term relationship evidenced here underlines the risk of a major drought crisis in the 21st century. Further paleoclimate reconstructions combined with paleoclimate modeling experiments are required to confirm and understand centennial scale Sahel hydroclimate variability and constrain greenhouse climate predictions in this region.

References

Allan RP, Soden BJCL (2007) Large discrepancy between observed and simulated precipitation trends in the ascending and descending branches of the tropical circulation. Geophysical Research Letters 34 http://dx.doi.org/10.1029/2007GL031460

Azzoug M (2012) Reconstitution des variations multidecennales et saisonnières de la mousson ouest-Africaine au cours des deux derniers millénaires à partir de l'étude sclérochronologique des amas coquilliers fossiles dans le delta du Saloum, Sénégal. Unpublished PhD, Université Montpellier 2

Azzoug M, Carré M, Chase BM, Deme A, Lazar A, Lazareth CE, Schauer AJ, Mandeng-Yogo M, Simier M, Thierno-Gaye A, de Morais LT (2012) Positive precipitation-evaporation budget from AD 460 to 1090 in the Saloum Delta (Senegal) indicated by mollusk oxygen isotopes. Global and Planetary Change 98-99:54-62.

Azzoug M, Carré M, Schauer AJ (2012a) Reconstructing the duration of the West African Monsoon season from growth patterns and isotopic signals of shells of Anadara senilis (Saloum Delta, Senegal). Palaeogeography, Palaeoclimatology, Palaeoecology 346-347:145-152.

Barusseau JP, Bâ M, Descamps C, Salif Diop EH, Giresse P, Saos JL (1995) Coastal Evolution in Senegal and Mauritania at 10^3, 10^2 and 10^1-year scales: Natural and human records. Quaternary International 29/30:61-73.

Biasutti M (2013) Forced Sahel rainfall trends in the CMIP5 archive. Journal of Geophysical Research: Atmospheres 118:1613-1623. http://dx.doi.org/10.1002/jgrd.50206

Bird BW, Abbott MB, Vuille M, Rodbell DT, Stansell ND, Rosenmeier MF (2011) A 2,300-year-long annually resolved record of the South American summer monsoon from the Peruvian Andes. Proc. Natl Acad. Sci. USA 108:8583-8588.

Blaauw M, Christen JA (2011) Flexible paleoclimate age-depth models using an autoregressive gamma process. Bayesian Analysis 6:457-474.

Brown ET, Johnson TC (2005) Coherence between tropical East African and South American records of the Little Ice Age. Geochemistry, Geophysics, Geosystems 6:Q12005. http://dx.doi.org/10.1029/2005GC000959

Byrne MP, Schneider T (2016) Narrowing of the ITCZ in a warming climate: physical mechanisms. Geophysical Research Letters:2016GL070396. http://dx.doi.org/10.1002/2016GL070396

Carré M, Sachs JP, Wallace JM, Favier C (2012) Exploring errors in paleoclimate proxy reconstructions using Monte Carlo simulations: paleotemperature from mollusk and coral geochemistry. Climate of the Past 8:433-450.

Christensen JH, Kanikicharla KK, Marshall G, Turner J (2013) Climate phenomena and their relevance for future regional climate change. In: Climate Change 2013, The physical science basis. Cambridge University Press, p 1217-1308

Cockerton HE, Holmes JA, Street-Perrott FA, Ficken KJ (2014) Holocene dust records from the West African Sahel and their implications for changes in climate and land surface conditions. Journal of Geophysical Research: Atmospheres 119:8684-8694. doi: 10.1002/2013JD021283

Cohn M, Urey HC (1938) Oxygen exchange reactions of organic compounds with water. Journal of the American Chemical Society 60:679-687.

Daveau S (1969) La découverte du climat au cours des navigations portugaises. Bull. Inst. Fr. Afr. Noire, série B 31:953-988.

Debenay JP, Leung Tack D, Ba M, Sy I (1994) Environmental conditions, growth and production of *Anadara senilis* (Linnaeus, 1758) in a Senegal lagoon. Journal of Molluscan Studies 60:113-121.

Diara M, Barusseau JP (2006) Late Holocene evolution of the Salum-Gambia double delta (Senegal). Geo-Eco-Marina 12:17-28.

El-Bekri, translated by De Slane MG (1859) Description de l'Afrique Septentrionale, Vol. Imprimerie Impériale, Paris

Elouard P, Rosso J-C (1977) Biogéographie et habitat des mollusques actuels laguno-marins du delta du Saloum (Sénégal). Geobios 10:275-296, IN271-IN273.

Faure H, Fontes JC, Hebrard L, Monteillet J, Pirazzoli PA (1980) Geoidal Change and Shore-Level Tilt Along Holocene Estuaries: Senegal River Area, West Africa. Science 210:421-423.

Fernandes V, Monod T, Mauny R (1951) Description de la côte occidentale d'Afrique:(Sénégal du Cap de Monte, Archipels), Centro de Estudos da Guiné Portuguesa

Folland CK, Palmer TN, Parker DE (1986) Sahel rainfall and worldwide sea temperatures, 1901-85. Nature 320:602-607. http://dx.doi.org/10.1038/320602a0

Gallego D, Ordóñez P, Ribera P, Peña-Ortiz C, García-Herrera R (2015) An instrumental index of the West African Monsoon back to the nineteenth century. Q. J. R. Meteorol. Soc. 141:3166-3176. http://dx.doi.org/10.1002/qj.2601

Giannini A, Saravanan R, Chang P (2003) Oceanic forcing of Sahel rainfall on interannual to interdecadal time scales. Science 302:1027-1030.

Gillikin DP, Lorrain A, Bouillon S, Willenz P, Dehairs F (2006) Stable carbon isotopic composition of Mytilus edulis shells: relation to metabolism, salinity, d13CDIC and phytoplankton. Organic Geochemistry 37:1371-1382.

Goodwin DH, Schöne BR, Dettman DL (2003) Resolution and fidelity of oxygen isotopes as paleotemperature proxies in bivalve mollusk shells: Models and observations. Palaios 18:110-125.

Grossman EL, Ku, Teh-Lung (1986) Oxygen and carbon fractionation in biogenic aragonite: temperature effect. Chemical Geology 59:59-74.

Hardy K, Camara A, Piqué R, Dioh E, Guèye M, Diadhiou HD, Faye M, Carré M (2016) Shellfishing and shell midden construction in the Saloum Delta, Senegal. Journal of Anthropological Archaeology 41:19-32.

Haug GH, Hughen KA, Sigman DM, Peterson LC, Röhl U (2001) Southward migration of the intertropical convergence zone through the Holocene. Science 293:1304-1308.

Held IM, Delworth TL, Lu J, Findell KL, Knutson TR (2005) Simulation of Sahel drought in the 20th and 21st centuries. Proc. Natl Acad. Sci. USA 102:17891-17896.

Held IM, Soden BJ (2006) Robust Responses of the Hydrological Cycle to Global Warming. Journal of Climate 19:5686-5699.

Kim S-T, Mucci A, Taylor BE (2007) Phosphoric acid fractionation factors for calcite and aragonite between 25 and 75 °C: Revisited. Chemical Geology 246:135-146.

Kuhnert H, Mulitza S (2011) Multidecadal variability and late medieval cooling of near-coastal sea surface temperatures in the eastern tropical North Atlantic. Paleoceanography 26:PA4224. http://dx.doi.org/10.1029/2011PA002130

Lau WKM, Kim K-M (2015) Robust Hadley Circulation changes and increasing global dryness due to CO2 warming from CMIP5 model projections. Proc. Natl Acad. Sci. USA 112:3630-3635. doi:10.1073/pnas.1418682112

Lavaud R, Thébault J, Lorrain A, van der Geest M, Chauvaud L (2013) Senilia senilis (Linnaeus, 1758), a biogenic archive of environmental conditions on the Banc d'Arguin (Mauritania). Journal of Sea Research 76:61-72.

Maley J (1981) Etudes palynologiques dans le bassin du Tchad et paléoclimatologie de l'Afrique nord-tropicale de 30 000 ans à l'époque actuelle. Travaux et documents de l'ORSTOM:pp. 586.

Mann ME, Zhang Z, Rutherford S, Bradley RS, Hughes MK, Shindell DT, Ammann C, Faluvegi G, Ni F (2009) Global signatures and dynamical origins of the Little Ice Age and Medieval Climate Anomaly. Science 236:1256-1260.

Martin ER, Thorncroft CD (2014) The impact of the AMO on the West African monsoon annual cycle. Quarterly Journal of the Royal Meteorological Society 140:31-46. http://dx.doi.org/10.1002/qj.2107

Mikhailov VN, Isupova MV (2008) Hypersalinization of river estuaries in West Africa. Water Resources 35:367-385.

Moberg A, Sonechkin DM, Holmgren K, Datsenko NM, Karlén W (2005) Highly variable northern hemisphere temperatures reconstructed from low- and high-resolution proxy data. Nature 433:613-617.

Mohino E, Janicot S, Bader J (2011) Sahel rainfall and decadal to multi-decadal sea surface temperature variability. Climate Dynamics 37:419-440. doi: 10.1007/s00382-010-0867-2

Mulitza S, Rühlemann C (2000) African Monsoonal Precipitation Modulated by Interhemispheric Temperature Gradients. Quaternary Research 53:270-274. doi:10.1006/qres.1999.2110

Mulitza S, Heslop D, Pittauerova D, Fischer HW, Meyer I, Stuut J-B, Zabel M, Mollenhauer G, Collins JA, Kuhnert H, Schulz M (2010) Increase in African dust flux at the onset of commercial agriculture in the Sahel region. Nature 466:226-228. doi:10.1038/nature09213

Nash DJ, De Cort G, Chase BM, Verschuren D, Nicholson SE, Shanahan TM, Asrat A, Lézine A-M, Grab SW (2016) African hydroclimatic variability during the last 2000 years. Quaternary Science Reviews 154:1-22.

Ndeye M (2008) Marine Reservoir Ages in Northern Senegal and Mauritania Coastal Waters. Radiocarbon 50:281-288. doi:10.1017/S0033822200033580

Neelin JD, Chou C, Su H (2003) Tropical drought regions in global warming and El Niño teleconnections. Geophysical Research Letters 30:2275. doi:10.1029/2003GL018625

Nicholson SE (2014) Spatial teleconnections in African rainfall: A comparison of 19th and 20th century patterns. The Holocene 24:1840-1848.

Nicholson SE, Dezfuli AK, Klotter D (2012) A Two-Century Precipitation Dataset for the Continent of Africa. Bull. Amer. Meteor. Soc. 93:1219-1231.

Nicholson SE, Nash DJ, Chase BM, Grab SW, Shanahan TM, Verschuren D, Asrat A, Lézine A-M, Umer M (2013) Temperature variability over Africa during the last 2000 years. The Holocene 23:1085-1094.

Pagès J, Citeau J (1990) Rainfall and salinity of a Sahelian estuary between 1927 and 1987. Journal of Hydrology 113:325-341.

PAGES-2k (2013) Continental-scale temperature variability during the past two millennia. Nature Geosci 6:339-346. doi:10.1038/ngeo1797

Pendergrass A, National Center for Atmospheric research Staff (2016) The Climate Data Guide: GPCP (Daily): Global Precipitation Climatology Project. https://climatedataguide.ucar.edu/climate-data/gpcp-daily-global-precipitation-climatology-project

Reimer PJ, Bard E, Bayliss A, Beck JW, Blackwell PG, Bronk Ramsey C, Buck CE, Cheng H, Edwards RL, Friedrich M, Grootes PM, Guilderson TP, Haflidason H, Hajdas I, Hatté C, Heaton TJ, Hoffmann DL, Hogg AG, Hughen KA, Kaiser KF, Kromer B, Manning SW, Niu M, Reimer RW, Richards DA, Scott EM, Southon JR, Staff RA, Turney CSM, van der Plicht J (2013) IntCal13 and Marine13 Radiocarbon Age Calibration Curves 0-50,000 Years cal BP. Radiocarbon 55:1869-1887.

Robert DS (1970) Les Fouilles de Tegdaoust. The Journal of African History 11:471-493.

Sachs JP, Sachse D, Smittenberg RH, Zhang Z, Battisti DS, Golubic S (2009) Southward movement of the Pacific intertropical convergence zone A.D. 1400-1850. Nature Geoscience 2:519-525.

Savenije HHG, Pagès J (1992) Hypersalinity: a dramatic change in the hydrology of Sahelian estuaries. Journal of Hydrology 135:157-174.

Shanahan TM, Overpeck JT, Anchukaitis KJ, Beck JW, Cole JE, Dettman DL, Peck JA, Scholz CA, King JW (2009) Atlantic Forcing of Persistent Drought in West Africa. Science 324:377-380.

Smith TM, Reynolds RW, Peterson TC, Lawrimore J (2008) Improvements to NOAA's Historical Merged Land-Ocean Surface Temperature Analysis (1880-2006). Journal of Climate 21:2283-2296. http://dx.doi.org/10.1175/2007JCLI2100.1

Street-Perrott FA, Perrott RA (1990) Abrupt climate fluctuations in the tropics: the influence of Atlantic Ocean circulation. Nature 343:607.

Street-Perrott FA, Holmes JA, Waller MP, Allen MJ, Barber NGH, Fothergill PA, Harkness DD, Ivanovich M, Kroon D, Perrott RA (2000) Drought and dust deposition in the West African Sahel: a 5500-year record from Kajemarum Oasis, northeastern Nigeria. The Holocene 10:293-302. 10.1191/095968300678141274

Su H, Jiang JH, Neelin JD, Shen TJ, Zhai C, Yue Q, Wang Z, Huang L, Choi Y-S, Stephens GL, Yung YL (2017) Tightening of tropical ascent and high clouds key to precipitation change in a warmer climate. Nature Communications 8:15771. doi:10.1038/ncomms15771

Thilmans G, Descamps C (1982) Amas et tumulus coquilliers du delta du Saloum. In: Recherches scientifiques dans les parcs nationaux du Sénégal, Vol 92. Mémoires de l'Institut Fondamental d'Afrique Noire, Dakar, p 31-50

Tierney JE, Smerdon JE, Anchukaitis KJ, Seager R (2013) Multidecadal variability in East African hydroclimate controlled by the Indian Ocean. Nature 493:389-392. http://dx.doi.org/10.1038/nature11785

Tierney JE, Ummenhofer CC, deMenocal PB (2015) Past and future rainfall in the Horn of Africa. Science Advances 1. doi: 10.1126/sciadv.1500682

Wade M, Mignot J, Lazar A, Gaye AT, Carré M (2015) On the spatial coherence of rainfall over the Saloum delta (Senegal) from seasonal to decadal time scales. Frontiers in Earth Science, Atmospheric Science 3:30. doi:10.3389/feart.2015.00030

Wodzicki KR, Rapp ADCJ (2016) Long-term characterization of the Pacific ITCZ using TRMM, GPCP, and ERA-Interim. Journal of Geophysical Research: Atmospheres 121:3153-3170. http://dx.doi.org/10.1002/2015JD024458

Yan H, Wei W, Soon W, An Z, Zhou W, Liu Z, Wang Y, Carter RM (2015) Dynamics of the intertropical convergence zone over the western Pacific during the Little Ice Age. Nature Geosci 8:315-320. http://dx.doi.org/10.1038/ngeo2375

Yancheva G, Nowaczyk NR, Mingram J, Dulski P, Schettler G, Negendank JFW, Liu J, Sigman DM, Peterson LC, Haug GH (2007) Influence of the intertropical convergence zone on the East Asian monsoon. Nature 445:74.

Zhang R, Delworth TLCL (2006) Impact of Atlantic multidecadal oscillations on India/Sahel rainfall and Atlantic hurricanes. Geophysical Research Letters 33. http://dx.doi.org/10.1029/2006GL026267

Acknowledgements:

The authors are thankful to César Tendeng, Ansu Mane, Iba Ndiaye, and Bernard Bassène for their assistance with fieldwork. We are thankful to Cyr Descamps for sharing his knowledge on archaeological shell middens. We thank the Institut de Recherche pour le Développement

(IRD) in Senegal for the logistical support during field trips. We thank Andrew Schauer and Marie Balasse for their support with isotopic analyses, Sharon Nicholson and Brian M. Chase for their valuable comments on the manuscript, and two anonymous reviewers. This research was funded by the University of Montpellier, the French CNRS-Institut National des Sciences de l'Univers through the LEFE program, and the ANR-Belmont Forum PACMEDY project (ANR- 15-JCLI-0003-01).